

# PACIFIC EARTHQUAKE ENGINEERING RESEARCH CENTER

## Performance-Based Seismic Assessment of Skewed Bridges

**Peyman Kaviani**

Department of Civil and Environmental Engineering  
University of California, Irvine

**Farzin Zareian**

Department of Civil and Environmental Engineering  
University of California, Irvine

**Ertugrul Taciroglu**

Department of Civil and Environmental Engineering  
University of California, Los Angeles

#### Disclaimer

The opinions, findings, and conclusions or recommendations expressed in this publication are those of the author(s) and do not necessarily reflect the views of the study sponsor(s) or the Pacific Earthquake Engineering Research Center.

# **Performance-Based Seismic Assessment of Skewed Bridges**

**Peyman Kaviani**

Department of Civil and Environmental Engineering  
University of California, Irvine

**Farzin Zareian**

Department of Civil and Environmental Engineering  
University of California, Irvine

**Ertugrul Taciroglu**

Department of Civil and Environmental Engineering  
University of California, Los Angeles

PEER Report 2014/01  
Pacific Earthquake Engineering Research Center  
Headquarters at the University of California

January 2014



## ABSTRACT

The objective of this study is to assess the seismic behavior of reinforced concrete bridges with skew-angled seat-type abutments through a performance-based methodology. Special attention is given to the exploration of variations in the seismic behavior of such bridges with respect to the angle of skew. Post-earthquake reconnaissance studies have reported that larger values of skew angle adversely affect performance. The idiosyncratic, “multi-phasic,” behavior of skew bridges—observed during initial simulations of the present study—led to the development of a novel assessment methodology. This methodology is applied to a comprehensive database of bridges, which comprise combinations of a variety of geometric properties including: (1) number of spans, (2) number of columns per bent, (3) column-bent height, (4) span arrangement, and (5) abutment skew angle. An extensive set of nonlinear response history analyses were conducted using distinct suites of ground motions representing records for rock and soil sites, and another set that contained pronounced velocity pulses.

The findings indicate that demand parameters for skew-abutment bridges—e.g., deck rotation, abutment unseating, and column drift ratio—are generally higher than those for straight bridges. Through detailed investigations of the sensitivity of various response parameters to variations in bridge geometry and ground motion characteristics, we observed that bridges with larger abutment skew angles bear a higher probability of collapse due to excessive rotations. We also found that shear keys can play a major role in abating deck rotations and thus the probability of collapse. It was further observed that the resultant peak ground velocity ( $PGV_{res}$ ) is the most efficient ground motion intensity measure ( $IM$ ) for assessing skewed bridges’ seismic response.

In view of the abrupt changes observed in the skewed bridges’ demand parameters due to shear key failure, we propose a new probabilistic assessment approach—the “Multi-Phase Probabilistic Assessment of Response to Seismic Excitations” or M-PARS—for computing the complementary probability distribution function of an engineering demand parameter given the ground motion intensity measure,  $G(EDP|IM)$ .



## **ACKNOWLEDGMENTS**

This work was supported by the State of California through the Transportation Systems Research Program of the Pacific Earthquake Engineering Research (PEER) Center. Any opinions, findings, conclusions, or recommendations expressed in this material are those of the authors and do not necessarily reflect those of the funding agency.

Authors would also like to acknowledge Dr. Anoosh Shamsabadi (Caltrans) and Dr. Majid Sarraf (TMAD Taylor & Gaines; formerly, Parsons) for their guidance in developing the bridge model matrix used in this study.



# CONTENTS

<b>ABSTRACT</b> .....	<b>iii</b>
<b>ACKNOWLEDGMENTS</b> .....	<b>v</b>
<b>TABLE OF CONTENTS</b> .....	<b>vii</b>
<b>LIST OF FIGURES</b> .....	<b>xi</b>
<b>LIST OF TABLES</b> .....	<b>xv</b>
<b>1 STUDY OVERVIEW</b> .....	<b>1</b>
<b>1.1 Damage to Bridges</b> .....	<b>1</b>
1.1.1 Skewed Bridge Damages .....	1
<b>1.2 A Brief Review of Literature on the Seismic Response of Skewed Bridges</b> .....	<b>6</b>
1.2.1 Skewed Bridge Rotation Mechanism .....	6
<b>2 MATRIX OF REPRESENTATIVE BRIDGE MODELS</b> .....	<b>11</b>
<b>2.1 Introduction</b> .....	<b>11</b>
<b>2.2 Characteristics of California’s Bridges</b> .....	<b>11</b>
2.2.1 Bridges by the Skew Angle of Their Abutments .....	11
2.2.2 Bridges by the Number of Their Spans.....	12
2.2.3 Bridges Classified by the Year They Were Built.....	13
2.2.4 Bridges Classified by the Type of Structural System .....	13
<b>2.3 Bridges Selected for This Study</b> .....	<b>14</b>
2.3.1 Bridge A.....	16
2.3.2 Bridge B.....	18
2.3.3 Bridge C.....	20
<b>2.4 Ground Motion Selection</b> .....	<b>22</b>
2.4.1 Pulse-like Ground Motion Set .....	24
2.4.2 Soil-Site Ground Motion Set .....	26
2.4.3 Rock-Site Ground Motion Set .....	27
<b>2.5 Sensitivity Parameters</b> .....	<b>27</b>
2.5.1 Geometrical Characteristics .....	27
2.5.2 Ground Motion Characteristics.....	28
<b>2.6 The Bridge Model Matrix</b> .....	<b>30</b>

<b>3</b>	<b>DEVELOPMENT OF BRIDGE MODELS</b> .....	<b>33</b>
3.1	Overview .....	33
3.2	Model Attributes .....	33
3.2.1	Material Properties.....	33
3.2.2	Mass Assignment.....	34
3.2.3	Damping.....	35
3.3	Component Models .....	35
3.4	Modeling of the Deck.....	37
3.5	Cap-Beam Modeling.....	37
3.6	Column-Bent Modeling.....	37
3.6.1	Material Modeling .....	38
3.6.2	Section Properties .....	39
3.6.3	Element Characteristics .....	40
3.7	Abutment Modeling.....	41
3.7.1	Overview.....	41
3.7.2	Proposed Abutment Models for Skewed Bridges.....	45
<b>4</b>	<b>ANALYSIS AND TREND OBSERVATIONS IN SKEWED BRIDGE RESPONSE TO SEISMIC EXCITATIONS</b> .....	<b>53</b>
4.1	Overview .....	53
4.2	Modal Analysis.....	53
4.3	Collapse Criteria .....	57
4.4	Response History Analysis .....	57
4.4.1	Collapse Potential Observations .....	58
4.5	The Effect of Ground Motion Type on Skewed Bridge Response.....	60
4.5.1	Trends in the Statistical Parameters of Collapse Fragility Curves .....	64
4.6	Trend Observations .....	65
4.6.1	Trends in Deck Rotation.....	66
4.6.2	Trends in Abutment Unseating Displacement .....	70
4.6.3	Trends in Column-Bent Drift Ratio .....	74
<b>5</b>	<b>MULTI-PHASE PROBABILISTIC ASSESSMENT OF STRUCTURAL RESPONSE TO SEISMIC EXCITATIONS (M-PARS)</b> .....	<b>79</b>
5.1	Overview .....	79
5.2	M-PARS Formulation .....	79
5.3	Application of M-PARS to Skew Bridges .....	81
5.3.1	Hazard Curve .....	82
5.3.2	Relationship Between Selected <i>EDP</i> and <i>IM</i> .....	82

5.3.3	Fragility Curve .....	85
5.3.4	Steps for Implementing M-PARS .....	86
<b>5.4</b>	<b>M-PARS Statistical Parameters for the Bridge Matrix Used in This Study.....</b>	<b>87</b>
<b>5.5</b>	<b>Case Studies Using M-PARS.....</b>	<b>87</b>
5.5.1	Seismic Hazard Level .....	87
5.5.2	$G(EDP IM)$ Probability Representation .....	88
<b>6</b>	<b>SUMMARY AND CONCLUSIONS.....</b>	<b>101</b>
6.1	An Overview of Findings.....	101
6.2	Novel Skewed Bridge Modeling Technique.....	101
6.3	Sensitivity of Bridge Response Parameters to Variations in Bridge Geometrical Properties and Ground Motion Characteristics .....	102
6.4	Efficient Ground Motion Intensity Measure for Assessing Skewed Bridge Seismic Response .....	102
6.5	M-PARS Method.....	103
6.6	Recommendations for Future Studies.....	103
	<b>REFERENCES.....</b>	<b>105</b>
	<b>APPENDIX A: FHWA BRIDGE TYPE CODING SYSTEM.....</b>	<b>111</b>
	<b>APPENDIX B: GROUND MOTION PROPERTIES .....</b>	<b>113</b>
	<b>APPENDIX C: DESCRIPTION OF THE SEED BRIDGE MODELS .....</b>	<b>121</b>
	<b>APPENDIX D: SHEAR KEY MODELING IN OPENSEES .....</b>	<b>127</b>
	<b>APPENDIX E: M-PARS STATISTICAL PARAMETERS FOR THE BRIDGE MATRIX .....</b>	<b>133</b>



## LIST OF FIGURES

Figure 1.1	Failure of columns of the FBU (source: Chen and Duan [2000]).....	3
Figure 1.2	Gavin Canyon Undercrossing collapse in the 1994 Northridge Earthquake (source: Chen and Duan [2000]).....	4
Figure 1.3	Santa Clara River Bridge pounding damage to the abutment in 1994 Northridge Earthquake (source: Chen and Duan [2000]). .....	4
Figure 1.4	Abutment of the Northwestern bridge of the FBU (source: Jennings et al. [1971]).....	5
Figure 1.5	Damage to a skewed bridge after the Chile Earthquake of February 27, 2010 (source: Yashinsky et al. [2010]). .....	5
Figure 1.6	Rotational moment due to abutment impact forces. ....	7
Figure 1.7	Effect of skew angle on eccentricity parameters. ....	8
Figure 1.8	Effect of skew angle on deck rotation index ( <i>DRI</i> ). ....	8
Figure 2.1	Distribution of bridges in California based on the abutment skew angle. ....	12
Figure 2.2	Distribution of bridges in California based on the number of spans. ....	12
Figure 2.3	Distribution of bridges in California based on the year of construction. ....	13
Figure 2.4	Distribution of bridges in California based on type of structure. ....	14
Figure 2.5	The <i>Jack Tone Road on-ramp overcrossing</i> (Bridge A) shown in (a) a photograph (source: Google Maps) and (b) elevation (source: California Department of Transportation structural drawings).....	17
Figure 2.6	The <i>La Veta Overcrossing</i> (Bridge B) shown in (a) a photograph (source: Google Maps) and (b) elevation (source: California Department of Transportation structural drawings). ....	19
Figure 2.7	The <i>Jack Tone Road Overhead</i> (Bridge C) shown in (a) a photograph (source: Google Maps) and (b) elevation (source: California Department of Transportation structural drawings).....	21
Figure 2.8	Response spectra of strike-normal (SN) and strike-parallel (SP) components of (a) pulse-like, (b) soil-site, and (c) rock-site ground motion types. ....	25
Figure 2.9	Ground velocity history of strike-normal (SN) component of three pulse-like ground motions. ....	26
Figure 2.10	Histogram of pulse periods in pulse-like ground motion set. ....	26
Figure 2.11	Comparison of three different ground motion sets. ....	29
Figure 2.12	Ground motion incidence angle scheme for the strike-normal component. ....	30
Figure 2.13	Scheme of the bridge matrix assigned to Bridge A. ....	31

Figure 3.1	Generic stress-strain curve for concrete.....	34
Figure 3.2	Generic model ( $\alpha^\circ$ skew) used for nonlinear response history analyses.....	36
Figure 3.3	Column modeling scheme.....	38
Figure 3.4	OpenSees stress-strain curves for concrete: (a) <i>Concrete01</i> and (b) <i>Concrete02</i> .....	39
Figure 3.5	OpenSees stress-strain curves for steel: (a) <i>Steel02</i> and (b) <i>ReinforcingSteel</i> .....	39
Figure 3.6	Configuration of typical seat-type abutment.....	41
Figure 3.7	The “interpreted Caltrans SDC [2010]” longitudinal stiffness for (a) seat-type abutment and (b) diaphragm abutment. ....	42
Figure 3.8	Abutment effective width for seat-type and diaphragm abutments. ....	43
Figure 3.9	Simplified abutment model.....	44
Figure 3.10	Vertical force-displacement backbone curve of the abutment ( $K_1$ : the elastomeric bearing pad stiffness, and $K_2$ : the stemwall and abutment embankment stiffness). ....	44
Figure 3.11	Spring abutment model. ....	45
Figure 3.12	Friction abutment model.....	47
Figure 3.13	Skewed Abutment Model, backfill soil springs. (a) Configuration diagram. (b) Backbone curves. ....	48
Figure 3.14	Cracking pattern at the end of Shear Key testing (Test 1B; Megally et al. [2002]).....	49
Figure 3.15	Strut-and-tie analogous model for shear keys (source: Megally et al. [2002]).....	50
Figure 3.16	Shear key force-deformation backbone curve. ....	52
Figure 3.17	Shear key for the seed bridges depicted in scale.....	52
Figure 4.1	Three first mode shapes of $0^\circ$ , $30^\circ$ , and $60^\circ$ skewed bridges (numbers in meters) for (a) Bridge A, (b) Bridge B, and (c) Bridge C.....	56
Figure 4.2	Pulse-like ground motions spectra for (a) strike-normal and (b) strike-parallel.....	59
Figure 4.3	Bridge A’s response sensitivity, with original column height and symmetric spans, to type of seismic excitation and abutment skew angle for (a) $PGA_{res}-\theta_{rot}$ and (b) $PGA_{res}-\theta_{col}$ . ....	61
Figure 4.4	Development of the collapse fragility curve for Bridge A (symmetrical span, original column height, $60^\circ$ abutment skew angle, and pulse-like ground motion [i.e., ALS4P]). ....	62

Figure 4.5	Dispersions in collapse fragility curves obtained for the bridge matrix using the pulse-like ground motion set and using logistic regressions of data for various <i>IMs</i> .....	63
Figure 4.6	Median and dispersion of collapse capacity, expressed in terms of $PGV_{res}$ for the bridge matrix obtained using the pulse-like ground motion set.....	65
Figure 4.7	$\theta_{rot}-PGV_{res}$ conditioned on no-collapse plots obtained for Bridge A using (a) pulse-like, (b) soil-site, and (c) rock-site ground motion sets.....	67
Figure 4.8	$\theta_{rot}-PGV_{res}$ conditioned on no-collapse plots obtained for Bridge B using (a) pulse-like, (b) soil-site, and (c) rock-site ground motion sets.....	68
Figure 4.9	$\theta_{rot}-PGV_{res}$ conditioned on no-collapse plots obtained for Bridge C using (a) pulse-like, (b) soil-site, and (c) rock-site ground motion sets.....	69
Figure 4.10	$\delta_{unseat}-PGV_{res}$ conditioned on no-collapse plots obtained for Bridge A using (a) pulse-like, (b) soil-site, and (c) rock-site ground motion sets.....	71
Figure 4.11	$\delta_{unseat}-PGV_{res}$ conditioned on no-collapse plots obtained for Bridge B using (a) pulse-like, (b) soil-site, and (c) rock-site ground motion sets.....	72
Figure 4.12	$\delta_{unseat}-PGV_{res}$ conditioned on no-collapse plots obtained for Bridge C using (a) pulse-like, (b) soil-site, and (c) rock-site ground motion sets.....	73
Figure 4.13	$\theta_{cot}-PGV_{res}$ conditioned on no-collapse plots obtained for Bridge A using (a) pulse-like, (b) soil site, and (c) rock-site ground motion sets.....	75
Figure 4.14	$\theta_{cot}-PGV_{res}$ conditioned on no-collapse plots obtained for Bridge B using (a) pulse-like, (b) soil-site, and (c) rock-site ground motion sets.....	76
Figure 4.15	$\theta_{cot}-PGV_{res}$ conditioned on no-collapse plots obtained for Bridge C using (a) pulse-like; (b) soil-site; and (c) rock-site ground motion sets.....	77
Figure 5.1	Schematic explanation of the M-PARS method.....	82
Figure 5.2	<i>EDP-IM</i> regression (AHA3P) using (a) multi-phase and (b) mono-phase.....	85
Figure 5.3	Development of fragility curve (AHA3P) using (a) multi-phase and (b) mono-phase.....	86
Figure 5.4	$\theta_{rot}$ -probability curves for Bridge A using (a) pulse-like, (b) soil-site, and (c) rock-site ground motion sets.....	89
Figure 5.5	$\theta_{rot}$ -probability curves for Bridge B using (a) pulse-like, (b) soil-site, and (c) rock-site ground motion sets.....	90
Figure 5.6	$\theta_{rot}$ -probability curves for Bridge C using (a) pulse-like, (b) soil site, and (c) rock-site ground motion sets.....	91
Figure 5.7	$\delta_{unseat}$ -probability curves for Bridge A using (a) pulse-like, (b) soil-site, and (c) rock-site ground motion sets.....	93
Figure 5.8	$\delta_{unseat}$ -probability curves for Bridge B using (a) pulse-like, (b) soil-site, and (c) rock-site ground motion sets.....	94

Figure 5.9	$\delta_{unseat}$ -probability curves for Bridge C using (a) pulse-like, (b) soil-site, and (c) rock-site ground motion sets. ....	95
Figure 5.10	$\theta_{cot}$ -probability curves for Bridge A using (a) pulse-like, (b) soil-site, and (c) rock-site ground motion sets. ....	97
Figure 5.11	$\theta_{cot}$ -probability curves for Bridge B using (a) pulse-like, (b) soil-site, and (c) rock-site ground motion sets. ....	98
Figure 5.12	$\theta_{cot}$ -probability curves for Bridge C using (a) pulse-like, (b) soil site, and (c) rock-site ground motion sets. ....	99
Figure C.1	Nodal and element designation of Bridge A. ....	123
Figure C.2	Nodal and element designation of Bridge B. ....	124
Figure C.3	Nodal and element designation of Bridge C. ....	125
Figure D.1	Transverse component of pulse-like ground motion number-11. ....	128
Figure D.2	Deck rotation of bridge ALS0P0 under Pulse-11 ground motion (Case I). ....	129
Figure D.3	Transverse spring deformation located in two different abutments, but on the same side (Case I). ....	129
Figure D.4	Backbone curve of the transverse spring during response history analysis (Case I). ....	130
Figure D.5	Deck rotation of the bridge ALS0P0 under Pulse-11 ground motion (Case II). ....	130
Figure D.6	Transverse spring deformation located in two different abutments, but on the same side (Case II). ....	131
Figure D.7	Backbone curve of the transverse spring during response history analysis (Case II). ....	131
Figure D.8	Backbone curve of the transverse spring during response history analysis (Case III). ....	132
Figure D.9	Backbone curve of the transverse spring during response history analysis (Case IV). ....	132

## LIST OF TABLES

Table 2.1	Selected characteristics of the seed bridges from the NBI database*.....	15
Table 2.2	Bridge A structural and geometric description. ....	18
Table 2.3	Bridge B structural and geometric description. ....	20
Table 2.4	Bridge C structural and geometric description. ....	22
Table 2.5	Span arrangements of bridges. ....	29
Table 2.6	Geometric and ground motion characteristics used in the sensitivity study.....	31
Table 3.1	Shear key strength contribution corresponding to the seed bridges. ....	51
Table 3.2	Shear key failure deformation of the seed bridges.....	51
Table 4.1	Fundamental periods of all studied bridges. ....	54
Table 4.2	Allowable unseating length of the seed bridges. ....	57
Table 4.3	Number of collapses for each bridge/ground motion set combination. ....	58
Table 4.4	Ground motion intensity measures ( <i>IMs</i> ) used in this study.....	61
Table 5.1	M-PARS component definitions for skewed bridges. ....	80
Table 5.2	<i>PGV</i> corresponding to a hazard level of 2% in 50 years. ....	88
Table A.1	The first digit descriptions (source: FHWA1995). ....	111
Table A.2	The second and third digit descriptions (source: FHWA1995). ....	112
Table B.1	Pulse-like ground motion properties.....	114
Table B.2	Soil-site ground motion properties.....	116
Table B.3	Rock-site ground motion properties.....	118
Table E.1	Statistical parameters for Bridge A with pulse-like ground motion and a deck rotation EDP.....	134
Table E.2	Statistical parameters for Bridge A with soil-site ground motion and a deck rotation EDP.....	135
Table E.3	Statistical parameters for Bridge A with rock-site ground motion and a deck rotation EDP.....	136

Table E.4	Statistical parameters for Bridge B with pulse-like ground motion and a deck rotation EDP .....	137
Table E.5	Statistical parameters for Bridge B with soil-site ground motion and a deck rotation EDP .....	138
Table E.6	Statistical parameters for Bridge B with rock-site ground motion and a deck rotation EDP .....	139
Table E.7	Statistical parameters for Bridge C with pulse-like ground motion and a deck rotation EDP .....	140
Table E.8	Statistical parameters for Bridge C with soil-site ground motion and a deck rotation EDP .....	141
Table E.9	Statistical parameters for Bridge C with rock-site ground motion and a deck rotation EDP .....	142
Table E.10	Statistical parameters for Bridge A with pulse-like ground motion and an abutment unseating EDP .....	143
Table E.11	Statistical parameters for Bridge A with soil-site ground motion and an abutment unseating EDP .....	144
Table E.12	Statistical parameters for Bridge A with rock-site ground motion and an abutment unseating EDP .....	145
Table E.13	Statistical parameters for Bridge B with pulse-like ground motion and abutment unseating EDP .....	146
Table E.14	Statistical parameters for Bridge B with soil-site ground motion and an abutment unseating EDP .....	147
Table E.15	Statistical parameters for Bridge B with rock-site ground motion and an abutment unseating EDP .....	148
Table E.16	Statistical parameters for Bridge C with pulse-like ground motion and an abutment unseating EDP .....	149
Table E.17	Statistical parameters for Bridge C with soil-site ground motion and an abutment unseating EDP .....	150
Table E.18	Statistical parameters for Bridge C with rock-site ground motion and an abutment unseating EDP .....	151
Table E.19	Statistical parameters for Bridge A with pulse-like ground motion and a column drift ratio EDP .....	152
Table E.20	Statistical parameters for Bridge A with soil-site ground motion and a column drift ratio EDP .....	153
Table E.21	Statistical parameters for Bridge A with rock-site ground motion and a column drift ratio EDP .....	154
Table E.22	Statistical parameters for Bridge B with a pulse-like ground motion and a column drift ratio EDP .....	155
Table E.23	Statistical parameters for Bridge B with soil-site ground motion and a column drift ratio EDP .....	156

Table E.24	Statistical parameters for Bridge B with rock-site ground motion and a column drift ratio EDP.....	157
Table E.25	Statistical parameters for Bridge C with pulse-like ground motion and a column drift ratio EDP.....	158
Table E.26	Statistical parameters for Bridge C with soil-site ground motion and a column drift ratio EDP.....	159
Table E.27	Statistical parameters for Bridge C with a rock-site ground motion and a column drift ratio EDP.....	160



# 1 Study Overview

## 1.1 DAMAGE TO BRIDGES

The main reasons for variations in the nature of damage experienced by bridges can be categorized as due to (i) the differences in the ground motion characteristics at the specific site; and (ii) the construction details of a particular bridge. Moehle and Eberhard—in the Bridge Engineering Handbook [Chen and Duan 2000]—classify bridge damage into *primary* and *secondary* damages. To wit, “damage caused by earthquake ground shaking or deformation that was the primary cause of damage to the bridge, and that may have triggered other damage or collapse” is classified as primary damage; and “damage caused by earthquake ground shaking or deformation that was the result of structural failures elsewhere in the bridge, and was caused by redistribution of internal actions for which the structure was not designed” is classified as secondary damage.

Generally, primary damage to bridges can be caused by three sources:

1. The overall factors contributing to bridge damage, including the site condition, construction era, and the bridge’s current condition.
2. The damage affected by the bridge configuration, including the skew of the abutment, curve layout, and redundancy.
3. Typical damage to the various bridge components, such as bridge superstructure, substructure, foundation, bearings, and restrainers.

Since this study focuses on skewed bridges, the following subsection addresses the damage to bridges affected by a skewed abutment.

### 1.1.1 Skewed Bridge Damages

The Foothill Boulevard Undercrossing (FBU) and the Painter Street Overcrossing (PSO) are typical examples of California’s bridges and have been the subjects of extensive studies (e.g., the FBU by Jennings et al. [1971] and Wakefield et al. [1991]; the PSO by Goel and Chopra [1997] and McCallen and Romstad [1994]). Both bridges experienced several earthquakes, and the former was severely damaged during the 1971 San Fernando Earthquake. The FBU is a four-span skewed bridge with a skew angle of approximately  $60^\circ$  and three columns per bent. The PSO is a two-span skewed bridge with a skew angle of nearly  $39^\circ$  and two columns per bent. The PSO was instrumented by the California Strong Motion Instrumentation Program (CSMIP), and

data recorded from various earthquakes at this station have been used frequently to evaluate the seismic behavior of short bridges.

In the rest of this section, we provide a basic review of damages to the aforementioned bridges as reported by different authors:

Superstructure response: Rigid body motion is expected for short bridges. The eccentric masses in the longitudinal and transverse directions of a skewed bridge can lead to the amplification of one or more of the six principal types of motion [Maragakis 1984], namely: (1) rigid-body longitudinal translation; (2) rigid-body lateral translation; (3) rigid-body in-plane rotation of the deck; (4) vertical flexure; (5) lateral flexure; and (6) torsional distortion of the bridge deck. Wakefield et al. [1991] concluded that in-plane rigid-body motion (translation as well as rotation) could have been the dominant response of the FBU Bridge during the 1971 San Fernando Earthquake. In their study, they assumed that the bridge deck was not rigidly connected to the abutments, which is the case for seat-type abutments. On the other hand, Goel and Chopra [1997] argued that the PSO Bridge experienced a significant torsional (rotational) motion about the deck's vertical axis during the main shock of the 1992 Cape Mendocino/Petrolia Earthquake.

Column-bent failure: Large abutment skew angles can induce torsional modes of vibration and lateral flexure, which may cause increase in axial forces, shear, moment, and torque in supporting piers. Figure 1.1 shows the damage to the intermediate piers of the FBU Bridge after the 1971 San Fernando Earthquake. This damage indicates that one of the major features of the collapse was the shear failure of the center column-bents. Meng and Lui [2000] concluded that inadequate shear strength, coupled with insufficient column cross-sectional sizes and transverse torsional reinforcement for the middle column-bents, were the main reasons for the column failures. Shear failures can occur at relatively low displacements of the bridge at the point where longitudinal reinforcement may not yet have yielded. On the other hand, because shear strength degrades with inelastic loading cycles, shear failures can also occur after flexural yielding.

Abutment unseating: An example of skewed bridge failure is the Gavin Canyon Undercrossing, which failed during the 1994 Northridge Earthquake [Earthquake Engineering Research Institute (EERI) 1995]. As shown in Figure 1.2, both skewed hinges became unseated during ground shaking and collapsed. In seat-type abutments, damage was also observed due to superstructures' pounding of the backwalls (see Figure 1.3). Similarly, the FBU rotated in its horizontal plane during the 1971 San Fernando Earthquake [Jennings et al. 1971]. This rotation caused a permanent offset of approximately 7.5 cm (i.e.,  $0.9 \times 10^{-3}$  radians of deck rotation) in the direction of increasing skew angle (see Figure 1.4).

Shear key failure: The reconnaissance report of the 2010 Chile Earthquake [Kawashima et al. 2010; Yashinsky et al. 2010] states that the skewed bridges in

affected regions rotated, mainly about their center of stiffness, and that those with weak exterior shear keys suffered higher damage levels due to transverse unseating (see Figure 1.5).



**Figure 1.1** Failure of columns of the FBU (source: Chen and Duan [2000]).



**Figure 1.2** Gavin Canyon Undercrossing collapse in the 1994 Northridge Earthquake (source: Chen and Duan [2000]).



**Figure 1.3** Santa Clara River Bridge pounding damage to the abutment in 1994 Northridge Earthquake (source: Chen and Duan [2000]).



Figure 1.4 Abutment of the Northwestern bridge of the FBU (source: Jennings et al. [1971]).



Figure 1.5 Damage to a skewed bridge after the Chile Earthquake of February 27, 2010 (source: Yashinsky et al. [2010]).

## 1.2 A BRIEF REVIEW OF LITERATURE ON THE SEISMIC RESPONSE OF SKEWED BRIDGES

In recent years, much research has been conducted on the seismic response of regular bridges [Aviram et al. 2008; Bignell et al. 2005; Johnson et al. 2009; Kappos and Sextos 2001; Kotsoglou and Pantazopoulou 2010; Mackie and Stojadinovic 2007; Paraskeva et al. 2006] as well as skewed bridges [Abdel-Mohti and Pekcan 2008; Asheboa et al. 2007a; Asheboa et al. 2007b; Dimitrakopoulos 2011; Kalantari and Amjadian 2010; Lou and Zerva 2004; Maleki 2005; Meng and Lui 2002; Saadeghvaziria and Yazdani-Motlagh 2008]. The development of analytical/numerical models that can capture the peculiar collapse mechanisms of skewed bridges under seismic excitation and can accurately quantify their damages has been a subject of research for quite some time.

Ghobarah and Tso [1974] used a spine-line model to represent bridge deck and columns; they concluded that the bridge's collapse was caused by coupled flexural-torsional motions of the bridge deck or by excessive compression demands that resulted in column failures. Using simplified beam models, Maragakis and Jennings [1987] concluded that the angle of the abutment skew and the impact between the deck and abutment govern the response of skewed bridges. Wakefield et al. [1991] conjectured that if the deck is not rigidly connected to the abutments, the bridge's dynamic response will be dominated by the deck's planar rigid body rotations rather than coupled flexural and torsional deformations.

A more recent study by Meng and Lui [2000] proposed that a bridge's seismic response is strongly influenced by column boundary conditions and skew angle. In a subsequent study [Meng and Lui 2002], they used a dual-beam stick model to represent the bridge deck and showed that in-plane deck rotations are due mostly to abutment reactions. Using nonlinear static and dynamic analyses, Abdel-Mohti and Pekcan [2008] investigated the seismic performance of a three-span continuous RC box-girder bridge for abutment skew angles spanning between 0° and 60°. They used detailed finite element models, as well as simplified beam-stick models, and concluded that simplified beam-stick models can capture skewed bridge's coupled lateral-torsional responses for moderate skew angles.

An approximate method for dynamic analysis of skewed bridges with continuous rigid decks was proposed by Kalantari and Amjadian [2010]. They developed a three-degree-of-freedom model to determine the natural frequencies, mode shapes, and internal forces for short skewed bridges.

### 1.2.1 Skewed Bridge Rotation Mechanism

The primary issue that distinguishes the behavioral differences between skewed and non-skewed bridges is the former's tendency to rotate. As shown in Figure 1.6, when a deck collides with the abutment, a rotational moment of  $M_R$  is produced around the deck's center of stiffness [Watanabe and Kawashima 2004; Singh and Chakraverty 1994].

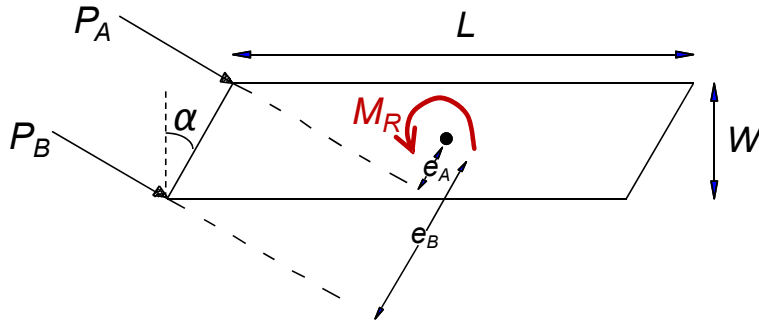


**Figure 1.6 Rotational moment due to abutment impact forces.**

If we assume that the moment direction shown in Figure 1.6 is the positive direction, then the rotational moment  $M_R$  can be shown in Equation (1.1).

$$M_R = P_A e_A + P_B e_B \quad (1.1)$$

where  $P_A$  and  $P_B$  are the impact abutment forces at obtuse and acute angles, respectively, perpendicular to the skewed abutment; and  $e_A$  and  $e_B$  represent the eccentricity of the impact forces from the mass center.

Considering the geometry of the shape illustrated in Figure 1.6, the eccentricity distances can be calculated as shown in Equations (1.2a), and (1.2b)

$$e_A = \frac{(L \times \sin \alpha - \frac{W}{\cos \alpha})}{2} \quad (1.2a)$$

$$e_B = \frac{(L \times \sin \alpha + \frac{W}{\cos \alpha})}{2} \quad (1.2b)$$

where  $\alpha$  is the abutment skew angle, and  $L$  and  $W$  are the superstructure's length and width in the longitudinal and transverse directions. Using Equations (1.1) and (1.2), one can derive the imposed rotational moment by the abutment impact, which depends on the abutment's skew angle and the deck's geometry.

The abutment skew angle's effect on two eccentricity parameters,  $e_A$  and  $e_B$ , is illustrated in Figure 1.7 for different aspect ratios (bridge length to deck width ratio  $[L/W]$ ). It is shown that for a  $0^\circ$  abutment skew angle, the curves representing eccentricities  $e_A$  and  $e_B$  have values of  $-0.5$  and  $0.5$ , respectively. The rate of increase in eccentricity increases as the bridge becomes narrower (i.e., larger  $L/W$ ). As shown in Figure 1.7, the eccentricity  $e_A$  has a negative value for a low abutment skew angle. At a certain value of the skew angle  $\alpha$ , the term of  $P_A e_A$  in Equation (1.1) becomes positive, and can increase the rotational moment  $M_R$ . This skew angle can be derived by equating the eccentricity of  $e_A$  to zero in Equation (1.2a), which yields Equation (1.3)

$$\sin 2\alpha_{cr} = \frac{2W}{L} \quad (1.3)$$

where  $\alpha_{cr}$  is termed “critical abutment skew angle” for skewed bridges. This angle depends on the bridge’s length ( $L$ ) and the superstructure’s width ( $W$ ). The abutment skew angle derived from Equation (1.3) is the angle at which a skewed bridge is geometrically vulnerable to deck rotation.

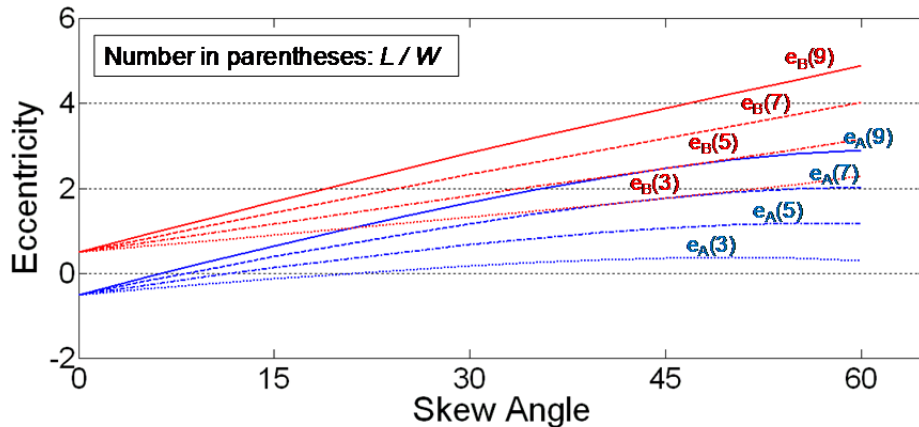


Figure 1.7 Effect of skew angle on eccentricity parameters.

To evaluate the deck rotation that is caused by the abutment skew angle, it is assumed that forces PA and PB in Equation (1.3) are constant and can be factorized from the equation. The deck rotation index, which represents the bridge’s tendency to rotate around the deck’s vertical axis, is introduced in Equation (1.4).

$$DRI = e_A + e_B \tag{1.4}$$

Figure 1.8 illustrates that in a high abutment skew angle, a large magnification of deck rotation is possible.

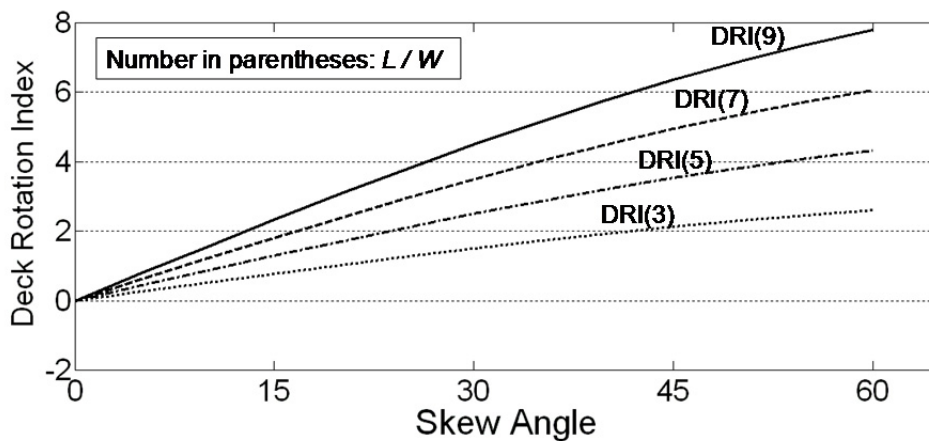


Figure 1.8 Effect of skew angle on deck rotation index (DRI).

Recent studies (e.g., Dimitrakopoulos [2011] and Dimitrakopoulos et al. [2009; 2010]) have revisited the seismic response of short skewed bridges with deck-abutment pounding joints. Dimitrakopoulos [2011] proposed a non-smooth rigid body approach to analyze the seismic response of pounding skewed bridges. They showed that the skewed bridges' tendency to rotate after deck-abutment impact is a factor of not only the skew angle ( $\alpha$ ) and geometry ( $L/W$ ), but also the coefficient of friction ( $\mu$ ). Two dimensionless skew ratios for frictionless ( $\eta_0$ ) and frictional ( $\eta_1$ ) contact, respectively, were introduced as shown in Equation (1.5):

$$\eta_0 = \frac{\sin 2\alpha}{2(W/L)} \quad (1.5a)$$

$$\eta_1 = \eta_0 \left( 1 + \frac{\mu}{\tan \alpha} \right) \quad (1.5b)$$

The parameters in Equation (1.5), such as abutment skew angle ( $\alpha$ ) and the geometry in plan ( $L/W$ ), enable the sign of two dimensionless skew ratios ( $\eta_0$  and  $\eta_1$ ) to be defined, which can specify the rotational moment  $M_R$  (Figure 1.6).



## **2 Matrix of Representative Bridge Models**

### **2.1 INTRODUCTION**

In this chapter, the matrix of representative bridge models used in the subsequent numerical studies is described. The objective is to develop a comprehensive database of bridge models with parameters that cover an adequately wide range of possible variations encountered in the field. In what follows, we first present some statistical information about the highway bridges in California and then discuss the geometrical and structural characteristics of three bridges selected for this study, which we refer to as the *seed bridges*. Finally, we discuss the development of the model matrix generated from these seed bridges.

### **2.2 CHARACTERISTICS OF CALIFORNIA'S BRIDGES**

There are nearly 610,000 public road bridges in the U.S., as discussed in the National Bridge Inventory (NBI) [Federal Highway Administration (FHWA) 2010]. Approximately 25,000 (4%) of these bridges are located in California. This section discusses some of the relevant statistical data about the characteristics of bridges in California, as derived from the NBI database, which is usually updated annually. The information presented here is based on the 2010 records.

#### **2.2.1 Bridges by the Skew Angle of Their Abutments**

The FHWA defines the skew angle in bridges as “the angle between the centerline of a pier and a line normal to the roadway centerline” [FHWA1995]. As shown in Figure 2.1, 60% of bridges located in California are skewed bridges. Skew angles are grouped using 15° increments from 1° to 60° of skew angle, and the last range includes skew angles greater than 60°. The lower ranges of skewed bridges, from 1° to 30°, represent a higher percentage of the skewed bridges in California. This study follows the same grouping approach, excluding skew angles larger than 60°.

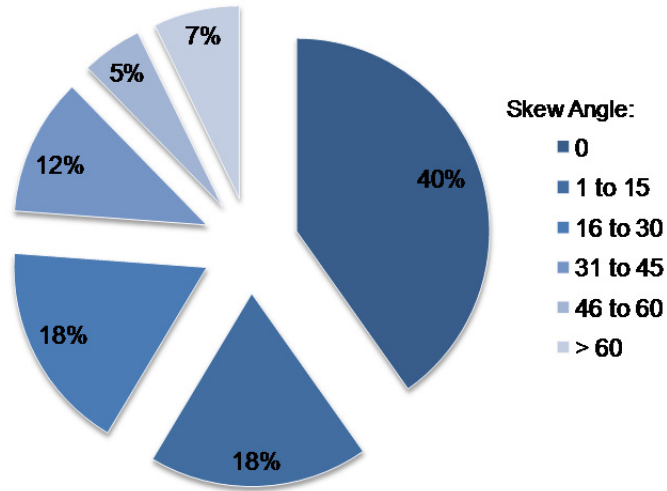


Figure 2.1 Distribution of bridges in California based on the abutment skew angle.

### 2.2.2 Bridges by the Number of Their Spans

We define bridges with single and double spans—the primary subject of this research effort—as *short bridges*, which are typically highway overcrossings. Bridges with three to five spans are considered as *intermediate bridges*, and those with a larger number of spans are defined as *long bridges*. The pie chart in Figure 2.2 shows that more than half of the bridges in California are short bridges and fewer than 10% of bridges are long bridges.

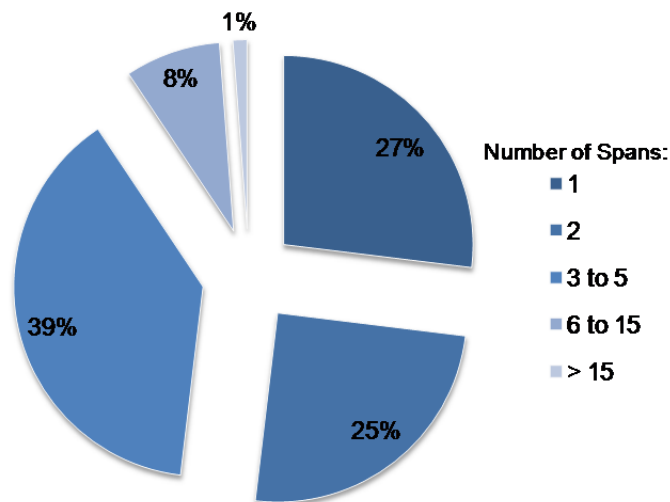


Figure 2.2 Distribution of bridges in California based on the number of spans.

### 2.2.3 Bridges Classified by the Year They Were Built

Bridge design philosophies in California continue to evolve rapidly (as also discussed briefly in Section 2.6); the primary stimuli have, arguably, always been major earthquakes (e.g., the 1971 San Fernando and the 1999 Loma Prieta). Figure 2.3 indicates that more than 50% of existing bridges in California were built between 1940 and 1971—i.e., before the significant modifications to bridge design philosophies that followed the San Fernando Earthquake. However, the focus of this study is confined to the most recent types of designs. Thus, we only examine bridges designed after 2000, which comprise 5% of the bridge stock in California (Figure 2.3).

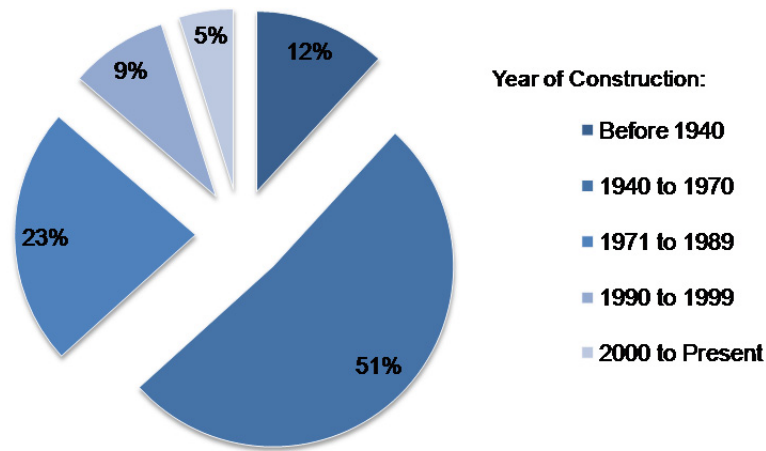
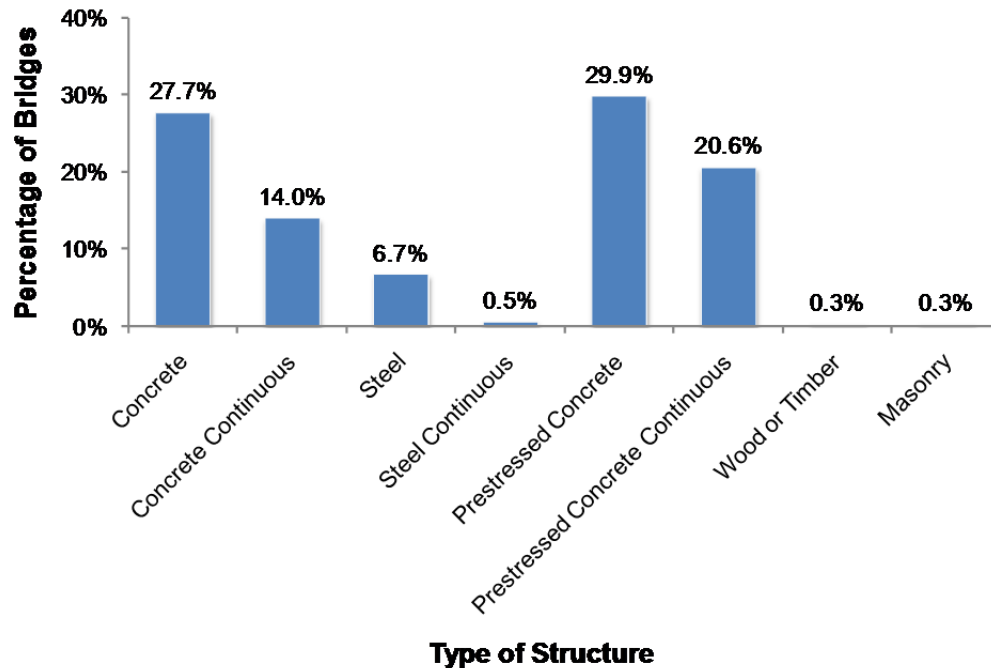


Figure 2.3 Distribution of bridges in California based on the year of construction.

### 2.2.4 Bridges Classified by the Type of Structural System

The FHWA uses a three-digit code to indicate the type of structure for the main span of a bridge [FHWA1995]. The first digit indicates the type of material and/or design, and the second and third digits indicate the predominant type of design and/or construction (see Appendix A for details about this code). In Figure 2.4, which displays the distribution of materials used to construct bridges in California built after year 2000, it can be seen that more than half of existing bridges are made of prestressed concrete.



**Figure 2.4** Distribution of bridges in California based on type of structure.

### 2.3 BRIDGES SELECTED FOR THIS STUDY

We selected three recently designed (constructed after year 2000) bridges, which bear the typical characteristics of modern short bridges in California. These are labeled as seed bridges, as other bridges in the subsequently developed model matrix were spawned from them through basic geometrical parameter variations.

The main considerations used for selecting the seed bridges were the numbers of their spans and columns per bent. The selection was biased towards bridges with fewer spans and supporting columns, as presumably they have less rotational stiffness—a characteristic that is especially pertinent for the present study, because skew bridges are prone to rotating in the plane of their decks. Given this, we considered two- and three-span bridges, and because a bridge’s overall torsional resistance relies largely on the number of columns per bent, the study considered both single-column and multi-column bents.

The first seed bridge we selected is the Jack Tone Road Overcrossing (Bridge A), which has two spans supported on a single column. The second bridge is the La Veta Avenue Overcrossing (Bridge B), with two spans supported on a two-column bent. As such, it has a larger global torsional stiffness than Bridge A. The third bridge is the Jack Tone Road Overhead (Bridge C), with three spans and two three-column bents. Table 2.1 displays the seed bridges’ characteristics as extracted from the NBI database [FHWA 2010]. The following sections discuss the major geometrical and structural aspects of the selected bridges.

**Table 2.1 Selected characteristics of the seed bridges from the NBI database\*.**

<b>NBI Data Item</b>	<b>Bridge A</b>	<b>Bridge B</b>	<b>Bridge C</b>
Structure number	29 0320	55 0938	29 0318
Features intersected	STATE ROUTE 99	ROUTE 55	UPRR, SB99 ONRP, KAMPS WY
Facility carried by structure	Jack Tone Road	La Veta Avenue OC	Jack Tone Road
Location	10-SJ-099-2.34-RIP	12-ORA-055-13.2-TUS	10-SJ-099-2.32-RIP
Toll	3 (toll-free)	3 (toll free)	3 (toll free)
Functional classification of inventory route	6 (minor arterial)	17 (collector)	6 (minor arterial)
Year built	2001	2001	2001
Lane on/under structure	107 (1 lane on, 7 lanes under)	414 (4 lanes on, 14 lanes under)	403 (4 lanes on, 3 lanes under)
Design load(the live load for which the structure was designed)	6 [MS 18+MOD (metric), HS 20+MOD (English)]	6 [MS 18+MOD (metric), HS 20+MOD (English)]	6 [MS 18+MOD (metric), HS 20+MOD (English)]
Approach roadway width (the normal width)	551 ft (168 m)	636.5 ft (194 m)	590 ft (180 m)
Skew(the angle between the centerline of a pier and a line normal to the roadway centerline)	33°	0°	36°
Structure flare (variation in the width of the structure)	0 (no flare)	0 (no flare)	0 (no flare)
Type of service	11 (highway on bridge, highway w/wo pedestrian under bridge)	51 (highway-pedestrian on bridge, highway w/wo pedestrian under bridge)	18 (highway on bridge, highway-waterway-railroad under bridge)
Structure type, main	606 (Appendix-I)	605 (Appendix-I)	606 (Appendix-I)
Number of span in main unit	2	2	3
Deck (overall condition rating of the deck)	7 (good condition, some minor problems)	6 (satisfactory condition, structural elements show some minor deterioration)	7 (good condition, some minor problems)
Superstructure (physical condition of all structural members)	8 (very good condition, no problem noted)	8 (very good condition, no problem noted)	8 (very good condition, no problem noted)]
Substructure (physical condition of piers, abutments, piles, fenders, footings or other components)	7 (good condition, some minor problems)	7 (good condition, some minor problems)	7 (good condition, some minor problems)
Inspection date (last routine inspection date)	309 (March 2009)	408 (April 2008)	309 (March 2009)
Deck structure type	1 (concrete cast-inplace)	1 (concrete cast-inplace)	1 (concrete cast-inplace)

Structure flare (variation in the width of the structure)	0 (no flare)	0 (no flare)	0 (no flare)
Type of service	11 (highway on bridge, highway w/wo pedestrian underbridge)	51 (Highway-pedestrian on bridge, highway w/wo pedestrian underbridge)	18 (Highway on bridge, highway-waterway-railroad underbridge)
Structure type, main	606 (Appendix-I)	605 (Appendix-I)	606 (Appendix-I)
Number of spans in main unit	2	2	3
Deck (overall condition rating of the deck)	7 (good condition, some minor problems)	6 (satisfactory condition, structural elements show some minor deterioration)	7 (good condition, some minor problems)
Superstructure (physical condition of all structural members)	8 (very good condition, no problem noted)	8 (very good condition, no problem noted)	8 (very good condition, no problem noted)
Substructure (physical condition of piers, abutments, piles, fenders, footings or other components)	7 (good condition, some minor problems)	7 (good condition, some minor problems)	7 (good condition, some minor problems)
Inspection date (last routine inspection date)	309 (March 2009)	408 (April 2008)	309 (March 2009)
Deck structure type	1 (concrete cast-in-place)	1 (concrete cast-in-place)	1 (concrete cast-in-place)

\*The definitions of some of the items are provided in the brackets [FHWA1995].

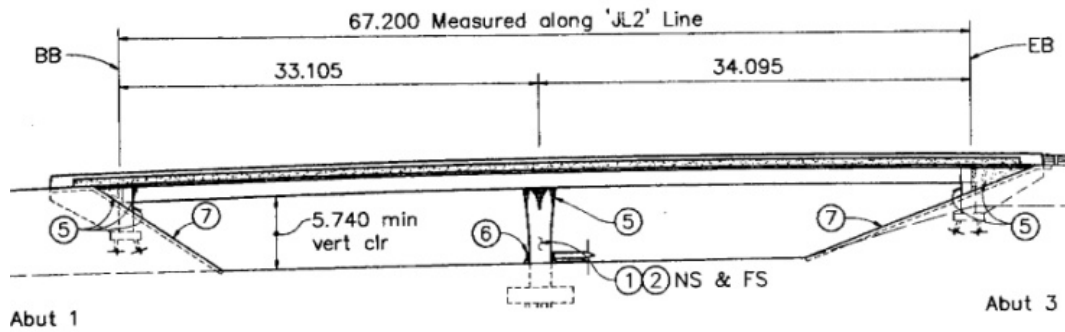
### 2.3.1 Bridge A

Bridge A, the Jack Tone Road On-Ramp Overcrossing (Figure 2.5), is located in the city of Ripon, California, at the intersection of Route 99 and Jack Tone Road (identification number 10-SJ-099-2.34-RIP) and was built in year 2001. The bridge has two spans, with a total length of 220.4 ft (67.2 m), and spans of 108.58 ft (33.105 m) and 111.82 ft (34.095 m), respectively. The bridge abutment has an approximately 33° skew angle, and crosses one lane of traffic on a seven-lane highway (Table 2.2).

The superstructure of Bridge A is a three-cell continuous prestressed, reinforced-concrete box girder. The bent has a half cap-beam integral with deck and a single reinforced-concrete circular column in the middle. The column of the bent is 5.51 ft (1.68 m) in diameter and is supported on 25 HP 305×79 steel piles. The column's longitudinal reinforcement ratio is approximately 2%. The abutments are seat-type, with four elastomeric bearing pads per abutment. A detailed description of Bridge A is provided in Table 2.2.



(a)



(b)

**Figure 2.5** The Jack Tone Road on-ramp overcrossing (Bridge A) shown in (a) a photograph (source: Google Maps) and (b) elevation (source: California Department of Transportation structural drawings).

**Table 2.2 Bridge A structural and geometric description.**

Parameters	Value/ Description
General bridge description	Ordinary standard single-column-per-bent bridge with 2 spans
Total length of bridge ( $L_{Total}$ )	220.4 ft (67.2 m)
Abutment skew angle ( $\alpha$ )	33°
Number of spans and length of each deck span	2 spans: 108.58 ft (33.105 m) and 111.82 ft (34.095 m)
Total deck width ( $W_{deck}$ )	27.13 ft (8.27 m)
Deck depth ( $d_d$ )	4.64 ft (1.415 m)
Deck cross-sectional geometry	$A= 97.546 \text{ ft}^2$ (9.067 m <sup>2</sup> ); $J= 341.442 \text{ ft}^4$ (2.954 m <sup>4</sup> ); $I_x= 180.328 \text{ ft}^4$ (1.558 m <sup>4</sup> ); $I_y= 3797.9 \text{ ft}^4$ (32.81 m <sup>4</sup> ); $A_{vx}= 18.92 \text{ ft}^2$ (1.759 m <sup>2</sup> ); $A_{vy}= 27.584 \text{ ft}^2$ (2.564 m <sup>2</sup> ); $S_x= 83.35 \text{ ft}^3$ (2.362 m <sup>3</sup> ); $Z_x= 115.143 \text{ ft}^3$ (3.263 m <sup>3</sup> ); $S_y= 279.97 \text{ ft}^3$ (7.934 m <sup>3</sup> ); $Z_y= 521.832 \text{ ft}^3$ (14.788 m <sup>3</sup> )
Number and clear height of each column bent ( $H_{col}$ )	1 column: 19.68 ft (6 m)
Column diameter ( $D_c$ )	5.51 ft (1.68 m)
Deck centroid ( $D_{c.g.}$ )	2.48 ft (0.756 m)
Length of cap beam to centroid of column bent ( $L_{cap}$ )	No cap beam
Cap beam dimension ( $B_{cap} \times d_d$ )	No cap beam
Location and size of expansion joints	No expansion joints specified
Support details for boundary conditions	Fixed foundations
Concrete material properties for concrete of superstructure ( $f'_c, E_c$ )	Elastic deck: $f'_c= 5 \text{ ksi}$ (34.5 MPa); $E_c=4030.5 \text{ ksi}$ (27,800 MPa)
Concrete and reinforcing material properties of column bents	Concrete: $f'_c= 5 \text{ ksi}$ (34.5 MPa); Steel: ASTM A706.
Reinforcement details of column bent cross section	Longitudinal reinforcement: 44#11 (bundles of 2), $\rho_l=2\%$ Transverse reinforcement: Spiral, #6 @3.34 in. (85 mm)
Abutment general geometry	Simplified abutment model
Number and properties of abutment bearing pads	4 elastomeric bearing pads used per abutment

### 2.3.2 Bridge B

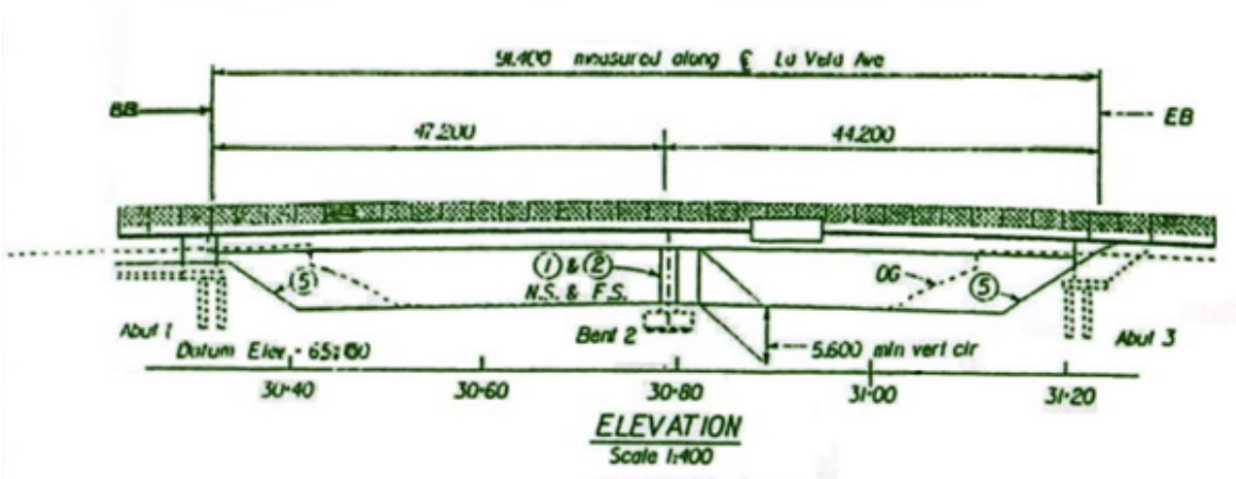
Bridge B, the La Veta Avenue Overcrossing (Figure 2.6), is located in the city of Tustin, California, at the intersection of Route 55 and La Veta Avenue (identification number 12-ORA-055-13.2-TUS) and was built in year 2001. This bridge has two spans, with a total length of 299.8 ft (91.4 m), individual spans of 154.82 ft (47.2 m) and 144.98 ft (44.2 m), and no skew (Table 2.3).

The superstructure of Bridge B is a six-cell, continuous, reinforced-concrete box girder with two lanes of traffic in each direction. The bent has a cap-beam integral with the bridge deck

and two reinforced-concrete circular columns. The columns of the bent are 5.58 ft (1.7 m) in diameter and are supported by 20-per-column 23.6 in. (600 mm) diameter CIDH (cast-in-drilled-hole) piles. The columns' longitudinal reinforcement ratio is approximately 1.9%. The abutments are seat-type, with seven elastomeric bearing pads per abutment. Further details about Bridge B can be found in Table 2.3.



(a)



(b)

Figure 2.6 The La Veta Overcrossing (Bridge B) shown in (a) a photograph (source: Google Maps) and (b) elevation (source: California Department of Transportation structural drawings).

**Table 2.3 Bridge B structural and geometric description.**

Parameters	Value/ Description
General bridge description	Ordinary standard multi-column bent bridge with 2 spans
Total length of bridge ( $L_{Total}$ )	299.8 ft (91.4 m)
Abutment skew angle ( $\alpha$ )	0°
Number of spans and length of each deck span	2 spans: 154.82 ft (47.2 m) and 144.98 ft (44.2 m)
Total deck width ( $W_{deck}$ )	75.5 ft (23 m)
Deck depth ( $d_d$ )	6.23 ft (1.9 m)
Deck cross-sectional geometry	$A=129.13 \text{ ft}^2$ (12.0 m <sup>2</sup> ); $J=2532 \text{ ft}^4$ (21.88 m <sup>4</sup> ); $I_x=791.76 \text{ ft}^4$ (6.84 m <sup>4</sup> ); $I_y=58352 \text{ ft}^4$ (504.2 m <sup>4</sup> ); $A_{vx}=33.18 \text{ ft}^2$ (3.08 m <sup>2</sup> ); $A_{vy}=78.66 \text{ ft}^2$ (7.31 m <sup>2</sup> ); $S_x=254.18 \text{ ft}^3$ (7.2 m <sup>3</sup> ); $Z_x=367.62 \text{ ft}^3$ (10.418 m <sup>3</sup> ); $S_y=1432.8 \text{ ft}^3$ (40.6 m <sup>3</sup> ); $Z_y=2119.36 \text{ ft}^3$ (60.06 m <sup>3</sup> )
Number and clear height of each column bent ( $H_{col}$ )	2 columns: 22 ft (6.7 m)
Column diameter ( $D_c$ )	5.58 ft (1.7 m)
Deck centroid ( $D_{c.g.}$ )	3.41 ft (1.04 m)
Length of cap beam to centroid of column bent ( $L_{cap}$ )	18.04 ft (5.5 m)
Cap beam dimension ( $B_{cap} \times d_d$ )	7.55 ft $\times$ 6.23 ft (2.3 m $\times$ 1.9 m)
Location and size of expansion joints	No expansion joints specified
Support details for boundary conditions	Pinned foundations
Concrete material properties for concrete of superstructure ( $f'_c, E_c$ )	Elastic deck: $f'_c=5 \text{ ksi}$ (34.5 MPa); $E_c=4030.5 \text{ ksi}$ (27,800 MPa)
Concrete and reinforcing material properties of column bents	Concrete: 5 ksi (34.5 MPa); Steel: ASTM A706.
Reinforcement details of column bent cross section	Longitudinal reinforcement: 44#11 (bundles of 2), $\rho_1=1.95\%$ ; Transverse reinforcement: Spiral, #4 @ 6 in. (152 mm)
Abutment general geometry	Simplified abutment model
Number and properties of abutment bearing pads	7 elastomeric bearing pads used per abutment

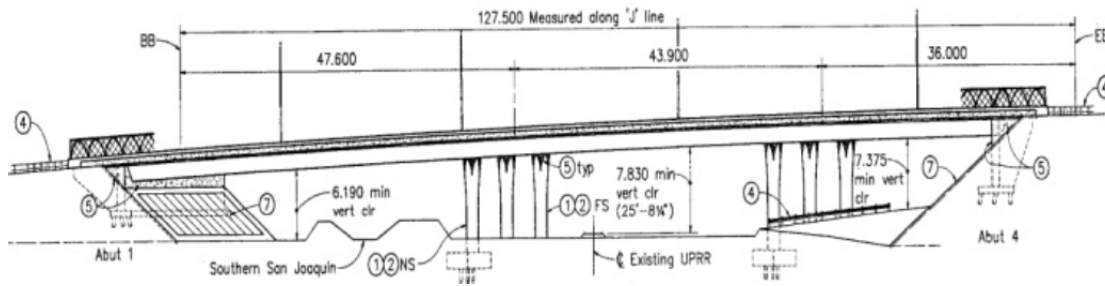
### 2.3.3 Bridge C

Bridge C, the Jack Tone Road Overhead (Figure 2.7), is located in the city of Ripon, California, where the Jack Tone Road intersects the UPRR track and the Southern San Joaquin Irrigation District canal (identification number 10-SJ-099-2.32-RIP) and was built in year 2001. It is a three-span bridge with a total length of 418.2 ft (127.5 m), and individual spans of 156.12 ft (47.6 m), 144 ft (43.9 m), and 118.08 ft (36.0 m). It is skewed at its abutments by approximately 36° (Table 2.4).

The superstructure is a seven-cell continuous reinforced-concrete box girder, which passes over four lanes of traffic. Intermediate bents have a cap-beam integral with the bridge deck and three reinforced concrete circular columns. The columns of the bent are 5.51 ft (1.68 m) in diameter, and are supported on 24 HP 305×79 steel piles per column bent. The columns' longitudinal reinforcement ratio is approximately 2.2%. The abutments are cantilever-seat-type, with nine elastomeric bearing pads per abutment. Further details are provided in Table 2.4.



(a)



(b)

**Figure 2.7** The Jack Tone Road Overhead (Bridge C) shown in (a) a photograph (source: Google Maps) and (b) elevation (source: California Department of Transportation structural drawings).

**Table 2.4 Bridge C structural and geometric description.**

Parameters	Value/ Description
General bridge description	Ordinary standard three columns per bent bridge with 3 spans
Total length of bridge ( $L_{Total}$ )	418.2 ft (127.5 m)
Abutment skew angle ( $\alpha$ )	36°
Number of spans and length of each deck span	3 spans: 156.12 ft (47.6 m) + 144 ft (43.9 m) + 118.08 ft (36.0 m)
Total deck width ( $W_{deck}$ )	77 ft (23.47 m)
Deck depth ( $d_d$ )	6.3 ft (1.92 m)
Deck cross-sectional geometry	$A=424.12 \text{ ft}^2$ (39.422 m <sup>2</sup> ); $J=2622.6 \text{ ft}^4$ (22.659 m <sup>4</sup> ); $I_x=1432.4 \text{ ft}^4$ (12.298 m <sup>4</sup> ); $I_y=161859 \text{ ft}^4$ (1398.43 m <sup>4</sup> ); $A_{vx}=55.88 \text{ ft}^2$ (5.194 m <sup>2</sup> ); $A_{vy}=88.96 \text{ ft}^2$ (8.269 m <sup>2</sup> ); $S_x=465.1 \text{ ft}^3$ (13.179 m <sup>3</sup> ); $Z_x=673.57 \text{ ft}^3$ (19.088 m <sup>3</sup> ); $S_y=4205.2 \text{ ft}^3$ (119.17 m <sup>3</sup> ); $Z_y=7159.8 \text{ ft}^3$ (202.9m <sup>3</sup> )
Number and clear height of each column bent ( $H_{col}$ )	3 columns: 24.6 ft (7.5 m)
Column diameter ( $D_c$ )	5.51 ft (1.68 m)
Deck centroid ( $D_{c.g.}$ )	3.23 ft (0.987 m)
Length of cap beam to centroid of column bent ( $L_{cap}$ )	Bent 2: 31.44 ft (9.585 m) + 31.67 ft (9.655 m); Bent 3: 33.538 ft (10.225 m) + 33.9 ft (10.335 m)
Cap beam dimension $B_{cap} \times d_d$	7.48 ft $\times$ 6.3 ft (2.28 m $\times$ 1.92 m)
Location and size of expansion joints	No expansion joints specified
Support details for boundary conditions	Pinned foundations
Concrete material properties for concrete of superstructure ( $f'_c, E_c$ )	Elastic deck: $f'_c=5 \text{ ksi}$ (34.5 MPa); $E_c=4030.5 \text{ ksi}$ (27,800 MPa)
Concrete and reinforcing material properties of column bents	Concrete: 5 ksi (34.5 MPa); Steel: ASTM A706.
Reinforcement details of column bent cross section	Longitudinal reinforcement: 34#14 (bundles of 2), $\rho_1=2.2\%$ Transverse reinforcement: Spiral, #6 @ 3.34 in. (85 mm)
Abutment general geometry	Simplified abutment model
Number and properties of abutment bearing pads	9 elastomeric bearing pads used per abutment

## 2.4 GROUND MOTION SELECTION

We employed three ground motion sets from the PEER (Pacific Earthquake Engineering Research) *Transportation Research Program Ground Motion Database* [Jayaram et al. 2010]. All ground motions were originally selected from the larger metadata PEER NGA (Next Generation Attenuation) Project ground motion library [Campbell and Bozorgnia 2008; Chiou et al. 2008].

In general, ground motion selection and scaling methods target a specific hazard level, and require information about the structure's location and some structural characteristics, such as fundamental period. However, the PEER Transportation Research Program ground motion selection project considered a wide variety of structural and geotechnical systems at a wide range of locations—an approach that did not result in ground motion sets for a target bridge and hazard level. Such an approach for ground motion selection and scaling provided a strong basis for the present research, as bridges in the model matrix had different structural characteristics, and the results of this research needed to be applicable to locations other than those of the seed bridges. Bridge response parameters were obtained using nonlinear response history analysis of each bridge model subjected to the ground motion sets from the PEER Transportation Research Program. We employed a novel regression analysis methodology to manage the relationship between ground motion hazard and bridge response [Kaviani 2011; Kaviani et al. 2012]. The following discussion briefly explains the methodology used for ground motion selection and scaling [Baker et al. 2011] first, and then presents the specific characteristics of each ground motion set.

In general, a ground motion selection and scaling methodology defines a suite of ground motions whose response spectra have specified mean and variance values. This approach selects structure-specific ground motions that have a specified spectral acceleration at the structure's fundamental periods. Baker et al. [2011] studied the response of Single Degree of Freedom (SDOF) and Multi Degree of Freedom (MDOF) structures across several ground motion scenarios and showed that considering response spectrum variance in the ground motion selection process did not significantly affect the median structural response, though it did tend to increase the response's mean and dispersion. The increased dispersion can result in more extreme responses, which can increase the probability of structural collapse.

A structure's average response is what often is referred to in loading codes [American Society of Civil Engineers (ASCE) 2005]. The average response is typically considered as mean response, but sometimes is considered as median response. If a structure's median response is considered as the target for assessing performance, then consideration of the response spectrum variance in the ground motion selection and scaling process does not significantly affect such an estimation. Nevertheless, if the structure's mean response is the target, then the consideration of response spectrum variance seems to increase the mean structural response.

The performance-based earthquake engineering (PBEE) approach often considers the full distribution of structural responses [ATC (Applied Technology Council) 2009]. Matching the target response spectrum variance increases the structural response dispersion, thereby affecting the structural response distribution. Consequently, the damage state and loss estimation calculation in the PBEE framework is negatively affected. Moreover, an increased dispersion in response can lead to a higher estimate of probability of collapse.

Based on the aforementioned research on ground motion selection and scaling [Baker et al. 2011], we used three sets of ground motions from the PEER Transportation Research Program ground motion database [Jayaram et al. 2010]. The first set of ground motions is characterized by strong velocity pulses with near-fault directivity effects (pulse-like). The other

two sets are “broadband” ground motions associated with earthquakes of moderately large magnitude (soil-site and rock-site). These ground motions were selected to match the target at periods between 0 and 5 sec, which are in the period range of the bridge structures considered in this study. Figure 2.8 displays the response spectra of both the strike-normal (SN) and the strike-parallel (SP) components of the three ground motion sets.

#### **2.4.1 Pulse-like Ground Motion Set**

This ground motion set includes 40 unscaled three-component ground motions; details are in Appendix B. Their SN components contain strong velocity pulses of varying periods. These velocity pulses are expected in ground motions from near-fault ruptures, due to directivity effects. Having a strong velocity pulse in the SN direction is considered in selecting this set of ground motions, as illustrated in Figure 2.9. Strong velocity pulses are also apparent in other orientations of this set of ground motions, but mainly are concentrated in the SN component.

Unlike the other two ground motion sets that will be described later; no matching to any target response spectrum has been applied for this set. This causes more dispersion in the characteristics of the selected ground motions, and accordingly more variations in the structural response.

A variety of pulse periods were chosen for the pulse-like ground motion set. It is known that the ratio of the pulse period to the periods of structure vibration is an important factor affecting structural response. The histogram of pulse periods in the pulse-like ground motion set is shown in Figure 2.10. Pulse periods range from 1.0 to 12.9 sec, with a mean of 5.5 sec. The high peak ground velocity (PGV) of pulse-like ground motions indicates that these ground motions are generally intense. The PGVs of the SN component range from 1 to 6 ft/sec (30 to 184 cm/sec), with a mean of 2.8 ft/sec (85 cm/sec). The PGVs of the SP component are somewhat smaller, ranging from 0.56 to 3.8 ft/sec (17 to 115 cm/sec), with a mean of 2 ft/sec (61 cm/sec), excepting the Chi-Chi TCU068 motion, which has a SP PGV of 8.2 ft/sec (250 cm/sec).

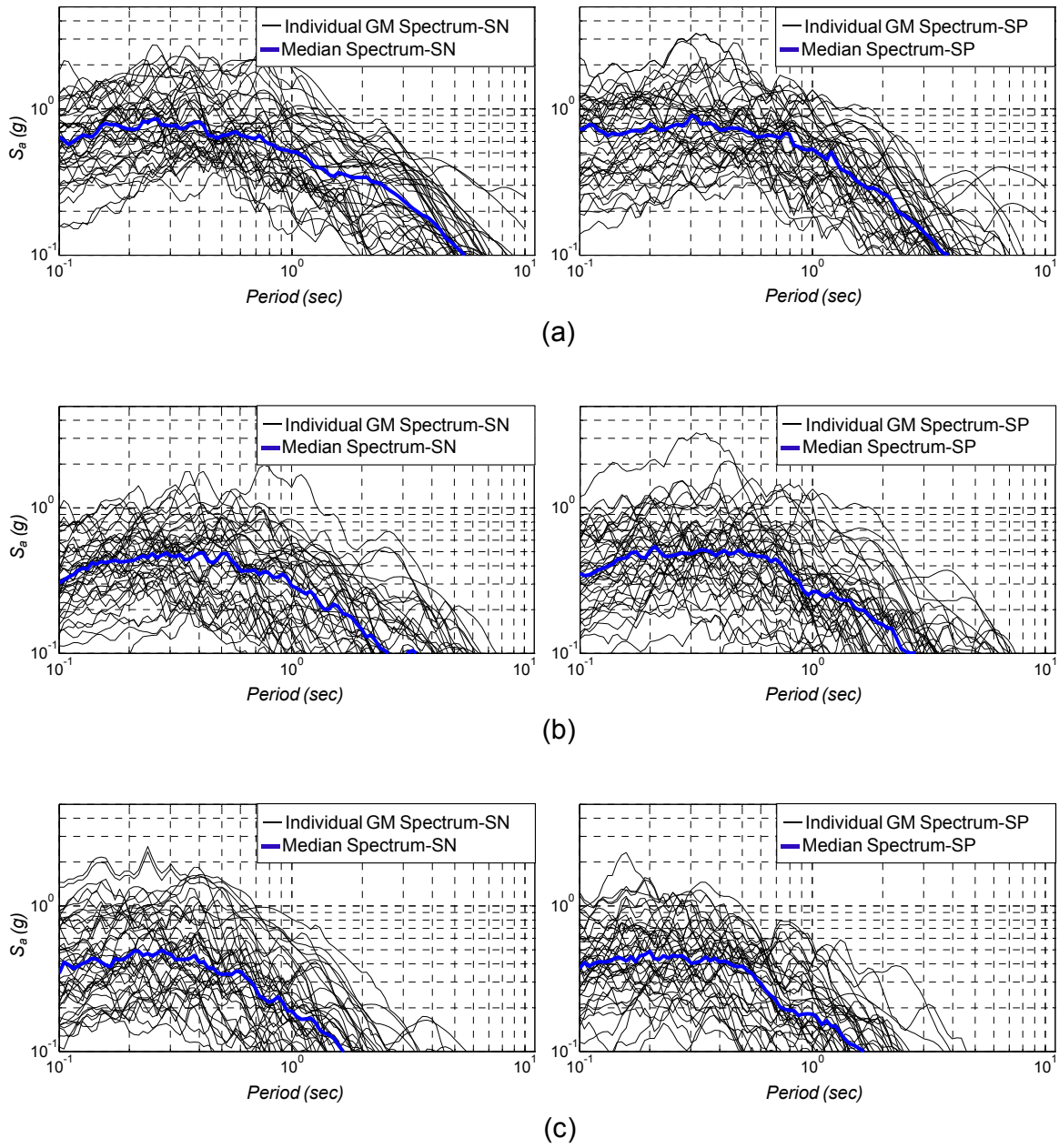


**Figure 2.8** Response spectra of strike-normal (SN) and strike-parallel (SP) components of (a) pulse-like, (b) soil-site, and (c) rock-site ground motion types.

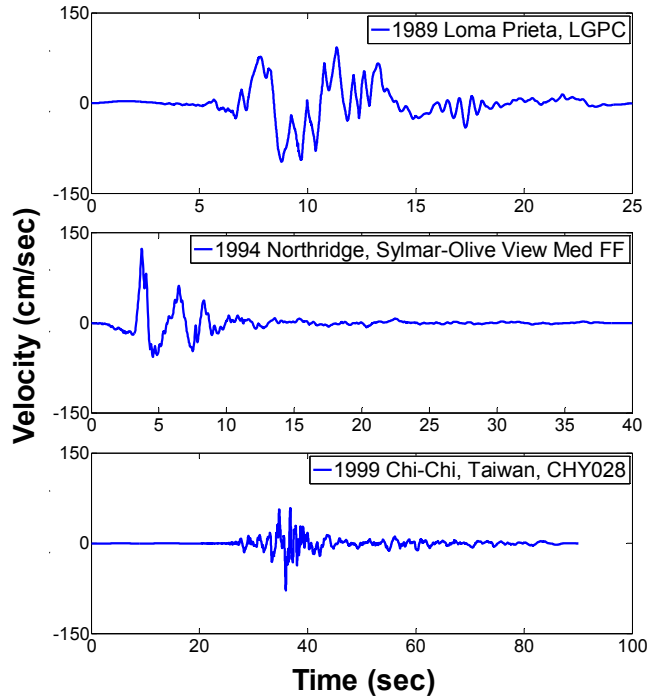


Figure 2.9 Ground velocity history of strike-normal (SN) component of three pulse-like ground motions.

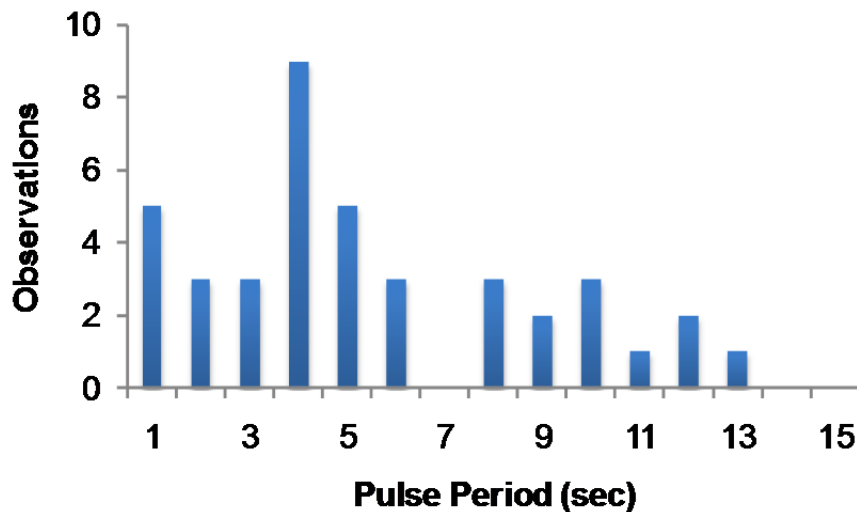


Figure 2.10 Histogram of pulse periods in pulse-like ground motion set.

### 2.4.2 Soil-Site Ground Motion Set

This ground motion set includes 40 unscaled three-component ground motions. These ground motions are selected based on matching their horizontal response spectra to the median and log standard deviations predicted from a magnitude-7 strike-slip earthquake at a distance of 6.2 miles (10 km). See Appendix B for a more detailed discussion. Since the selected ground motions in

this set are primarily specified to be used at soil sites, only ground motions with recorded  $V_{s30}$  (average shear wave velocity in the top 98.4 ft [30 m]) between 656 to 1,312 ft/sec (200 and 400 m/sec) were considered for these selections.

### 2.4.3 Rock-Site Ground Motion Set

This ground motion set includes 40 unscaled three-component ground motions. Similar to the soil-site ground motion set, the selected ground motion response spectra match the median and log standard deviations predicted for strike slip earthquakes with a magnitude of 7 at a distance of 6.2 miles (10 km). A site with  $V_{s30}$  of 2,493 ft/sec (760 m/sec) was assumed; this shear velocity is the only value that differs from the soil-site ground motion set. All ground motions in this set have  $V_{s30} > 2,034$  ft/sec (620 m/sec)—see Appendix B for further discussion. These ground motions are intended to be representative of bedrock-level ground motions.

## 2.5 SENSITIVITY PARAMETERS

While developing the bridge matrix used in this study, we had identified two groups of geometrical and ground motion characteristics that could affect seismic response of skewed bridges [Kaviani et al. 2010a, 2010b; Kaviani 2011]. In the bridge model matrix, variations in these characteristic parameters were considered to subsequently quantify—through numerical simulations—the sensitivities of various response measures. In the following subsections, we describe the selected sensitivity parameters and the rationale for choosing them.

### 2.5.1 Geometrical Characteristics

The geometrical characteristics that we varied in the bridge matrix are the skew angle, column-bent height, and span arrangement. The variations in the bridges' geometrical properties follow practical values. The definition and range of each parameter are as follows.

*Abutment skew angle:* The angle between an abutment's (or pier's) centerline and the line normal to the roadway centerline is defined as the abutment skew angle. As it was discussed before (Figure 2.1), the skew angles of most bridges in California vary between  $0^\circ$  and  $60^\circ$ . Given this, we considered the aforementioned variation range in  $15^\circ$  increments. The abutment skew angles studied here are, therefore,  $0^\circ$ ,  $15^\circ$ ,  $30^\circ$ ,  $45^\circ$ , and  $60^\circ$ .

*Column-bent height:* We consider two column height variations (original column height of  $Col_{orig}$  and extended column height of  $Col_{ext} = 1.5 \times Col_{orig}$ ). The lower level ( $Col_{orig}$ ) of column elevation refers to the original column-bent height. The higher-level column ( $Col_{ext}$ ) elevation is defined by a 50% extension of the original column-bent height. The higher level column elevation is less than eight times the column diameter ( $8 \times D_{col}$ ), a value that *reasonably* represents the maximum column height.

*Span arrangement:* We study two types span arrangement: symmetrical (i.e., equal span lengths) and asymmetrical (i.e., a ratio of span lengths equal to 1.2). In an asymmetric arrangement, the length of two adjacent spans varies by 20% (Table 2.5). To maintain the bridge's original properties, the variation of the span length is limited to 20%. Again, these selections were based on discussions with practicing engineers, and by consulting the NBI database [FHWA 2010].

## 2.5.2 Ground Motion Characteristics

This study considers two characteristics regarding the ground motions—*viz.*, the ground motion type and the ground motion incidence angle.

*Ground motion type:* We employ three sets of ground motions, as explained in Section 2.4 (soil-site, rock-site, and pulse-like). Each set of ground motions contained 40 pairs of ground motions, distinguished in two components: strike-normal (SN) and strike-parallel (SP). These ground motions are not selected to represent a specific hazard level, but rather, are selected to cover the variety of bridges at generic—albeit seismically vulnerable—sites (Figure 2.11). The method of selecting these ground motions was based on matching the target spectra at periods between 0 and 5 sec, which encompasses the period range of bridge structures used in this study.

*Incidence angle:* The ground motion incidence angle is the angle between ground motion strike-normal direction and the bridge's longitudinal direction (Figure 2.12). Because ground motions can strike a generic bridge structure at an arbitrary angle of incidence, we considered variations in this parameter. Specifically, we considered six incidence angles ( $0^\circ$ ,  $30^\circ$ ,  $60^\circ$ ,  $90^\circ$ ,  $120^\circ$ , and  $150^\circ$ ). In a  $0^\circ$ -incident event, the ground motion's strike-normal component is applied in the longitudinal direction, and consequently the strike-parallel component is applied in the transverse direction. In a  $90^\circ$ -incident event, the two ground motion components would be switched compared to the  $0^\circ$ -incident event.

**Table 2.5 Span arrangements of bridges.**

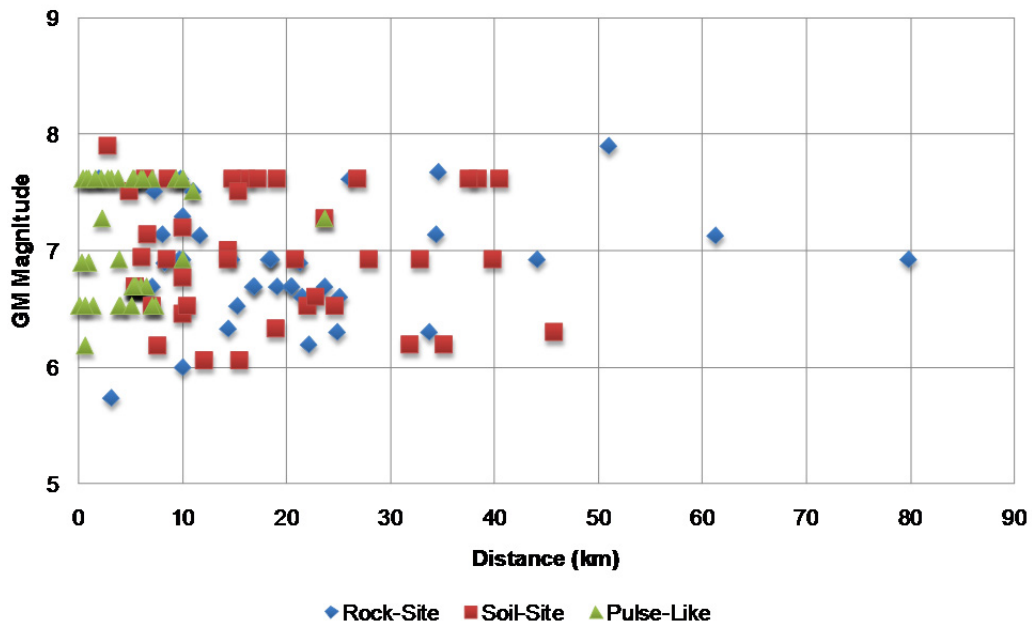
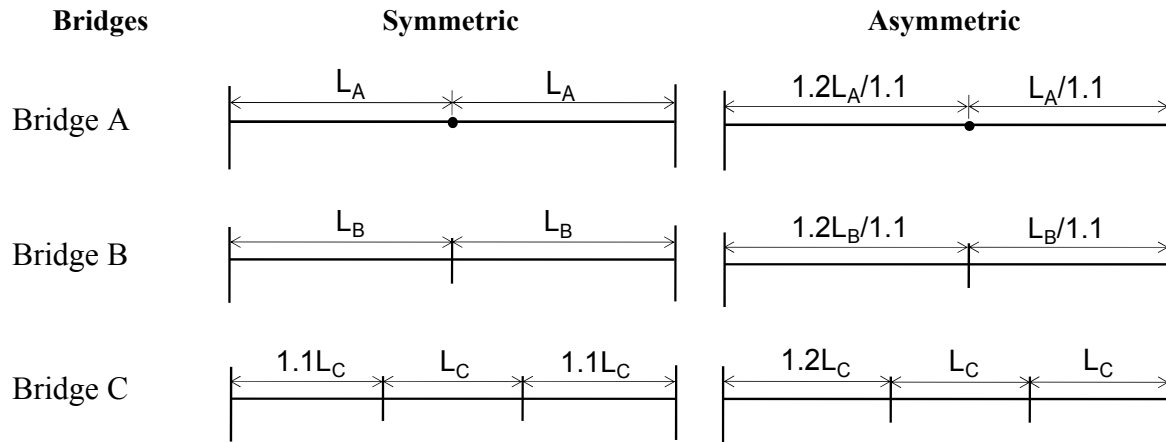


**Figure 2.11 Comparison of three different ground motion sets.**

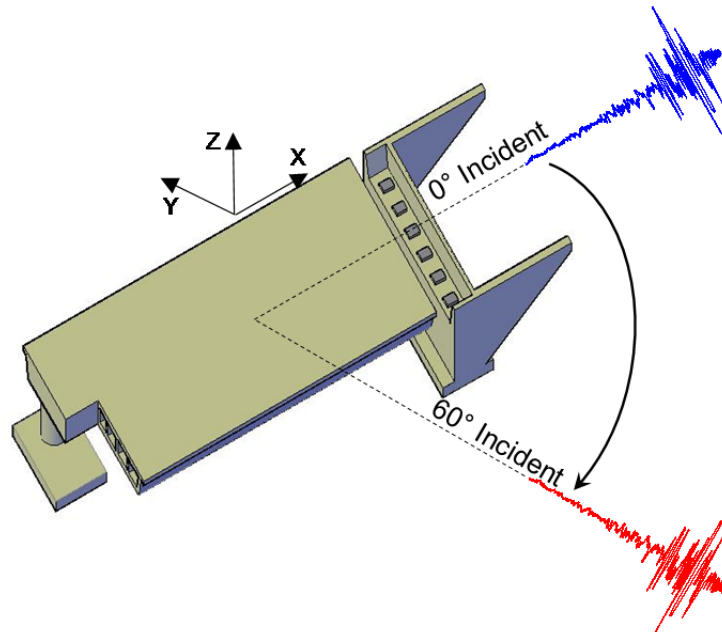


**Figure 2.12** Ground motion incidence angle scheme for the strike-normal component.

## 2.6 THE BRIDGE MODEL MATRIX

The bridge matrix used in this study is developed based on the rules discussed in the preceding sections and is summarized in Table 2.6. Figure 2.13 illustrates the scheme of the bridge matrix for one of the seed bridges (Bridge A) in a logic tree format. A shorthand notation is devised to identify the specific analytical bridge model. For example, the designation “AHS2R2” indicates a model for the seed Bridge A (denoted as A) with a higher-level column height (denoted as H), symmetrical span arrangement (denoted as S), and abutment skew of  $30^\circ$  (denoted as 2), and to which a rock type of ground motion (denoted as R) is applied with an incidence angle of  $60^\circ$  (denoted as 2). A similar figure to Figure 2.13 can be developed for the other seed bridges. The remainder of the text will employ this naming convention.

**Table 2.6 Geometric and ground motion characteristics used in the sensitivity study.**

Sensitivity Parameters		Variation Range
Geometric characteristics	Abutment skew angle (deg.)	0, 15, 30, 45, 60
	Span arrangement	Symmetrical (span ratio = 1.0)
		Asymmetrical (span ratio = 1.2)
Column height	$Col_{orig}$ = Original column size $Col_{ext}$ = $1.5 Col_{orig}$	
Ground motion characteristics	Ground motion type	Soil-site
		Rock-site
		Pulse-like
Angle of incidence (deg.)	0, 30, 60, 90, 120, 150	

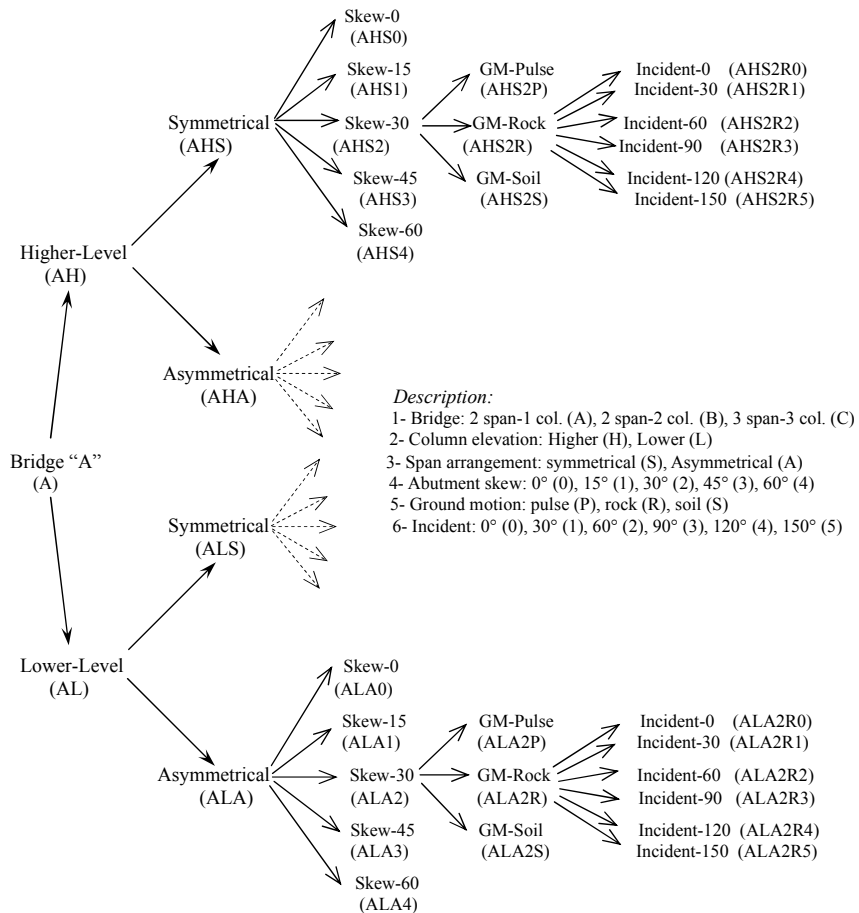


**Figure 2.13 Scheme of the bridge matrix assigned to Bridge A.**



## **3 Development of Bridge Models**

### **3.1 OVERVIEW**

In this chapter we describe the numerical models for bridges in the model matrix described in Chapter 2. These are prestressed concrete bridges with box-girder decks that are supported by column-bents and seat-type abutments. Our starting points in developing these models are the recommendations provided in the Caltrans Seismic Design Criteria (SDC) Version 1.6 [Caltrans 2010] and the research conducted by Aviram et al. [2008]. We also sought recommendations from a number of design engineers during this process to ensure that the salient features the bridges in consideration are adequately represented in the simulation models.

### **3.2 MODEL ATTRIBUTES**

The bridge models were created in two nonlinear finite element analytical programs, SAP2000 Nonlinear [Computers & Structures Inc. (CSI) 2005] and OpenSees [McKenna et al. 2000], for which the modeling procedures and analysis techniques are fairly similar. Nevertheless, our discussion here will focus only on OpenSees for brevity. When necessary, we will explain various notable differences between the models developed in OpenSees and SAP2000.

OpenSees (ver. 2.2.2) provides an adequate element and material library for earthquake engineering applications. The program enables scripted execution of repetitive nonlinear response history analyses through which the model parameters and input ground motions can be systematically varied. The OpenSees scripts of all parametric simulations implemented in this report are provided as attachments to this PEER report. The descriptions of the models are detailed in Appendix C, as well.

#### **3.2.1 Material Properties**

Material properties are assigned in accordance with Caltrans SDC [2010]. For the reinforced concrete column, the model by Mander et al. [1988] is used. Caltrans SDC [2010] recommends that both confined and unconfined concrete should be used for determining the local capacity of ductile concrete members (see Figure 3.1).

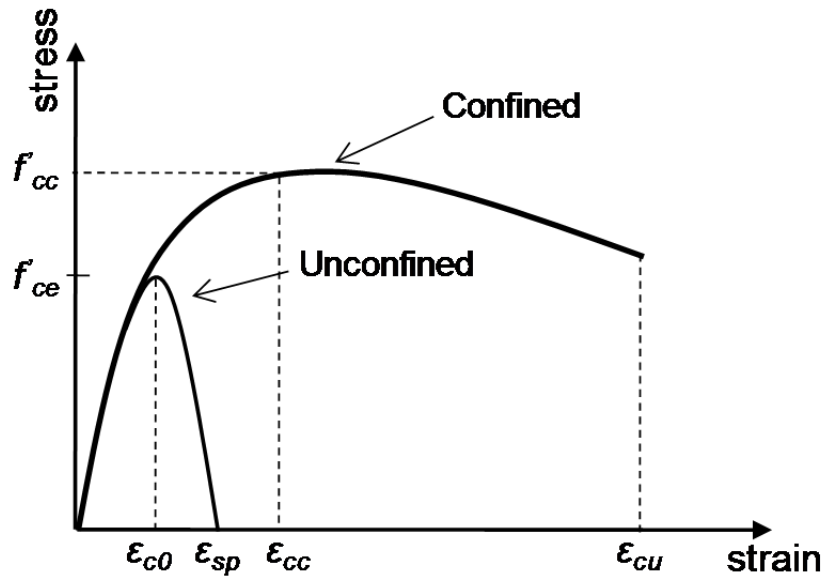


**Figure 3.1** Generic stress-strain curve for concrete.

We considered  $\epsilon_{c0} = 0.0028$ ,  $f'_{ce} = 5$  ksi (34.5 MPa), and  $\epsilon_{sp} = 0.005$  for unconfined concrete. For confined concrete, we employed  $f'_{cc} = 6.6$  ksi (45 MPa),  $\epsilon_{cc} = 0.008$ . For the ultimate compression strain—which is the point where strain energy equilibrium between the concrete and the confinement steel is reached—we used  $\epsilon_{cu} = 0.025$ . The concrete modulus of elasticity, as given by Caltrans SDC [2010], is shown in Equation (3.1)

$$E_c = 0.043 \times w^{1.5} \times \sqrt{f'_c} \text{ (MPa)}, E_c = 33 \times w^{1.5} \times \sqrt{f'_c} \text{ (psi)} \quad (3.1)$$

where  $w$  is the unit weight of concrete, with  $w = 143.96$  lb/ft<sup>3</sup> (2,286.05 kg/m<sup>3</sup>) and  $f'_c$  is the compressive strength of unconfined concrete, with  $f'_c = 5$  ksi (34.5 MPa).

The reinforcing steel used in the models is A706/A706M. From Caltrans SDC [2010], the steel modulus of elasticity and the expected yield strength were set as  $E_s = 29,000$  ksi (200,000 MPa) and  $f_{ye} = 68$  ksi (475 MPa), respectively.

### 3.2.2 Mass Assignment

The weight of normal concrete is specified by Caltrans SDC as  $w = 143.96$  lb/ft<sup>3</sup> (2,286.05 kg/m<sup>3</sup>), and therefore a mass of  $\rho_c = 4.471$  lb-sec<sup>2</sup>/ft<sup>4</sup> (233.03 kg-sec<sup>2</sup>/m<sup>4</sup>) is used when specifying material properties for concrete. SAP2000 automatically calculates the translational mass of all longitudinal elements in the three global directions of the bridge (longitudinal, transverse, and vertical) and assigns them as a lumped mass at each node, based on tributary lengths. However, in an OpenSees model, the mass should be defined by the user. In order to achieve an accurate distribution of mass along the length of the superstructure, a sufficient number of nodes and segments should be defined in the OpenSees model. After consultation

with Caltrans engineers, we divided each bridge span into ten segments. To achieve greater accuracy in the predicted dynamic responses and fundamental modes of the bridge—particularly for those modes associated with the torsional and transverse motions—the assignment of rotational mass (mass moment of inertia) is required for the superstructure and column-bents of a spine-line model of the bridge. The rotational moment of inertia of a segment of superstructure can be calculated by Equation (3.2)

$$M_{XX} = \frac{M d_w^2}{12} = \frac{(m/L) L_{trib} d_w^2}{12} \quad (3.2)$$

where  $M_{XX}$  is the rotational mass of the superstructure;  $M$  is the total mass of the superstructure segment, tributary to the node;  $m/L = \rho_c \times A_{deck}$  is mass of the superstructure per unit length;  $L_{trib}$  is the tributary length;  $d_w$  is the superstructure width.  $L$  is the length of the superstructure as shown in Equation (3.3)

$$M_{ZZ} = \frac{M R_{col}^2}{2} = \frac{(m/L) L_{trib} D_{col}^2}{8} \quad (3.3)$$

where  $M_{ZZ}$  is the rotational mass of the column;  $M$  is the total mass of the column segment, tributary to the node;  $m/L = \rho_c \times A_{col}$  is the mass of the column per unit length;  $L_{trib}$  is the tributary length;  $R_{col}$  and  $D_{col}$  are the radius and the diameter of the column; and  $L$  is the length of the superstructure.

### 3.2.3 Damping

We employed modal (Rayleigh) damping and considered 5% of critical damping in the first two modes of vibration [Aviram et al. 2008]. As shown in Equation (3.4), the damping matrix  $[D]$  is classical and is specified as a linear combination of the stiffness and mass matrices [Clough and Penzien 1994].

$$[D] = \alpha_0 [M] + \alpha_1 [K] \quad (3.4)$$

where  $[D]$  is the damping matrix,  $[M]$  the mass matrix,  $[K]$  the stiffness matrix, and  $\alpha_0$  and  $\alpha_1$  are the coefficients of proportionality, which can be calculated from Equation (3.5).

$$\zeta_n = \frac{\alpha_0}{2\omega_n} + \frac{\alpha_1 \omega_n}{2} \quad \text{for } n = 1, 2 \quad (3.5)$$

In Equation (3.5),  $\zeta_n$  and  $\omega_n$  are the damping coefficient and the frequency associated to the  $n^{\text{th}}$  mode of vibration, respectively.

## 3.3 COMPONENT MODELS

Various modeling assumptions are known to have significant effects on the predicted dynamic response characteristics of short bridges. Based on findings reported in open literature [Priestley et al. 1996; Aviram et al. 2008], we opted to use three-dimensional spine-line models for the

bridge superstructures, with line elements located at the centroids of the cross-sections following the bridge alignment. This type of model strikes a good balance between computational efficiency and accuracy. A representative bridge model that is used in the simulations is displayed in Figure 3.2, which—besides the spine-line discretization of the superstructure—comprises seat-type abutments, shear keys, expansion joints, column-bents, and the superstructure. The nonlinear behaviors of individual components are included, which include column plastic hinges as well as transverse and longitudinal springs and gap components for the abutments. Based on a reduced set of preliminary simulations, the superstructure and the cap-beam are considered as linear elastic components to alleviate some of the computational burden of the subsequent parametric studies. Similarly, the connection of the column bent to the pile cap is considered to be rigid for single-column bridges (i.e., Bridges A) and pinned for multi-column bridges (i.e., Bridges B and C).

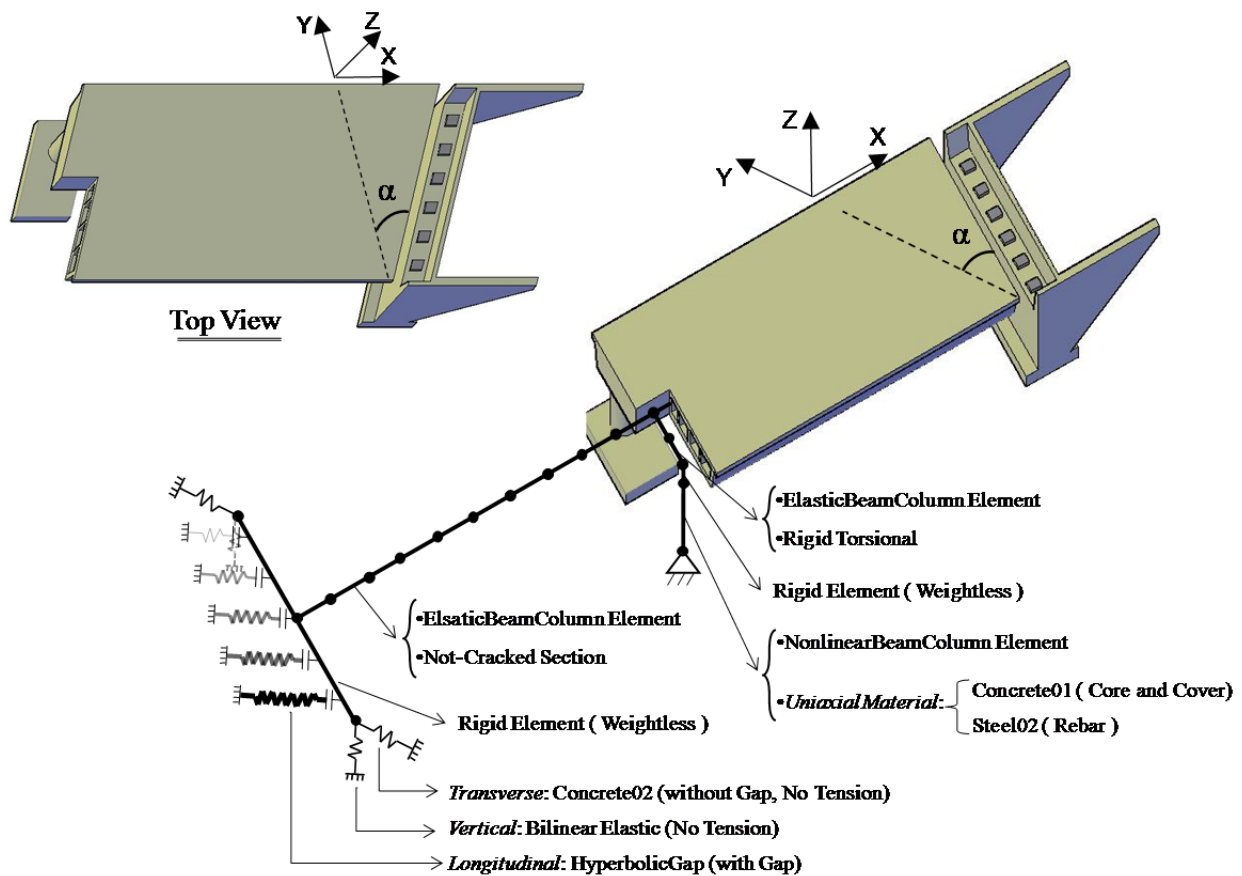


Figure 3.2 Generic model ( $\alpha^\circ$  skew) used for nonlinear response history analyses.

Important assumptions and main aspects of the modeling process of each individual component are described in the following sections.

### 3.4 MODELING OF THE DECK

As mentioned above, the prestressed concrete box-girder decks are modeled as “spine-lines,” using elastic beam-column elements. The elastic beam is used because flexural yielding of the deck during seismic response is not expected. Cracked section properties are used in the model to obtain realistic values for the structure’s period and the seismic demands generated from the analyses [Shamsabadi and Taciroglu 2013]. The effective moment of inertia of the box girder, denoted as  $I_{eff}$ , depends on the extent of cracking. For conventional reinforced concrete box-girder sections,  $I_{eff} = 0.5I_g$  (or)  $0.75I_g$ . However, according to Caltrans SDC [2010], no stiffness reduction is recommended for prestressed concrete box-girder sections (i.e.,  $I_{eff} = I_g$ ).

### 3.5 CAP-BEAM MODELING

For the two multi-column bridges (i.e., Bridge B and Bridge C), an elastic element representing the cap-beam is modeled as a frame element with a solid rectangular cross-section and dimensions according to the structural drawings. The cap-beam is connected through a fully restrained connection to the superstructure, because both components are usually constructed monolithically without any joints. As such, the superstructure’s flexural stiffness enhances the torsional stiffness of the cap-beam. The actual dimensions of the cap-beam-superstructure system resisting torsion are greater than the cross-sectional dimensions of the cap-beam element alone. The torsional constant of the cap beam  $J$  is therefore artificially magnified (by a factor of  $10^5$ ). The cap-beam is also assumed to be rigid for bending in the plane of the superstructure; however, the beam behaves flexibly out of the plane of the deck.

### 3.6 COLUMN-BENT MODELING

Progression of column yielding and damage is expected under strong ground motions, and thus nonlinear force-based beam elements are used to represent the columns (Figure 3.3). All fiber sections are assigned with the *UniaxialMaterial* model tag in the OpenSees [McKenna et al. 2000] model. Three different constitutive rules are used simultaneously within a cross-section: (i) confined concrete, (ii) unconfined concrete, and (iii) steel rebar (Figure 3.3). Details of the modeling of columns—such as selecting material properties, aggregating the fiber section in shear and torsion, and the type of nonlinear element—are provided in the following subsections.

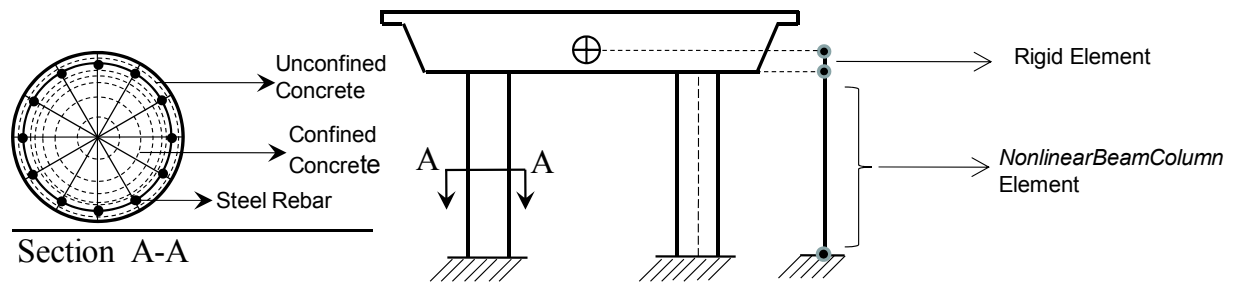


**Figure 3.3** Column modeling scheme.

### 3.6.1 Material Modeling

OpenSees has a rich collection of material models; in what follows, a brief explanation of each material obtained from the OpenSees material library and used in the modeling process is discussed.

Concrete Material: Two types of *UniaxialMaterial* having diverse capabilities in modeling concrete behavior in OpenSees were employed:

*Concrete01:* A uniaxial Kent-Scott-Park concrete material object with degraded linear unloading/reloading stiffness according to the work of Karsan-Jirsa and no tensile strength [OpenSees Wiki 2010].

*Concrete02:* A uniaxial concrete material object with tensile strength and linear tension softening [OpenSees Wiki 2010]. Assigned stress-strain backbone curves for two *concrte01* and *concrete02* materials are shown in Figure 3.4.

Steel Material: Three types of *UniaxialMaterial* for steel were considered:

*Steel02:* A uniaxial Giuffre-Menegotto-Pinto steel material object with isotropic strain hardening [OpenSees Wiki 2010] as shown in Figure 3.5(a). The advantage of *Steel02* to *Steel01* can be expressed as the smooth translation of backbone curve from elastic range to plastic range, which causes less of a convergence problem.

*ReinforcingSteel:* A uniaxial material for the reinforcing steel, which is proposed by Chang and Mander [1994] as shown in Figure 3.5(b).

*Hysteretic:* A uniaxial bilinear hysteretic material object with pinching of force and deformation, damage due to ductility and energy, and degraded unloading stiffness based on ductility [OpenSees Wiki 2010]. In this type of material, the stress-strain curve can be defined by three pairs of points for stress and strain in both tension and compression regions. In this study, *concrete02* and *ReinforcingSteel* are remodeled as hysteretic materials.

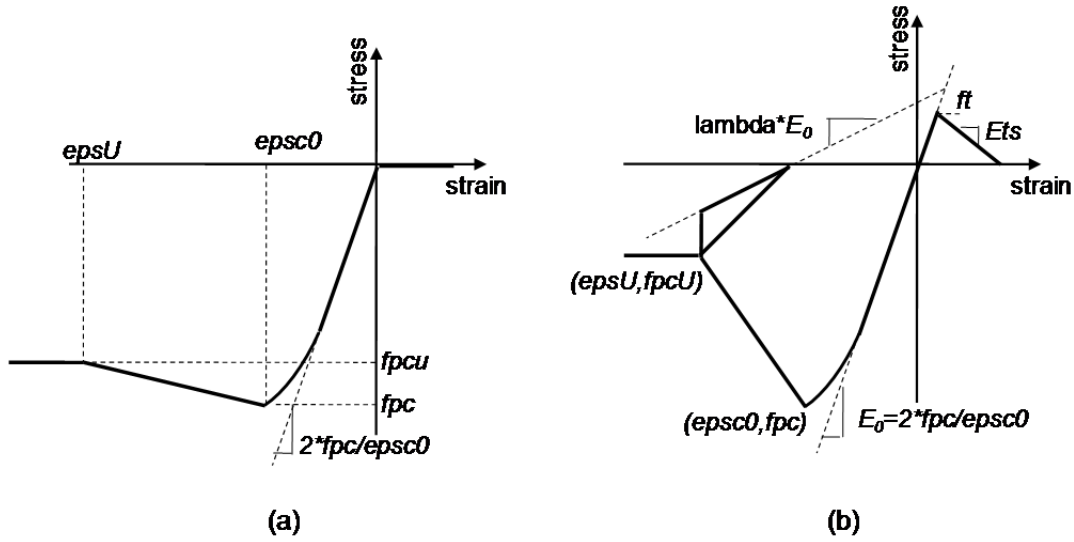


Figure 3.4 OpenSees stress-strain curves for concrete: (a) *Concrete01* and (b) *Concrete02*.

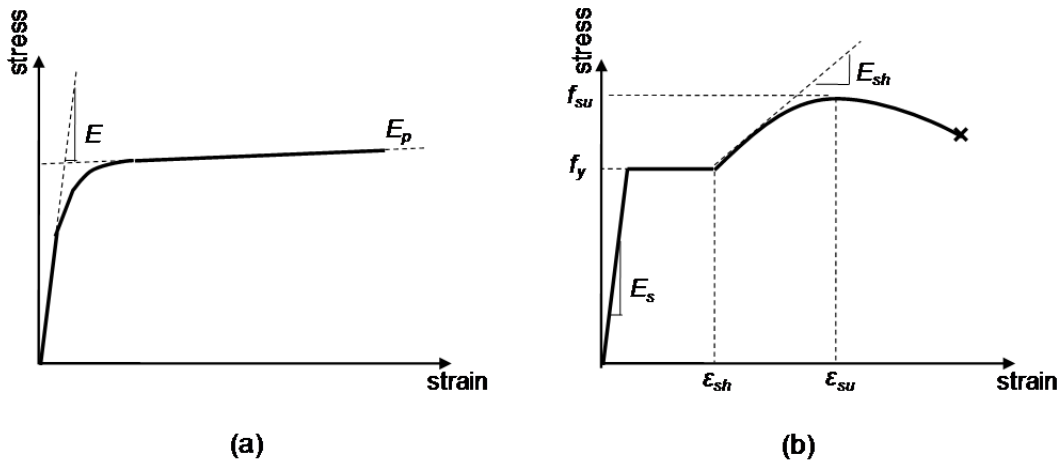


Figure 3.5 OpenSees stress-strain curves for steel: (a) *Steel02* and (b) *ReinforcingSteel*.

### 3.6.2 Section Properties

In order to combine the shear and torsional rigidities in column-bent modeling, we used the section aggregator in OpenSees. To aggregate the shear deformation in the section analysis of the column, an elastic material is defined with elastic shear stiffness shown in Equation (3.6), where  $G_{conc}$  is the shear modulus of concrete and  $A_{col}$  is the cross-section area of the column. A shape factor of 0.9 is applied because of the circular cross-sections of column-bents.

$$\left(\frac{9}{10}\right) \times G_{conc} \times A_{col} \quad (3.6)$$

To aggregate the torsional deformation in the fiber section of the column, an elastic material that relates the torque to the angle of twist per unit length of the column is used. The torsional stiffness that is assigned to the backbone curve is shown in Equation (3.7),

$$0.2 \times G_{conc} \times J_{col} \quad (3.7)$$

where  $G_{conc}$  is the shear modulus of concrete and  $J_{col}$  is the polar moment of inertia of the cross-section of the column. Due to cracking of the column cross-section, the torsional stiffness is reduced by a factor of 0.2 [Aviram et al. 2008].

### 3.6.3 Element Characteristics

A single force-based element with 10 quadrature points is used per column, and this is usually deemed to provide adequate accuracy. In order to model the portion of the column-bent embedded in the superstructure, a rigid element is attached to the top of the nonlinear beam-column element.

*Nonlinear Beam-columnElement:* Two formulations—force-and displacement-based—exist for this element type. The element model *dispBeamColumn* in OpenSees is a beam-column element model based on a displacement-based formulation, and *nonlinearBeamColumn* is a beam-column element based on a force-based formulation. A study by Neuenhofer and Filippou [1997] indicated that the solution of force interpolation functions only includes a numerical integration error, which can be reduced by increasing the number of integration points. As such, we employed a force-based element, *nonlinearBeamColumn*, for the column-bent modeling and used only one element per column with 10 integration points to control the numerical integration errors.

*Rigid Links:* As mentioned earlier, all elements are modeled in the centerline of the bridge components. Therefore, in order to model the portion of that column-bent that is embedded in the superstructure, a rigid element with the length of  $D_{c.g.}$  (distance between the soffit flange of superstructure box-girder centroid cross-section and the column top) is used on top of the nonlinear element (Figure 3.3).

In SAP2000 [CSI 2005], plastic hinges are considered with zero length—i.e., distributed plasticity was not considered. In those models, a beam-column element connects each of the nodes at the geometric centroid of the column cross-section, and five elements are used to model the column. Plastic hinges can develop at column ends near the point of fixity. In the plastic hinge zone, the plastic moment and curvature are assumed constant; otherwise assumed linear variation. The analytical length of the plastic hinge in the column is designated in Section 7.6.2 of Caltrans SDC [2010], which is reproduced in Equation (3.8)

$$L_p = \begin{cases} 0.08L + 0.15f_{ye}d_{bl} \geq 0.3f_{ye}d_{bl} \text{ (in., ksi)} \\ 0.08L + 0.022f_{ye}d_{bl} \geq 0.044f_{ye}d_{bl} \text{ (mm, MPa)} \end{cases} \quad (3.8)$$

where  $L$  is the column height,  $f_{ye}$  is the expected yield stress for A706 reinforcement, and  $d_{bl}$  is the nominal bar diameter of the longitudinal column diameter. Per Equation (3.8), the plastic hinge length depends on the column height, the longitudinal reinforcement size, and the strength of rebar. Column hinges are modeled with fiber elements. Such a model can incorporate the P-M-M interaction, representing the loss of stiffness caused by concrete cracking, yielding of reinforcing steel due to flexural yielding, and strain hardening.

### 3.7 ABUTMENT MODELING

Numerous studies have addressed the issues inherent in abutment modeling [Aviram et al. 2008; Bozorgzadeh et al. 2006; Bozorgzadeh et al. 2008; Goel and Chopra 1997; Shamsabadi et al. 2007; Shamsabadi et al. 2010; Wilson and Tan 1990a; Wilson and Tan 1990b]. This study focuses on seat-type skewed angle abutment modeling (Figure 3.6).

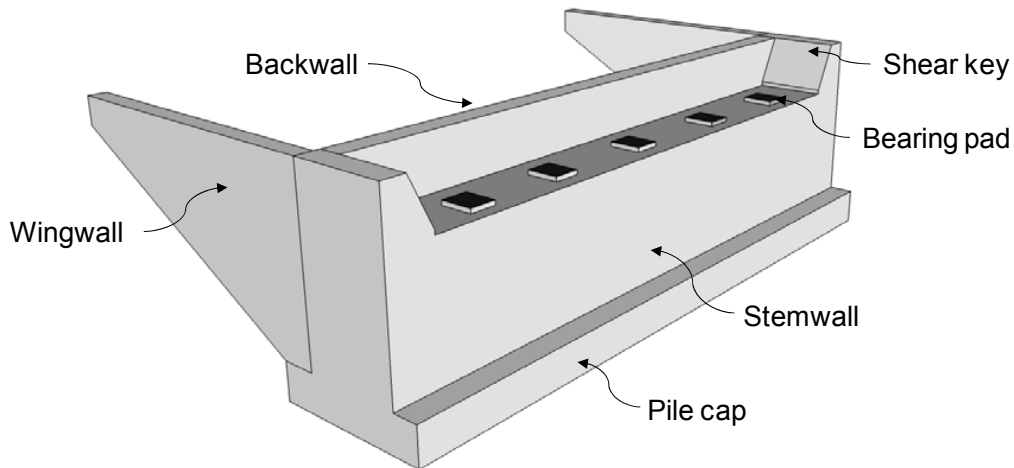


Figure 3.6 Configuration of typical seat-type abutment.

#### 3.7.1 Overview

Guidelines for abutment modeling are provided in Caltrans SDC [2010]. In the longitudinal direction, a backbone curve representing the passive earth pressure based on results from large-scale abutment testing at UC Davis [Maroney 1995] and UCLA [Stewart et al. 2007] are used. Equation (3.9) provides the initial stiffness of this backbone curve. The formula is proportionally adjusted to the backwall/diaphragm height, which is equal to 5.5 ft (1.7 m).

$$K_{abut} = \begin{cases} 25 \frac{\text{kip/in.}}{\text{ft}} \times w \times \left(\frac{h}{5.5}\right) \text{ (ft, Kip)} \\ 14.35 \frac{\text{kN/mm}}{\text{m}} \times w \times \left(\frac{h}{1.7}\right) \text{ (m, kN)} \end{cases} \quad (3.9)$$

In Equation (3.9),  $w$  and  $h$  denote the width and height of the backwall or the diaphragm abutments, respectively. The force-displacement backbone curves of the seat-type and diaphragm abutments in longitudinal direction are shown in Figure 3.7. The effective longitudinal displacement at the idealized yield point, which delineates full the mobilization of the passive soil resistance, is denoted by  $\Delta_{eff}$  [SDC Caltrans 2010]. For the seat-type abutments,  $\Delta_{gap}$  is the gap distance between seat-type abutment and superstructure, which can be estimated from structural drawings (e.g.,  $\Delta_{gap}=1$  in. or 2.54 cm). The resistance force assigned to seat-type abutment,  $P_{bw}$ , and diaphragm abutment,  $P_{dia}$ , are defined in Equations (3.10) and (3.11)

$$P_{bw} \text{ or } P_{dia} = \begin{cases} A_e \times 5.0 \text{ ksf} \times \left( \frac{h_{bw} \text{ or } h_{dia}}{5.5} \right) & \text{(ft, kip)} \\ A_e \times 239 \text{ kPa} \times \left( \frac{h_{bw} \text{ or } h_{dia}}{1.7} \right) & \text{(m, kN)} \end{cases} \quad (3.10)$$

where

$$A_e = \begin{cases} h_{bw} \times w_{bw} & \text{Seat-type abutments} \\ h_{dia} \times w_{dia} & \text{Diaphragm abutments} \end{cases} \quad (3.11)$$

In Equation (3.11),  $h_{bw}$  is the effective height of the backwall in seat-type abutments,  $h_{dia}$  is the effective height of the diaphragm, which is designed for full soil pressure,  $w_{bw}$  is the width of the backwall in seat-type abutment, and  $w_{dia}$  is the width of the diaphragm abutment (Figure 3.8).

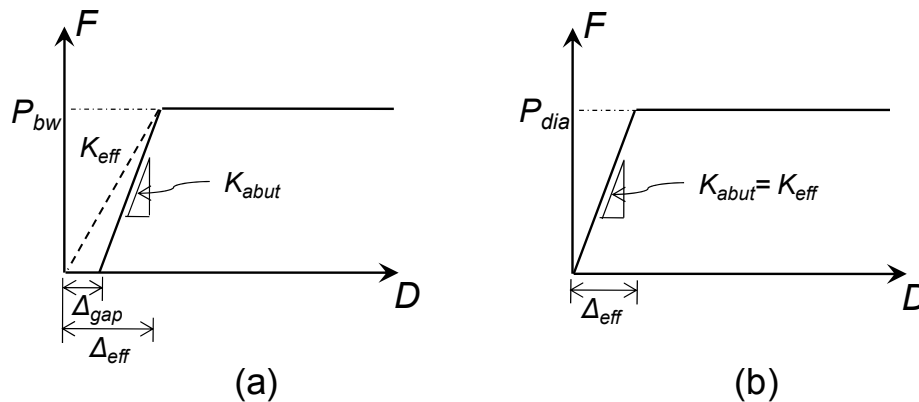


**Figure 3.7** The “interpreted Caltrans SDC [2010]” longitudinal stiffness for (a) seat-type abutment and (b) diaphragm abutment.

Caltrans SDC [2010] provisions dictate that seat-type abutments are designed to behave elastically in the transverse direction for service and moderate earthquake loads. In extreme events, shear keys are likely to respond nonlinearly; Caltrans SDC [2010] recommends that the transverse stiffness of a seat-type abutment should be assumed to be negligible unless the designer can demonstrate that the force-deflection and stiffness of each component that contributes to the transverse response. Caltrans SDC [2010] recommends a nominal transverse spring,  $K_{nom}$  equal to 50% of the adjacent bent for the elastic domain. For the diaphragm-type

abutments supported on standard piles, ignoring the wingwall effect, 40 kips/in. (7.0 KN/mm) stiffness per pile, is conservatively considered adequate for transverse resistance.

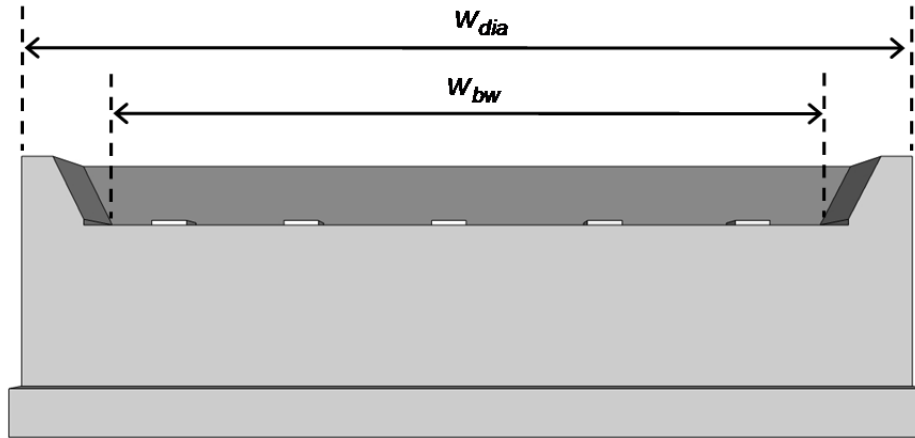


Figure 3.8 Abutment effective width for seat-type and diaphragm abutments.

### 3.7.1.1 A Simplified Abutment Model

Herein, we devise a simplified abutment model, in which the abutment is represented by a rigid element with a length of  $d_w$  (superstructure width), connected through a rigid joint to the superstructure's centerline. Three nonlinear springs—longitudinal, transverse, and vertical—are used to connect each end of the rigid element (Figure 3.9). In the longitudinal direction, a zero-length element is assigned with an elastic-perfectly-plastic (EPP) backbone curve representing the abutment backwall. The longitudinal stiffness accounts for the gap and embankment fill response where passive pressure is produced by the abutment backwall. In comparison to embankment fill stiffness, the shear stiffness of the bearing pads may be ignored.

In the transverse direction, a zero-length element is defined at each end of the rigid link with an assigned EPP backbone curve representing the backfill-wingwall-pile system. The abutment stiffness and strength for the longitudinal direction are modified using factors corresponding to wall effectiveness ( $C_L = 2/3$ ) and participation coefficients ( $C_W = 4/3$ ) according to Maroney and Chai [1994]. It is assumed that the wingwall length is varied, ranging from 1/3 to 1/2 of the backwall length. The resistance of the (brittle) shear keys and distributed bearing pads are ignored in this model for simplicity.

In the vertical direction, an elastic spring is defined at each end of the rigid link with a stiffness representing the vertical stiffness of bearing pads  $k_v$ . All assigned nonlinear zero-length elements work only in compression. The effect of the vertical embankment stiffness is not accounted for in this modeling technique. As shown in Figure 3.10, we consider a force-displacement backbone curve with two different stiffnesses working in compression. The first stiffness represents the more flexible portion of the bearing pad, which is  $K_1 = 1,200$  kips/in.

(210 KN/mm) effective in  $\Delta = 0.6$  in. (15 mm) deformation of the bearing fiber pad. The second stiffness ( $K_2$ ) is a large value and represents the rigid behavior of the abutment stemwall.

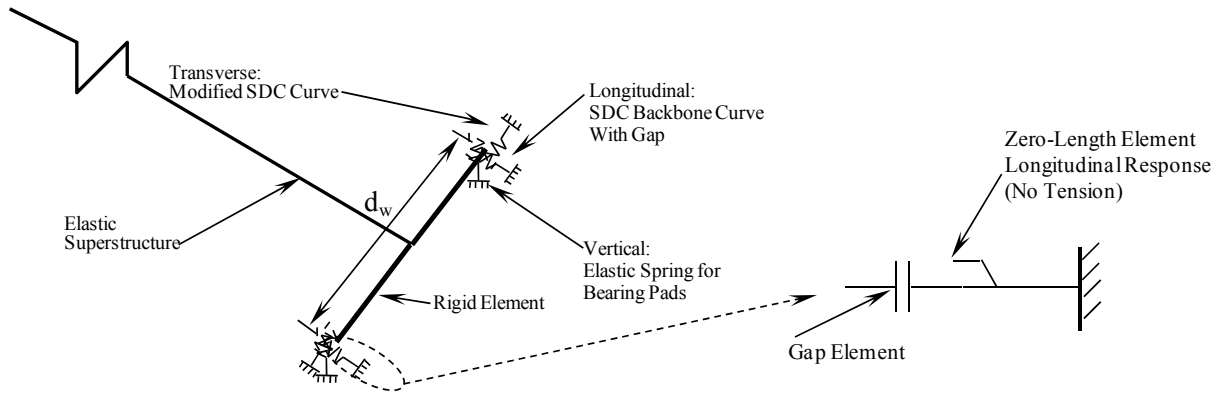


**Figure 3.9 Simplified abutment model.**

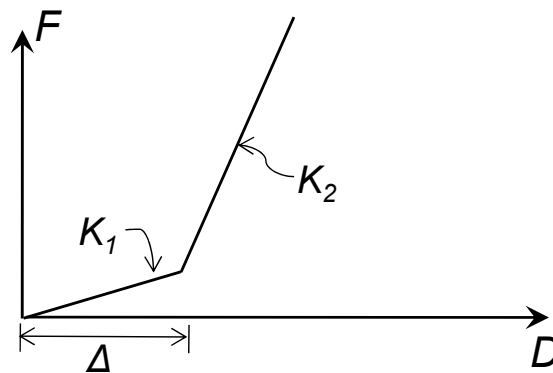


**Figure 3.10 Vertical force-displacement backbone curve of the abutment ( $K_1$ : the elastomeric bearing pad stiffness, and  $K_2$ : the stemwall and abutment embankment stiffness).**

### 3.7.1.2 Spring Abutment Model

This more complex abutment model was developed by Mackie and Stojadinovic [2006]. The refined longitudinal, transverse, and vertical nonlinear abutment response, as well as the participating mass corresponding to the concrete abutment and mobilized embankment soil, are accounted for in the spring abutment model (Figure 3.11).

In the longitudinal direction, the effects of elastomeric bearing pads, gap, abutment backwall, abutment piles, and soil backfill material are considered. Longitudinal response can be expressed at two distinct levels of deformation demand: (1) before gap closure—which corresponds to less deformation demand—and (2) after gap closure. In the first level of modeled behavior (i.e., before gap closure) the superstructure forces are transmitted to the stemwall through elastomeric pads, and then to the piles and the backfill. In the second level of the

modeled behavior (i.e., after gap closure), the superstructure collides directly with the abutment backwall and mobilizes the full passive backfill pressure.

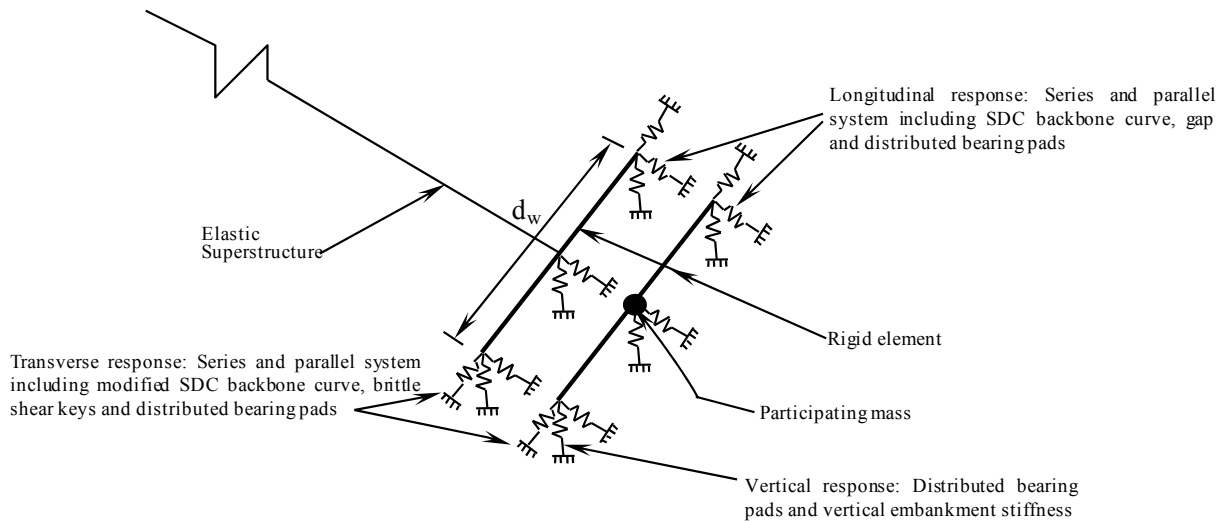


**Figure 3.11 Spring abutment model.**

In the transverse direction, the effects of elastomeric pads, exterior concrete shear keys, abutment piles, wingwalls, and backfill material are accounted for. Bearing pad modeling is uncoupled with respect to the longitudinal direction. The exterior shear key modeling is derived from experimental data [Megally et al. 2002]. According to Caltrans SDC [2010], the ultimate strength of the shear key is assumed to be 30% of the superstructure dead load. A hysteric material with a tri-linear response backbone curve—possessing two hardening and one softening stiffness parameters—is used. The bearing pads and shear keys are defined to act in parallel. This combined bearing pad-shear key system is in series with the transverse abutment stiffness and strength.

In the vertical direction, the abutment model consists of the vertical bearing pads stiffness in series with the vertical stiffness of the trapezoidal embankment, obtained from Zhang and Makris [2002a, 2002b].

### 3.7.2 Proposed Abutment Models for Skewed Bridges

We herein propose two different models—namely, the *Friction Abutment Model* and the *Skewed Abutment Model*—that feature the skew effect. Each model is discussed in more detail in the following subsections. While devising these models, we sought to find a balance between the sophistication of the modeling technique and the present capabilities of the employed software platforms (i.e., OpenSees and SAP2000). We finally opted to use the *simpler* Skewed Abutment Model for the extensive parametric studies that followed. This model was easy to construct using

the version of OpenSees available at the time of this study (ver. 2.2.2), and its numerical performance was adequately robust.

### 3.7.2.1 Friction Abutment Model

Figure 3.12 shows the proposed seat-type skewed abutment with a skew angle of  $\alpha$ . Each component of the Friction Abutment Model is coded in accordance with the type of element used in OpenSees. Code “B” represents the *elasticBeamColumn* element, “Z” represents the *zeroLength* element, and “L” represents the *twoNodeLink* element. We describe each component:

- B1: A rigid element with length equal to the superstructure width and which connects rigidly to the spine-line representing superstructure in the middle.
- B2: An elastic beam element with properties of the backwall.
- Z1: An Elastic Perfectly Plastic, EPP *zeroLength* element representing the external shear key. The initial stiffness and strength of the backbone curve is based on experimental data in UCSD [Bozorgzadeh et al. 2006] and Caltrans SDC [2010].
- Z2: An EPP with gap *zeroLength* element representing the gap between deck and backwall as well as the active backfill soil pressure behind the backwall. Depending on the length of the bridge, a gap length of 1 in. (2.54 cm) to 2 in. (5.08 cm) is considered. The stiffness and strength are derived from Caltrans SDC [2010] for the skewed length of the abutment.
- Z3: An EPP *zeroLength* element representing the shear stiffness of the backfill soil behind the backwall.
- L1: A *twoNodeLink* element that only transfers forces perpendicular to the abutment. To achieve this response, a large value is assigned to the local longitudinal stiffness; however, a very small stiffness value is assigned in other directions.

In the vertical direction, the model includes two elastic *zeroLength* elements that work in parallel. As shown in Figure 3.10 and previously explained in the simplified abutment model, the first *zeroLength* element represents the flexible portion of the elastomeric bearing pad in vertical direction ( $K_1$ ) and the second one represents the vertical stiffness of the stemwall and abutment embankment ( $K_2$ ).

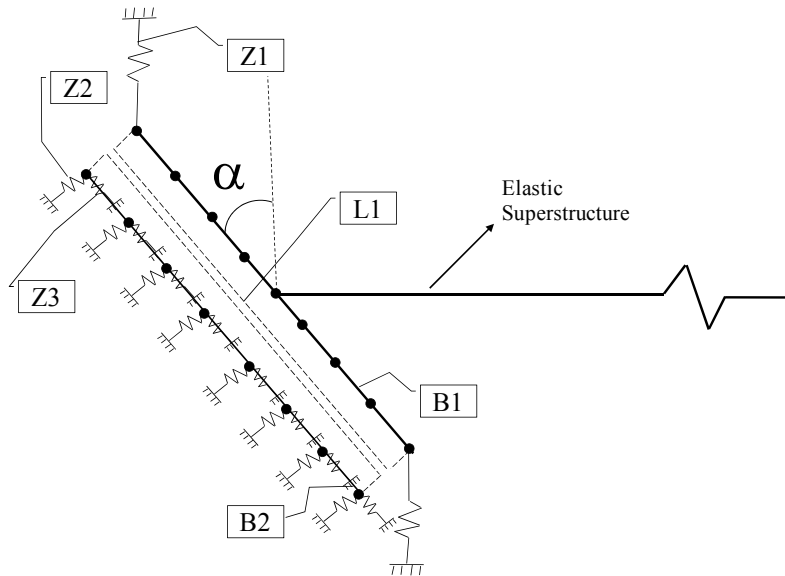
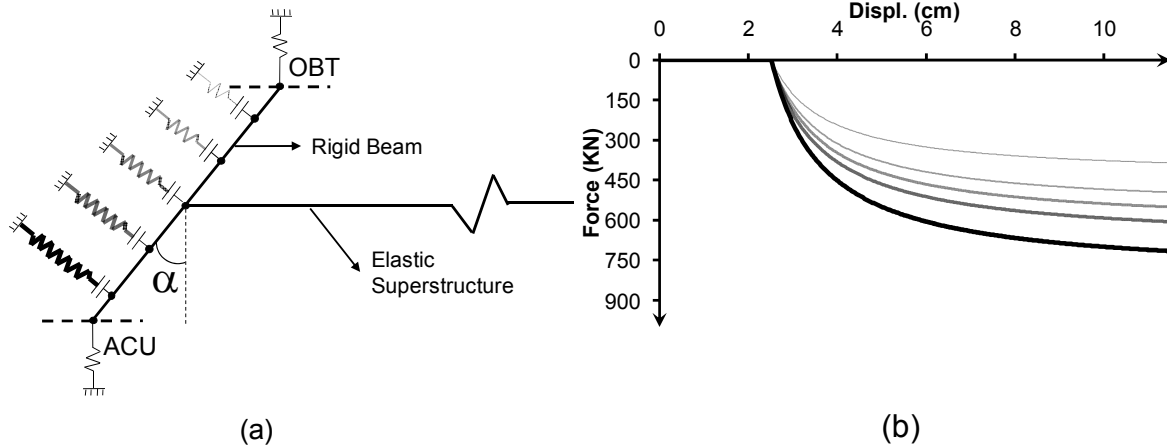


Figure 3.12 Friction abutment model.

### 3.7.2.2 Skewed Abutment Model

The Skewed Abutment Model is a simpler version of the Friction Abutment Model where only three characteristics of the Friction Abutment Model are explicitly considered: (1) longitudinal response of the backfill (passive pressure) and the expansion joint, (2) transverse response of the shear keys, and (3) vertical response of the bearing pads and the stemwall. Other elements in the Friction Abutment Model are omitted, as their contributions to the overall response and their effects on failure modes were found to be insignificant in preliminary numerical simulations.

*Longitudinal response:* Experimental data on lateral passive response of abutment backfills are limited [Bozorgzadeh et al. 2006; Romstad et al. 1995; Shamsabadi et al. 2010; Stewart et al. 2007]. At the time of the writing of this report—and to the best of the authors’ knowledge—there are no data sets from controlled experiments on backfill response for skewed abutments. Therefore, the intuitive model devised here is not experimentally validated. That said, the longitudinal response is modeled by using five nonlinear springs in series with gap elements as shown in Figure 3.13(a). The nonlinear springs and the gap elements represent the passive backfill response and the expansion joint, respectively. The strength and initial stiffness of the soil springs are obtained from recommendations provided in the Caltrans SDC [2010], which, in turn, were derived from large scale abutment testing [Romstad et al. 1995; Stewart et al. 2007].



**Figure 3.13 Skewed Abutment Model, backfill soil springs. (a) Configuration diagram. (b) Backbone curves.**

For all abutment skew angles, the direction of the backfill passive pressure is assumed to be perpendicular to the backwall. The backfill springs are equally spaced and attached to a rigid bar representing the deck. Properties of the five abutment nonlinear hyperbolic springs are slightly different from each other, depending on their relative location to the obtuse angle between the backwall and the longitudinal/traffic direction (point OBT in Figure 3.13). The stiffness and strength of these springs are assumed to increase linearly with increasing the abutment skew angle and distance from point OBT. We argue here that the volume of engineered backfill soil that can be mobilized per unit wall-width in the event of backwall breakage is larger as we move from point OBT towards the acute side (point ACU in Figure 3.13). We also maintain that this variation is linear, which is the simplest—and therefore the most reasonable—assumption that can be adopted without direct guidance from experimental observations. Finally, we postulate that the maximum stiffness/strength variation occurs for the largest skew angle (60°) and that it is equal to 30%. Therefore, the stiffness/strength variation factor  $\beta$  for a given skew angle  $\alpha$  can be computed in Equation (3.12).

$$\beta = 0.3 \times \frac{\tan \alpha}{\tan 60^\circ} \quad (3.12)$$

Multiple analyses conducted with different values of the maximum variation between OBT and ACU springs [i.e., 30% in Equation (3.12)] indicate that the results are not highly sensitive to variations in  $\beta$  (less than 2% difference in the median of deck rotation of Bridge A when  $\beta$  is varied from 0 to 60%). As such, the aforementioned modeling assumptions are reasonable extensions of those adopted in previous attempts (see, for example, Shamsabadi et al. [2007]).

*Transverse response:* The resistance provided by the exterior shear key is accounted for modeling the transverse response in the Skewed Abutment Model. The capacity of the exterior shear key can be evaluated using three models, as discussed by Megally et al. [2002]: (1) the sliding shear friction model, (2) the strut-and-tie analogy, and (3) moment-curvature analysis.

According to the shear key rebar details of the seed bridges used in this study, we can assign the Test 1B (Figure 3.14) of the model matrix [Megally et al. 2002] to the seed bridge shear keys. Megally et al. [2002] concluded that no sliding between shear key and abutment occurs when a shear key is constructed monolithically with the abutment backwall and the wingwall. Such a shear key would not behave as a structural fuse does. This, then, would be in contrast with Caltrans SDC [2010], which considers shear keys as a fuse-type structural component.

Based on Megally’s observations, the “strut-and-tie model” results in the most theoretically accurate estimates of the capacity and the strength of shear keys. As shown in Figure 3.14, the lateral load is transferred from the shear key to the abutment through a compressive diagonal strut. A diagonal crack develops from the shear key to the toe of the abutment stemwall. Therefore, we use the strut-and-tie model to calculate strength and initial stiffness of shear keys. The capacity of the shear key in the strut-and-tie model is shown in Equation (3.13).

$$V_N = V_C + V_S \quad (3.13)$$

where  $V_C$  and  $V_S$  are the concrete and reinforcing steel contributions to the shear key capacity, respectively. The strength of the shear key provided by concrete is given by Equation (3.14) where  $f'_c$  is the compressive strength of concrete,  $h$  is the height of abutment stemwall, and  $b$  is the stemwall width.

$$V_C = \begin{cases} 2.4\sqrt{f'_c} \times b \times h & (\text{psi}) \\ 0.2\sqrt{f'_c} \times b \times h & (\text{MPa}) \end{cases} \quad (3.14)$$



**Figure 3.14** Cracking pattern at the end of Shear Key testing (Test 1B; Megally et al. [2002]).

As shown in Figure 3.15, the steel contribution,  $V_S$ , can be calculated via the equilibrium of forces along the diagonal crack, AB. We assume that the impact force imposed by the superstructure on the shear key,  $V$ , is applied in a distance, denoted as  $a$ , from the seating level of the abutment. The resisting moments in this mechanism are:

The moment developed by the tension tie  $T_1$ :  $M_A = A_{s,1}f_{y,1}h$ , where  $A_{s,1}$  is the total area of steel along the horizontal tension tie  $T_1$ ;  $f_{y,1}$  is the tension yield stress of the reinforcing bars along  $T_1$  and  $h$  is height of the abutment stemwall.

The moment developed by the first row of steel bars crossing the shear key interface  $T_2$ :  $M_B = A_{s,2}f_{y,2}d$ , where  $A_{s,2}$  is the total area of steel along  $T_2$ ;  $f_{y,2}$  is the tension yielding stress of the reinforcing bars along  $T_2$  and  $d$  is width of the shear key and the abutment stemwall interface.

The moments developed by the horizontal and vertical reinforcement located on the side faces of the abutment stemwall intersecting the diagonal crack.

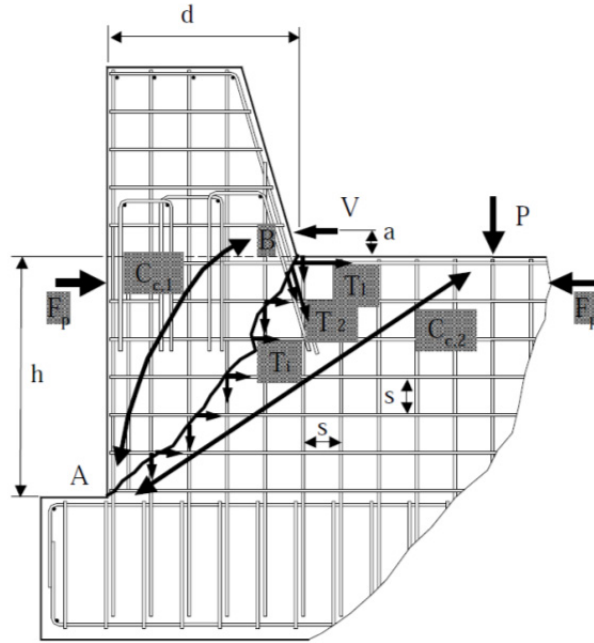


**Figure 3.15** Strut-and-tie analogous model for shear keys (source: Megally et al. [2002]).

Therefore, the steel contribution to the capacity of the shear key can be described by Equation (3.15) where  $n_h$  and  $n_v$  are the numbers of side faces with horizontal and vertical side reinforcements;  $f_{y,s}$  is the tension yield stress of the side reinforcements and  $A_{s,s}$  is the cross sectional area of the side reinforcements. Table 3.1 illustrates the concrete and reinforcing steel contributions to the shear key capacity and the total shear key strength corresponding to each seed bridge.

$$V_S = \left[ A_{s,1}f_{y,1}h + A_{s,2}f_{y,2}d + n_h A_{s,s}f_{y,s} \frac{h^2}{2s} + n_v A_{s,s}f_{y,s} \frac{d^2}{2s} \right] \left( \frac{1}{h+a} \right) \quad (3.15)$$

We develop the force-deformation backbone curve of each seed bridge based on the preceding formulations and the actual size of the seed bridges. Figure 3.16 illustrates the shear key backbone curves of each seed bridge. All tri-linear backbone curves degrade to zero-stiffness at a certain deformation. We refer to this deformation level as the *shear key failure deformation* (Table 3.2). In the following chapters, each response history analysis filtered for “no-collapse” will be discriminated based on the shear key failure status. Within this subset, if only one of the bridge shear keys exceeds its failure deformation ( $\Delta_{SK-f}$ ) during the response history analysis, we assign that analysis to the *shear key failure* category; otherwise, we assign it to the *shear key survival* category. Figure 3.17 displays the partial scaled sketch of the seed bridge abutments. Our analysis shows that the shear key dimensions largely affect the transverse response backbone curve.

Vertical response: The two proposed abutment models have the same modeling in vertical response. As Figure 3.10 shows, the vertical response is modeled by two parallel springs. The first spring represents the flexible portion of the elastomeric bearing pad in the vertical direction ( $K_1$ ) and the second one represents the vertical stiffness of the stemwall and abutment embankment ( $K_2$ ). In Appendix D, we discuss the modeling issue that we confront in shear key modeling by OpenSees.

**Table 3.1 Shear key strength contribution corresponding to the seed bridges.**

	$V_C$	$V_S$	$V_N$
Bridge A	1984 KN (446 kips)	1379 KN (310 kips)	3363 KN (756 kips)
Bridge B	2549 KN (573 kips)	5493 KN (1235 kips)	8042 KN (1808 kips)
Bridge C	5071 KN (1140 kips)	5435 KN (1222 kips)	10506 KN (2362 kips)

**Table 3.2 Shear key failure deformation of the seed bridges.**

	$\Delta_{SK-f}$
Bridge A	6.2 cm (2.45 in)
Bridge B	19.1 cm (7.51 in)
Bridge C	21.7 cm (8.56 in)

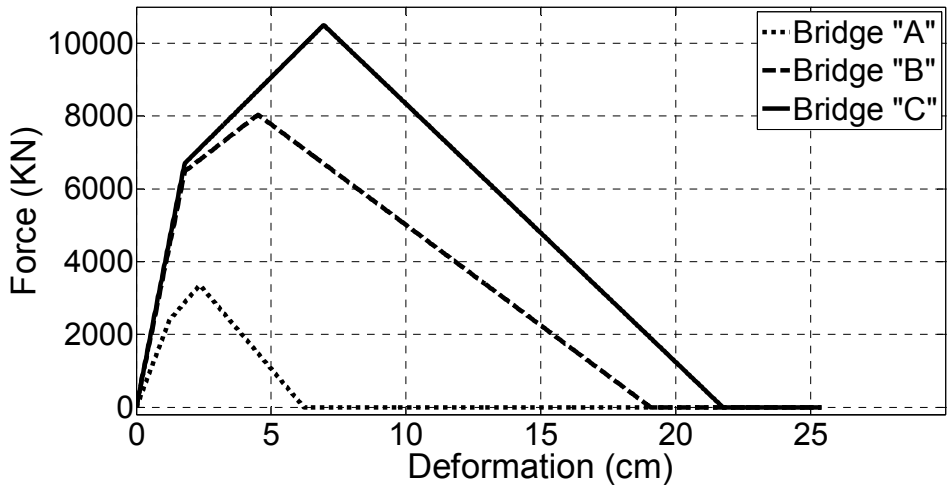


Figure 3.16 Shear key force-deformation backbone curve.

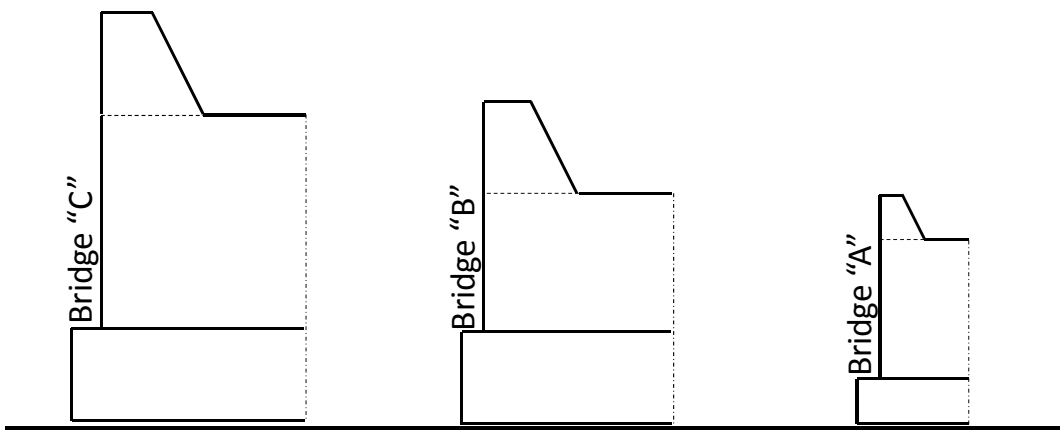


Figure 3.17 Shear key for the seed bridges depicted in scale.

## 4 Analysis and Trend Observations in Skewed Bridge Response to Seismic Excitations

### 4.1 OVERVIEW

This chapter provides an assessment of skewed bridge performance under seismic excitations and identifies trends in the simulated response values. A detailed review of the current state-of-the-art on this subject has been provided in Section 1.3. This trend identification makes use of the bridge model matrix that was generated from three seed bridges located in California, as discussed in Chapter 2. Results are based on 3D nonlinear response history analyses of bridge models described in Chapter 3.

The present research encompasses a broader set of parameters and variations than past studies. Through extensive parametric study conducted using nonlinear response history analyses, trends in the seismic response of skewed bridges are sought by considering variations in the configuration parameters of the models and in the ground motion characteristics. The varied configuration parameters and attributes include global torsional resistance, abutment skew angle, column-bent height, and span arrangements. The applied ground motions are those that were recorded on rock or soil, and those that contained pronounced velocity pulses. The examined seismic response parameters include maximum planar deck rotation ( $\theta_{rot}$ ), maximum abutment unseating ( $\delta_{unseat}$ ), and maximum column-bent drift ratio ( $\theta_{col}$ ).

### 4.2 MODAL ANALYSIS

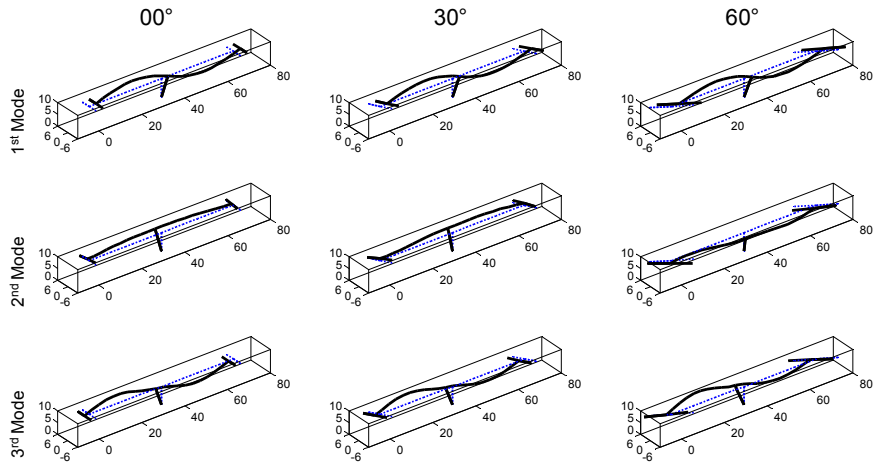
A bridge's geometrical properties naturally have a significant effect on its modal properties. Table 4.1 displays the first three periods of all bridges in the bridge matrix. Abutment skew angle has a less pronounced effect on the fundamental period of a single-column bridge (Bridge A) than on the fundamental periods of other multi-column bridges (Bridges B and C). Fundamental periods of bridges similar to Bridge B are the most affected by the abutment skew angle. Such bridges' fundamental periods increase with an increase in the abutment skew angle, as the bridge's effective stiffness in the longitudinal direction is decreased. The effects of the column-bent boundary condition, as well as the skewed cap-beams of multi-column bridges, are the two reasons that the fundamental periods of multi-column bridges are influenced more significantly by the abutment skew angle. Extension of the column-bent height caused all

bridges' fundamental periods to increase. This trend was expected, as the bridge global stiffness decreases with an increase in the column-bent height. The span arrangements had no significant effect on the bridges' fundamental periods.

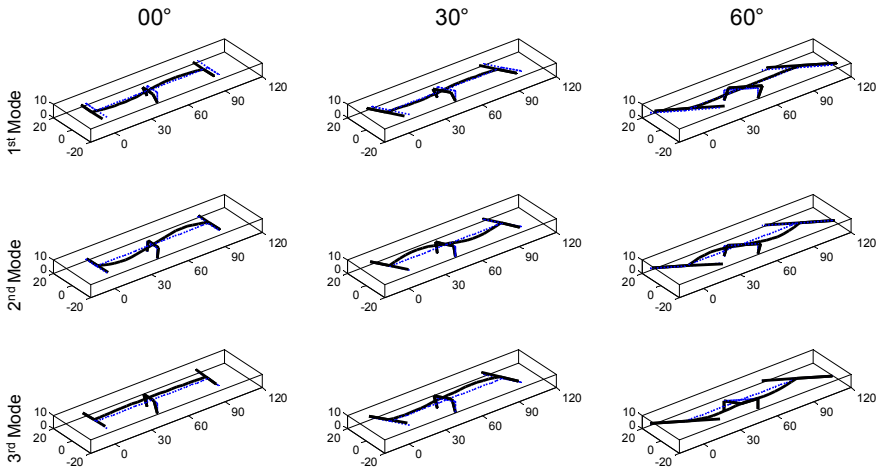
**Table 4.1** Fundamental periods of all studied bridges.

Bridge	Column	Span	Mode	0°	15°	30°	45°	60°
Bridge A	Lower	Symm.	1st	0.606	0.605	0.604	0.600	0.589
			2nd	0.379	0.378	0.377	0.376	0.376
			3rd	0.350	0.349	0.345	0.335	0.320
		Asymm.	1st	0.613	0.613	0.612	0.609	0.601
			2nd	0.383	0.404	0.408	0.416	0.429
			3rd	0.380	0.382	0.379	0.375	0.368
	Higher	Symm.	1st	0.877	0.876	0.875	0.871	0.862
			2nd	0.434	0.433	0.432	0.430	0.427
			3rd	0.416	0.414	0.405	0.386	0.352
		Asymm.	1st	0.877	0.877	0.875	0.872	0.863
			2nd	0.447	0.467	0.473	0.481	0.492
			3rd	0.434	0.445	0.440	0.432	0.419
Bridge B	Lower	Symm.	1st	1.090	1.117	1.195	1.372	2.352
			2nd	0.465	0.462	0.451	0.448	0.560
			3rd	0.353	0.356	0.369	0.400	0.510
		Asymm.	1st	1.093	1.116	1.205	1.371	2.364
			2nd	0.496	0.495	0.490	0.488	0.580
			3rd	0.344	0.416	0.414	0.423	0.510
	Higher	Symm.	1st	1.804	1.839	1.998	2.297	3.090
			2nd	0.481	0.473	0.455	0.449	0.569
			3rd	0.359	0.360	0.373	0.406	0.508
		Asymm.	1st	1.802	1.840	1.998	2.326	3.094
			2nd	0.511	0.506	0.493	0.490	0.584
			3rd	0.358	0.439	0.439	0.443	0.508
Bridge C	Lower	Symm.	1st	0.816	0.814	0.817	0.841	1.020
			2nd	0.588	0.593	0.623	0.691	0.792
			3rd	0.557	0.556	0.558	0.584	0.665
		Asymm.	1st	0.818	0.818	0.820	0.846	0.973
			2nd	0.608	0.609	0.631	0.702	0.782
			3rd	0.591	0.597	0.611	0.627	0.675
	Higher	Symm.	1st	1.397	1.392	1.379	1.386	1.424
			2nd	0.774	0.770	0.776	0.800	1.050
			3rd	0.569	0.567	0.576	0.646	0.755
		Asymm.	1st	1.398	1.393	1.385	1.389	1.429
			2nd	0.776	0.771	0.776	0.803	0.957
			3rd	0.623	0.622	0.627	0.672	0.731

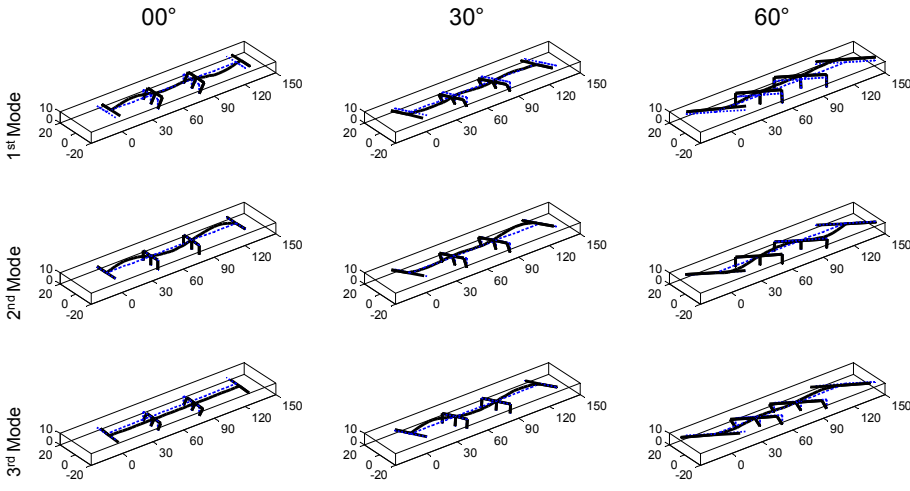
Figure 4.1 displays the first three mode shapes of Bridges A, B, and C for  $0^\circ$ ,  $30^\circ$ , and  $60^\circ$  skews, respectively. We consider the symmetrical arrangement of spans with original column-bent height as the representative sample of the bridge matrix. All bridges' first mode shapes are longitudinal; however, rotational mode contributes more when the abutments' skew increases from  $0^\circ$  to  $60^\circ$ . This contribution is more predominant for multi-column bridges (Bridges B and C). This trend emphasizes the skewed cap beam's effect on skewed bridges' modal properties.



(a)



(b)



(c)

**Figure 4.1** Three first mode shapes of 0°, 30°, and 60° skewed bridges (numbers in meters) for (a) Bridge A, (b) Bridge B, and (c) Bridge C.

### 4.3 COLLAPSE CRITERIA

The simplified modeling technique and structural analysis software adopted in this study are not capable of simulating every conceivable collapse mechanism. This is particularly true for sequential collapse scenarios. With that proviso, we post-processed the analysis output in order to identify the collapse cases using predefined collapse criteria. We define non-simulated collapse criteria as follows:

Column-bent maximum drift ratio (CDR) is greater than 8%. It was shown by Hutchinson et al.[2004] that if a column maximum drift ratio is less than 8%, that column's maximum residual drift ratio can be considered to be less than 1%—a number that provides an indication of the bridge's serviceability after an earthquake [ JRA (Japan Road Association) 1996].

Deck displacement relative to the abutment in the longitudinal unseating direction is greater than the seat length. The deck's longitudinal displacement relative to the abutment is accounted as another collapse criterion where the allowable abutment unseating length is defined based on the seat length provided for each seed bridge (Table 4.2).

**Table 4.2 Allowable unseating length of the seed bridges.**

	Unseating length
Bridge A	29.5 in. (75 cm)
Bridge B	29.5 in. (75 cm)
Bridge C	35.4 in. (90 cm)

### 4.4 RESPONSE HISTORY ANALYSIS

The bridge models of the bridge matrix were systematically analyzed using the selected ground motion sets under multiple angles of incidence. Each bridge/ground motion set combination results in a total of 240 response history analyses (40 ground motion records in each set and 6 angles of incidence per ground motion record). In total, the study conducted 43,200 response history analyses and scrutinized the results to identify dependencies, correlations, and trends.

To that end, three sets of seismic response parameters were obtained: maximum planar deck rotations ( $\theta_{rot}$ ), maximum abutment unseating displacements ( $\delta_{unseat}$ ), and maximum column-bent drift ratios ( $\theta_{col}$ ). Detailed investigation of simulated data suggested the necessity of dividing results into groups based on three distinct regimes of skewed bridge behavior: bridge collapse (according to the collapse criteria discussed in Section 4.3), bridge survival with shear key failure (Chapter 3), and bridge survival with shear key survival.

#### 4.4.1 Collapse Potential Observations

Table 4.3 shows the number of response history analyses that caused collapse as a function of seed bridge configuration, ground motion (GM) types, and abutment skew angle. The total number of response history analyses for each cell in Table 4.3 is 960—that is, 40 ground motion records in each set, multiplied by 6 angles of incidence per ground motion record, by two column height configurations ( $Col_{orig}$  and extended column height  $Col_{ext} = 1.5 \times Col_{orig}$ ), and by two span arrangements (symmetrical with equal span lengths and asymmetrical with ratio of span lengths equal to 1.2). The most collapses were observed in Bridge C and in bridges with larger abutment skew angles.

**Table 4.3** Number of collapses for each bridge/ground motion set combination.

GM type	Bridge	0°	15°	30°	45°	60°
Pulse-like	A	35	56	97	88	150
	B	48	72	153	162	295
	C	243	317	372	444	470
Soil-site	A	0	0	4	10	17
	B	3	4	24	28	57
	C	90	107	132	173	174
Rock-site	A	0	0	0	2	3
	B	1	2	29	6	19
	C	25	31	27	34	46

Pulse-like ground motions caused the largest number of collapses among all bridges; therefore, this study focuses on the set of collapses with pulse-like ground motion—in total, 40. In particular, pulse-like ground motion numbers—11, 18, 19, 28, and 31 (see Appendix B)—were the most significant; their response spectra are illustrated in Figure 4.2 with colored lines. This figure simultaneously illustrates the first fundamental periods of three sample bridges corresponding to a 60° abutment skew, which caused the largest number of collapses. Using information illustrated in Figure 4.2, it is clear that the most destructive records are those that have a large spectral acceleration for a broad range of periods.

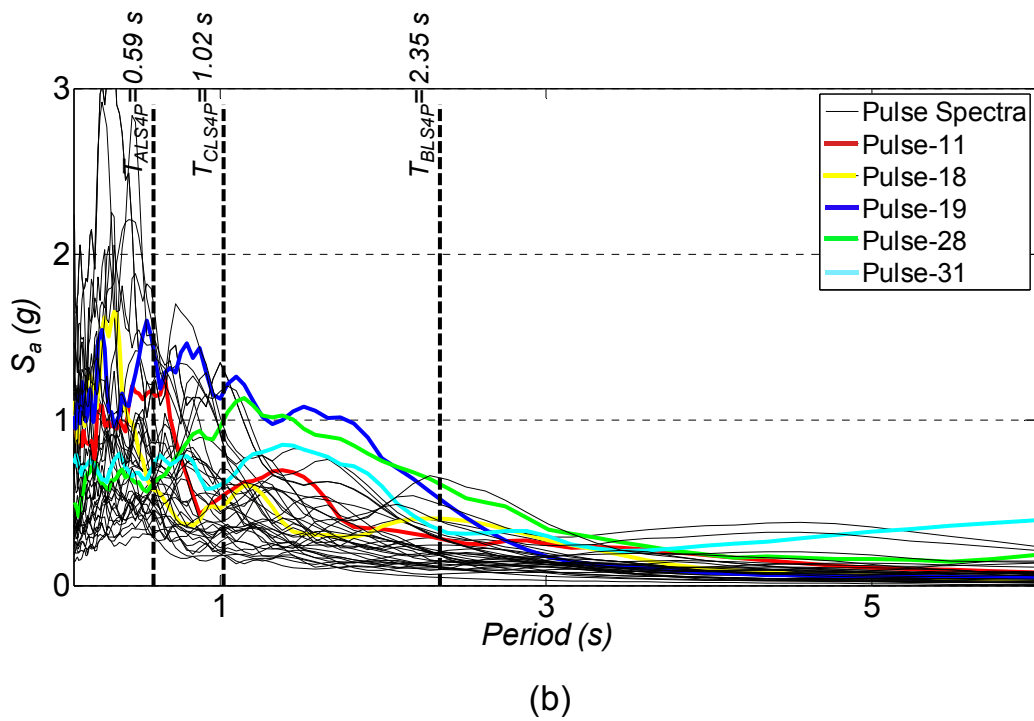
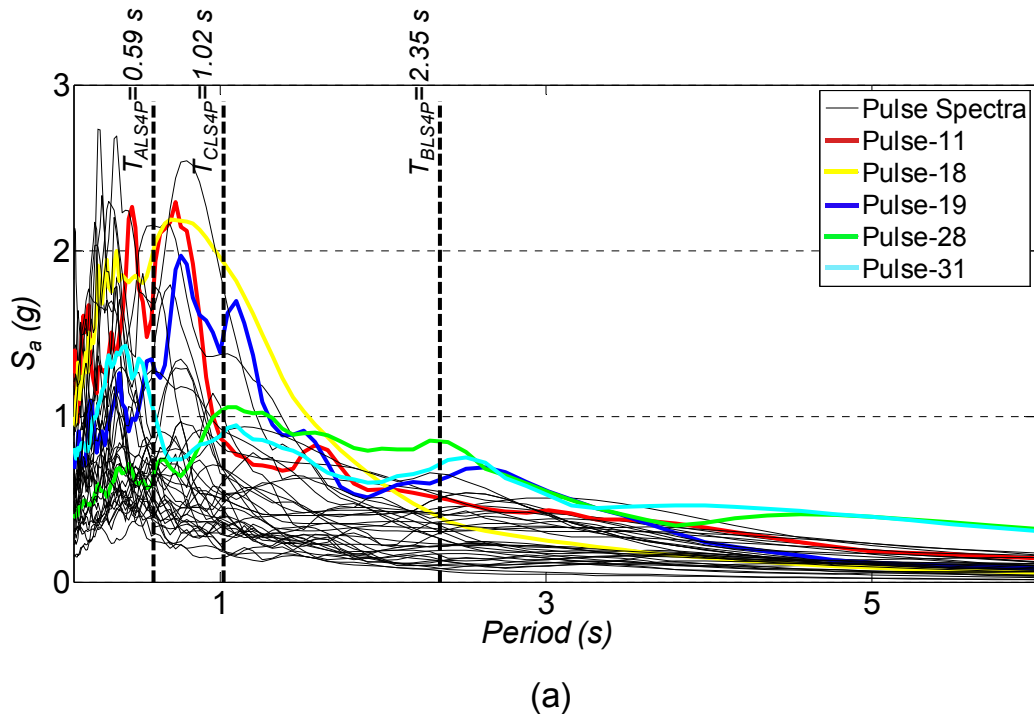


Figure 4.2 Pulse-like ground motions spectra for (a) strike-normal and (b) strike-parallel.

## 4.5 THE EFFECT OF GROUND MOTION TYPE ON SKEWED BRIDGE RESPONSE

In this section, we discuss the effect of ground motion characteristics on skewed bridge response and propose the use of an efficient ground motion intensity measure to express the *IM-EDP* (Engineering Demand Parameter) curves. Because the ground motion sets used in this study are not tuned for a target hazard level, it is necessary to interpret the results using *IM-EDP* curves that are conditioned on no-collapse (henceforth denoted simply as *IM-EDP* curves) and the probability of collapse (given *IM*).

Skewed bridges' seismic response parameters are significantly sensitive to the characteristics of applied seismic excitations: higher values of response parameters and incidences of collapse are observed for skewed bridges that experience pulse-like ground motions. Figure 4.3 displays the variation of  $\theta_{rot}$  and  $\theta_{col}$  for no-collapse cases as a function of ground motion peak acceleration  $PGA_{res}$  (maximum of the resultant of two SN and SP components) for all ground motion sets, and for five variations of the abutment skew angle. This figure is generated only for Bridge A with its original column height and by assuming symmetric spans, but other variations in bridge geometrical properties display similar trends for  $\theta_{rot}$  and  $\theta_{col}$ . Each plot divides *EDPs* into two categories, based on whether the shear keys survived (circles in Figure 4.3) or lost resistance (squares) during seismic excitation. These results clearly indicate that the probability of shear key failure is higher when the bridge experiences a pulse-like motion (higher concentration of black squares) for any abutment skew angle. Given the significance of pulse-like ground motions in imposing high seismic demands compared to other types of ground motions, the trend observations will henceforth be emphasized more in those analyses that are carried out using the pulse-like ground motion set. However, results from the soil- and rock-site ground motion sets are mentioned as well.

Selecting an appropriate *IM* that can represent seismic motion has been a challenge for researchers. The Federal Emergency Management Agency's (FEMA's) loss assessment program HAZUS [FEMA 1997] recommends using one of two intensity measures of peak ground acceleration (*PGA*) and permanent ground deformation (*PGD*). The later version of HAZUS [FEMA 2003] has switched to the use of spectral acceleration at a period of 1 sec [ $S_a(1.0)$ ] and *PGD*. Introducing a single intensity measure that works for all structural systems and all *EDPs* is not feasible. Baker and Cornell [2006] suggested that efficiency may be improved if more than one intensity measure is used. Mackie and Stojadinovic [2003] identified 23 intensity measures that could be used for assessing highway bridges' seismic responses. They evaluated each intensity measure based on an efficiency factor and found that those intensity measures that are related to spectral quantities (e.g., spectral acceleration and spectral displacement) tend to be the most efficient.

In this study, we opted to use the resultant peak ground velocity ( $PGV_{res}$ ) as the ground motion intensity measure for generating *IM-EDP* curves. The  $PGV_{res}$  is computed as the maximum of the SN and SP components' resultant velocity histories. The efficiency of different intensity measures was studied by monitoring the variations in *IM-EDP* plots (similar to Figure 4.3 but with different *IMs*) as well as dispersion of collapse fragility curves, considering a wide

range of  $IMs$  as collapse potential indicators. As shown in Table 4.4, other  $IMs$  that were considered include spectral acceleration at the first mode period of the strike-normal component, denoted as  $Sa_{SN}(T_1)$ , peak ground acceleration of the strike-normal component ( $PGA_{SN}$ ), the peak ground velocity of the strike-normal component ( $PGV_{SN}$ ), and peak resultant ground acceleration ( $PGA_{res}$ ).

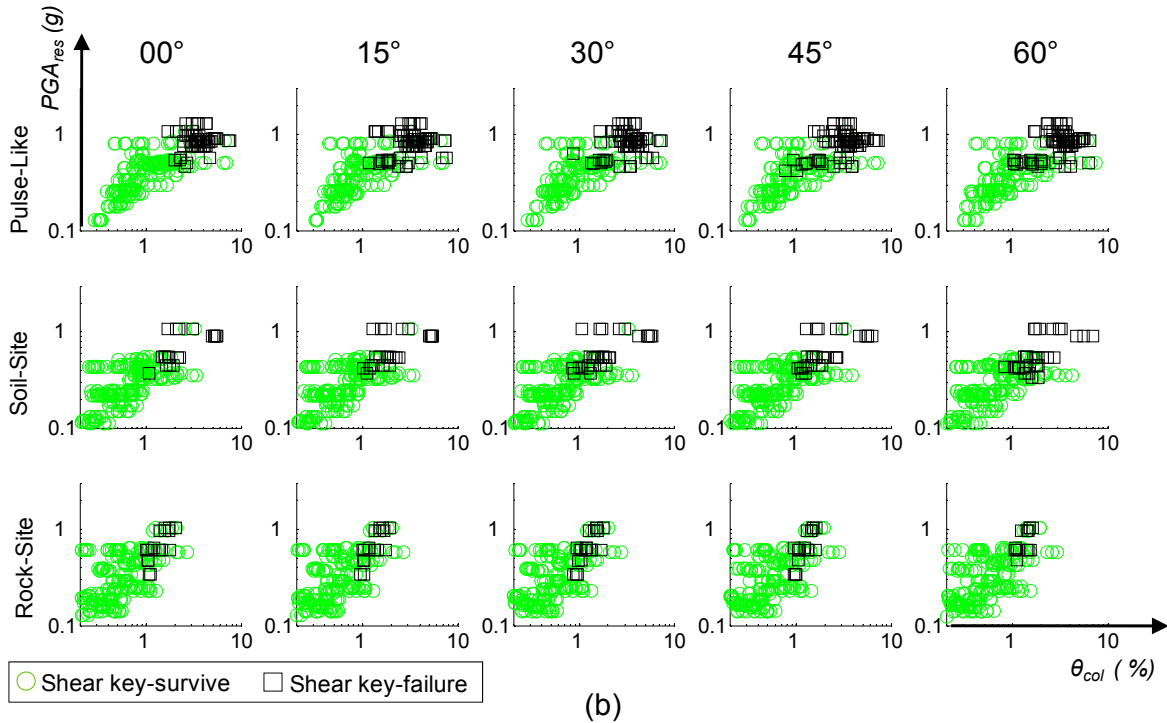


**Figure 4.3** Bridge A's response sensitivity, with original column height and symmetric spans, to type of seismic excitation and abutment skew angle for (a)  $PGA_{res}-\theta_{rot}$  and (b)  $PGA_{res}-\theta_{col}$ .

**Table 4.4** Ground motion intensity measures ( $IMs$ ) used in this study.

$IMs$	Descriptions
$Sa_{SN}(T_1)$	Spectral acceleration at the first mode period of strike-normal component
$PGA_{SN}$	Peak ground acceleration of strike-normal component
$PGA_{res}$	Peak resultant ground acceleration
$PGV_{SN}$	Peak ground velocity of strike-normal component
$PGV_{res}$	Peak resultant ground velocity

Figure 4.4 displays a sample collapse fragility curve derived for Bridge A with original column height, symmetric span, and 60° abutment skew angle, subjected to the pulse-like ground motion set. To generate this collapse fragility curve, a logistic regression was applied to the 240 data points (resulting from 40 ground motion records and 6 angles of incidence). Data points shown in Figure 4.4 are pairs of  $PGV_{res}$  and an indicator parameter, which is equal to “1” if the ground motion caused collapse and “0” otherwise. Using this approach, the collapse fragility curves of all bridges in the bridge matrix were obtained along with the median and dispersion values of fitted log-normal distributions [Shinozuka et al. 2000; Shinozuka et al. 2003].

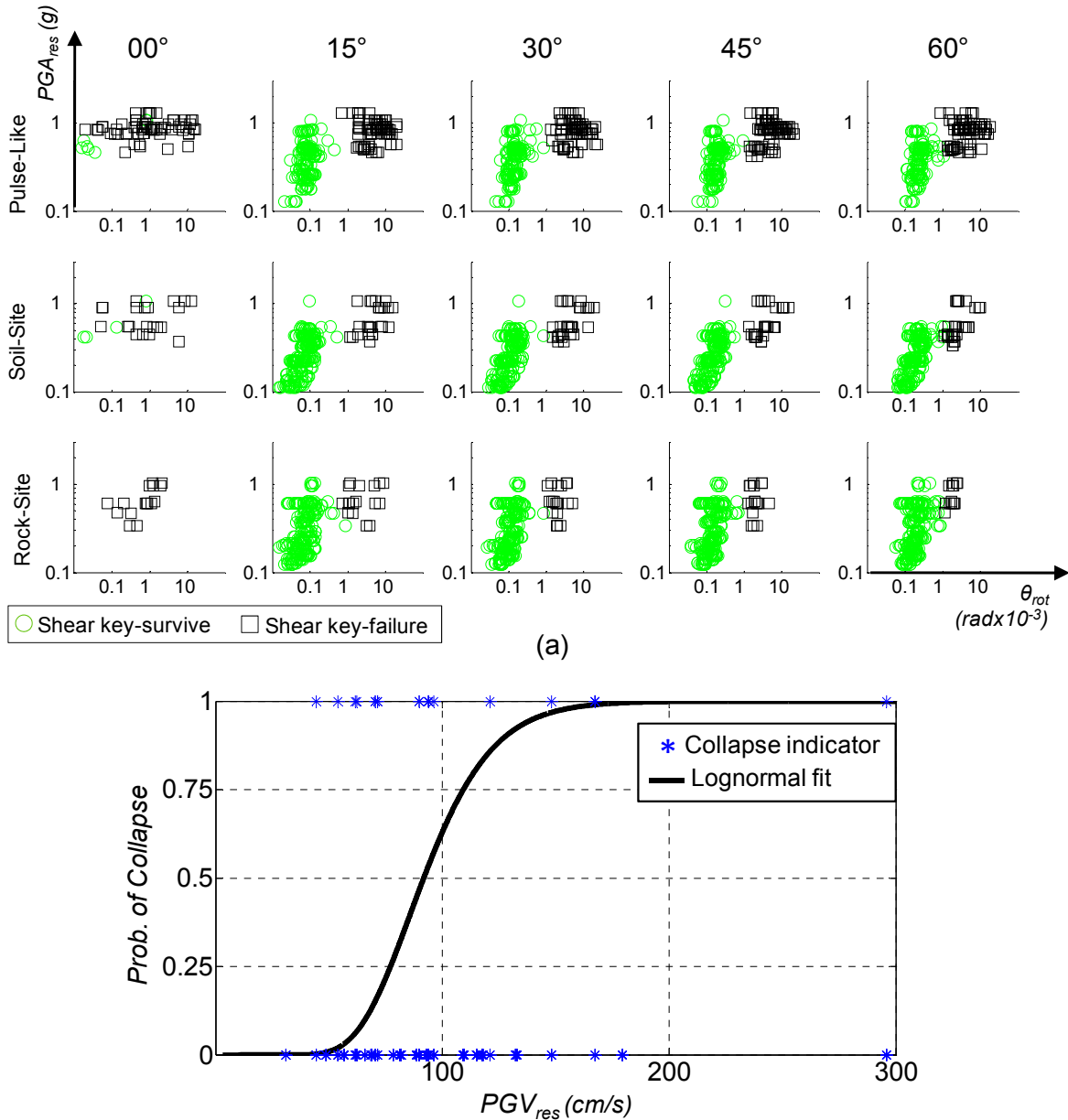


**Figure 4.4** Development of the collapse fragility curve for Bridge A (symmetrical span, original column height, 60° abutment skew angle, and pulse-like ground motion [i.e., ALS4P]).

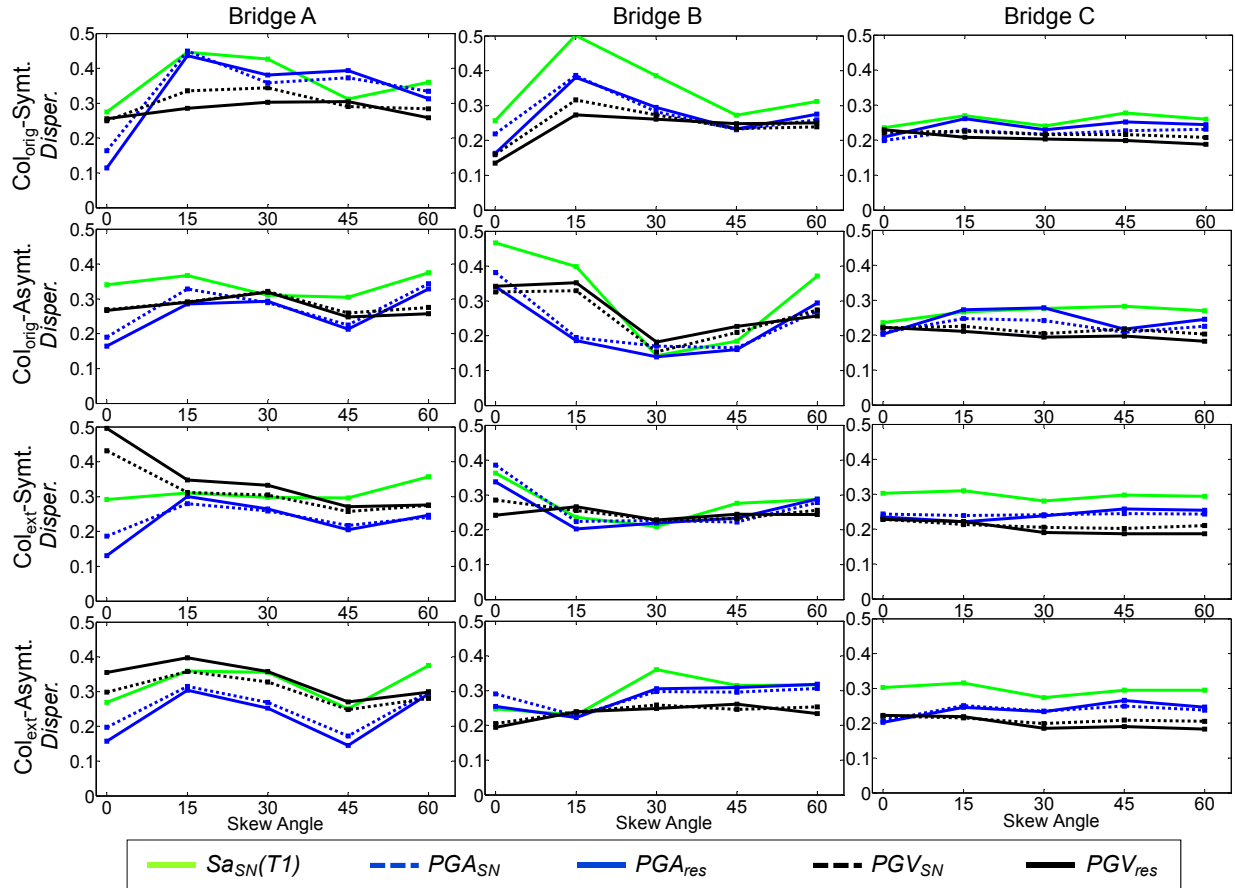


**Figure 4.5** Dispersions in collapse fragility curves obtained for the bridge matrix using the pulse-like ground motion set and using logistic regressions of data for various *IMs*.

The implication that  $PGV_{res}$  is a superior *IM* compared to other *IMs* may be deduced from Figure 4.5, which presents the dispersions of various candidate collapse-potential indicator *IMs*. Figure 4.5 displays these collapse-potential *IM* dispersions for three bridge types (A, B, and C) and four combinations of column height and span arrangements:

- Original column height with symmetric span ( $Col_{orig-Symm.}$ )
- Original column height with asymmetric span ( $Col_{orig-Asymm.}$ )
- Extended column height with symmetric span ( $Col_{ext-Symm.}$ )
- Extended column height with asymmetric span ( $Col_{ext-Asymm.}$ )

Each plot shows the dispersion as a function of assumed abutment skew angle.

These results indicate that the dispersion of collapse fragility curves—obtained using  $PGV_{res}$  as the collapse potential indicator—is consistently smaller on average than those of other *IMs* for Bridges B and C. A similar trend is observed for Bridge A; however,  $PGA_{res}$  exhibits a

smaller dispersion compared to  $PGV_{res}$  for cases with extended column height. It is clear that no single  $IM$  (i.e., no truncated/reduced model or ground motion parameter) by itself can capture all aspects of seismic hazard [Baker and Cornell 2006]; nevertheless, given the observed superiority of  $PGV_{res}$  for most cases, it will be used for identifying collapse potential and for obtaining the  $IM$ - $EDP$  curves throughout the rest of this report.

#### 4.5.1 Trends in the Statistical Parameters of Collapse Fragility Curves

Given the level of ground motion intensity, probability of collapse is sensitive to the type of seismic excitation, abutment skew angle, bridge column height, and span arrangement. Fragility curves of all bridges in the bridge matrix were developed using  $PGV_{res}$  as the collapse potential indicator and using logistic regression as described above. Figure 4.6 displays the median collapse capacity and the associated dispersion for all bridges considered, obtained by using the pulse-like ground motion set. The rock- and soil-site ground motion sets had significantly fewer instances of collapse, so these results are omitted here.

The effect of abutment skew angle on bridges' collapse potential is found to be a function of bridge type. For a single-column two-span bridge (i.e., Bridge A) the collapse potential is small at zero skew angle (note the high median collapse potential at zero skew angle for Bridge A in Figure 4.6). The median collapse potential drops for higher skew angles, exhibiting a higher probability of collapse at the same level of ground motion intensity. Bridge C, in contrast, does not show a similar correlation between the abutment skew angle and the collapse potential. This phenomenon can arguably be attributed to the type of failure resulting from the column-base boundary conditions. Based on information gathered from the structural drawings, Bridges A and C were modeled with fixed- and pinned-base boundary conditions, respectively. As a consequence, there is a high moment demand at the tops of the Bridge C columns, regardless of the abutment skew angle, which can rapidly exhaust column load-resistance capacity and lead to collapse. In contrast, Bridge A's single fixed-base column can better handle the moment demand at zero skew angle. However, for larger abutment skew angles, the bridge becomes susceptible to deck rotation, which may increase its collapse potential.

Certain combinations of abutment skew angle, column height, and span arrangement can create a condition in which the bridge is more susceptible to deck rotations, increasing the probability of collapse. Figure 4.6 shows this phenomenon for Bridge B: the median collapse potential decreases for skew angles between  $0^\circ$  and  $15^\circ$ , once original column heights and symmetric span are considered. However, for the same column size and asymmetric span, the median collapse capacity increases.

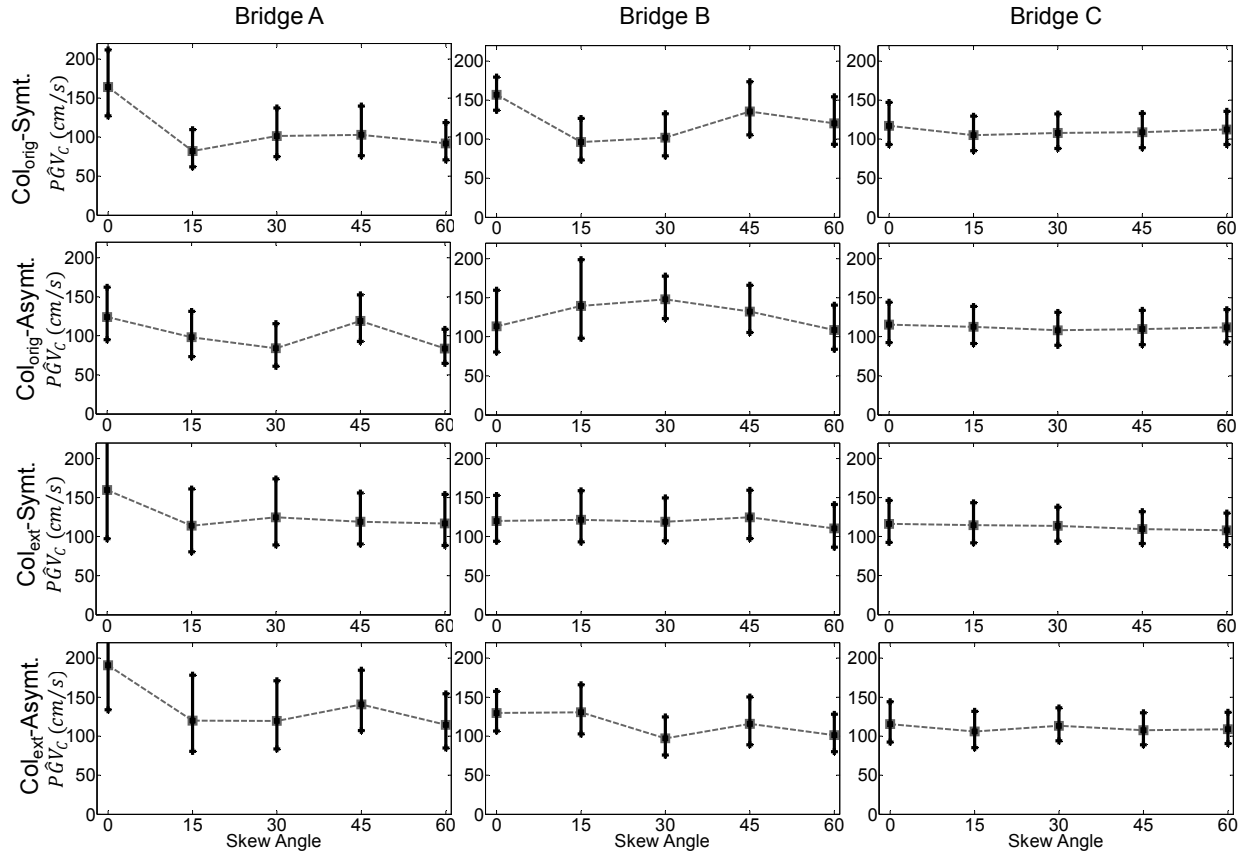


**Figure 4.6** Median and dispersion of collapse capacity, expressed in terms of  $PGV_{res}$  for the bridge matrix obtained using the pulse-like ground motion set.

#### 4.6 TREND OBSERVATIONS

To study the trends in the variations in skewed bridges' response parameters, we developed the *IM-EDP* curves, taking into consideration three seismic response parameters: maximum planar deck rotation ( $\theta_{rot}$ ), maximum abutment unseating displacement ( $\delta_{unseat}$ ), and maximum column-bent drift ratio ( $\theta_{col}$ ). The resultant peak ground velocity ( $PGV_{res}$ ) was used as the ground motion intensity measure for generating the *IM-EDP* curves.

We investigated the simulated data filtered for no-collapse bridge cases according to the collapse criteria discussed in Section 4.3. Again, based on the distinct regimes of skewed bridge behavior in relation to the shear key failure status (Chapter 3), *EDPs* were divided into two categories, based on whether the shear keys survived (green circles) or lost resistance (black squares) during seismic excitation. In each plot, we considered four combinations of column height and span arrangements—original column height with symmetric span ( $Col_{orig-Symm.}$ ), original column height with asymmetric span ( $Col_{orig-Asymm.}$ ), extended column height with symmetric span ( $Col_{ext-Symm.}$ ), and extended column height with asymmetric span ( $Col_{ext-Asymm.}$ )—for the abutment skew angles  $0^\circ$ ,  $15^\circ$ ,  $30^\circ$ ,  $45^\circ$ , and  $60^\circ$ . The response parameter

trends were studied corresponding to each *EDP* and sorted based on the seed bridges for different ground motion sets.

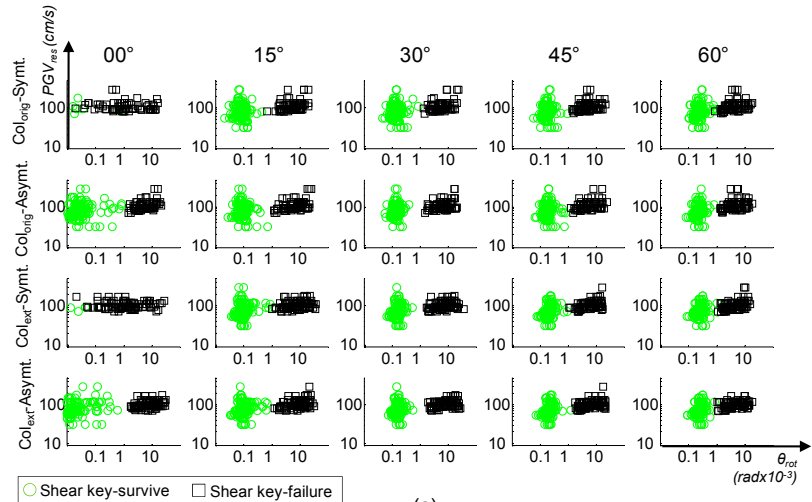
#### 4.6.1 Trends in Deck Rotation

Shear key strength has a large influence on bridge deck rotation. For larger skew angles, the probability of shear key failure—and hence, the probability of a large deck rotation—increases. Figures 4.7, 4.8, and 4.9 show the variations in  $\theta_{rot}$  for Bridges A, B, and C, respectively, as a function of  $PGV_{res}$  obtained from the pulse-like, soil-site, and rock-site ground motion sets. These figures display the sensitivity of  $\theta_{rot}$  to five variations in abutment skew angle and to various combinations of span configuration and column height. As before, the cases in each plot where shear keys survived (circles in Figure 4.7) or have lost resistance (squares) during seismic excitation are marked. Data points representing ground motions for which the bridge collapsed are not shown. Higher  $\theta_{rot}$  is expected once a shear key fails. Moreover, span arrangements appear to have less effect than column height on deck rotation demand.

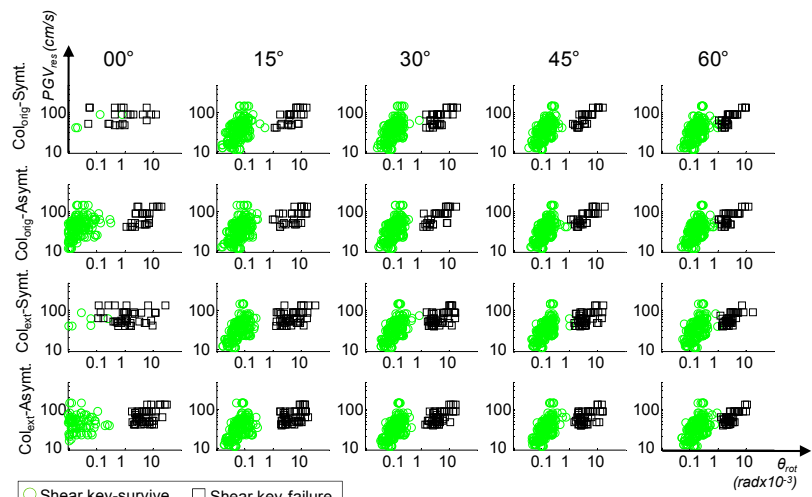
The incidence of shear key failure is higher for Bridge A (a two-span single-column bridge) than for Bridges B or C, and Bridge A's seismic response is more affected by abutment behavior than those of other bridges. Particularly for the pulse-like ground motion type, the two cases of shear key survival and failure have seemingly divided the *IM-EDP* plots into two distinct regions. However, in Bridge B, these regions overlap somewhat, suggesting that the incidences of collapse in Bridge B are not dominated by excessive deck rotations and that excessive translations play a significant role.

Deck rotations can be detected even for symmetrical bridges that have 0° skew as shown in Figure 4.7(a). These rotations are caused by column-bents that become asymmetrically damaged (concrete losing strength in tension, etc.) during the course of strong motions. Bridge column-bents and shear keys experience loads exceeding their yield capacity and behave nonlinearly. This eliminates the initial symmetry in geometry and boundary conditions, leading to the initiation of deck rotations and, in some cases, ultimately to collapse.

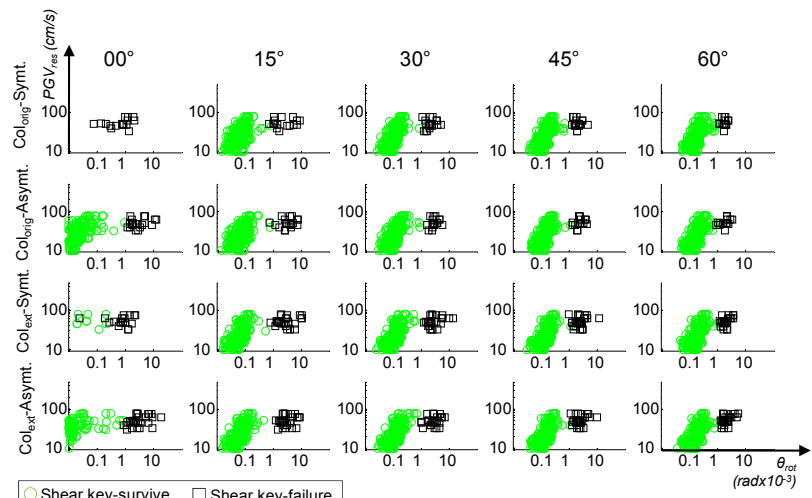
Considering ground motion type influence on shear key failure status reveals that soil-site and mainly rock-site ground motion sets, which have less  $PGV_{res}$  compared to pulse-like ground motion sets (Appendix B), caused fewer shear key failures. For instance, Figure 4.8(c) shows shear key survival for all non-collapsed analyses. This trend observation can be generalized to all studied trends in the following corresponding plots.



(a)

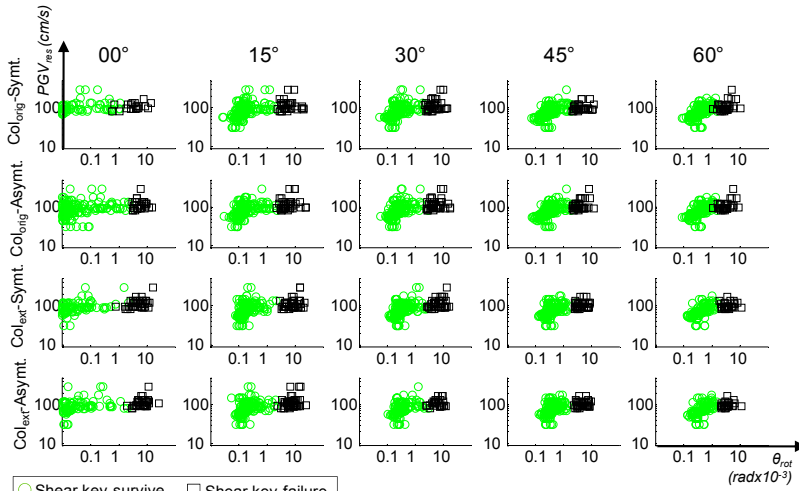


(b)

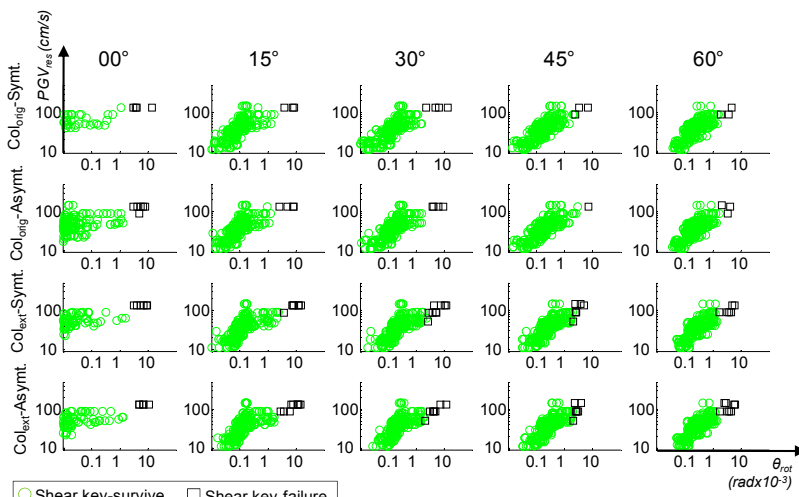


(c)

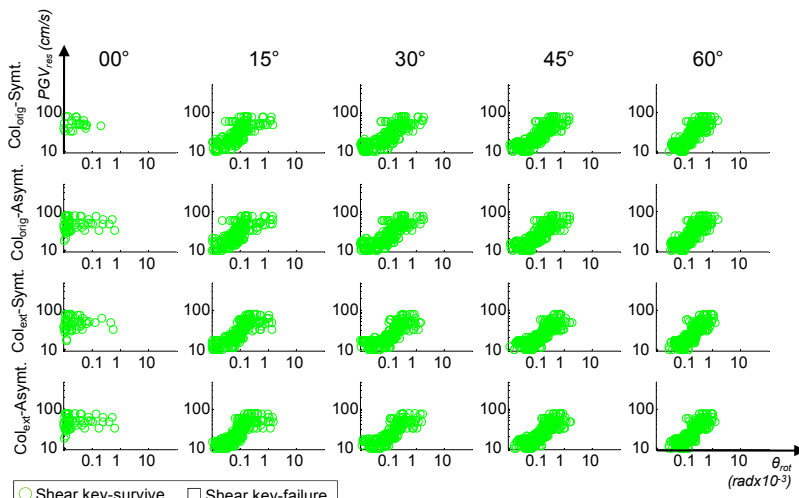
**Figure 4.7**  $\theta_{rot}$ - $PGV_{res}$  conditioned on no-collapse plots obtained for Bridge A using (a) pulse-like, (b) soil-site, and (c) rock-site ground motion sets.



(a)



(b)



(c)

Figure 4.8  $\theta_{rot}$ - $PGV_{res}$  conditioned on no-collapse plots obtained for Bridge B using (a) pulse-like, (b) soil-site, and (c) rock-site ground motion sets.

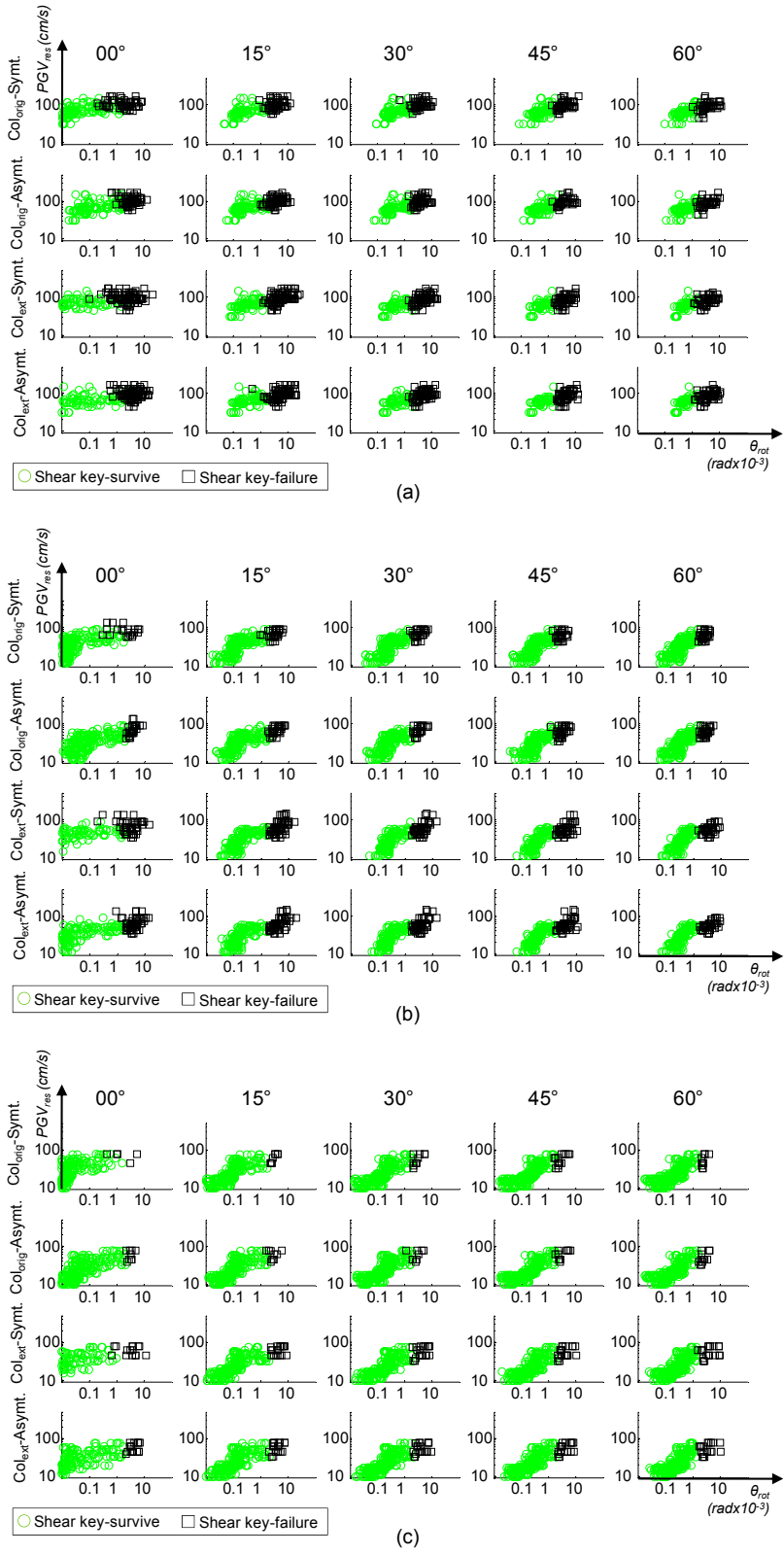


**Figure 4.9**  $\theta_{rot}-PGV_{res}$  conditioned on no-collapse plots obtained for Bridge C using (a) pulse-like, (b) soil-site, and (c) rock-site ground motion sets.

#### 4.6.2 Trends in Abutment Unseating Displacement

Figures 4.10 through 4.12 display the variation of maximum abutment unseating displacement ( $\delta_{unseat}$ ) for bridges A, B, and C, respectively. In contrast to the deck rotation trend observations, shear key strength has less effect on the bridge abutment unseating response (i.e., the points in figures are continuous). The analysis shows that geometrical properties such as abutment skews and span arrangements have only a minor influence on variations in  $\delta_{unseat}$ ; however, column-bent height effect has a significant influence. This trend suggests that, in the longitudinal direction, there is less global bridge stiffness, which was caused by column-bent height extension.

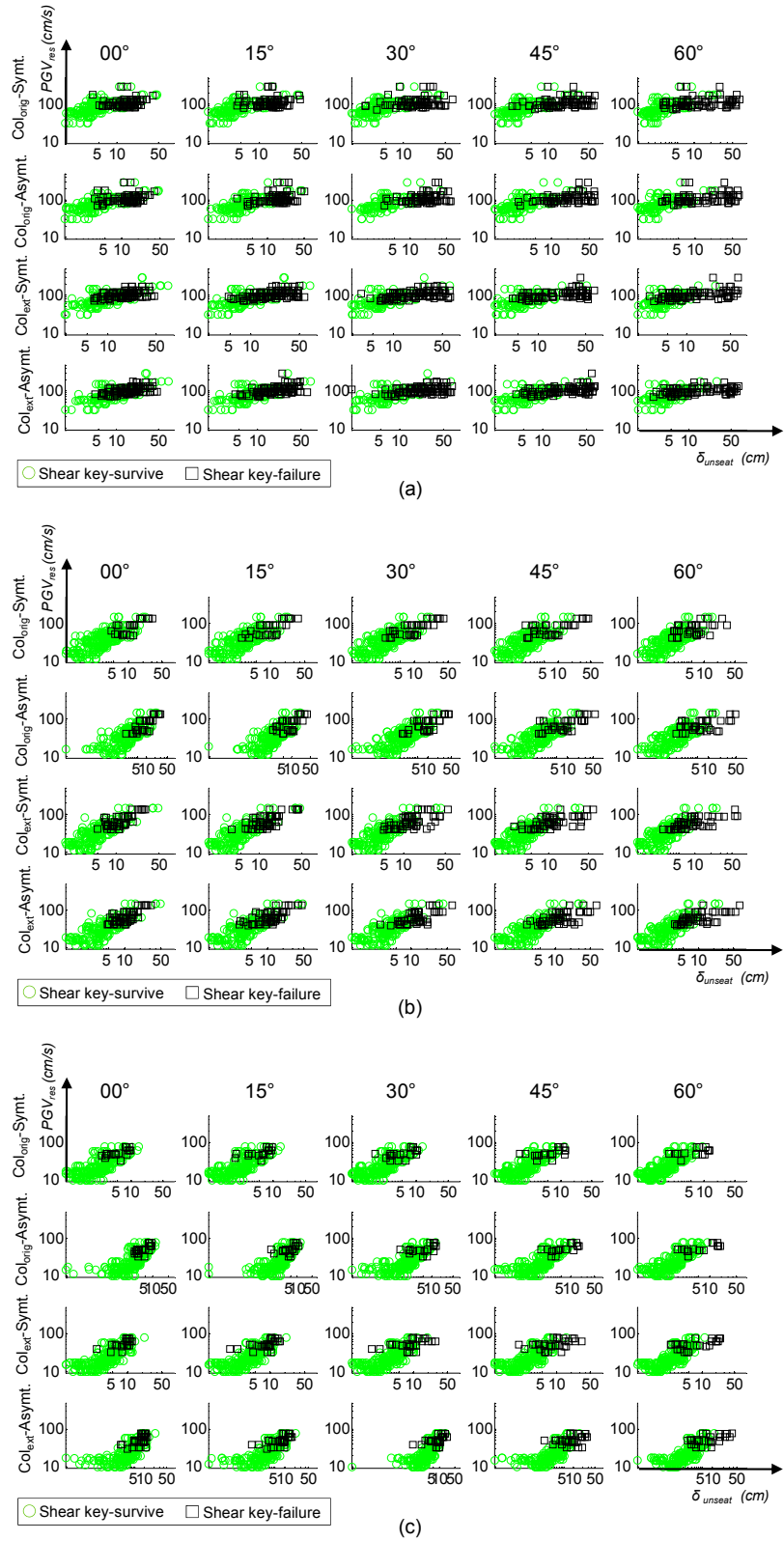


Figure 4.10  $\delta_{unseat}$ - $PGV_{res}$  conditioned on no-collapse plots obtained for Bridge A using (a) pulse-like, (b) soil-site, and (c) rock-site ground motion sets.

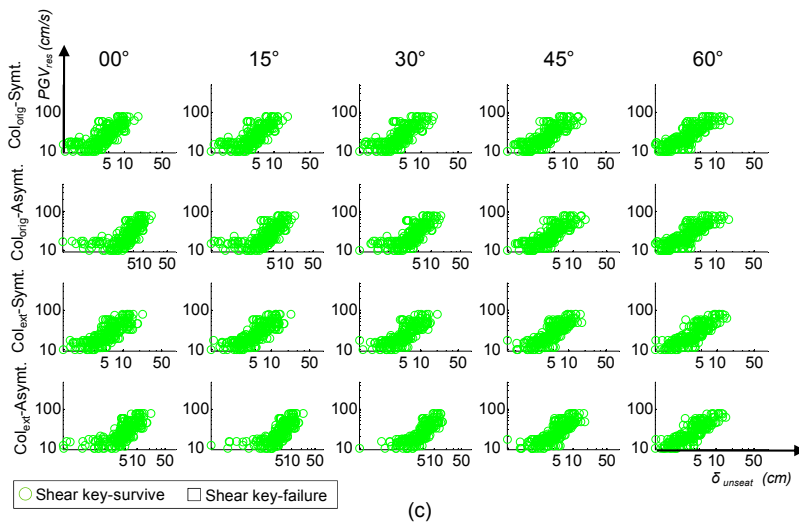
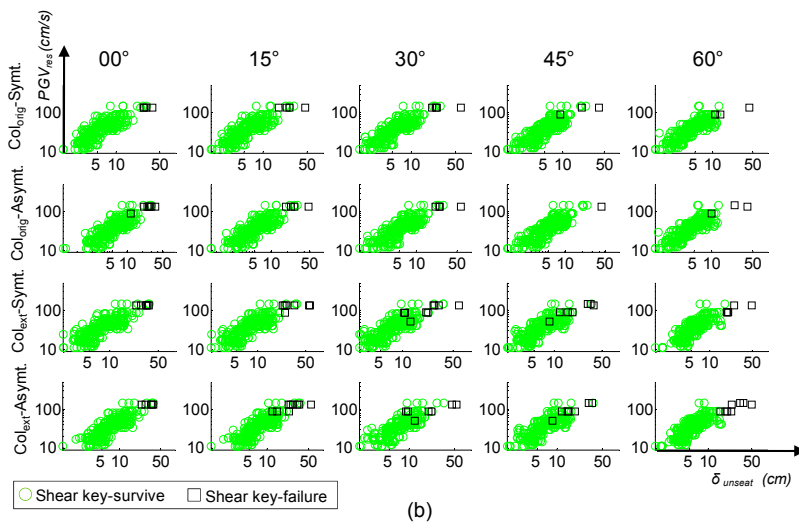
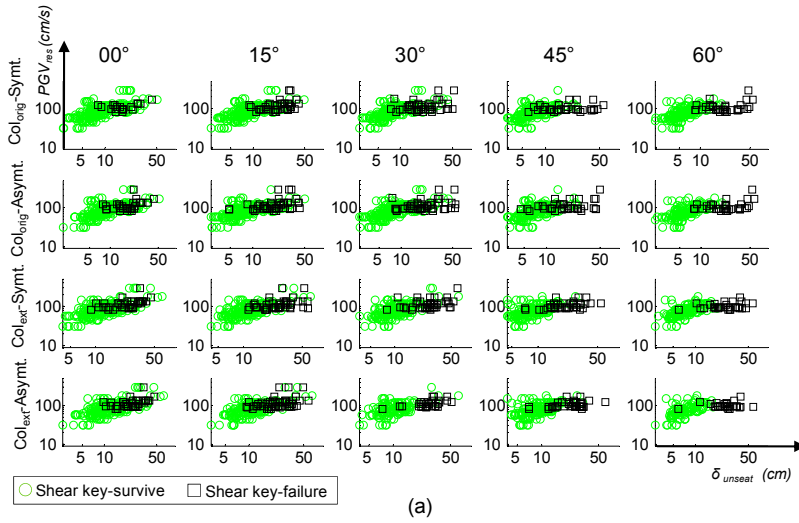


Figure 4.11  $\delta_{unsear}$ - $PGV_{res}$  conditioned on no-collapse plots obtained for Bridge B using (a) pulse-like, (b) soil-site, and (c) rock-site ground motion sets.

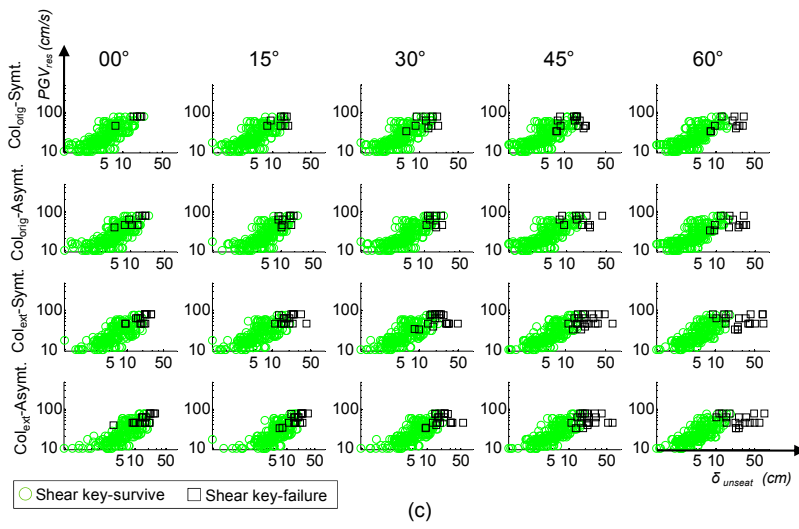
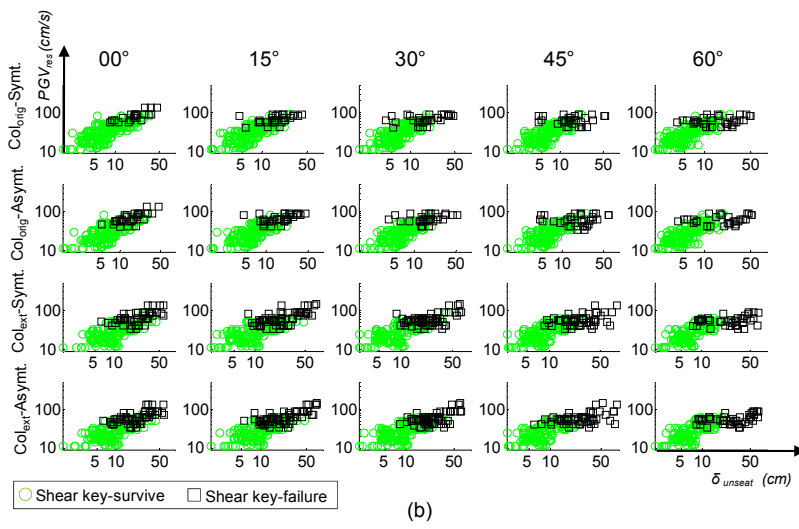
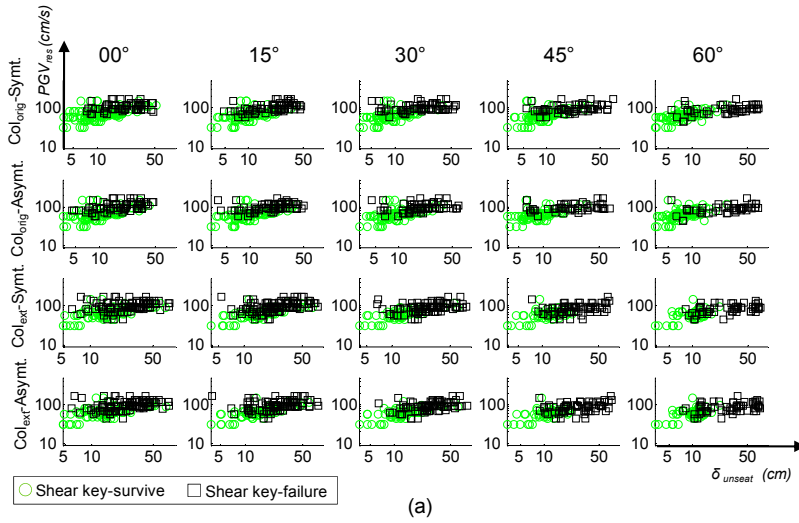


Figure 4.12  $\delta_{unsear}$ - $PGV_{res}$  conditioned on no-collapse plots obtained for Bridge C using (a) pulse-like, (b) soil-site, and (c) rock-site ground motion sets.

### 4.6.3 Trends in Column-Bent Drift Ratio

For a single-column bridge, the column drift ratio is a response parameter that depends on the bridge deck's translation in two longitudinal and transverse directions. However, in multi-column skewed bridges, deck rotation results in an additional translation of the column-top, and this can potentially increase the maximum column drift ratio for these bridges compared to their zero-skew counterparts. Figures 4.13 through 4.15 clearly display this effect, where  $PGV_{res}$  and  $\theta_{col}$  data pairs are shown for Bridges A, B, and C, respectively, for cases where collapse has not occurred.

The first row of plots in Figure 4.13(a), which is for Bridge A with symmetric spans and original column heights under pulse-like ground motion set, reveals that  $\theta_{col}$  is not sensitive to abutment skew angle. However, the first row of Figure 4.14(a), which is for Bridge B, indicates that  $\theta_{col}$  increases with the skew angle. Similar trends may be observed with a one-to-one comparison between the plots in Figures 4.13 and 4.14, where the effect of deck rotation in increasing the column drift ratio for higher skew angles in Bridge B (multi-column) or lack of it for Bridge A (single-column) is evident.

$\theta_{col}$  for Bridge C shows a behavior similar to that for Bridge A, despite the fact that Bridge C is a multi-column three-span bridge (Figure 4.15). This behavior may be attributed to Bridge C's torsional rigidity, in which the two multi-columns provide a relatively high stiffness against transverse rotation. However, given this study's modeling assumptions, which model the column bases in a multi-column with pinned connections, there is a sudden drop in stiffness once the moment capacity of the columns exceeds the yield moment capacity, at which point the bridge is likely to collapse.

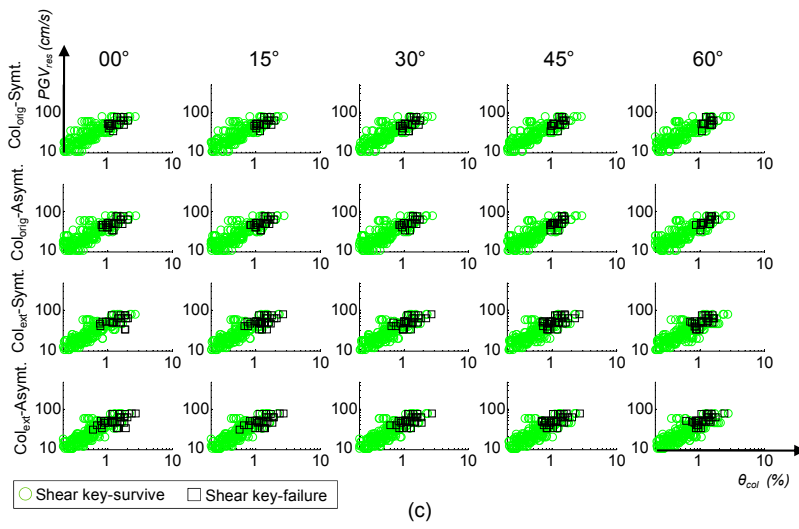
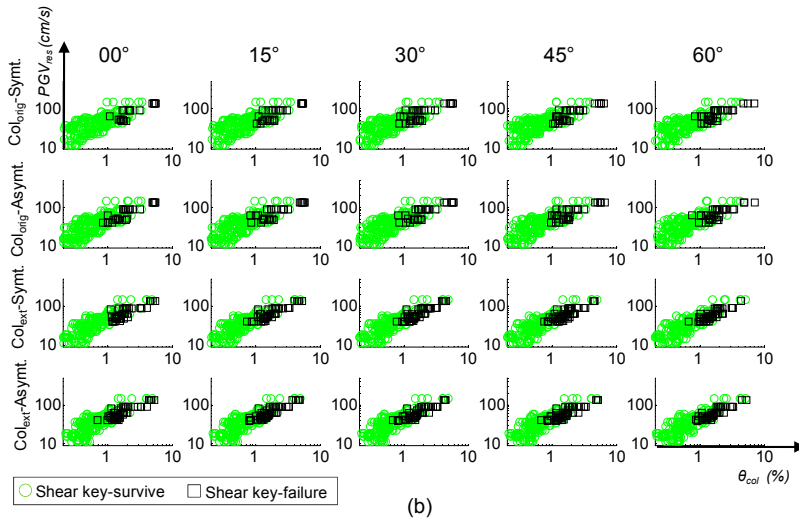
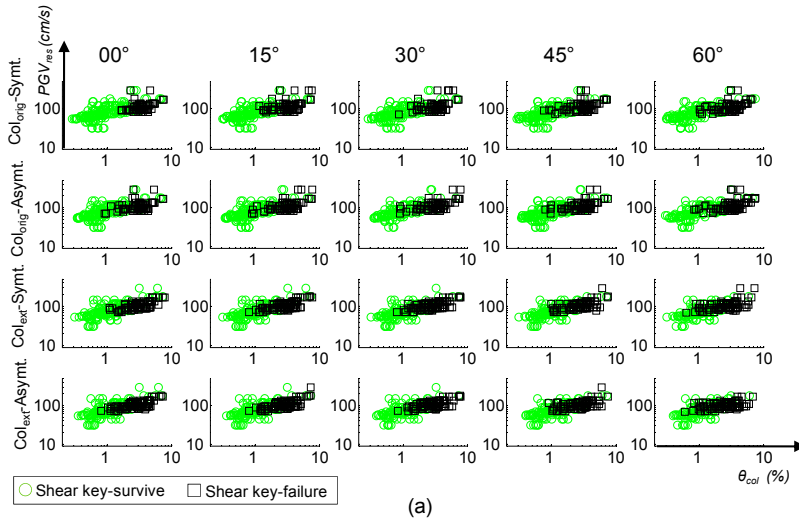
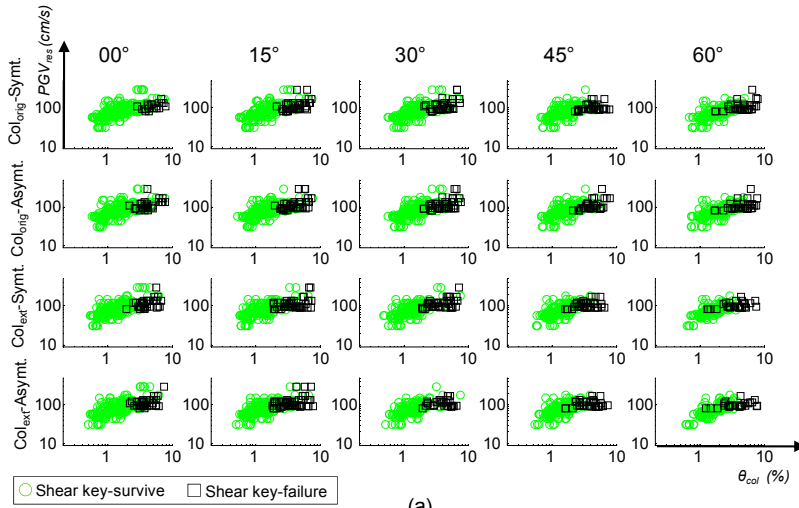
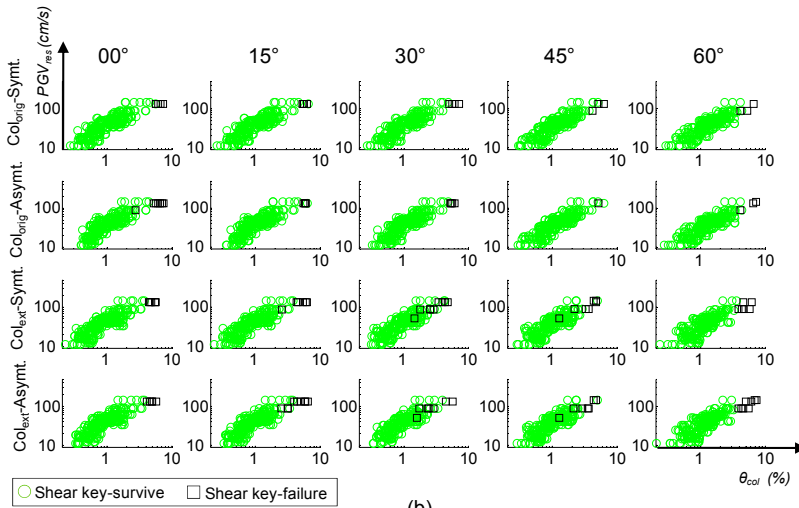


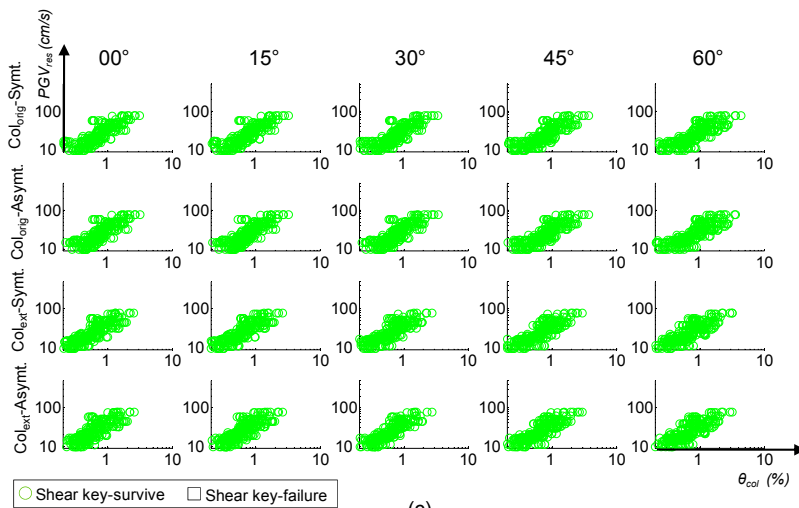
**Figure 4.13**  $\theta_{col}$ - $PGV_{res}$  conditioned on no-collapse plots obtained for Bridge A using (a) pulse-like, (b) soil site, and (c) rock-site ground motion sets.



(a)



(b)



(c)

**Figure 4.14**  $\theta_{col}$ - $PGV_{res}$  conditioned on no-collapse plots obtained for Bridge B using (a) pulse-like, (b) soil-site, and (c) rock-site ground motion sets.

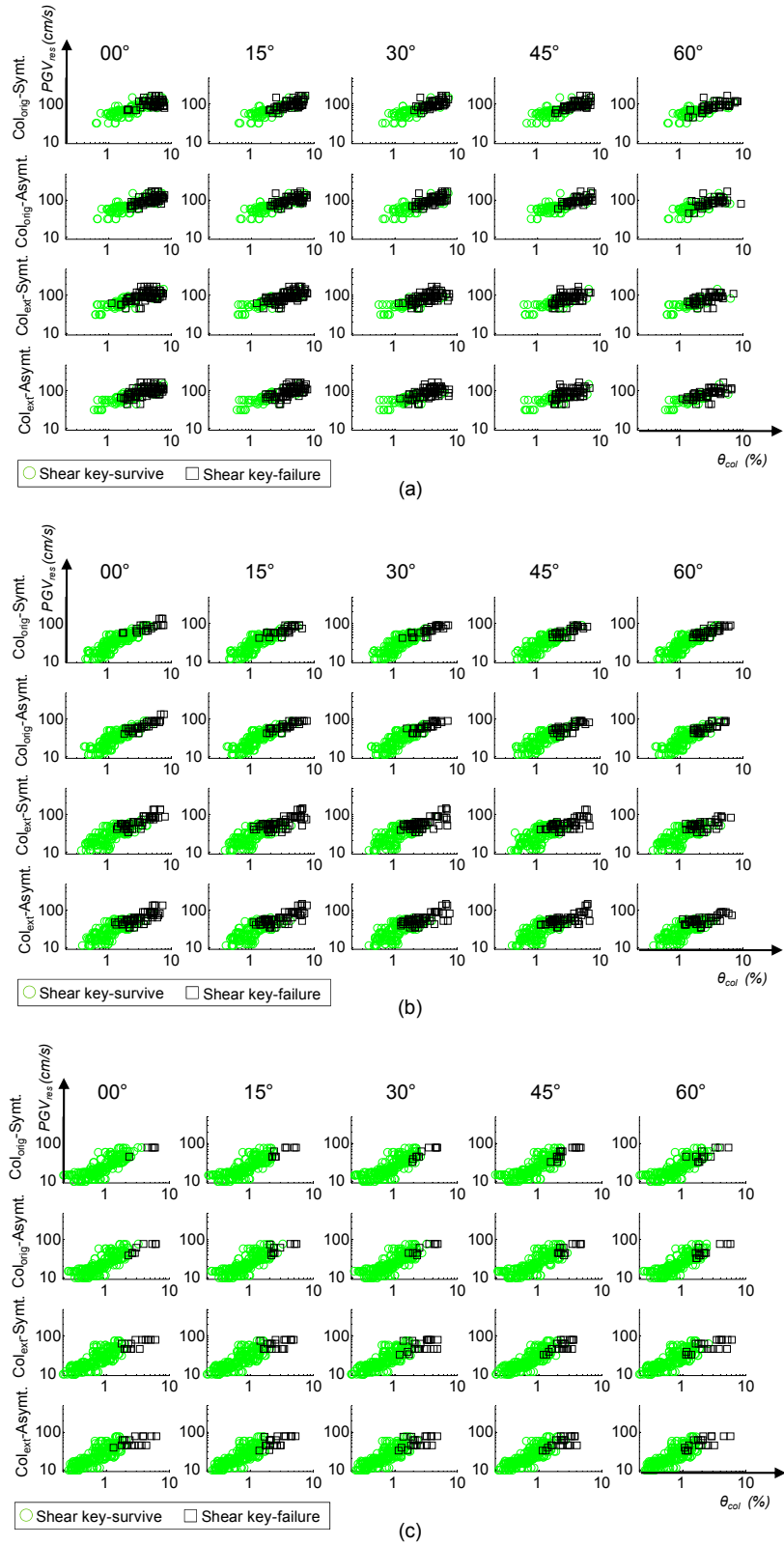


Figure 4.15  $\theta_{col}$ - $PGV_{res}$  conditioned on no-collapse plots obtained for Bridge C using (a) pulse-like; (b) soil-site; and (c) rock-site ground motion sets.



# 5 Multi-Phase Probabilistic Assessment of Structural Response to Seismic Excitations (M-PARS)

## 5.1 OVERVIEW

In recent years, probabilistic seismic response assessment methods have been the subject of significant research efforts [Shom and Cornell 1999; Cornell et al. 2002; Jalayer and Cornell 2003; Nielson 2005]. In particular, Jalayer and Cornell [2003] proposed a technical framework for performance-based earthquake engineering, which contained a closed-form formulation that uses seismic hazard information and yields an estimate of the mean annual frequency of exceeding a given seismic response. More specifically, the Jalayer-Cornell proposed formulation provides an estimate of the mean annual frequency (MAF) of failure by combining two pieces of information: (1) the *IM* and its hazard, and (2) the relation between *IM* and an *EDP* associated a predefined limit state.

In what follows, we propose an enhancement to the approach proposed by Jalayer and Cornell [2003] to account for various distinct phases of structural behavior at different ground motion intensity measures. Such a multi-phasic behavior is evident in skewed bridges (see Chapter 4), particularly in deck rotations. Lumping these distinct phases into a single assessment formula provides only a coarse probabilistic appraisal of performance and filters out some of the useful information in the process.

We propose an approach for seismic response assessment of structures that explicitly considers abrupt changes in the nature of the structure's response as the ground motion intensity measure increases. This approach—coined here as “Multi-Phase Probabilistic Assessment of Structural Response to Seismic Excitations” or M-PARS—is an enhancement to the formulation devised by Jalayer and Cornell [2003]. In this chapter, we describe and apply this method to skewed bridges.

## 5.2 M-PARS FORMULATION

The formulation of M-PARS applied to a structure with  $m$  number of phases is shown in Equation (5.1) where the complementary probability distribution function of an engineering

demand parameter given the ground motion intensity measure, denoted as  $G(EDP|IM)$ , is estimated. In Equation (5.1),  $S_{i_1 i_2 \dots i_m}$  is the phase-state indicator parameter; there are  $m$  different phases, each of which can have a finite number of states as:  $N_1, N_2, \dots, N_m$ , respectively.

$$G(EDP|IM) = P[edp > EDP|IM] = \sum_{i_1=1}^{N_1} \sum_{i_2=1}^{N_2} \dots \sum_{i_m=1}^{N_m} (P[edp > EDP|IM, S_{i_1 i_2 \dots i_m}] \times P[S_{i_1 i_2 \dots i_m}|IM]) \quad (5.1)$$

Our findings in Chapter 4 indicates that the adoption of Equation (5.1) for assessing seismic response of skew bridges requires consideration of two phases ( $m = 2$ ), each of which has two states ( $N_1 = 2, N_2 = 2$ ). The first phase is the bridge collapse phase, with two possible states: “Bridge Collapsed” and “Bridge Survived” (denoted as BC and BS, respectively). The second phase is the shear key failure phase, with two possible states: “Shear Key Failure” and “Shear Key Survived” (denoted as SKF and SKS, respectively). Table 5.1 shows the two phases and their states.

**Table 5.1 M-PARS component definitions for skewed bridges.**

State Indicator	Notation	Definition
$S_{11}$	BS-SKS	Bridge Survival plus Shear Key Survival
$S_{12}$	BS-SKF	Bridge Survival plus Shear Key Failure
$S_{21}$	BC-SKS	Bridge Collapse plus Shear Key Survival
$S_{22}$	BC-SKF	Bridge Collapse plus Shear Key Failure

For assessing skewed bridge responses based on the definitions of the two phases and their states, Equation (5.1) is reduced to Equation (5.2), which can be expanded in the form of Equation (5.3).

$$G(EDP|IM) = P[edp > EDP|IM] = \sum_{i_1=1}^2 \sum_{i_2=1}^2 (P[edp > EDP|IM, S_{i_1 i_2}] \times P[S_{i_1 i_2}|IM]) \quad (5.2)$$

$$\begin{aligned} G(EDP|IM) &= P[edp > EDP|IM] \\ &= \overbrace{P[edp > EDP|IM, S_{11}] \times P[S_{11}|IM]}^A \\ &\quad + \overbrace{P[edp > EDP|IM, S_{12}] \times P[S_{12}|IM]}^B \\ &\quad + \overbrace{P[edp > EDP|IM, S_{21}] \times P[S_{21}|IM]}^C \\ &\quad + \overbrace{P[edp > EDP|IM, S_{22}] \times P[S_{22}|IM]}^D \end{aligned} \quad (5.3)$$

To simplify the explanations that follow, we identify the terms on the right-hand side of Equation (5.3) as *A*, *B*, *C*, and *D*. Expression *A* represents the state in which the bridge has not collapsed and the shear keys have not failed (BS-SKS). Expression *B* is similar to *A*; however, at least one shear key has failed (BS-SKF). Expressions *C* and *D* represent cases where the bridge has collapsed (BC-SKS and BC-SKF), so both terms of  $P[edp > EDP|IM, S_{21}]$  and  $P[edp > EDP|IM, S_{22}]$  are equal to unity. Therefore, we can further reduce Equation (5.3) to the form given in Equation (5.4) by introducing a new probability term,  $P[BC|IM]$ , which denotes the probability of bridge collapse given *IM*, as shown in Equation (5.5). In Equation (5.4),  $P[BS - SKF|IM]$  is the probability of bridge not reaching its collapse state but shear key(s) fail given *IM*; Equation (5.4) is the simplest form of formulating a probabilistic response assessment for a skewed bridge according to the M-PARS concept. Evidently, the two main states of the shear key failure phase—namely, Shear Key Survival (SKS) and Shear Key Failure (SKF)—dominate the bridge’s seismic response in the no-collapse regime. To examine Equation (5.4), one must determine the different conditional probability quantities as noted in this equation. We show this exercise in the following sections.

$$\begin{aligned}
G(EDP|IM) &= P[edp > EDP|IM] \\
&= \{(P[edp > EDP|IM, S_{11}]) \times (1 - P[BC|IM])\} \\
&\quad \times (1 - P[BS - SKF|IM])\} \\
&\quad + \{(P[edp > EDP|IM, S_{12}]) \times (1 - P[BC|IM])\} \\
&\quad \times (P[BS - SKF|IM])\} \quad + \{P[BC|IM]\}
\end{aligned} \tag{5.4}$$

$$P[BC|IM] = 1.0 \times (P[S_{21}|IM] + P[S_{22}|IM]) \tag{5.5}$$

### 5.3 APPLICATION OF M-PARS TO SKEW BRIDGES

The application of M-PARS requires consideration of two phases of bridge behavior, each of which has two states as formulated in Equation (5.4). Figure 5.1 schematically displays the complete probabilistic seismic response assessment for a skewed bridge through M-PARS.

Four major sections are shown in Figure 5.1; from left to right, these sections are: (1) Hazard curve; (2) *EDP-IM* curves; (3) Bridge collapse fragility curve; and (4) Shear key failure fragility curve. Each of the aforementioned sections provides information about the terms in Equation (5.4) for the computation of  $G(EDP|IM)$ . In particular, *EDP-IM* curves provide information on  $P[edp > EDP|IM, S_{11}]$  and  $P[edp > EDP|IM, S_{12}]$ , the bridge collapse fragility curve provides information on  $P[BC|IM]$ , and the shear key failure fragility curve provides information on  $P[BS-SKF|IM]$ . The following subsections discuss each of the sections in Figure 5.1. We frequently switch between the general case of M-PARS and its specific

application for addressing the seismic response of skewed bridges in order to keep its broader applicability within the reader’s perspective.

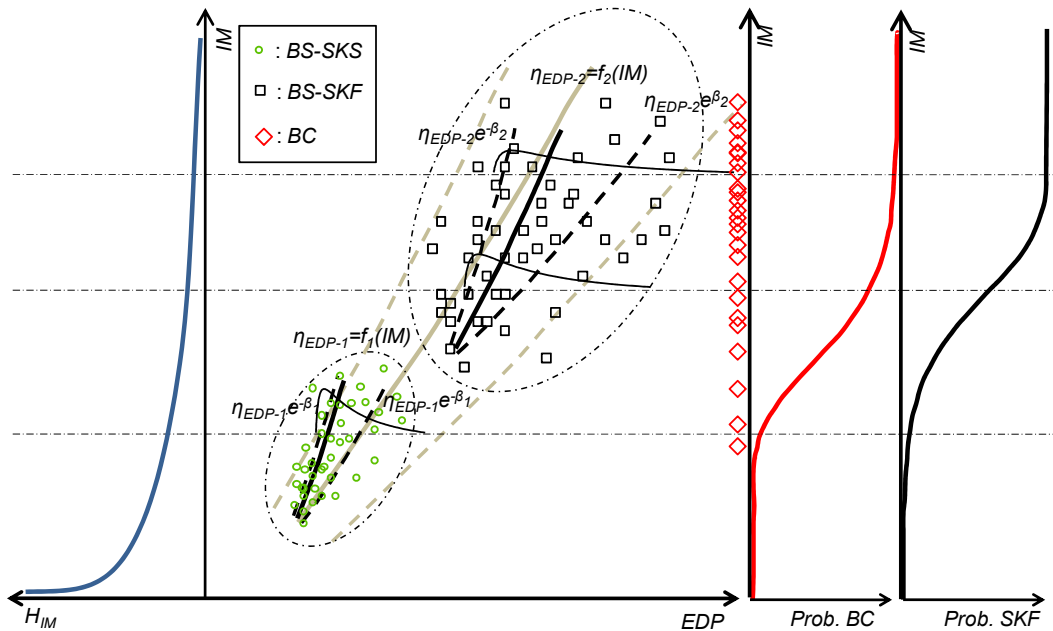


Figure 5.1 Schematic explanation of the M-PARS method.

### 5.3.1 Hazard Curve

The hazard curve,  $H_{IM}$ , defines the relationship between the ground motion hazard and a target  $IM$ . It measures the mean annual frequency of exceeding an  $IM$  value. The hazard curve for an intensity measure can be obtained using available tools, such as OpenSHA (Open Source Seismic Hazard Analysis), which is accessible online ([www.opensha.org](http://www.opensha.org)) and is based on the geographical coordinates of the structure location and some other required data that are usually structure-specific, such as the first mode period. Discussion of the seismic hazard curve is beyond the scope of this report, and the reader is referred to the wealth of information available in open literature, including, among others, Kennedy and Ravindra [1984], Kramer [1996], Field et al. [2003; 2005a], and Maechling [2005a; 2005b].

### 5.3.2 Relationship Between Selected $EDP$ and $IM$

The structural demands ( $EDPs$ ) derived from response history analyses using several ground motions are shown as scattered points in the  $EDP-IM$  plot. We split this data according to pre-defined phases of the structural seismic response. The seismic response of skewed bridges is categorized here into two phases of behavior, each of which has also two states. As shown in Equation (5.3), this results in four combinations of conditions that are mutually exclusive and collectively exhaustive. Practically, the number of combinations is reduced from four to three given the simplification recognized in Equation (5.5), which combines the two combinations in which the bridge collapses. Two of these combinations can be shown in the  $EDP-IM$  section of

Figure 5.1, which represents combinations in which the bridge has not collapsed. The first combination is *no-collapse plus shear key survival*,  $S_{11}$ , and the other is *no-collapse plus shear key failure*,  $S_{12}$ . In Figure 5.1, the *EDP-IM* pairs from the response history analysis of a bridge that did not collapse and where the shear key survived are shown in gray circles (green in color print). The *EDP-IM* pairs from the analyses that resulted in shear key failure are shown as black squares.

For a given level of ground motion intensity,  $IM$ , the estimate of *EDP* will show two types of variability: aleatory and epistemic. This study is concerned only with aleatory variability in estimating *EDPs* for a given  $IM$ , which is also known as record-to-record variability. Figure 5.1 indicates that the variability in the estimation of *EDP* for a given  $IM$  is recognized by the scatter in the results shown in the combination of two conditions of  $S_{11}$  and  $S_{12}$ .

To obtain  $P[edp > EDP|IM, S_{11}]$  and  $P[edp > EDP|IM, S_{12}]$ , we show a functional relationship between the conditional *EDPs*—that is,  $EDP|S_{11}$  and  $EDP|S_{12}$ , and  $IM$ . We begin this discussion by identifying the median of conditional *EDPs* given  $IM$ , while later paragraphs graduate to discussing the dispersion in such estimations. The medians of conditional *EDPs* given  $IM$  are denoted as  $\eta_{EDP|S_{11},IM}$ , and  $\eta_{EDP|S_{12},IM}$ , and are obtained using the data derived from response history analyses. Equations (5.6) and (5.7) show the conditional medians in a mathematical format.

$$\eta_{EDP|S_{11},IM}(x) = f_{11}(x) \quad (5.6)$$

$$\eta_{EDP|S_{12},IM}(x) = f_{12}(x) \quad (5.7)$$

We have tried to introduce a functional relationship that can both match our observations of the bridge seismic response curve and simplify future analytical efforts. We have employed linear regression in logarithmic space with the format shown in Equations (5.8) and (5.9) for states  $S_{11}$  and  $S_{12}$ , respectively. This method is introduced in order to fit a power-law function [Equations (5.10) and (5.11)] to data of *EDP* and  $IM$  pairs. In Equations (5.8) through (5.11),  $a_0$  and  $a_1$  are the coefficients of regression for the corresponding states.

$$\ln \eta_{EDP|S_{11},IM}(x) = \ln a_{0S_{11}} + a_{1S_{11}} \ln x \quad (5.8)$$

$$\ln \eta_{EDP|S_{12},IM}(x) = \ln a_{0S_{12}} + a_{1S_{12}} \ln x \quad (5.9)$$

$$\eta_{EDP|S_{11},IM}(IM) = a_{0S_{11}} \cdot IM^{a_{1S_{11}}} \quad (5.10)$$

$$\eta_{EDP|S_{12},IM}(IM) = a_{0S_{12}} \cdot IM^{a_{1S_{12}}} \quad (5.11)$$

We can account for the variability of the data shown in Figure 5.1 by constructing a full probabilistic model as shown in Equations (5.12) and (5.13), where  $\varepsilon_{S_{11}}$  and  $\varepsilon_{S_{12}}$  are random variables with a log-normal probabilistic distribution (based on observation of data) with a median equal to unity, as shown in Equations (5.14) and (5.15), respectively. The term  $\eta_{\varepsilon_{S_{11}}}$  denotes the median values of  $\varepsilon_{S_{11}}$ ,  $\sigma_{\ln(\varepsilon_{S_{11}})}$  is the standard deviation of  $\ln \varepsilon_{S_{11}}$ , and

$\beta_{EDP|S_{11},IM}$  is the dispersion of data. For the  $S_{12}$  combination, similar values apply to  $\eta_{\varepsilon_{S_{12}}}, \varepsilon_{S_{12}}, \sigma_{\ln(\varepsilon_{S_{12}})}$ , and  $\beta_{EDP|S_{12},IM}$ .

$$EDP|S_{11},IM = \eta_{EDP|S_{11},IM}(x) \cdot \varepsilon_{S_{11}} = f_{11}(x) \cdot \varepsilon_{S_{11}} \quad (5.12)$$

$$EDP|S_{12},IM = \eta_{EDP|S_{12},IM}(x) \cdot \varepsilon_{S_{12}} = f_{12}(x) \cdot \varepsilon_{S_{12}} \quad (5.13)$$

$$\begin{cases} \eta_{\varepsilon_{S_{11}}} = e^{mean((\ln \varepsilon_{S_{11}}))} = 1 \\ \sigma_{\ln(\varepsilon_{S_{11}})} = \beta_{EDP|S_{11},IM} \end{cases} \quad (5.14)$$

$$\begin{cases} \eta_{\varepsilon_{S_{12}}} = e^{mean((\ln \varepsilon_{S_{12}}))} = 1 \\ \sigma_{\ln(\varepsilon_{S_{12}})} = \beta_{EDP|S_{12},IM} \end{cases} \quad (5.15)$$

By substituting Equation (5.10) in Equation (5.12), we obtain Equation (5.16), which is an expression for computing  $P[edp > EDP|IM, S_{11}]$ . Similarly, by substituting Equation (5.11) in Equation (5.13), Equation (5.17) is obtained to estimate  $P[edp > EDP|IM, S_{12}]$ . In Equations (5.16) and (5.17),  $\varepsilon_{S_{11}}$  and  $\varepsilon_{S_{12}}$  are log-normal variables; therefore,  $EDP|IM, S_{11}$  and  $EDP|IM, S_{12}$  are variables with log-normal distributions whose statistical properties are shown in Equations (5.18) and (5.19), respectively.

$$EDP|S_{11}(IM) = a_{0S_{11}} \cdot IM^{a_{1S_{11}}} \cdot \varepsilon_{S_{11}} \quad (5.16)$$

$$EDP|S_{12}(IM) = a_{0S_{12}} \cdot IM^{a_{1S_{12}}} \cdot \varepsilon_{S_{12}} \quad (5.17)$$

$$\begin{cases} \eta_{EDP|S_{11},IM} = a_{0S_{11}} \cdot IM^{a_{1S_{11}}} \\ \sigma_{\ln(\varepsilon_{S_{11}})} = \beta_{EDP|S_{11},IM} \end{cases} \quad (5.18)$$

$$\begin{cases} \eta_{EDP|S_{12},IM} = a_{0S_{12}} \cdot IM^{a_{1S_{12}}} \\ \sigma_{\ln(\varepsilon_{S_{12}})} = \beta_{EDP|S_{12},IM} \end{cases} \quad (5.19)$$

Figure 5.1 graphically presents the variability of  $EDP$  for a given  $IM$ , and the conditional log-normal distribution that is fitted to the data, together with the hazard curve. For each combination of  $S_{11}$  and  $S_{12}$ , the median of  $EDP$  times the exponential of the conditional dispersion is referred to as the “median plus one sigma” curve, as it corresponds to the 84<sup>th</sup> percentile of the data for a log-normal variable. Similarly, the conditional median  $EDP$  divided by the exponential of the conditional dispersion is referred to as the “median minus one sigma” curve, as it corresponds to the 16<sup>th</sup>-percentile of the data.

Figure 5.2 reveals the benefit of using the M-PARS approach, in which the response assessment explicitly recognizes the multi-phasic nature of a skewed bridge’s behavior, in contrast to the older method, which does not consider phases. We have applied the process for obtaining  $EDP|IM$  to one of the bridges in the bridge matrix, coded as AHA3P. This bridge has the following properties: two spans with a single column, high column height, asymmetric span,

and 45° abutment skew angle. Figure 5.2(a) shows the nature of the M-PARS method’s response assessment, and Figure 5.2(b) shows the response assessment using an older method by Jalayer and Cornel [2003]. The  $EDP$  selected is column drift ratio (CDR); and  $PGV_{res}$  is considered as the  $IM$ . Figure 5.2 shows that the consideration of shear key failure as one phase enables the assessment to exhibit less dispersion. Figure 5.2 suggests that dividing the  $EDP-IM$  no-collapse domain into two states according to shear key failure can significantly reduce the bias in estimating  $EDP$  for a given  $IM$ .

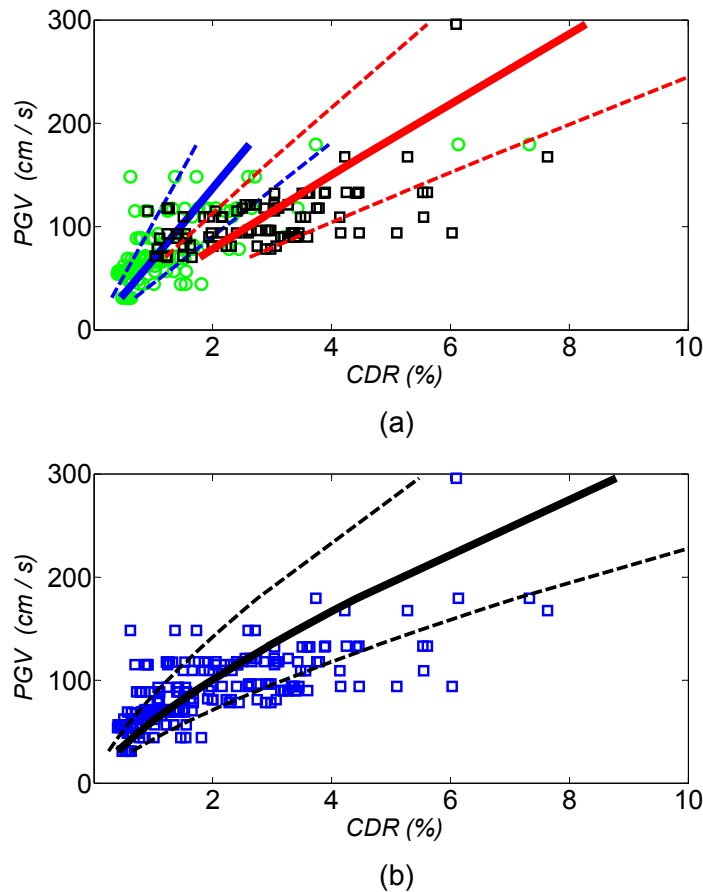


Figure 5.2  $EDP-IM$  regression (AHA3P) using (a) multi-phase and (b) mono-phase.

### 5.3.3 Fragility Curve

In general, the structural fragility for a specified limit state is defined as exceeding the probability of the limit-state capacity for a given  $IM$  level. As a general format, structural fragility can be formulated as shown in Equation (5.20), where  $F_{LS}(im)$  is the structural fragility at intensity measure of  $im$  for the limit state of  $LS$ , and  $IM_C$  is the random intensity measure capacity. Structural fragility can also be expressed as the cumulative distribution function of the random capacity  $IM_C$ . As shown in Figure 5.1, the M-PARS approach defines two fragility curves: bridge collapse (BC) and shear key failure (SKF). The following discussion briefly outlines the approach to constructing each fragility curve.

$$F_{LS}(im) = P[IM \geq IM_C | IM = im] = P[im \geq IM_C] \quad (5.20)$$

For each bridge in the bridge model matrix and ground motion types, we can obtain a total of 240 *EDP-IM* pairs from response history analyses (40 GMs times 6 incident angles). Based on the collapse criteria discussed in Section 4.3, the 240 response history analyses of each set can be categorized into two states: bridge collapsed (BC) with an indicator  $I_{BC} = 1$ , and bridge survived (BS) with an indicator  $I_{BC} = 0$ . Fitting a log-normal distribution to the bridge collapse indicator points that are scattered along the considered intensity measure enables us to obtain the bridge collapse fragility curve. We can construct the fragility curve for shear key failure, similar to the bridge collapse fragility curve using the data associated with  $I_{BC} = 0$  (i.e., cases where collapse has not happened).

Figure 5.3 illustrates the fragility curves for one of the bridges in the bridge model matrix (AHA3P). This figure displays the collapse fragility curve using a continuous red line and the shear key failure fragility curve with a black dashed line. The median collapse capacity in terms of  $PGV_{res}$  is higher than the median of shear key capacity.

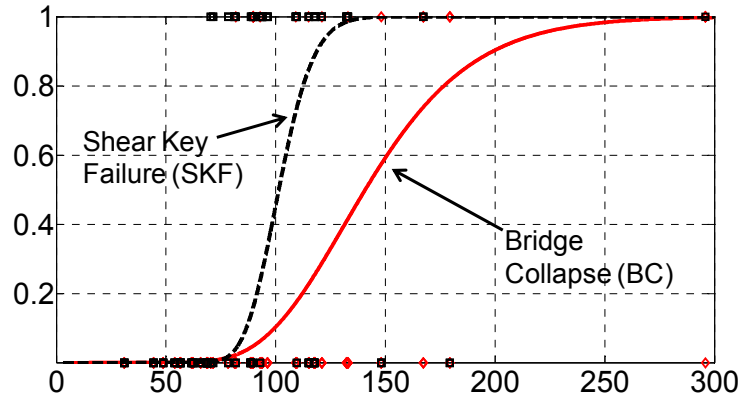


**Figure 5.3** Development of fragility curve (AHA3P) using (a) multi-phase and (b) mono-phase.

### 5.3.4 Steps for Implementing M-PARS

The step-by-step procedure for applying the M-PARS approach is as follows:

1. Obtain a model for the target bridge and select ground motion sets representative of the region's seismicity.
2. Perform nonlinear response history analyses using the bridge model and ground motion set to obtain pairs of *IM-EDPs*.
3. Use the extracted data from the response history analysis to obtain *IM-EDP* curves for each response phase, collapse fragility curves, and shear key failure fragility curves.
4. Compute  $G(EDP|IM)$  using Equation (5.4).

## 5.4 M-PARS STATISTICAL PARAMETERS FOR THE BRIDGE MATRIX USED IN THIS STUDY

We have analyzed the bridge model matrix described in Chapter 2 to obtain a database of statistical parameters required for exercising Equation (5.4). A complete set of statistical parameters for these bridges is shown in the tables in Appendix E. These tables provide the statistical parameters of three considered *EDPs*: deck rotation, abutment unseating, and column drift ratio. In the tables referenced in Appendix E, the coefficients  $a_{0S_{11}}$  and  $a_{1S_{11}}$ , mentioned in Equation (5.8), are tabulated under  $a_0$  and  $a_1$  for the  $S_{11}$  state (bridge survival-shear key survival). Similarly,  $a_{0S_{12}}$  and  $a_{1S_{12}}$ , mentioned in Equation (5.9), are tabulated under  $a_0$  and  $a_1$  for the  $S_{12}$  state (bridge survival-shear key failure). Each fit's dispersion is shown by  $\beta_{S_{11}}$  (i.e.,  $\beta_{EDP|S_{11},IM}$ ) and  $\beta_{S_{12}}$  (i.e.,  $\beta_{EDP|S_{12},IM}$ ), respectively. The last four columns of the tables show the median ( $\eta_{BC}$  and  $\eta_{SKF}$ ) and dispersion ( $\beta_{BC}$  and  $\beta_{SKF}$ ) of the bridge collapse (BC) and shear key failure (SKF) fragility curves. Blank cells in the tables show that no meaningful value could be assigned for that parameter.

## 5.5 CASE STUDIES USING M-PARS

We demonstrate the advantage of using the M-PARS method for estimation of  $G(EDP|IM)$  for a case study compared to the traditional method. The intention is to exercise Equation (5.4) using the information tabulated in Appendix E. We focus on three *EDPs*: deck rotation, abutment unseating displacement, and column drift ratio. This exercise uses peak ground velocity-resultant ( $PGV_{res}$ ) as the *IM*. To investigate the effect of the abutment skew angle on the induced demands, we seek  $G(EDP|IM)$  for abutment skew angles equal to  $0^\circ$ ,  $15^\circ$ ,  $30^\circ$ ,  $45^\circ$ , and  $60^\circ$ .

### 5.5.1 Seismic Hazard Level

We consider estimating  $G(EDP|IM)$  at an *IM* level associated with 2,500-year return period (i.e., 2% probability of exceeding in 50 years). We focus on three different sites located in California (see Table 5.2):

1. A site in the city of San Fernando, which is a site that is close to a fault zone (i.e., near field).
2. A site in the city of Ripon, which can be counted as a far field site, on soil.
3. A site in the city of Ripon, similar to site 2, but with stiff soil.

We employ OpenSHA [Field et al. 2003] to calculate the seismic hazard curves using Campbell and Bozorgnia's [2008] *PGV* attenuation relation (the random component is considered). We assume  $V_{s30} = 656$  ft/sec (200 m/sec) and  $PGV_{res} = 33$  in./sec (85 cm/sec) for Site 1,  $V_{s30} = 656$  ft/sec (200m/sec) and  $PGV_{res} = 22$  in./sec (55 cm/sec) for Site 2, and  $V_{s30} = 2,493$  ft/sec (760 m/sec) and  $PGV_{res} = 10$  in./sec (25 cm/sec) for Site 3.

We envision using the results obtained from nonlinear analysis of the bridge matrix used in this study in the following fashion: results from the "near-field" ground motion set for Site 1,

results from the “soil-site” ground motion set for Site 2, and results from the “rock-site” ground motion set for Site 3.

**Table 5.2 PGV corresponding to a hazard level of 2% in 50 years.**

GM Type	Distance	Location	$V_{s30}$	$PGV_{res}$
Pulse-like	Near-field	City of San Fernando	656 ft/sec (200 m/sec)	33 in./sec (85 cm/sec)
Soil site	Far-field	City of Ripon	656 ft/sec (200 m/sec)	22 in./sec (55 cm/sec)
Rock-site	Far-field	City of Ripon	2,493 ft/sec (760 m/sec)	10 in./sec (25 cm/sec)

### 5.5.2 $G(EDP|IM)$ Probability Representation

For each  $EDP$  under consideration, we separately study the  $G(EDP|IM)$  curves derived using the M-PARS approach. Each of the following figures includes four plots, and each plot displays  $G(EDP|IM)$  for a combination of column heights and span arrangements. Within each plot, five series show  $G(EDP|IM)$  for five different abutment skew angles. Given the discussion in Subsection 6.5.1 about the seismic hazard used in this exercise,  $G(EDP|IM)$  for two soil-site and rock-site ground motion sets are comparable. However, the  $G(EDP|IM)$  for the pulse-like ground motion set can only reflect the near-to-fault effects on the studied bridges.

Figures 5.4 through 5.6 display  $G(EDP|IM)$ , where the  $EDP$  is the deck rotation ( $\theta_{rot}$ ) for Bridges A, B, and C, respectively. All bridges exhibit more sensitivity to the abutment skew angle for pulse-like ground motions compared to other ground motion types. The probability of bridge collapse due to soil-site ground motions is larger than that for rock-site ground motions.

A high probability of collapse can result in high values for  $G(\theta_{rot}|IM)$ , even at small  $\theta_{rot}$  values. This condition is particularly evident in the lower right corner of Figure 5.5(b), which shows the data for a two-span multi-column bridge with high columns and asymmetric spans whose abutment skew angle is equal to  $45^\circ$  and is subjected to ground motions on a soil-site. This type of behavior can be also observed for other  $EDPs$  with identical geometrical and ground motion properties.

Large deck rotations can be detected for Bridge C, whose larger induced seismic demands result from the column-bent foundation modeling assumption employed in this study. As discussed in Chapter 3, we consider a simple support boundary condition for multi-column bridges—an assumption that forces a plastic hinge on the column-top. Therefore, such bridges’ column-bents are more vulnerable than those with fixed column-bases for the single-column bridges. The two-phase seismic response behavior is more detectable in Bridge C, as evidenced by the two visible differences in the curvatures of the curves shown in Figure 5.6. For the range of deck rotations ( $\theta_{rot}$ ) that occur with shear key failure (SKF), smaller curvatures are observed.

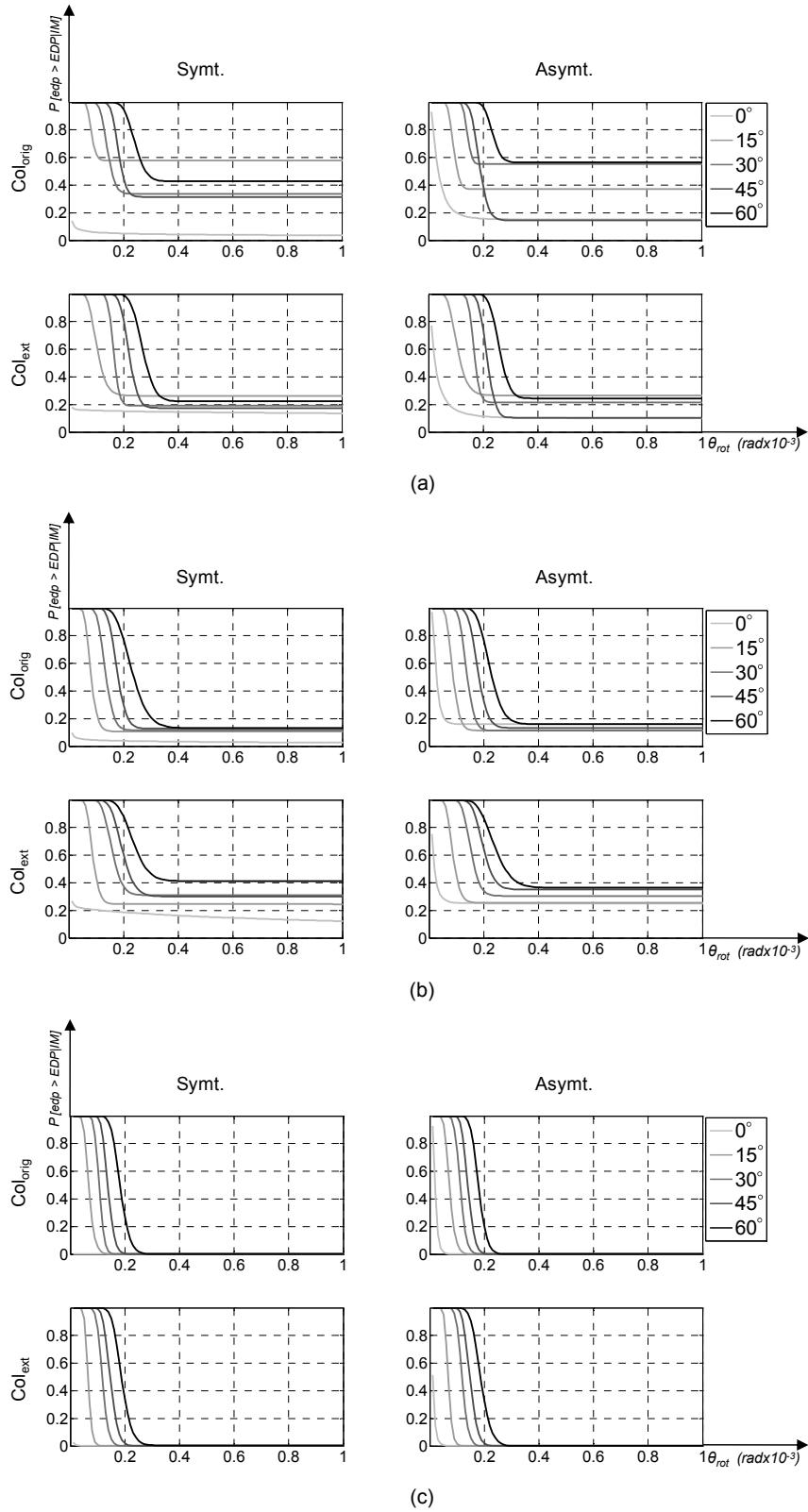


Figure 5.4  $\theta_{rot}$ -probability curves for Bridge A using (a) pulse-like, (b) soil-site, and (c) rock-site ground motion sets.

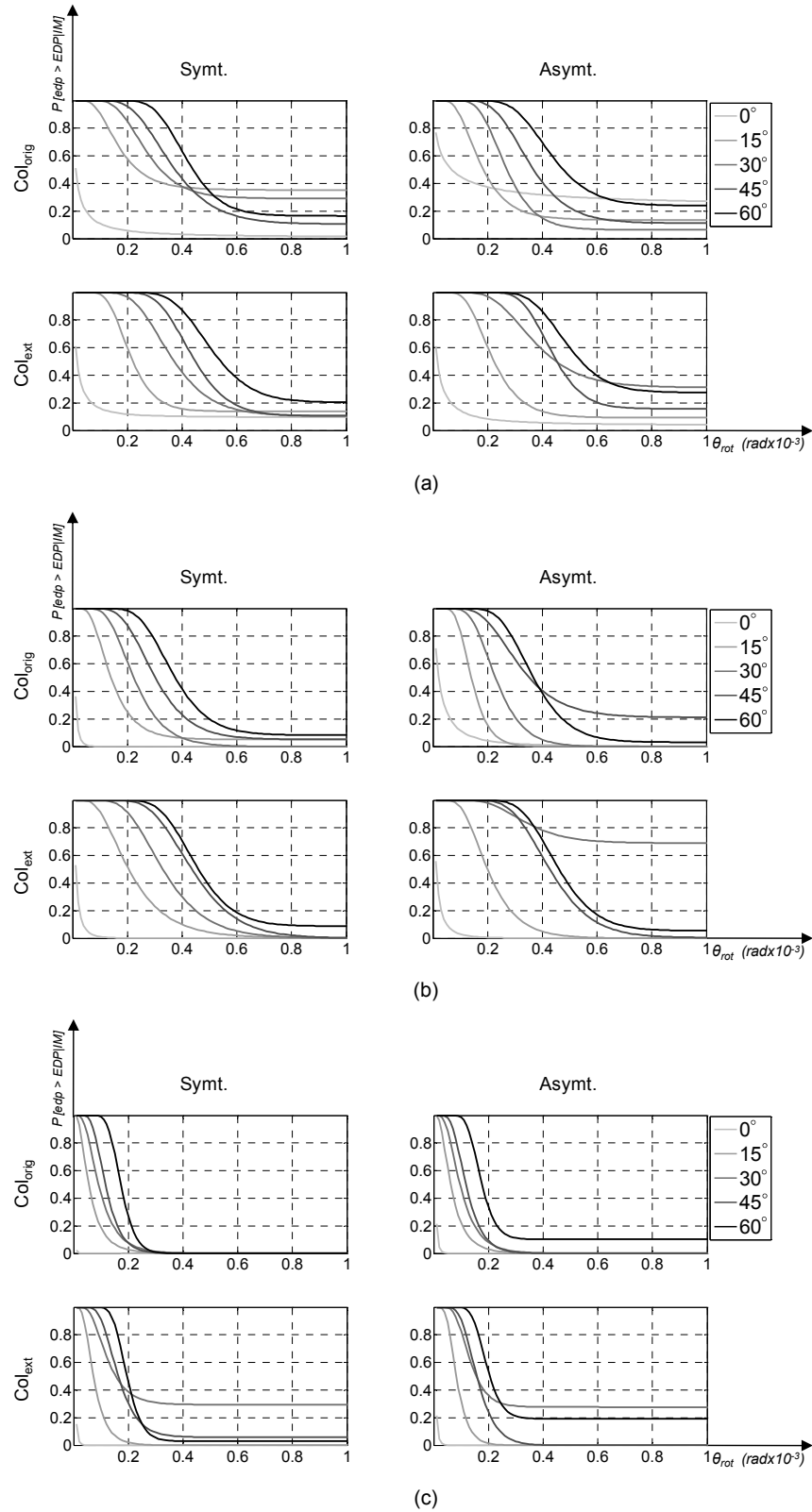


Figure 5.5  $\theta_{rot}$ -probability curves for Bridge B using (a) pulse-like, (b) soil-site, and (c) rock-site ground motion sets.

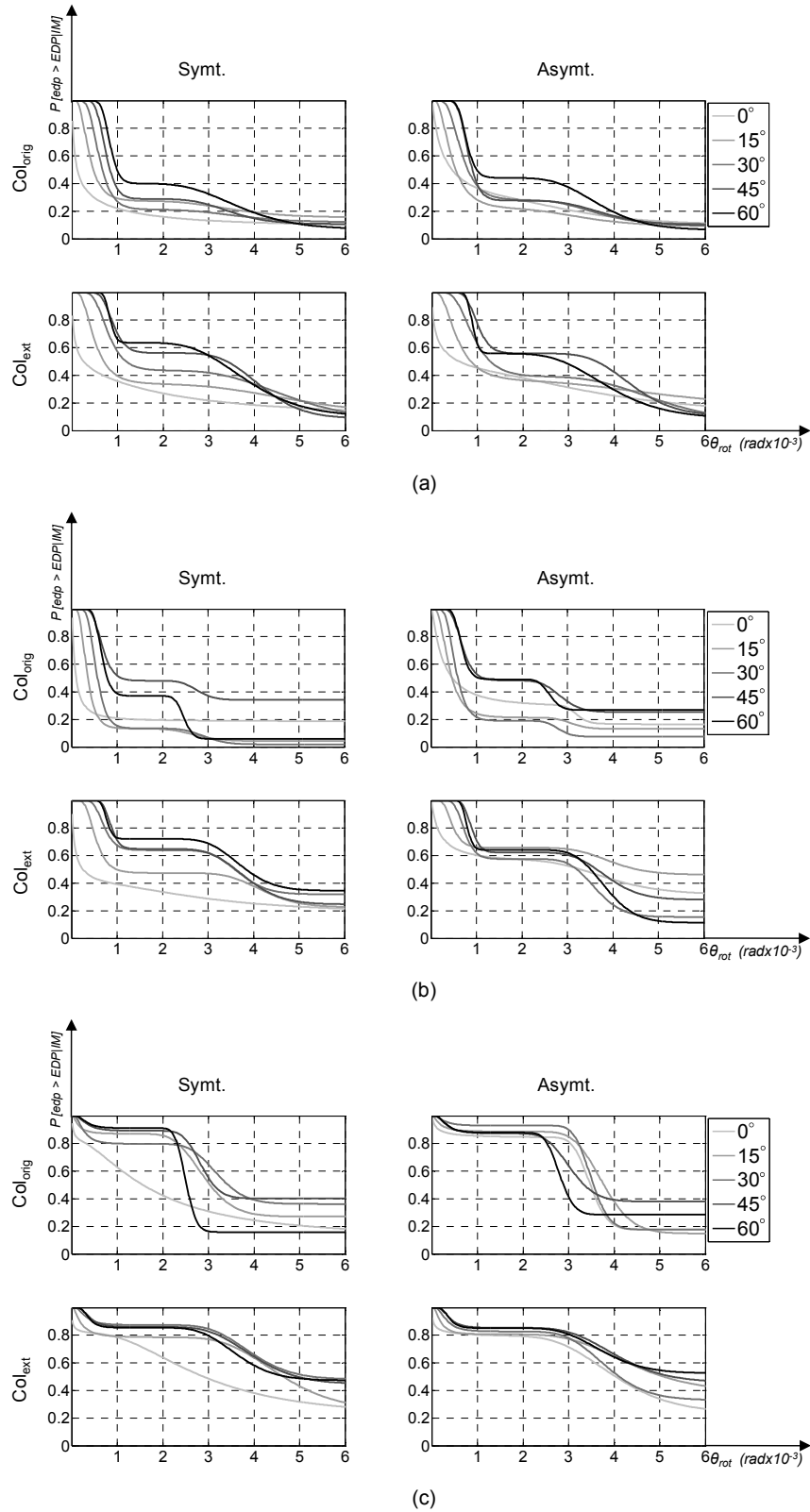


Figure 5.6  $\theta_{rot}$ -probability curves for Bridge C using (a) pulse-like, (b) soil site, and (c) rock-site ground motion sets.

Figures 5.7 through 5.9 display the  $G(EDP|IM)$  where the  $EDP$  is the abutment unseating displacement ( $\delta_{unseat}$ ) for Bridges A, B, and C, respectively. As a general trend,  $G(\delta_{unseat} | IM)$  for  $60^\circ$  skewed abutment is usually to the left of similar information for other skew angles, which suggests that, at larger skew angles, unseating is less likely. However, at large skew angles, the probability of collapse is higher. This phenomenon stems from the fact that the expansion joint (i.e., the gap element in the model) is assigned in the orthogonal direction to the skewed abutment, but abutment unseating is measured in the traffic direction (orthogonal to the non-skewed abutment).

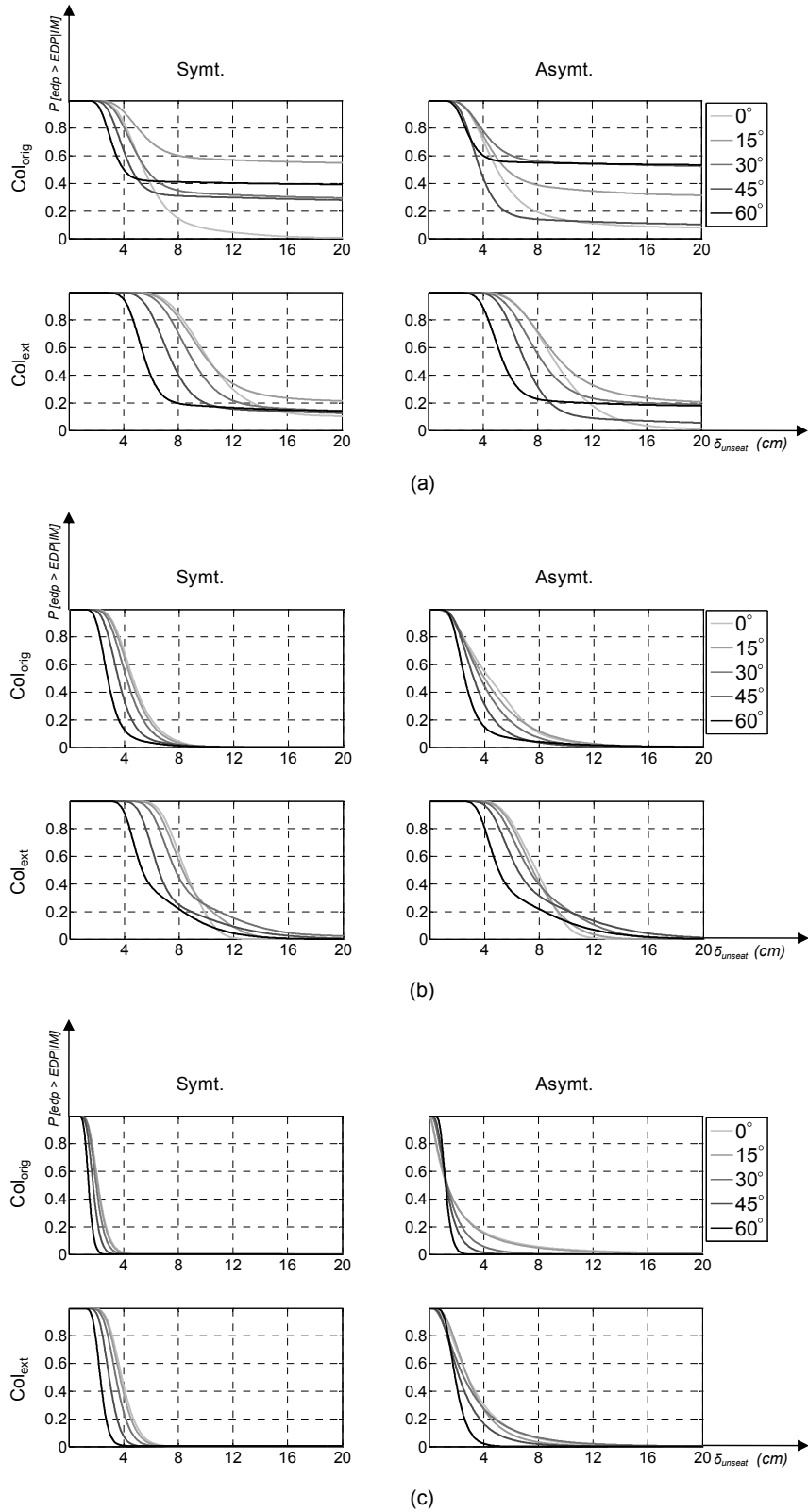


Figure 5.7  $\delta_{unseat}$ -probability curves for Bridge A using (a) pulse-like, (b) soil-site, and (c) rock-site ground motion sets.

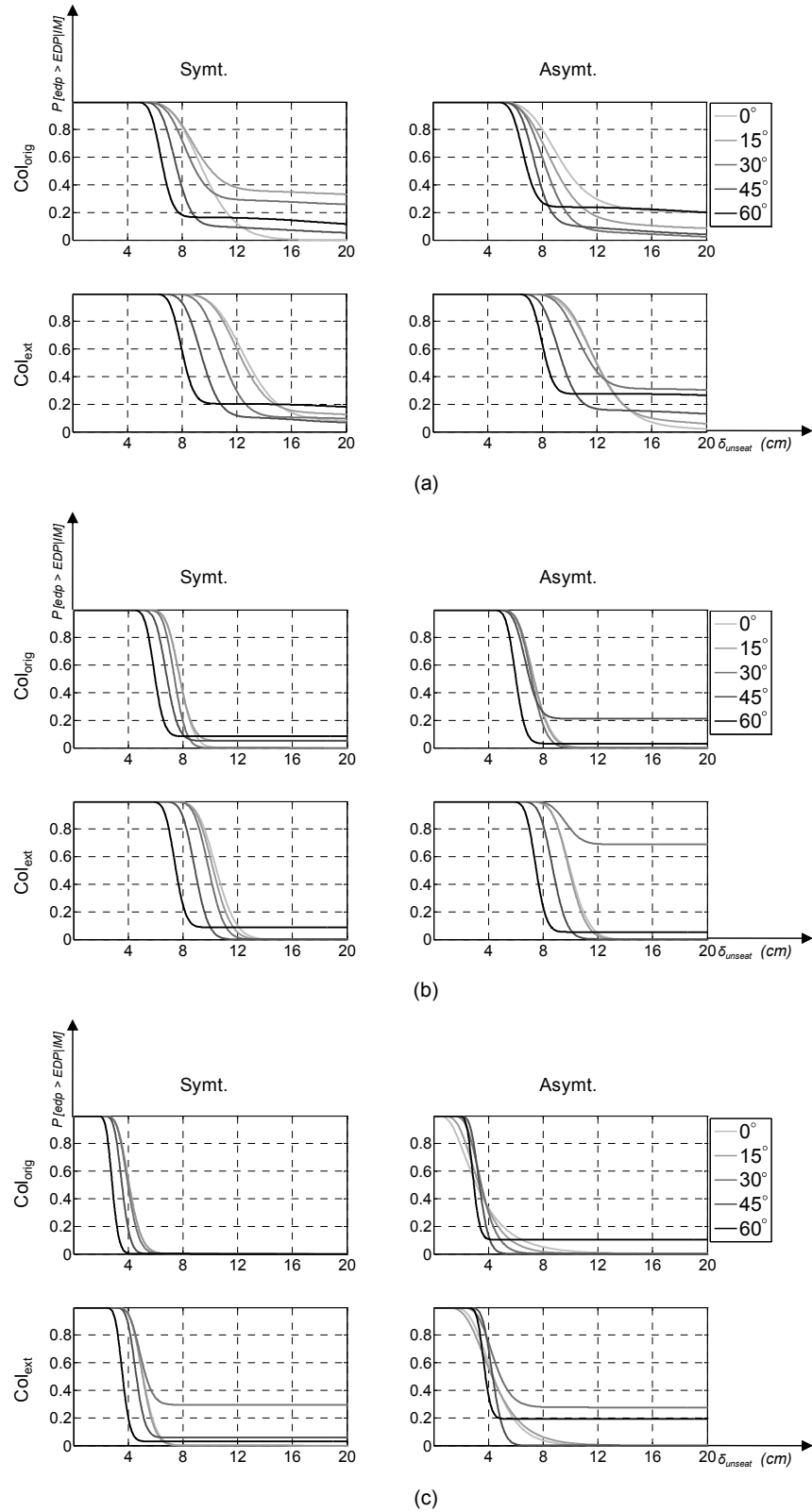


Figure 5.8  $\delta_{unseat}$ -probability curves for Bridge B using (a) pulse-like, (b) soil-site, and (c) rock-site ground motion sets.

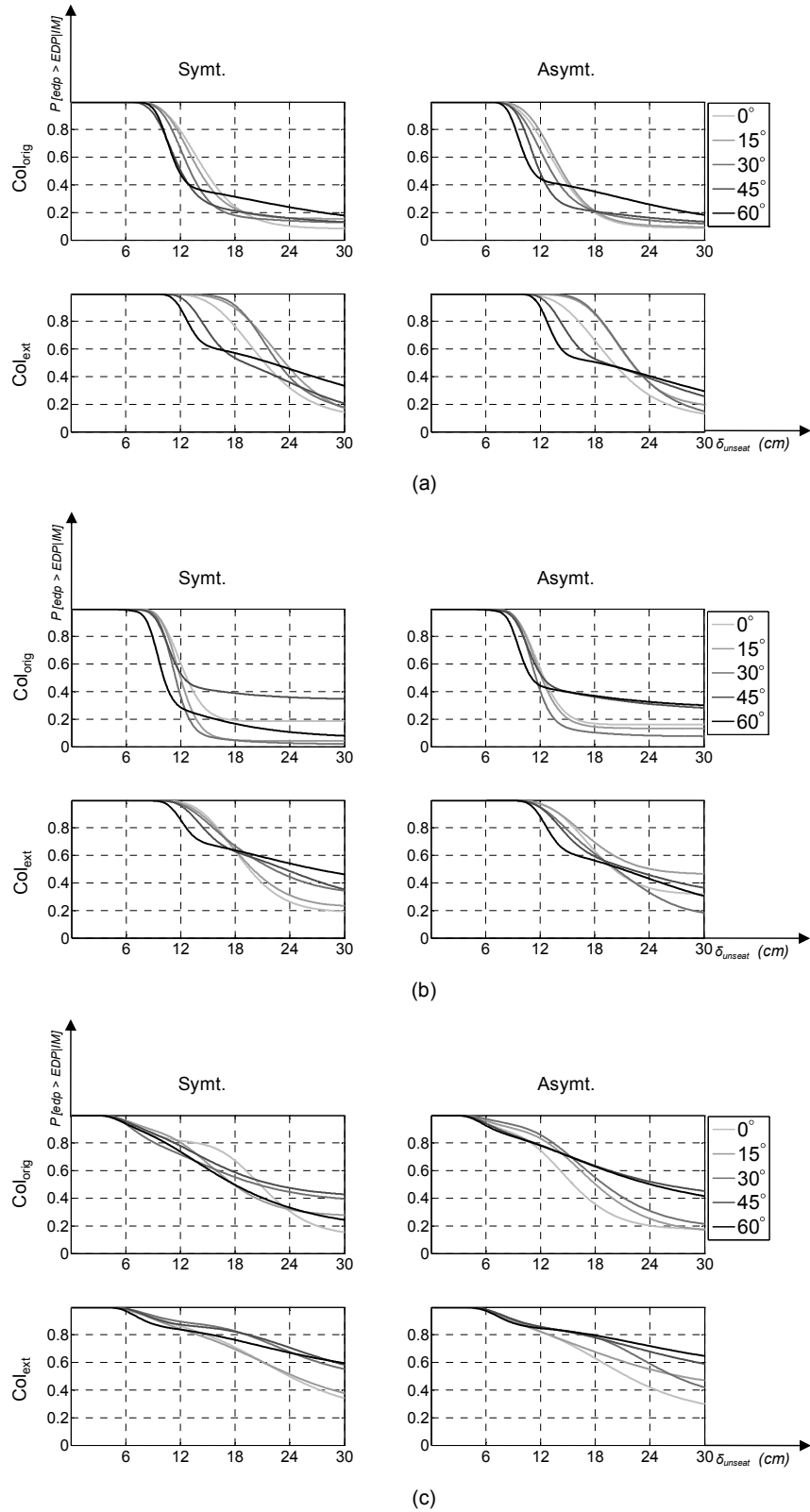


Figure 5.9  $\delta_{unseat}$ -probability curves for Bridge C using (a) pulse-like, (b) soil-site, and (c) rock-site ground motion sets.

The column drift ratio ( $\theta_{col}$ ) is the ratio of the maximum resultant displacement (i.e., resultant of longitudinal and transverse displacements) of the column-top to the column height. We consider the side column bent of Bridge C, because of higher induced seismic demands therein comparison to the central columns. The  $\theta_{col}$ -probability diagrams are shown in Figures 5.10 through 5.12.

Comparing the column drift ratio probability curves for a single-column bridge (Figure 5.10) with those for multi-column bridges (Figures 5.11 and 5.12) shows that the single-column bridge (Bridge A) is less sensitive to the abutment skew angle variation. This type of behavior has been expected, based on the discussion on Chapter 4, which suggests that side column-top deformation of multi-column bridges is more affected by variations in the abutment skew angle. However, for Bridge A, the column drift ratio is more sensitive to abutment skew angle variations, due to the pulse-like ground motion set in comparison with other ground motion types. As shown in Figure 5.11, the soil-site ground motion set induces larger column drifts in Bridge B than the rock-site ground motion type. Similar to deck rotation ( $\theta_{rot}$ ), for Bridge C, the probability curves' two-phase behavior is more noticeable.

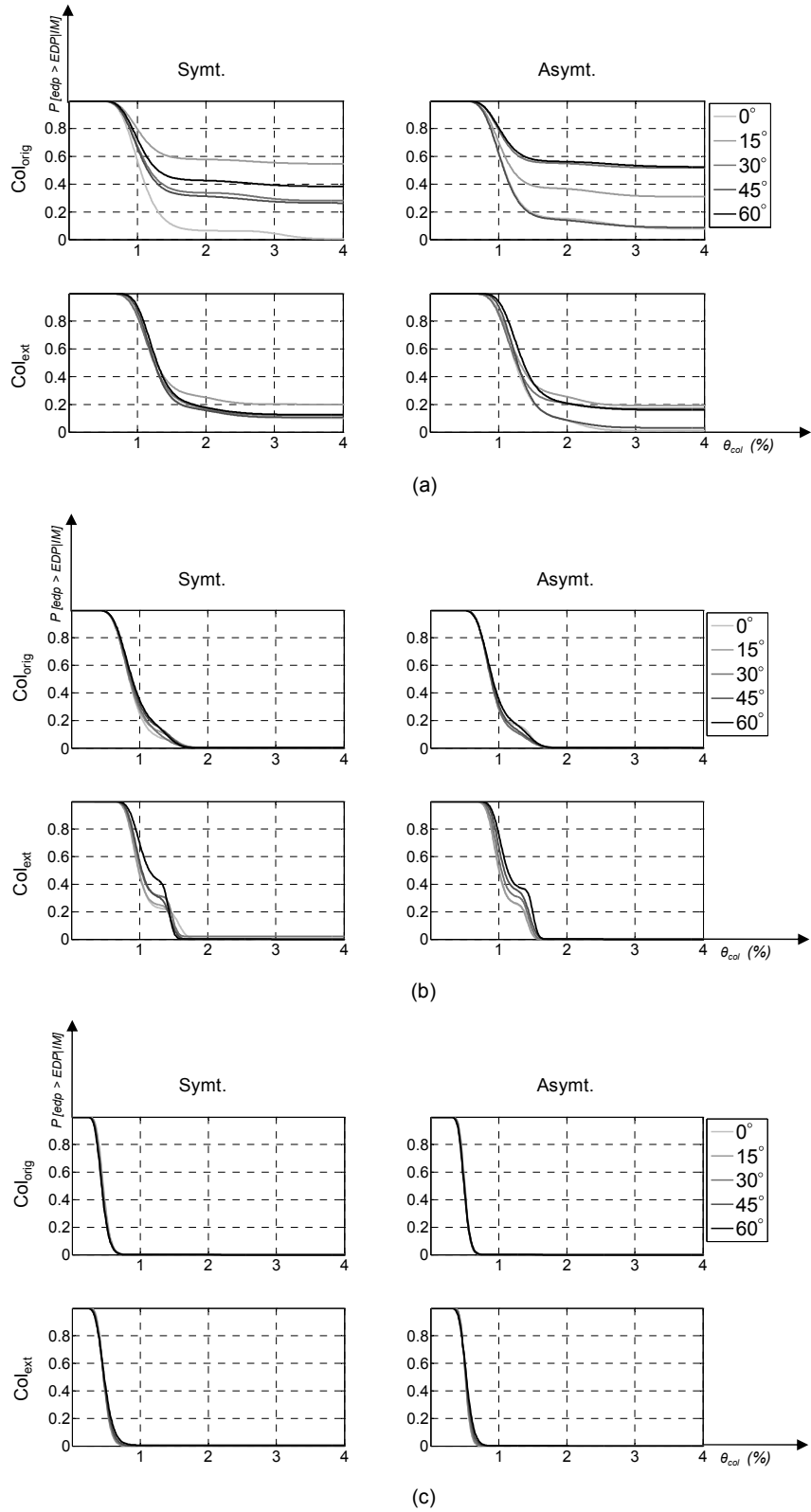


Figure 5.10  $\theta_{col}$ -probability curves for Bridge A using (a) pulse-like, (b) soil-site, and (c) rock-site ground motion sets.

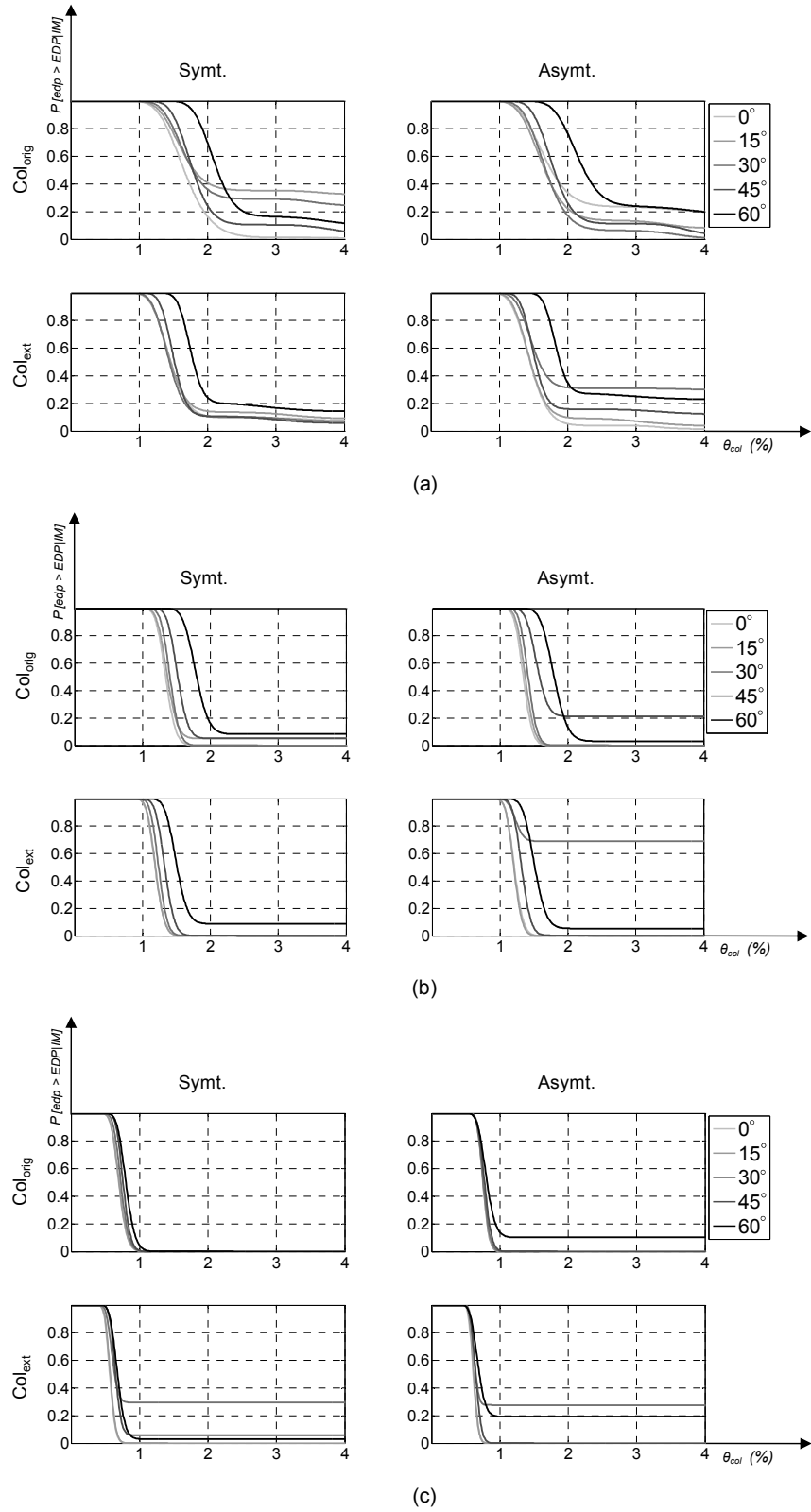
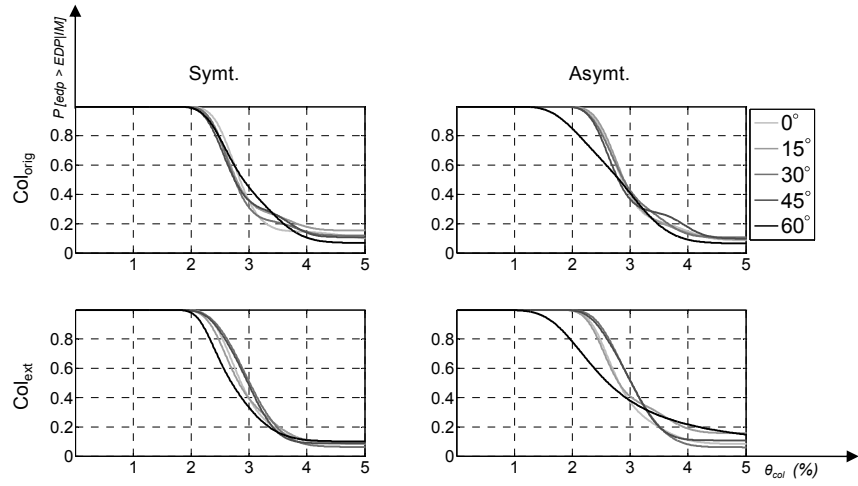
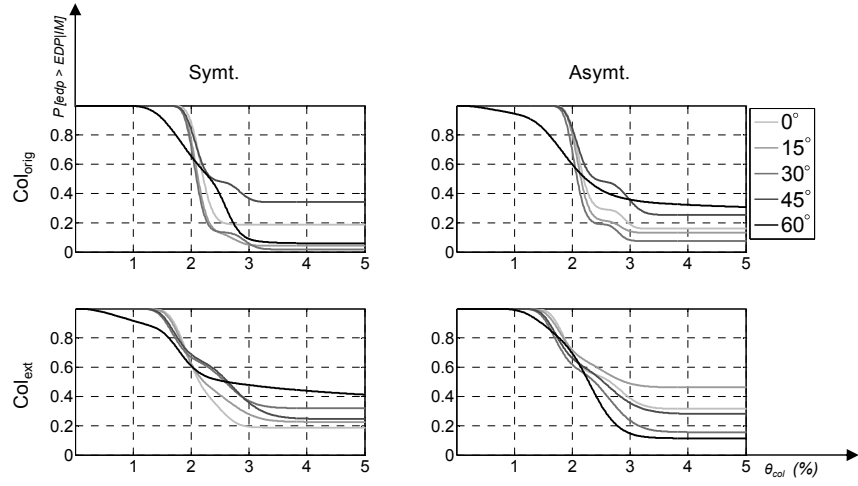


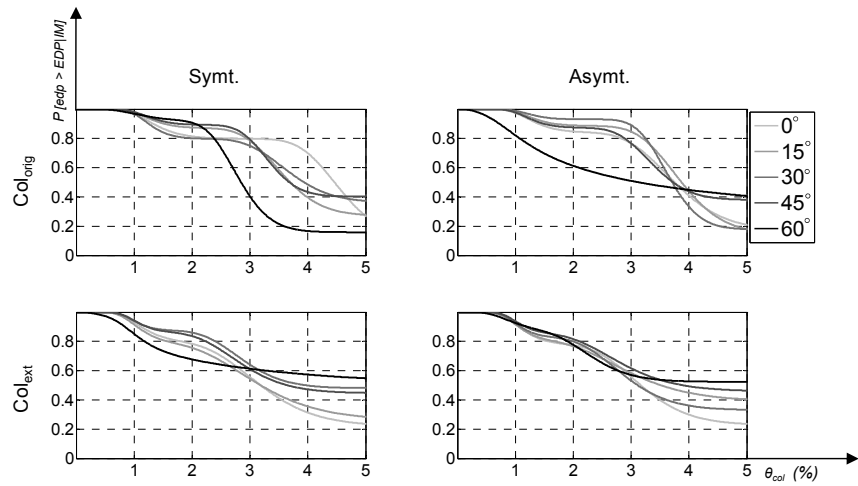
Figure 5.11  $\theta_{col}$ -probability curves for Bridge B using (a) pulse-like, (b) soil-site, and (c) rock-site ground motion sets.



(a)



(b)



(c)

**Figure 5.12**  $\theta_{col}$ -probability curves for Bridge C using (a) pulse-like, (b) soil site, and (c) rock-site ground motion sets.



## **6 SUMMARY AND CONCLUSIONS**

### **6.1 AN OVERVIEW OF FINDINGS**

This study was conducted to improve knowledge about the behavior of skewed bridges and provide the engineering community with recommendations for their design. The study proposes a novel probabilistic-based methodology that addresses the multi-phase behavior of such bridges under various seismic excitation regimes. This methodology is applied to a database of 3D models of a bridge matrix (Chapter 2) that was generated from three existing bridges located in California. We performed a total of 43,200 response history analyses using three ground motion sets. We identified the sensitivity in skewed bridge response due to variations in the bridges' geometrical and ground motion properties. This research's contributions can be summarized as follows:

1. It proposes a novel skewed bridge modeling technique through which the behavior of skewed abutments can be modeled more accurately and efficiently.
2. It quantifies the sensitivity of bridge response parameters to variations in bridge geometrical properties and ground motion characteristics.
3. It proposes a more efficient ground motion intensity measure for assessing skewed bridges' seismic responses.
4. It proposes a novel probabilistic framework—the Multi-Phase Probabilistic Assessment of Structural Response to Seismic Excitations (M-PARS)—for assessing structures' multi-phase behavior under various seismic regimes.

### **6.2 NOVEL SKEWED BRIDGE MODELING TECHNIQUE**

We focused on modeling two main components of bridge structures: column-bent and abutment. Accounting for the distributed plasticity along the column height had a significant effect on the global seismic behavior of bridge structures, and particularly of single-column bridges. The asymmetric behavior of a column section's fiber discretizations during seismic excitation can force the bridge into a virtual asymmetric geometry, a phenomenon that previous studies have not addressed. Employing force-based nonlinear elements in place of conventional displacement-

based elements for column-bent modeling can result in fewer numerical convergence problems and a smaller number of elements.

Abutment behavior dominates the global seismic response of short bridges. We proposed two analytical spine-line models (Chapter 3), which were enhanced specifically for skewed bridges. We modeled abutment in the longitudinal direction with five nonlinear springs attached to a rigid element simulating passive backfill soil pressure. We accounted for the backfill pressure's non-uniform distribution due to the abutment skew by linearly increasing these springs' longitudinal stiffness and strength from the obtuse corner toward the acute corner. In the transverse direction, we modeled shear key using the strut-and-tie method.

### **6.3 SENSITIVITY OF BRIDGE RESPONSE PARAMETERS TO VARIATIONS IN BRIDGE GEOMETRICAL PROPERTIES AND GROUND MOTION CHARACTERISTICS**

We concluded that shear key strength has a significant effect on skewed bridges' seismic response. Results showed that the fate of the shear key (failure vs. survival) delineates a skewed bridge's mode of behavior, and hence, its induced seismic response. This effect is more noticeable in deck rotations, and particularly under pulse-like ground motions. For *EDPs* such as abutment unseating or column drift ratio, the shear key strength effect is less significant.

Other trends we observed are as follows:

1. By increasing the abutment skew angle, we observed a larger number of bridge collapses and shear key failures.
2. Pulse-like ground motions—i.e., those involving high velocity pulses—induced greater seismic demands on skewed bridges.
3. The probability of shear key failure is higher for single-column bridges (Bridge A) due to induced seismic demands in the abutments' transverse direction.
4. Column-bent height affects induced seismic demands in skewed bridges, and higher column elevations resulted in greater seismic demands. However, span configuration was less influential.
5. The detected deck rotation for a symmetrical span arrangement of a single-column bridge (Bridge A) was caused by the asymmetrical yielding surface of the column section modeled by fiber sections.

### **6.4 EFFICIENT GROUND MOTION INTENSITY MEASURE FOR ASSESSING SKEWED BRIDGE SEISMIC RESPONSE**

We concluded that for skewed bridges the peak resultant ground velocity, denoted as  $PGV_{res}$ , is the most efficient ground motion intensity measure among five *IMs*:  $Sa_{SN}(T_I)$ ,  $PGA_{SN}$ ,  $PGA_{res}$ ,  $PGV_{SN}$ , and  $PGV_{res}$ . We considered three main criteria for selecting the most efficient *IM*:

(1) less dispersion in estimating collapse capacity, (2) independence from structural properties, and (3) the selected  $IM$ 's convenience for structural hazard calculations.

## 6.5 M-PARS METHOD

Based on the studied bridges' observed  $IM-EDP$  trends as discussed in Chapter 4, we recognized two regimes (i.e., phases) that dominate skewed bridges' seismic behavior : (1) bridge collapse status and (2) shear key failure status. Chapter 5 proposed a probabilistic methodology for assessing structures based on their multi-phase seismic response: the Multi-Phase Probabilistic Assessment of Structural Response to Seismic Excitations (M-PARS). The general formulation of the M-PARS method was illustrated in Equation (5.1), with special application for skewed bridges in Equation (5.4). Using the simulations conducted as part of this research, we obtained the information required for using Equation (5.4) to assess skewed bridges. We provided and carried out the procedures for computing the probability of exceeding an  $EDP$  with a given  $IM$  using this study's results for three  $EDPs$ — $\theta_{rot}$ ,  $\delta_{unseat}$ , and  $\theta_{col}$ —for a “2% in 50 years” seismic hazard level.

## 6.6 RECOMMENDATIONS FOR FUTURE STUDIES

This report summarizes a general assessment of the seismic response of skewed bridges. We employed state-of-the-art techniques to develop the numerical models of the bridges studied here and proposed a novel method for modeling the skewed abutments. We further developed a methodology for assessing the seismic response of structures with multi-phase behavior under various seismic regimes. We envision the following research topics as areas of interest for continuing the work presented in this report:

1. We studied the effect of abutment skew angle on skewed bridges' seismic response. Curved bridges—those with a curved superstructure in plan—are the other type of short bridges whose geometry is irregular. A study on the effects on seismic response of a curved deck alignment in combination with skewed abutment is recommended.
2. As discussed in Chapter 3, we studied the seismic response of bridges built after 2000, which were based on the most recent design specifications. However, more than 50% of existing bridges in California were built before 1970, with a less rigorous seismic design. Therefore, we recommend a study that assesses the seismic performance of older bridges in California and suggests efficient retrofit methods.
3. Abutment modeling can significantly influence skewed bridges' seismic response. To validate the numerical modeling, a full-scale experimental study on skewed seat-type abutment is strongly recommended. Simulation issues related to skewed abutment seismic response depend not only on backfill soil–abutment–structure interaction, but also on different failure surfaces of skewed abutment backfill soil.

4. An analysis of soil-pile (or foundation)–structure interaction is recommended. The current study considered a fixed base connection for a single-column bridge (Bridge A) and a pinned base connection for multi-column bridges (Bridges B and C). For Bridge C, the study showed that disregarding the soil stiffness in foundation modeling can induce greater seismic demands on the bridge structure.
5. Based on previous studies and empirical observations, we considered two bridge collapse criteria: (1) at an 8% column drift ratio and (2) at abutment unseating. However, further research is needed to provide more detailed collapse criteria for bridge structures. These collapse criteria can be categorized to ductility-based (global) and capacity-based (local). The results of such a study could lead to more effective design specifications.

## REFERENCES

- Abdel-Mohti A., Pekcan G. (2008). Seismic response of skewed RC box-girder bridges. *Earthq. Eng. Eng. Vib.*, 7(4): 415–426.
- ASCE (2005). Minimum design loads for buildings and other structures. *ASCE 7-05*, American Society of Civil Engineers/Structural Engineering Institute, Reston, VA.
- Asheboa D.B., Chana T.H.T., Yua L. (2007a). Evaluation of dynamic loads on a skew box girder continuous bridge part I: field test and modal analysis. *Eng. Struct.*, 29(6): 1052–1063.
- (2007b). Evaluation of dynamic loads on a skew box girder continuous bridge part II: parametric study and dynamic load factor. *Eng. Struct.*, 29(6): 1064–1073.
- ATC (2009). Guidelines for seismic performance assessment of buildings, 50% Draft. *Report No. ATC-58*, Applied Technology Council, Redwood City, CA.
- Aviram A., Mackie K.R., Stojadinovic B. (2008). Guidelines for nonlinear analysis of bridge structures in California. *Report PEER 2008/3*, Pacific Earthquake Engineering Research Center, University of California, Berkeley, CA.
- Baker J., Lin T., Shahi S.K., Jayaram N. (2011). New ground motion selection procedures and selected motions for the PEER Transportation Research Program. *Report PEER 2011/03*, Pacific Earthquake Engineering Research Center, University of California, Berkeley, CA.
- Baker J., Cornell A.C. (2006). Correlation of response spectral values for multicomponent ground motions. *B. Seismol. Soc. Am.*, 96(1): 215–227.
- Bignell J.L., LaFave J.M., Hawkins N.M. (2005). Seismic vulnerability assessment of wall pier supported highway bridges using nonlinear pushover analyses. *Eng. Struct.*, 27(14): 2044–2063.
- Bozorgzadeh A., Ashford S.A., Restrepo J.I. (2008). Effect of backfill soil type on stiffness and ultimate Capacity of bridge abutments. *Geotech. SP. IV ASCE*.
- Bozorgzadeh A., Megally S., Restrepo J.I., Ashford S.A. (2006). Capacity evaluation of exterior sacrificial shear keys of bridge abutments. *ASCE J. Bridge Eng.*, 11(5): 555–565.
- Caltrans (2010). Caltrans Seismic Design Criteria Version 1.6. California Department of Transportation, Sacramento, CA.
- Campbell K.W., Bozorgnia Y. (2008). NGA ground motion model for the geometric mean horizontal component of PGA, PGV, PGD and 5% damped linear elastic response spectra for periods ranging from 0.01 to 10 s. *Earthq. Spectra*, 24(1): 139–171.
- Chang G.A., Mander J.B. (1994). Seismic energy based fatigue damage analysis of bridge columns: part I - evaluation of seismic capacity. *Report NCEER-94-0006*, National Center for Earthquake Engineering Research, State University of New York, Buffalo, NY.
- Chen W.F., Duan L. (2000). *Bridge engineering handbook*. New York: CRC Press.
- Chiou B., Darragh R., Gregor N., Silva W. (2008). NGA project strong-motion database. *Earthq. Spectra*, 24(1): 23–44.
- Clough R.W., Penzien J. (1994). *Dynamics of structures*. 2nd Edition, New York: McGraw-Hill, Inc.
- Cornell C.A., Jalayer F., Hamburger R.O., Foutch D.A. (2002). The probabilistic basis for the 2000 SAC/FEMA steel moment frame guidelines. *ASCE J. Struct. Eng.*, 128(4): 526–533.
- CSI (2005). *SAP 2000-linear and nonlinear static and dynamic analysis and design of three-dimensional structures: basic analysis reference manual*. Computers and Structures, Inc.
- Dimitrakopoulos E.G. (2011). Seismic response analysis of skew bridges with pounding deck-abutment joints. *Eng. Struct.*, 33(3): 813–826.

- Dimitrakopoulos E.G., Makris N., Kappos A.J. (2010). Dimensional analysis of the earthquake response of a pounding oscillator. *ASCE J. Eng. Mech.*, 136(3): 299–310.
- Dimitrakopoulos E.G., Makris N., Kappos A.J. (2009). Dimensional analysis of the earthquake-induced pounding between adjacent structures. *Earthq. Eng. Struct. Dyn.*, 38(7): 867–886.
- EERI (1995). Northridge earthquake reconnaissance report. *Earthq. Spectra*, Special Suppl. to Vol. 11, 523 pp.
- FEMA (1997). *HAZUS 97: Technical Manual*. Federal Emergency Management Agency, Washington, D.C.
- FEMA (2003). *HAZUS-MH MRI: Technical Manual*. Vol. Earthquake Model. Federal Emergency Management Agency, Washington, D.C.
- FHWA (2010). Bridge programs NBI data. Retrieved August 2010, from U.S. Department of Transportation Federal Highway Administration <<http://www.fhwa.dot.gov/bridge/britab.cfm>>.
- FHWA (1995). Recording and coding guide for the structure inventory and appraisal of the nation's bridges. *FHWA-PD-96-001*, Washington, D.C.
- Field E.H., Gupta N., Gupta V., Blanpied M., Maechling P., Jordan T.H. (2005a). Hazard calculations for the WGCEP-2002 earthquake forecast using OpenSHA and distributed object technologies. *Seismol. Res. Lett.*, 76: 161–167, DOI: 10.1785/gssrl.76.2.161.
- Field E.H., Jordan T.H., Cornell C.A. (2003). OpenSHA: a developing community-modeling environment for seismic hazard analysis. *Seismol. Res. Lett.*, 74(4): 406–419.
- Ghobarah A.A., Tso W.K. (1974). Seismic analysis of skewed highway bridges with intermediate supports. *Earthquake Eng. Struct. Dyn.*, 2(3): 235-248.
- Goel R.K., Chopra A.K. (1997). Evaluation of bridge abutment capacity and stiffness during earthquakes. *Earthq. Spectra*, 13(1): 1–24.
- Hutchinson T.C., Chai Y.H., Boulanger R.W. (2004). Inelastic seismic response of extended pile-shaft-supported bridge structures. *Earthq. Spectra*, 20(4): 1057–1080.
- Jalayer F., Cornell C.A. (2003). A technical framework for probability-based demand and capacity factor design (DCFD) seismic formats. *Report PEER 2003/8*, Pacific Earthquake Engineering Research Center, University of California, Berkeley, CA.
- JRA (1996). *Design specification for highway bridges, Part V: seismic design*. Japan Road Association, Tokyo, Japan.
- Jayaram N., Shahi S., Baker J. (2010). Ground motion for PEER Transportation Research Program: <[http://peer.berekeley.edu/transportation/gm\\_peer\\_transportation.html](http://peer.berekeley.edu/transportation/gm_peer_transportation.html)>.
- Jennings P.C., (editor), Housner G.W., Hudson D.E., Trifunac M.D., Frazier G.A., Wood J.H., Scott R.F., Iwan W.D., Brady A.G. (1971). Engineering features of the San Fernando earthquake of February 9, 1971. *Report No. EERI 71-02*, California Institute of Technology, Pasadena, CA.
- Johnson N., Saiidi M.S., Sanders D. (2009). Nonlinear earthquake response modeling of a large-scale two-span concrete bridge. *ASCE J. Bridge Eng.*, 14(6): 460–471.
- Kalantari A., Amjadian M. (2010). An approximate method for dynamic analysis of skewed highway bridges with continuous rigid deck. *Eng. Struct.*, 32(9): 2850–2860.
- Kappos A.J., Sextos A.G. (2001). Effect of Foundation Type and Compliance on Seismic Response of RC Bridges. *ASCE J. Bridge Eng.*, 6(2): 120–130.
- Kaviani P., Zareian F., Taciroglu E. (2012). Seismic behavior of reinforced concrete bridges with skew-angled seat-type abutment. *Eng. Struct.*, 45: 137–150.
- Kaviani P. (2011). *Performance-based seismic assessment of skewed bridges*. Ph.D. Dissertation. University of California, Irvine, CA.
- Kaviani P., Zareian F., Taciroglu E., Sarraf M. (2011). Simplified method for seismic performance assessment of skewed bridges. *Proceedings of 3rd International Conference on Computational Methods in Structural Dynamics and Earthquake Engineering*, Corfu, Greece.

- Kaviani P., Zareian F., Sarraf M. (2010a). Comparison of seismic response of skewed bridges to near vs. far field motions. *Proceedings of 7th International Conference on Urban Earthquake Engineering & 5th International Conference on Earthquake Engineering*, Tokyo, Japan.
- Kaviani P., Zareian F., Sarraf M., Pla-Junca P. (2010b). Sensitivity of skewed-bridges response to seismic excitations. *Proceedings of 14th European Conference on Earthquake Engineering*, Ohrid, Republic of Macedonia.
- Kawashima K., Unjoh S., Hoshikuma J., Kosa, K. (2010). *Damage of transportation facility due to 2010 Chile earthquake (April 5, 2010)*. Bridge Team Dispatched by Japan Society of Civil Engineers: <[http://peer.berkeley.edu/publications/chile\\_2010/reports\\_chile.html](http://peer.berkeley.edu/publications/chile_2010/reports_chile.html)>.
- Kennedy R.P., Ravindra M.K. (1984). Seismic fragilities for nuclear power plant risk studies. *Nucl. Eng. Des.*, 79(1): 47–68.
- Kotsoglou A., Pantazopoulou S. (2010). Response simulation and seismic assessment of highway overcrossings. *Earthq. Eng. Struct. Dyn.*, 9(9): 991–1013.
- Kramer S.L. (1996). *Geotechnical earthquake engineering*. New Jersey: Prentice Hall.
- Lou L., Zerva A. (2004). Effects of spatially variable ground motions on the seismic response of a skewed, multi-span, RC highway bridge. *Soil Dyn. Earthq. Eng.*, 25(10): 729–740.
- Mackie K., Stojadinovic B. (2007). Performance-based seismic bridge design for damage and loss limit states. *Earthq. Eng. Struct. Dyn.*, 36(13): 1953–1971.
- Mackie K., Stojadinovic B. (2006). Seismic vulnerability of typical multi-span California highway bridges. *Proceedings of Fifth National Seismic Conference on Bridges and Highways*, San Francisco, CA.
- Mackie K., Stojadinovic B. (2003). Seismic demands for performance-based design of bridges. *Report PEER 312*, Pacific Earthquake Engineering Research Center, University of California, Berkeley, CA.
- Maechling P., Gupta V., Gupta N., Field E.H., Okaya D., Jordan T.H. (2005a). Seismic hazard analysis using distributed computing in the SCEC community modeling environment. *Seismol. Res. Lett.*, 76(2): 177–181.
- Maechling P., Gupta V., Gupta N., Field E.H., Okaya D., Jordan T.H. (2005b). Grid computing in the SCEC community modeling environment. *Seismol. Res. Lett.*, 76(5): 581–587.
- Maleki S. (2005). Seismic modeling of skewed bridges with elastomeric bearings and side retainers. *ASCE J. Bridge Eng.*, 10(4): 442–449.
- Mander J.B., Priestley M.J.N., Park R. (1988). Theoretical stress-strain model for confined concrete. *ASCE J. Struct. Eng.*, 114(8): 1804–1825.
- Maragakis E.A. (1984). *A Model for the Rigid Body Motions of Skew Bridges*. Ph.D. Dissertation. California Institute of Technology, Pasadena, CA.
- Maragakis E.A., Jennings P.C. (1987). Analytical models for the rigid body motions of skew bridges. *Earthq. Eng. Struct. Dyn.*, 15(8): 923–944.
- Maroney B.H. (1995). *Large scale abutment tests to determine stiffness and ultimate strength under seismic loading*. Ph.D. Dissertation. University of California, Davis, CA.
- Maroney B.H., Chai Y.H. (1994). Seismic design and retrofitting of reinforced concrete bridges. *Proceedings of 2nd International Workshop, Earthquake Commission of New Zealand*, Queenstown, New Zealand.
- McCallen D.B., Romstad K.M. (1994). Dynamic analysis of a skewed short-span box-girder overpass. *Earthq. Spectra*, 10(4): 729–755.
- McKenna F., Fenves G.L., Scott M.H. (2000). *Open system for earthquake engineering simulation*. University of California, Berkeley, CA: <<http://opensees.berkeley.edu>>, Version 2.2.2.
- Megally S., Silva P.F., Seible F. (2002). Seismic response of sacrificial shear keys in bridge abutments. *Report No. SSRP-2001/23*, University of California, San Diego, CA.
- Meng J.Y., Lui E.M. (2002). Refined stick model for dynamic analysis of skew highway bridges. *ASCE J. Bridge Eng.*, 7(3): 184–194.

- . 2000. Seismic analysis and assessment of a skew highway bridge. *Eng. Struct.*, 22(11): 1433–1452.
- Neuenhofer A., Filippou F.C. (1997). Evaluation of nonlinear frame finite-element models. *ASCE J. Struct. Eng.*, 123(7): 958–966.
- Nielson B.G. (2005). *Analytical fragility curves for highway bridges in moderate seismic zones*. Ph.D. Dissertation. Georgia Institute of Technology, GA.
- OpenSees Wiki: <[http://opensees.berkeley.edu/wiki/index.php/Command\\_Manual](http://opensees.berkeley.edu/wiki/index.php/Command_Manual)> (Last Access: April, 2010).
- Paraskeva T.S., Kappos A.J., Sextos A.G. (2006). Extension of modal pushover analysis to seismic assessment of bridges. *Earthq. Eng. Struct. Dyn.*, 35(10): 1269–1293.
- Priestley M.J.N., Calvi G.M., Seible F. (1996). *Seismic design and retrofit of bridges*. New York: John Wiley & Sons.
- Romstad K.M., Kutter B., Maroney B., Vanderbilt E., Griggs M., Chai Y.H. (1995). Experimental measurements of bridge abutment behavior. *Report No. UCD STR 95 1*, University of California, Structural Engineering Group, Davis, CA.
- Saadeghvaziria M.A., Yazdani-Motlagh A.R. (2008). Seismic behavior and capacity/demand analyses of three multi-span simply supported bridges. *Eng. Struct.*, 30(1): 54–66.
- Shamsabadi A., Taciroglu E. (2013). A frequency-time domain handshake method for seismic soil-foundation-structure interaction analysis of long-span bridges. *Proceeding 7th National Seismic Conference on Bridges and Highways*, Oakland, CA.
- Shamsabadi A., Khalili-Tehrani P., Stewart J.P., Taciroglu E. (2010). Validated simulation models for lateral response of bridge abutments with typical backfills. *ASCE J. Bridge Eng.*, 15(3): 302–311.
- Shamsabadi A., Rollins K.M., Kapuskar M. (2007). Nonlinear soil–abutment–bridge structure interaction for seismic performance-based design. *ASCE J. Geotech. Geoenviron.*, 133(6): 707–720.
- Shinozuka M., Feng M.Q., Kim H., Uzawa T., Ueda T. (2003). Statistical analysis of fragility curves. *Report No. MCEER-03-0002*, MCEER. University of Southern California, Los Angeles, CA.
- Shinozuka M., Feng M.Q., Kim H.-K., Kim S.-H. (2000). Nonlinear static procedure for fragility curve development. *ASCE J. Eng. Mech.*, 126(12): 1287–1296.
- Shinozuka M., Feng M.Q., Lee J., Naganuma T. (2000). Statistical analysis of fragility curves. *ASCE J. Eng. Mech.*, 126(12): 1224–1231.
- Shome N., Cornell C.A. (1999). Probabilistic seismic demand analysis of non-linear structures. *Report No. RMS-35*, Stanford University, Stanford, CA.
- Singh B., Chakraverty S. (1994). Flexural vibration of skew plates using boundary characteristic orthogonal polynomials in two variables. *J. Sound Vibration*, 173(2): 157–178.
- Stewart J.P., Wallace J.W., Taciroglu E., Ahlberg E.R., Lemnitzer A., Rha C., Tehrani P.K., Keowen S., Nigbor R.L., Salamanca A. (2007). Full scale cyclic testing of foundation support systems for highway bridges. Part II: abutment backwalls. *Report No. UCLA SGEL 2007/02*, University of California, Los Angeles, CA.
- Wakefield R.R., Nazmy A.S., Billington D.P. (1991). Analysis of seismic failure in skew RC bridge. *ASCE J. Struct. Eng.*, 117(3): 972–986.
- Watanabe G., Kawashima K. (2004). Effectiveness of cable-restrainer for mitigating rotation of a skewed bridge subjected to strong ground shaking. *Proceedings, 13th World Conference on Earthquake Engineering*, Paper No. 789, Vancouver, Canada.
- Wilson J.C., Tan B.S. (1990a). Bridge abutments: formulation of simple model for earthquake response analysis. *ASCE J. Eng. Mech.*, 116(8): 1828–1837.
- . (1990b). Bridge abutments: assessing their influence on earthquake response of Meloland road overpass, *ASCE J. Eng. Mech.*, 116(8): 1838–1856.

- Yashinsky M., Oviedo R., Ashford S.A., Fargier-Gabaldon L., Hube M. (2010). Performance of highway and railway structures during the February 27, 2010 Maule Chile earthquake. *EERI/PEER/FHWA Bridge Team Report*: < [http://peer.berkeley.edu/publications/chile\\_2010/reports\\_chile.html](http://peer.berkeley.edu/publications/chile_2010/reports_chile.html)>.
- Zhang J., Makris N. (2002a). Kinematic response functions and dynamic stiffnesses of bridge embankments. *Earthq. Eng. Struct. Dyn.*, 31(11): 1933–1966.
- Zhang J., Makris N. (2002b). Seismic response analysis of highway overcrossings including soil-structure interaction. *Earthq. Eng. Struct. Dyn.*, 31(11): 1967–1991.



# Appendix A: FHWA Bridge Type Coding System

The Report *FHWA-PD-96-001* [FHWA 1995] provides a three-digit coding system for bridges to represent their basic properties. This code is composed of three designator digits. The first digit indicates the type of material and/or design, as shown in Table A.1. The second and third digits indicate the predominant type of design and/or type of construction; Table A.2 displays the typical values for the second and third digits.

**Table A.1      The first digit descriptions (source: FHWA1995).**

Code	Description
1	Concrete
2	Concrete continuous
3	Steel
4	Steel continuous
5	Prestressed concrete*
6	Prestressed concrete continuous*
7	Wood or timber
8	Masonry
9	Aluminum, wrought iron, or cast iron
0	Other

\* Post-tensioned concrete should be coded as prestressed concrete.

**Table A.2 The second and third digit descriptions (source: FHWA1995).**

<b>GM Type</b>	<b>Distance</b>
01	Slab
02	Stringer/multi-beam or girder
03	Girder and floorbeam system
04	Tee beam
05	Box beam or girders – multiple
06	Box beam or girders – single or spread
07	Frame (except frame culverts)
08	Orthotropic
09	Truss – deck
10	Truss – thru
11	Arch – deck
12	Arch – thru
13	Suspension
14	Stayed – girder
15	Moveable – lift
16	Moveable – bascule
17	Moveable – swing
18	Tunnel
19	Culvert (include frame culverts)
20	Mixed types
21	Segmental box girder
22	Channel beam
00	other

***Examples:***

Wood or timber through truss:	710
Masonry culvert:	819
Steel suspension:	313
Continuous concrete multiple box girders:	205
Simple span concrete slab:	101
Tunnel in rock:	018

## Appendix B: Ground Motion Properties

Tables B.1 through B.3 describe the ground motions properties used in this study [Jayaram et al. 2010]. The definition of each column in the following tables is indicated in order, below:

**No.:** Number of record used in this study (No. 1 for pulse-like GM represents Pulse-1).

**EQ Name:** Earthquake name (from the NGA Flat file).

**Year:** Year of the earthquake.

**Station:** Recording station name (from NGA Flat file).

**M:** Moment magnitude of earthquake.

**D:** Closest distance in meter ( $m$ ) from the recording site to the ruptured area.

$V_{s30}$ : Average shear velocity (m/sec) between 0- and 30-m depth.

$PGA_{SN}$ : Peak ground acceleration of strike-normal component in  $g$ .

$PGA_{SP}$ : Peak ground acceleration of strike-parallel component in  $g$ .

$PGA_{res}$ : Peak resultant ground acceleration in  $g$ .

$PGV_{SN}$ : Peak ground velocity of strike-normal component in cm/sec.

$PGV_{SP}$ : Peak ground velocity of strike-parallel component in cm/sec.

$PGV_{res}$ : Peak resultant ground velocity in cm/sec.

**Table B.1 Pulse-like ground motion properties.**

#	EQ Name	Year	Station	<i>M</i>	<i>D</i>	<i>V</i> <sub>s30</sub>	<i>PGA</i> <sub>SN</sub>	<i>PGA</i> <sub>SP</sub>	<i>PGA</i> <sub>res</sub>	<i>PGV</i> <sub>SN</sub>	<i>PGV</i> <sub>SP</sub>	<i>PGV</i> <sub>res</sub>
1	Imperial Valley-06	1979	EC County Center FF	6.53	7.31	192.05	0.18	0.22	0.24	54.49	42.96	68.81
2	Imperial Valley-06	1979	EC Meloland Overpass FF	6.53	0.07	186.21	0.38	0.27	0.38	115.04	27.30	115.08
3	Imperial Valley-06	1979	El Centro Array #4	6.53	7.05	208.91	0.36	0.47	0.52	77.93	40.14	81.88
4	Imperial Valley-06	1979	El Centro Array #5	6.53	3.95	205.63	0.38	0.53	0.55	91.48	49.00	92.89
5	Imperial Valley-06	1979	El Centro Array #6	6.53	1.35	203.22	0.44	0.40	0.45	111.87	64.72	117.44
6	Imperial Valley-06	1979	El Centro Array #7	6.53	0.56	210.51	0.46	0.33	0.52	108.82	44.53	109.46
7	Imperial Valley-06	1979	El Centro Array #8	6.53	3.86	206.08	0.47	0.59	0.64	48.55	51.98	70.26
8	Imperial Valley-06	1979	El Centro Diff. Array	6.53	5.09	202.26	0.42	0.44	0.49	59.61	51.38	71.31
9	Morgan Hill	1984	Coyote Lake Dam (SW)	6.19	0.53	597.12	0.81	1.08	1.31	62.30	70.15	81.13
10	Loma Prieta	1989	Gilroy - Gavilan Coll.	6.93	9.96	729.65	0.29	0.41	0.45	30.81	26.62	30.86
11	Loma Prieta	1989	LGPC	6.93	3.88	477.65	0.94	0.54	0.98	97.02	72.18	109.18
12	Landers	1992	Lucerne	7.28	2.19	684.94	0.70	0.81	0.81	140.65	48.35	148.17
13	Landers	1992	Yermo Fire Station	7.28	23.62	353.63	0.61	0.81	0.81	56.64	31.25	56.65
14	Northridge-01	1994	Jensen Filter Plant	6.69	5.43	373.07	0.52	1.07	1.08	67.43	64.45	89.64
15	Northridge-01	1994	Jensen Filter Plant Gen.	6.69	5.43	525.79	0.52	1.07	1.08	67.38	65.28	89.82
16	Northridge-01	1994	Newhall - Fire Sta	6.69	5.92	269.14	0.72	0.65	0.75	120.27	50.57	121.11
17	Northridge-01	1994	Newhall - W Pico Canyon	6.69	5.48	285.93	0.43	0.28	0.47	87.75	74.75	93.84
18	Northridge-01	1994	Rinaldi Receiving Sta	6.69	6.50	282.25	0.87	0.42	0.87	167.20	62.71	167.23
19	Northridge-01	1994	Sylmar - Converter Sta	6.69	5.35	251.24	0.59	0.80	0.91	130.27	93.30	132.90
20	Northridge-01	1994	Sylmar - Converter Sta East	6.69	5.19	370.52	0.83	0.53	0.84	113.57	80.17	117.92
21	Northridge-01	1994	Sylmar -Olive View Med	6.69	5.30	440.54	0.73	0.60	0.84	122.72	54.67	132.36
22	Kobe, Japan	1995	KJMA	6.90	0.96	312.00	0.85	0.55	0.85	96.27	53.67	96.27
23	Kobe, Japan	1995	Takarazuka	6.90	0.27	312.00	0.65	0.70	0.76	72.65	83.23	89.78
24	Kocaeli, Turkey	1999	Gebze	7.51	10.92	792.00	0.24	0.14	0.26	51.16	28.67	56.46
25	Chi-Chi, Taiwan	1999	CHY028	7.62	3.14	542.61	0.66	0.85	0.89	77.66	66.93	93.70

#	EQ Name	Year	Station	<i>M</i>	<i>D</i>	<i>V</i> <sub>530</sub>	<i>PGA</i> <sub>SN</sub>	<i>PGA</i> <sub>SP</sub>	<i>PGA</i> <sub>res</sub>	<i>PGV</i> <sub>SN</sub>	<i>PGV</i> <sub>SP</sub>	<i>PGV</i> <sub>res</sub>
26	Chi-Chi, Taiwan	1999	CHY101	7.62	9.96	258.89	0.38	0.43	0.51	75.29	114.5	115.05
27	Chi-Chi, Taiwan	1999	TCU049	7.62	3.78	487.27	0.29	0.25	0.33	46.10	58.91	65.77
28	Chi-Chi, Taiwan	1999	TCU052	7.62	0.66	579.10	0.38	0.39	0.51	165.55	113.1	179.46
29	Chi-Chi, Taiwan	1999	TCU053	7.62	5.97	454.55	0.22	0.14	0.22	40.90	41.32	48.69
30	Chi-Chi, Taiwan	1999	TCU054	7.62	5.30	460.69	0.16	0.19	0.19	60.39	39.13	61.70
31	Chi-Chi, Taiwan	1999	TCU068	7.62	0.32	487.34	0.56	0.43	0.57	184.60	250.8	295.99
32	Chi-Chi, Taiwan	1999	TCU075	7.62	0.91	573.02	0.33	0.27	0.33	88.58	37.61	88.59
33	Chi-Chi, Taiwan	1999	TCU076	7.62	2.76	614.98	0.31	0.42	0.42	67.82	58.71	88.76
34	Chi-Chi, Taiwan	1999	TCU082	7.62	5.18	472.81	0.23	0.19	0.26	57.81	43.08	68.97
35	Chi-Chi, Taiwan	1999	TCU087	7.62	7.00	473.90	0.13	0.12	0.13	43.68	36.26	53.89
36	Chi-Chi, Taiwan	1999	TCU101	7.62	2.13	272.60	0.21	0.24	0.26	68.35	51.78	68.40
37	Chi-Chi, Taiwan	1999	TCU102	7.62	1.51	714.27	0.30	0.16	0.30	109.04	77.55	117.67
38	Chi-Chi, Taiwan	1999	TCU103	7.62	6.10	494.10	0.13	0.17	0.18	62.13	27.70	62.18
39	Chi-Chi, Taiwan	1999	TCU122	7.62	9.35	475.46	0.22	0.26	0.26	42.43	34.40	44.30
40	Chi-Chi, Taiwan	1999	WGK	7.62	9.96	258.89	0.30	0.49	0.50	67.64	74.42	78.22

**Table B.2 Soil-site ground motion properties.**

#	EQ Name	Year	Station	<i>M</i>	<i>D</i>	<i>V</i> <sub>s30</sub>	<i>PGA</i> <sub>SN</sub>	<i>PGA</i> <sub>SP</sub>	<i>PGA</i> <sub>res</sub>	<i>PGV</i> <sub>SN</sub>	<i>PGV</i> <sub>SP</sub>	<i>PGV</i> <sub>res</sub>
1	'Mammoth Lakes-1'	1980	'Long Valley Dam (LAbut)'	6.06	15.46	345.40	0.24	0.45	0.46	13.71	15.84	24.69
2	'Chi-Chi, Taiwan'	1999	'CHY036'	7.62	16.06	233.10	0.32	0.20	0.32	36.26	39.92	41.59
3	'Cape Mendocino'	1992	'Rio Dell Overpass - FF'	7.01	14.33	311.80	0.42	0.54	0.55	39.15	38.04	51.45
4	'Imperial Valley-06'	1979	'Delta'	6.53	22.03	274.50	0.24	0.32	0.35	23.52	27.75	33.75
5	'Kocaeli, Turkey'	1999	'Yarimca'	7.51	4.83	297.00	0.28	0.31	0.38	48.24	68.85	72.94
6	'Imperial Valley-06'	1979	'Calipatria Fire Station'	6.53	24.60	205.80	0.13	0.08	0.14	16.60	12.35	18.31
7	'Chi-Chi, Taiwan'	1999	'CHY034'	7.62	14.82	378.80	0.29	0.34	0.34	28.73	51.47	55.44
8	'Chi-Chi, Taiwan'	1999	'NST'	7.62	38.43	375.30	0.37	0.43	0.44	15.04	32.76	32.76
9	'Kocaeli, Turkey'	1999	'Duzce'	7.51	15.37	276.00	0.37	0.43	0.44	52.22	41.11	62.27
10	'Trinidad'	1980	'Rio Dell Overpass, E Gr.'	7.20	10.00	311.80	0.37	0.43	0.44	8.84	11.03	11.25
11	'Spitak, Armenia'	1988	'Gukasian'	6.77	10.00	274.50	0.37	0.43	0.44	14.33	20.55	29.25
12	'Loma Prieta'	1989	'Gilroy Array #4'	6.93	14.34	221.80	0.35	0.26	0.42	35.75	23.36	39.89
13	'Chi-Chi, Taiwan'	1999	'TCU060'	7.62	8.53	272.60	0.21	0.11	0.22	25.72	47.09	48.70
14	'Victoria, Mexico'	1980	'Chihuahua'	6.33	18.96	274.50	0.21	0.13	0.22	15.86	27.00	27.42
15	'Loma Prieta'	1989	'Fremont - Emerson Court'	6.93	39.85	284.80	0.21	0.20	0.22	8.58	10.34	17.00
16	'Chalfant Valley-02'	1986	'Zack Brothers Ranch'	6.19	7.58	271.40	0.38	0.41	0.45	30.33	46.92	47.18
17	'Chi-Chi, Taiwan'	1999	'TCU118'	7.62	26.84	215.00	0.11	0.09	0.12	29.37	31.68	35.55
18	'Denali, Alaska'	2002	'TAPS Pump Station #10'	7.90	2.74	329.40	0.33	0.28	0.35	53.92	49.85	146.58
19	'Imperial Valley-06'	1979	'El Centro Array #4'	6.53	7.05	208.90	0.36	0.47	0.52	77.85	40.13	81.88
20	'Big Bear-01'	1992	'San Bernardino - E & H.'	6.46	10.00	271.40	0.08	0.10	0.11	12.96	13.84	14.37
21	'Landers'	1992	'Yermo Fire Station'	7.28	23.62	353.60	0.22	0.22	0.25	39.59	24.83	56.42
22	'Northridge-01'	1994	'Sylmar - Converter Sta'	6.69	5.35	251.20	0.59	0.80	0.91	69.47	75.14	132.90

#	EQ Name	Year	Station	<i>M</i>	<i>D</i>	<i>V</i> <sub>s30</sub>	<i>PGA</i> <sub>SN</sub>	<i>PGA</i> <sub>SP</sub>	<i>PGA</i> <sub>res</sub>	<i>PGV</i> <sub>SN</sub>	<i>PGV</i> <sub>SP</sub>	<i>PGV</i> <sub>res</sub>
23	'San Fernando'	1971	'LA - Hollywood Stor FF'	6.61	22.77	316.50	0.22	0.21	0.24	17.60	18.41	19.66
24	'N. Palm Springs'	1986	'Morongo Valley'	6.06	12.07	345.40	0.22	0.23	0.23	23.46	39.41	41.16
25	'Loma Prieta'	1989	'Hollister - South & Pine'	6.93	27.93	370.80	0.27	0.30	0.37	47.19	23.27	62.45
26	'Chi-Chi, Taiwan'	1999	'TCU055'	7.62	6.36	272.60	0.25	0.20	0.25	28.33	42.23	51.59
27	'Chi-Chi, Taiwan'	1999	'CHY025'	7.62	19.09	277.50	0.16	0.15	0.17	48.19	28.71	50.32
28	'Imperial Valley-06'	1979	'Brawley Airport'	6.53	10.42	208.70	0.16	0.21	0.23	36.10	35.85	45.05
29	'Chi-Chi, Taiwan'	1999	'CHY088'	7.62	37.48	272.60	0.15	0.22	0.22	15.33	20.71	22.11
30	'Duzce, Turkey'	1999	'Duzce'	7.14	6.58	276.00	0.36	0.52	0.55	61.75	62.85	87.41
31	'Chi-Chi, Taiwan'	1999	'TCU061'	7.62	17.19	272.60	0.14	0.14	0.15	40.98	43.73	44.68
32	'Loma Prieta'	1989	'Saratoga - Aloha Ave'	6.93	8.50	370.80	0.36	0.38	0.52	31.49	23.48	55.95
33	'Imperial Valley-02'	1940	'El Centro Array #9'	6.95	6.09	213.40	0.21	0.29	0.32	21.13	38.34	38.58
34	'Chi-Chi, Taiwan-3'	1999	'TCU123'	6.20	31.79	272.60	0.08	0.06	0.08	9.98	10.41	12.22
35	'Northridge-01'	1994	'Jensen Filter Plant'	6.69	5.43	373.10	0.52	1.07	1.08	49.83	64.42	89.61
36	'Chi-Chi, Taiwan-3'	1999	'CHY104'	6.20	35.05	223.20	0.11	0.08	0.12	23.02	19.53	30.09
37	'Loma Prieta'	1989	'Salinas - John & Work'	6.93	32.78	271.40	0.10	0.09	0.12	13.53	12.79	15.68
38	'Loma Prieta'	1989	'Coyote Lake Dam (Dow.)'	6.93	20.80	295.00	0.16	0.19	0.19	10.21	22.60	23.08
39	'Chi-Chi, Taiwan'	1999	'CHY008'	7.62	40.44	210.70	0.12	0.13	0.13	23.33	30.58	32.00
40	'Chi-Chi, Taiwan-6'	1999	'TCU141'	6.30	45.72	215.00	0.13	0.15	0.16	14.04	8.89	15.45

**Table B.3 Rock-site ground motion properties.**

#	EQ Name	Year	Station	<i>M</i>	<i>D</i>	<i>V</i> <sub>s30</sub>	<i>PGA</i> <sub>SN</sub>	<i>PGA</i> <sub>SP</sub>	<i>PGA</i> <sub>res</sub>	<i>PGV</i> <sub>SN</sub>	<i>PGV</i> <sub>SP</sub>	<i>PGV</i> <sub>res</sub>
1	'San Fernando'	1971	'Lake Hughes #4'	6.61	25.07	821.70	0.15	0.19	0.19	8.44	5.37	9.60
2	'Loma Prieta'	1989	'Gilroy Array #6'	6.93	18.33	663.30	0.16	0.18	0.18	17.45	11.45	17.53
3	'Kocaeli, Turkey'	1999	'Izmit'	7.51	7.21	811.00	0.15	0.22	0.24	22.60	27.31	30.02
4	'Northridge-01'	1994	'LA - Wonderland Ave'	6.69	20.30	1222.5	0.16	0.12	0.17	11.38	5.62	13.29
5	'Imperial Valley-06'	1979	'Cerro Prieto'	6.53	15.19	659.60	0.15	0.17	0.19	15.34	11.42	18.79
6	'Hector Mine'	1999	'Hector'	7.13	11.66	684.90	0.34	0.31	0.34	37.02	29.51	44.16
7	'San Fernando'	1971	'Pasadena-Old Seismo Lab'	6.61	21.50	969.10	0.09	0.19	0.20	6.96	9.71	11.53
8	'Duzce, Turkey'	1999	'Lamont 531'	7.14	8.03	659.60	0.16	0.12	0.16	9.71	12.95	16.13
9	'Hector Mine'	1999	'Heart Bar State Park'	7.13	61.21	684.90	0.07	0.09	0.10	7.15	11.64	14.01
10	'Chi-Chi, Taiwan'	1999	'TCU138'	7.62	9.79	652.90	0.20	0.23	0.23	40.66	40.80	44.47
11	'Chi-Chi, Taiwan-6'	1999	'TCU129'	6.30	24.80	664.40	0.34	0.19	0.37	16.50	10.35	16.97
12	'Coyote Lake'	1979	'Gilroy Array #6'	5.74	3.11	663.30	0.45	0.33	0.48	51.54	27.14	51.55
13	'Taiwan SMART1'	1986	'SMART1 E02'	7.30	10.00	659.60	0.12	0.15	0.15	12.52	14.14	14.51
14	'Irpinia, Italy-01'	1980	'Bagnoli Irpinio'	6.90	8.18	1000.0	0.19	0.13	0.21	29.34	23.35	32.69
15	'Loma Prieta'	1989	'San Jose-Santa Teresa Hill'	6.93	14.69	671.80	0.27	0.22	0.29	25.69	21.92	26.56
16	'Irpinia, Italy-01'	1980	'Bisaccia'	6.90	21.26	1000.0	0.12	0.08	0.12	16.27	15.83	23.49
17	'Chi-Chi, Taiwan'	1999	'TCU045'	7.62	26.00	704.60	0.60	0.29	0.61	42.03	33.72	46.96
18	'Kocaeli, Turkey'	1999	'Gebze'	7.51	10.92	792.00	0.60	0.29	0.61	26.12	25.01	56.46
19	'Northridge-01'	1994	'Pacoima Dam (downstr)'	6.69	7.01	2016.1	0.60	0.29	0.61	18.49	13.83	49.97
20	'Denali, Alaska'	2002	'Carlo (temp)'	7.90	50.94	963.90	0.60	0.29	0.61	9.96	5.76	10.85
21	'Helena, Montana-1'	1935	'Carroll College'	6.00	10.00	659.60	0.60	0.29	0.61	5.15	9.90	16.52
22	'Northridge-01'	1994	'Vasquez Rocks Park'	6.69	23.64	996.40	0.60	0.29	0.61	17.78	13.65	18.86
23	'Chi-Chi, Taiwan'	1999	'WNT'	7.62	1.84	664.40	0.96	0.63	0.97	69.16	41.19	73.58
24	'Loma Prieta'	1989	'Golden Gate Bridge'	6.93	79.81	641.60	0.14	0.25	0.25	28.60	29.92	38.08
25	'Loma Prieta'	1989	'UCSC'	6.93	18.51	714.00	0.37	0.31	0.39	12.04	11.57	15.46

#	EQ Name	Year	Station	<i>M</i>	<i>D</i>	<i>V</i> <sub>s30</sub>	<i>PGA</i> <sub>SN</sub>	<i>PGA</i> <sub>SP</sub>	<i>PGA</i> <sub>res</sub>	<i>PGV</i> <sub>SN</sub>	<i>PGV</i> <sub>SP</sub>	<i>PGV</i> <sub>res</sub>
26	'Victoria, Mexico'	1980	'Cerro Prieto'	6.33	14.37	659.60	0.63	0.60	0.64	26.13	19.71	31.91
27	'Northridge-01'	1994	'Santa Susana Ground'	6.69	16.74	715.10	0.23	0.27	0.29	14.34	19.87	22.20
28	'Loma Prieta'	1989	'Gilroy - Gavilan Coll.'	6.93	9.96	729.70	0.29	0.41	0.45	30.79	15.30	30.82
29	'Duzce, Turkey'	1999	'Mudurnu'	7.14	34.30	659.60	0.11	0.07	0.13	10.07	15.79	16.76
30	'Northridge-01'	1994	'Burbank - Howard Rd.'	6.69	16.88	821.70	0.11	0.14	0.16	7.29	5.79	9.55
31	'Chi-Chi, Taiwan-3'	1999	'TCU138'	6.20	22.15	652.90	0.13	0.13	0.14	19.72	9.88	21.20
32	'Chi-Chi, Taiwan-6'	1999	'TCU138'	6.30	33.63	652.90	0.06	0.05	0.07	8.41	7.37	11.34
33	'Loma Prieta'	1989	'UCSC Lick Observatory'	6.93	18.41	714.00	0.41	0.51	0.52	17.69	18.69	19.78
34	'Loma Prieta'	1989	'Gilroy Array #1'	6.93	9.64	1428.0	0.43	0.44	0.47	38.57	17.08	38.58
35	'Northridge-01'	1994	'LA Dam'	6.69	5.92	629.00	0.58	0.42	0.58	35.56	40.75	77.39
36	'Northridge-01'	1994	'LA 00'	6.69	19.07	706.20	0.38	0.33	0.42	22.07	31.81	38.01
37	'Sitka, Alaska'	1972	'Sitka Observatory'	7.68	34.61	659.60	0.09	0.09	0.10	5.61	14.70	14.71
38	'Northridge-01'	1994	'LA - Chalon Rd'	6.69	20.45	740.10	0.19	0.23	0.24	18.57	29.21	29.42
39	'Loma Prieta'	1989	'Belmont - Envirotech'	6.93	44.11	627.60	0.14	0.10	0.14	19.97	7.63	19.97
40	'Chi-Chi, Taiwan'	1999	'TCU129'	7.62	1.84	664.40	1.01	0.64	1.03	60.16	35.37	61.23



# Appendix C: Description of the Seed Bridge Models

A comprehensive description of the numerical models developed for each seed bridge is presented here. These models are developed using OpenSees script package:

- Bridge A (two-span and single-column bridge).
- Bridge B (two-span and multi-column bridge).
- Bridge C (three-span and multi-column bridge).

## C.1 NODAL AND ELEMENT DESIGNATIONS

Illustrative descriptions of the nodal and element designations corresponding to the seed bridges used in this study are shown in Figures C.1 through C.3. These figures should be useful for understanding the bridge models that accompany this report. The nodes, beam elements, and *zeroLength* elements are represented by different shapes/markers. For brevity, not all of the labels are displayed in the aforementioned figures.

## C.2 OPENSEES SCRIPTS

The descriptions of different OpenSees scripts are explained in this subsection. These scripts are named based on the bridge matrix format discussed in Chapter 3. For each modeling script, the naming format comprises of two parts: the first part (i.e., before the underscore character) represents the seed bridge title followed by the column-bent element structural characterization. For instance, ALS represents Bridge A for the case where lower-height column and symmetrical span arrangement is considered. The second portion (after the underscore character) describes a sub-component of the bridge mode

The OpenSees script titled *Analyzer.tcl* is the mother/main file and calls the other required scripts for analysis. The abutment skew angles (0°, 15°, 30°, 45°, and 60°) and the incidence angles (0°, 30°, 60°, 90°, 120°, and 150°) are generated by the *Analyzer.tcl* script. In the following itemized list, brief descriptions of the functions of the said scripts are provided:

*AFIU\_Abutments.tcl*: Constructs two abutment models [A1: Simplified abutment model; and AAA2: Skewed abutment model (Chapter 4)].

*AFIU\_Analyzer.tcl*: The mother script, sources all other scripts (the global geometry of the bridge, types of analyses, type of material properties and abutment types).

*AFIU\_ColSection.tcl*: Generates geometrical properties of the column-bent fiber section.

*AFIU\_EQ.tcl*: Runs 40 response history analyses for 40 ground motions in one ground motion set and records element forces and nodal displacements.

*AFIU\_FP.tcl*: Records first three fundamental periods of the bridge.

*AFIU\_GM.tcl*: Reads ground motion records from the predefined address path and performs response history analysis (*UniformExcitation*).

*AFIU\_GravityLoad.tcl*: Assigns gravity loading.

*AFIU\_Materials.tcl*: Defines material properties (Concrete: *Concrete01*, *Concrete02*, and *Hysteretic*, simulating *concrete02*; and Steel: *Steel02*, *ReinforcingSteel*, and *Hysteretic*, simulating *ReinforcingSteel*).

*AFIU\_Modal.tcl*: Generates nodal coordinates and displacements of the first three mode shapes of the bridge.

*AFIU\_Model.tcl*: Generates nodal coordinates based on the incidence angle (i.e., *GMskew* variable in the script), constructs linear superstructure and nonlinear column-bent elements, and performs the static and modal analyses.

*AFIU\_Nodes.tcl*: Defines original coordinates of the nodes.

*AFIU\_POL.tcl*: Performs push-over analysis in longitudinal direction.

*AFIU\_POT.tcl*: Performs push-over analysis in transverse direction.

*BuildRCcircSection.tcl*: Builds circular fiber section of the column-bent.

*ReadSMDFile.tcl*: Modifies ground motion record format to format readable by OpenSees.

*Units&Constants.tcl*: Defines constants and converts US and SI unit systems.

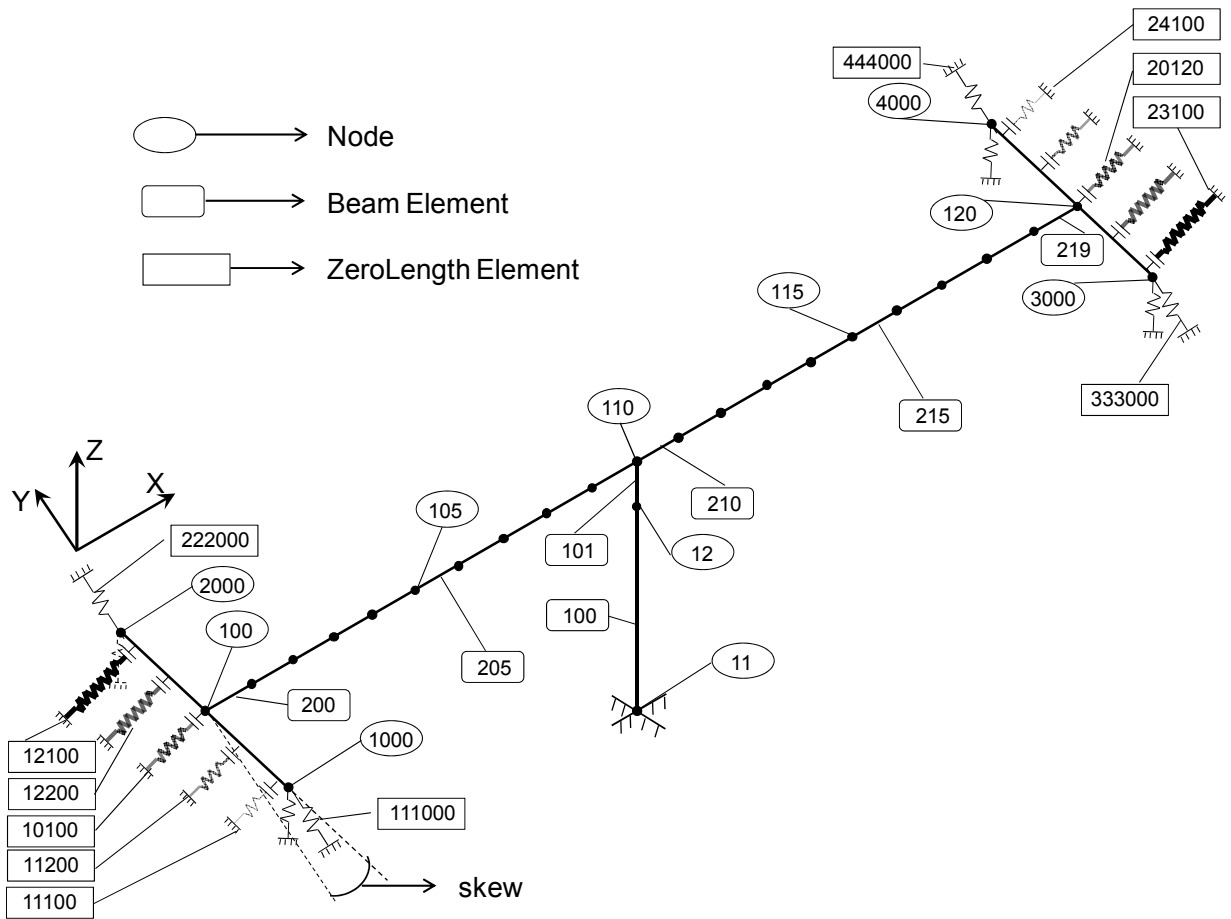


**Figure C.1 Nodal and element designation of Bridge A.**

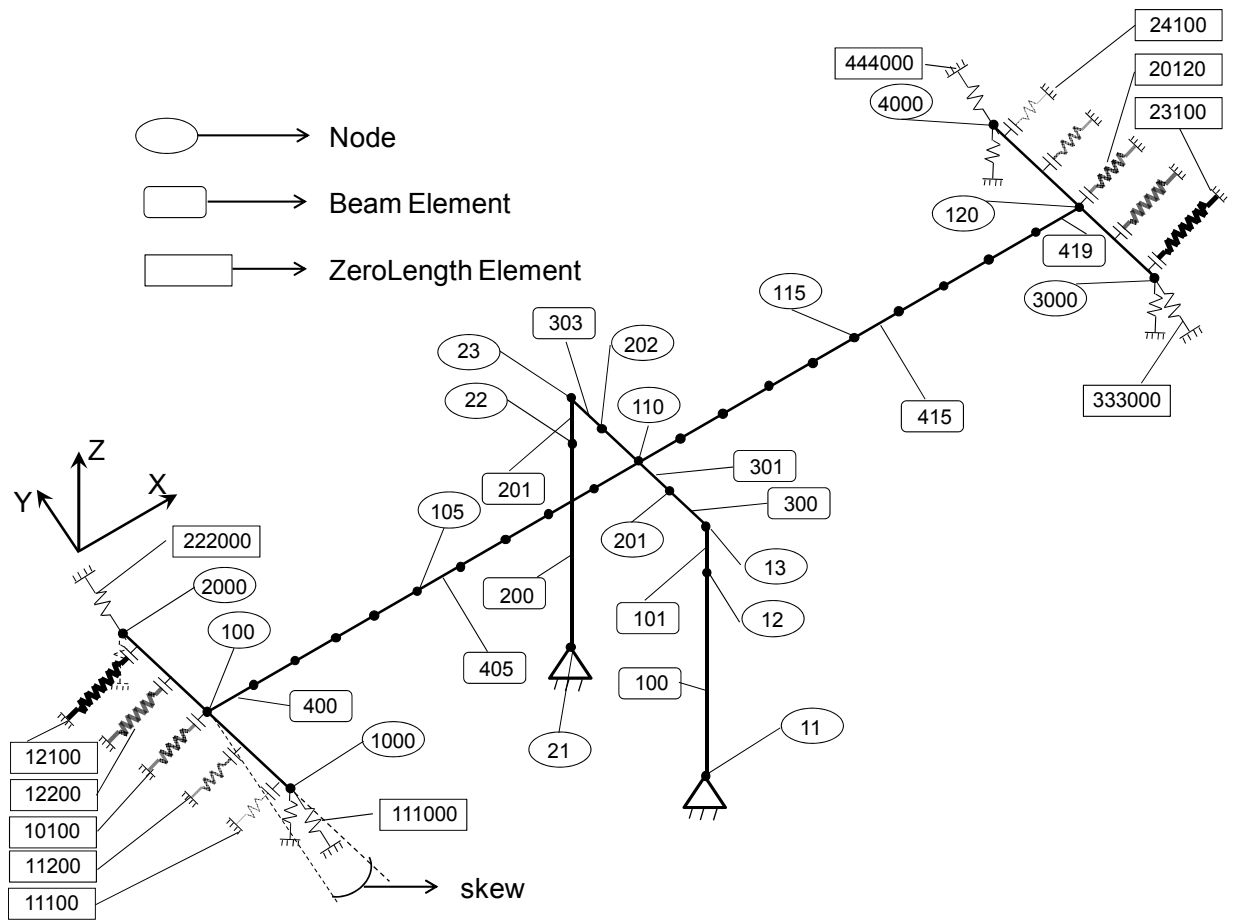
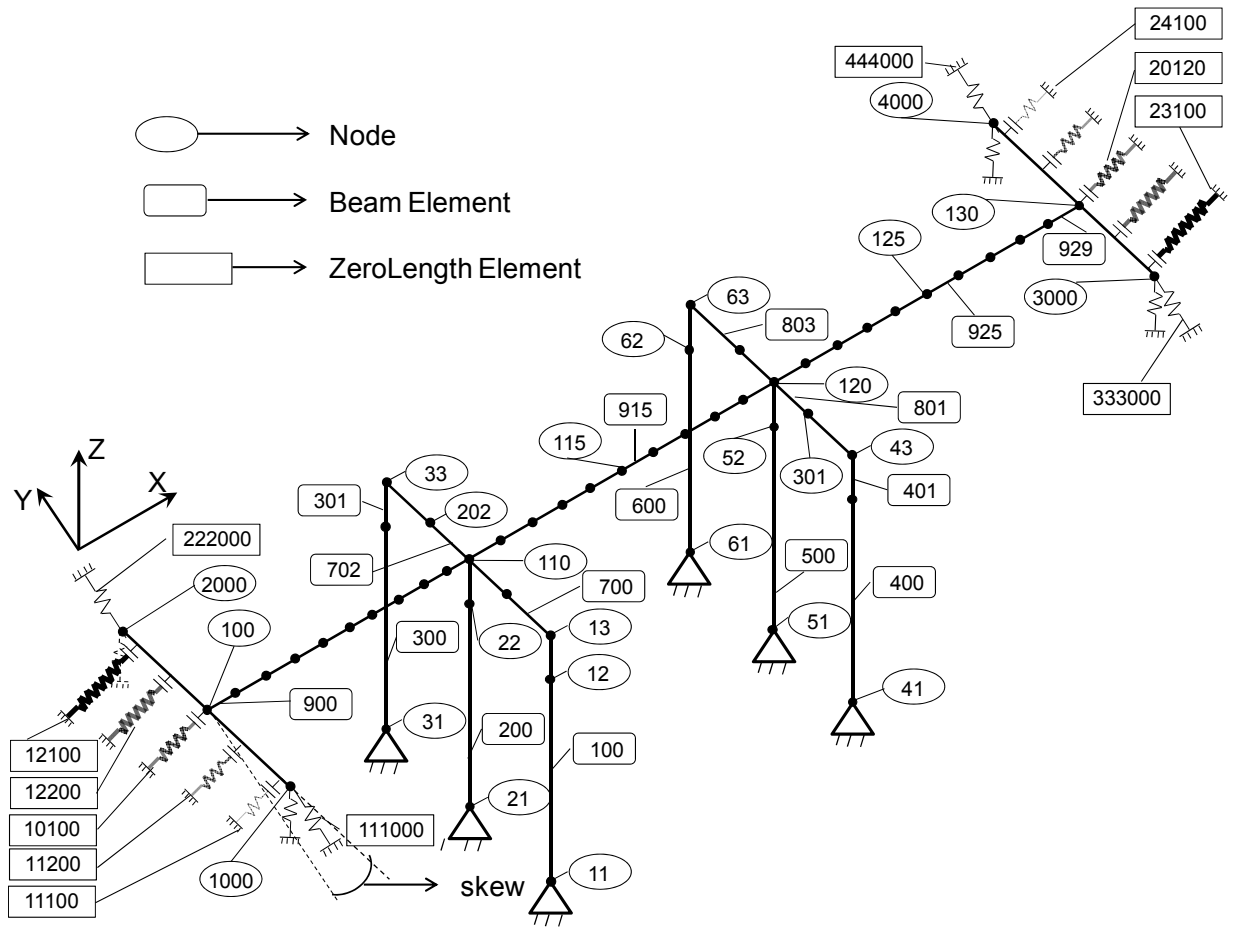


Figure C.2 Nodal and element designation of Bridge B.



**Figure C.3 Nodal and element designation of Bridge C.**



## Appendix D: Shear Key Modeling In OpenSees

In the first attempt for modeling the shear keys, we attempted to model the transverse response of the skewed abutment by using two macro-elements—i.e., the shear keys and the pile group—in a series arrangement. This combination was devised to resist only in compression. Two springs were connected to the rigid bar ends in the transverse direction to represent the abutment resistance in the transverse direction. We employed a *hysteretic* material to model the shear key behavior, and an elastic material with no-tension stiffness to model the pile group. We then studied the response history of a representative bridge from the bridge matrix that had asymmetric span and no skew angle, under an intense ground motion—namely, ALS0P0 (i.e., Bridge A with lower height column-bent, symmetrical span arrangement, incident angle of  $0^\circ$  and non-skewed abutment under a pulse-like ground motion). The transverse component of this pulse-like ground motion—i.e., number 11, Loma Prieta, LGPG (Appendix B)—is shown in Figure D.1. To attain the most appropriate OpenSees element to model the system, we considered the following four alternatives:

**Case I:** Force-deformation backbone for the transverse spring.

Due to symmetry in the numerical model, rotation of the deck was not expected. However, as shown in Figure D.2, we observed deck rotation once we employed this modeling technique. Deck rotation appeared approximately at 15sec into the ground motion. The deformation of the transverse spring located in different abutments—yet, at the same side of the bridge in the transverse direction—is shown in Figure D.3. We expected to observe identical deformations in both springs; however as shown in Figure D.3, spring deformations began to diverge at the 17.75 sec into the analysis. Figure D.4 shows the transverse spring response history. It was found that whenever the backbone curve reached a negative stiffness, there was a numerical convergence problem.

**Case II:** Elastic-perfectly-plastic force-deformation backbone curve resisting only compression.

We modified the force-deformation (backbone) curve of the transverse spring in the plastic domain from negative stiffness to zero stiffness. This results in an elastic-perfectly-plastic (EPP) backbone curve, which only resists compression. This setting resulted in an unexpected deck rotation as well (see Figure D.5). Figures D.6 and D.7 display the transverse spring deformation and the development of the hysteretic curve during response history analysis. Similar to Case I, the zero-stiffness, which occurs during the reloading cycle, causes a convergence problem in the iterative solution towards equilibrium.

**Case III:** The elastic-perfectly-plastic force-deformation backbone curve resisting both compression and tension.

In order to avoid the previously mentioned numerical problems caused by zero-stiffness, we considered using an elastic-perfectly-plastic system that resists both tension and compression. In this case, the capacity is halved to save the uniformity. As shown in Figure D.8, no divergence in the transverse spring deformation occurred under this approach. However, this method was deemed unusable in the numerical bridge models of this study, because the behavior of a skewed abutment is not compatible with the assumptions employed in this modeling technique.

**Case IV:** Shear key modeled by uniaxialMaterial *concrete02*.

We modeled the shear key by using *concrete02* from the *uniaxialMaterial* library of OpenSees. This *uniaxialMaterial* defines concrete material with tension resistance. As shown in Figure D.9, no convergence problem occurred. The simultaneous parallel force balance problem is solved by defining a small strength in tension.

Given the findings from various approaches summarized above, we opted to use the modeling technique described in Case IV to represent the responses of the shear keys.

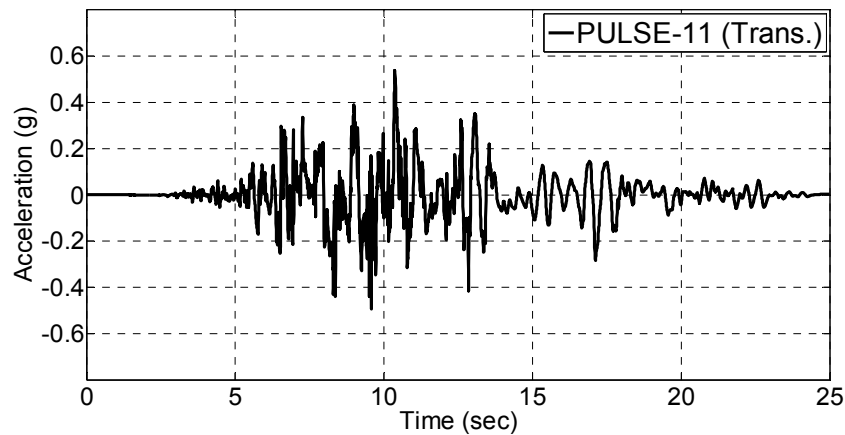


**Figure D.1** Transverse component of pulse-like ground motion number-11.

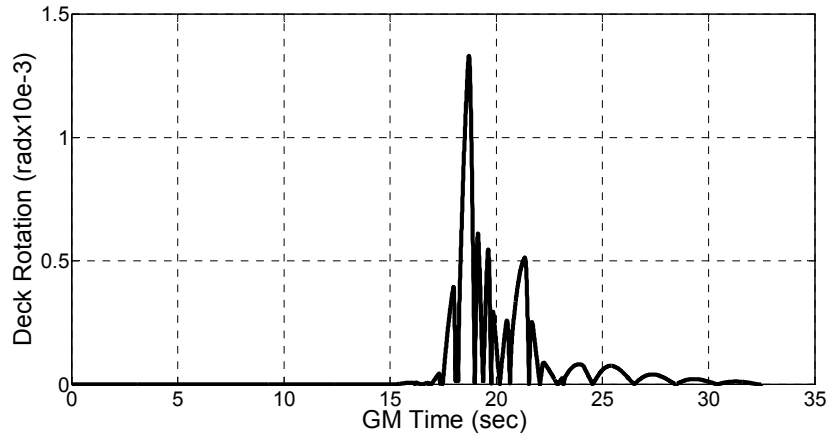


Figure D.2 Deck rotation of bridge ALS0P0 under Pulse-11 ground motion (Case I).

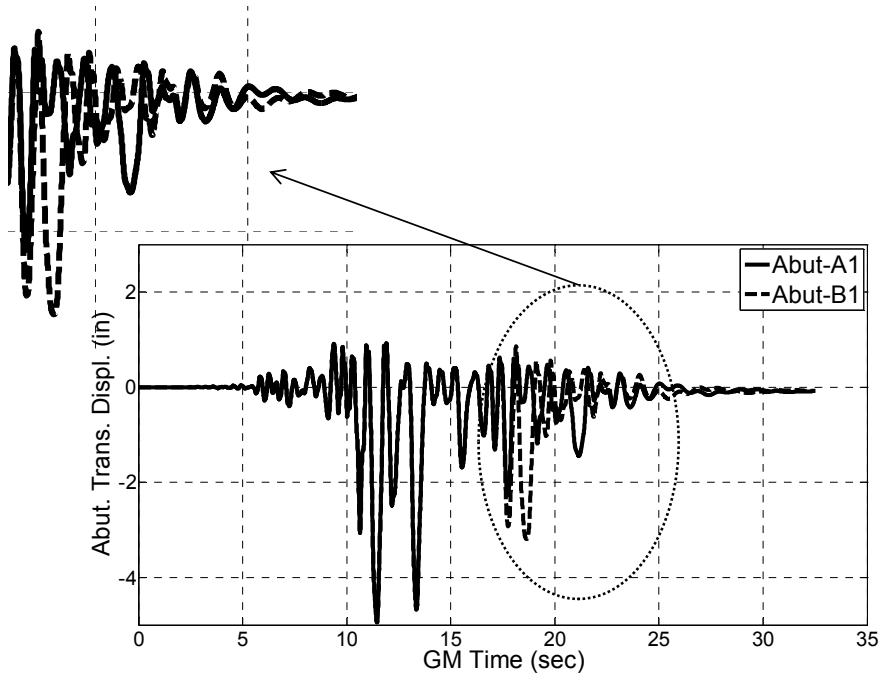
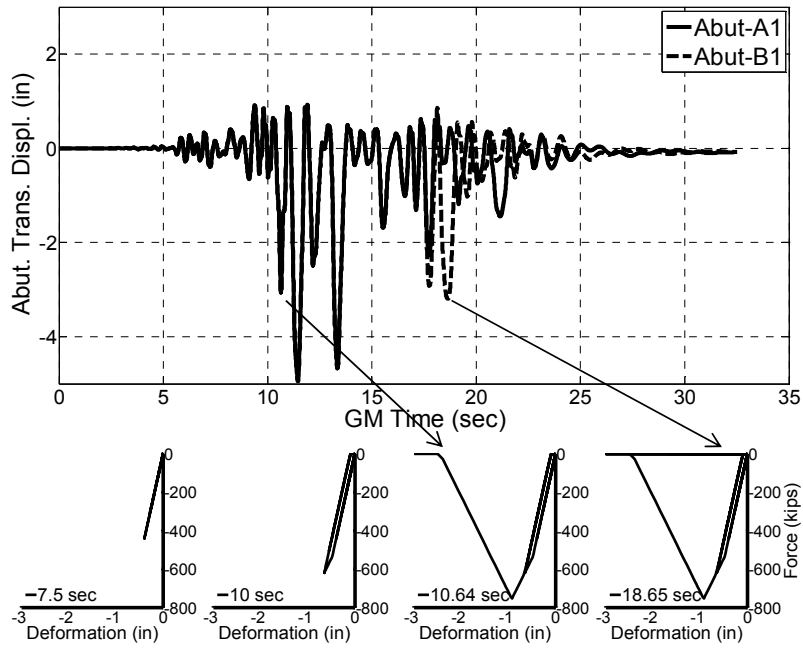
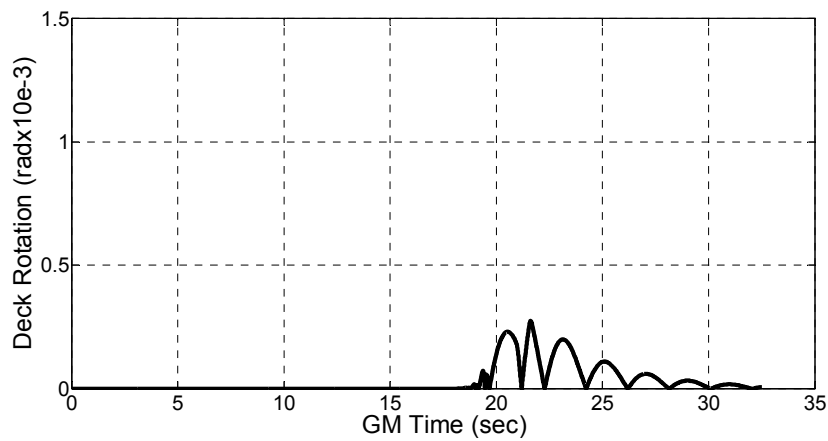


Figure D.3 Transverse spring deformation located in two different abutments, but on the same side (Case I).



**Figure D.4 Backbone curve of the transverse spring during response history analysis (Case I).**



**Figure D.5 Deck rotation of the bridge ALS0P0 under Pulse-11 ground motion (Case II).**

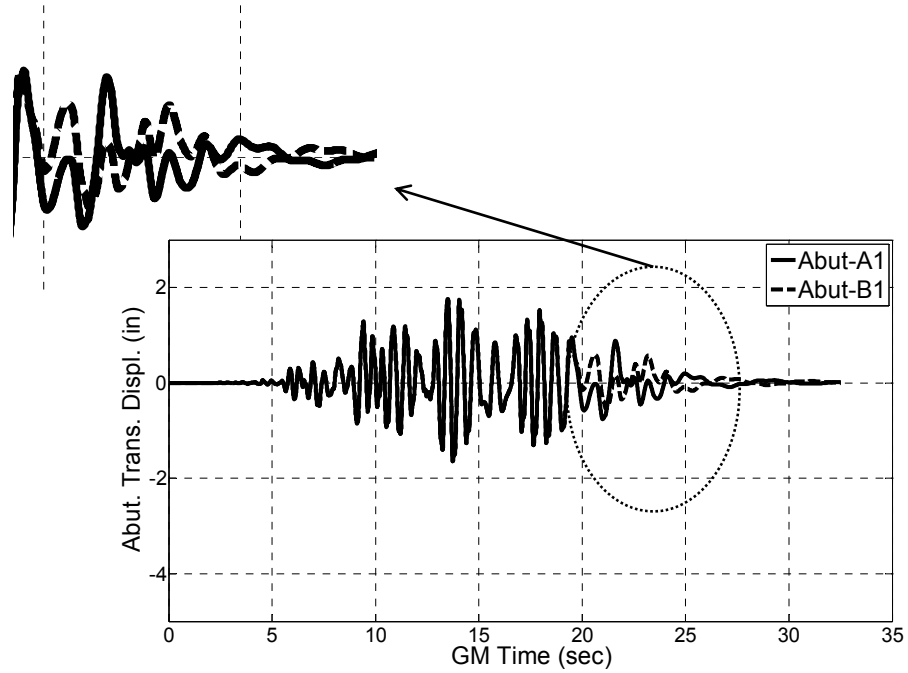


**Figure D.6** Transverse spring deformation located in two different abutments, but on the same side (Case II).

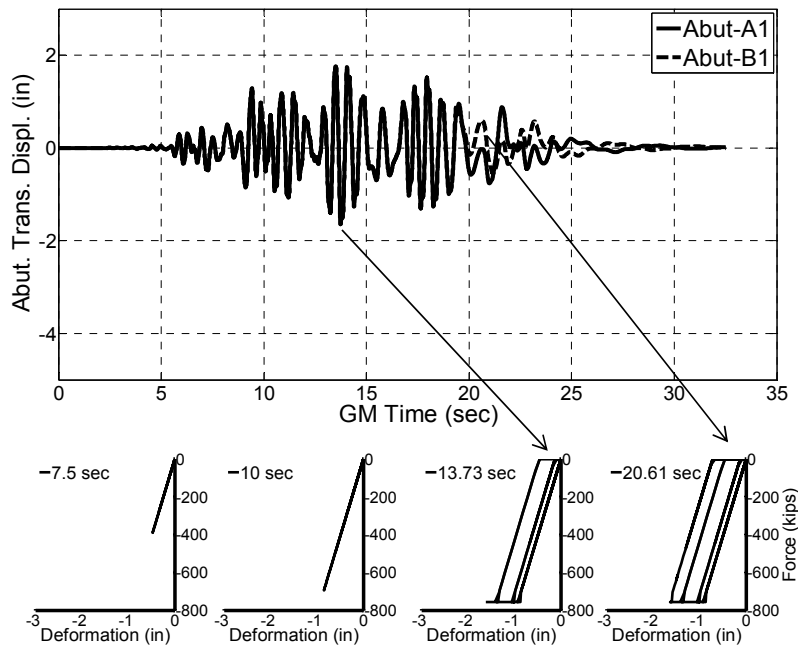


**Figure D.7** Backbone curve of the transverse spring during response history analysis (Case II).

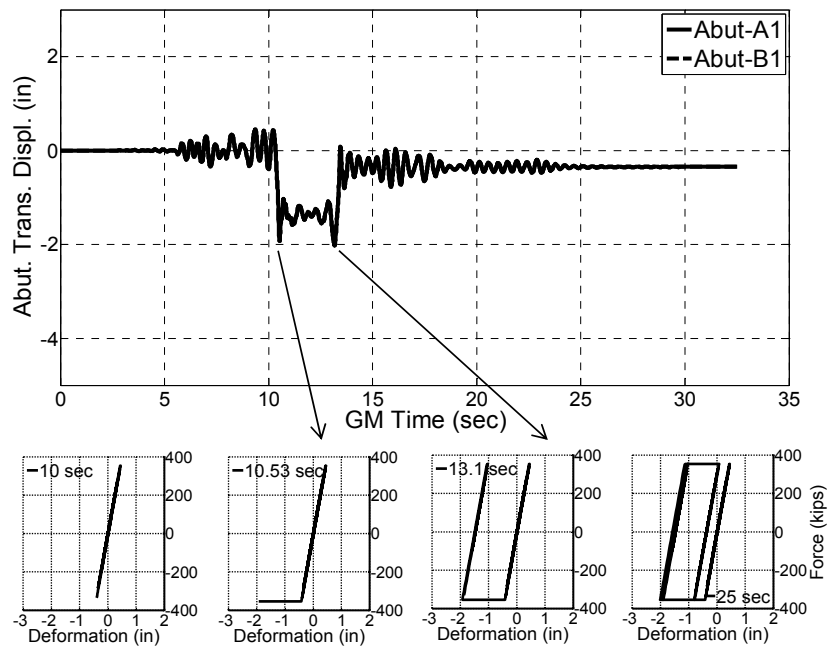


**Figure D.8 Backbone curve of the transverse spring during response history analysis (Case III).**

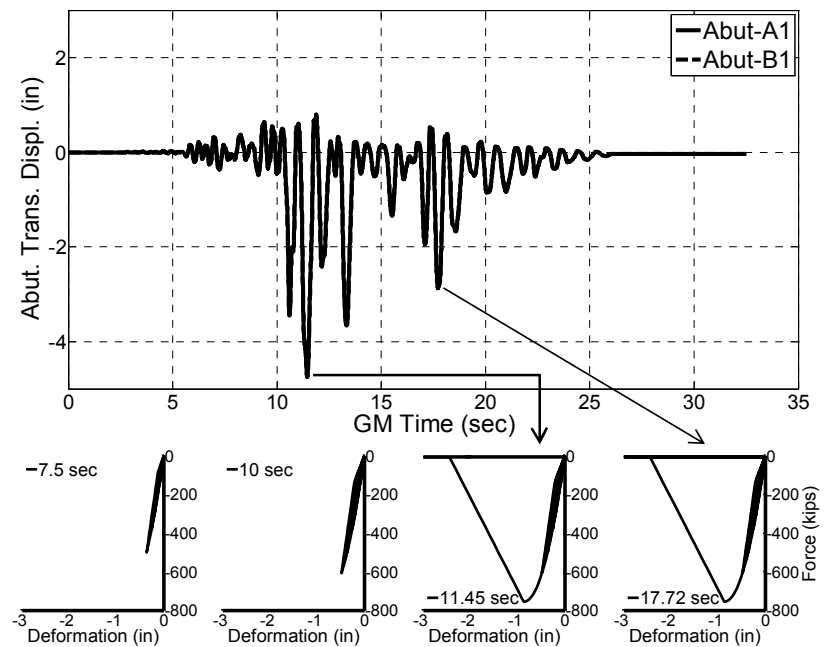


**Figure D.9 Backbone curve of the transverse spring during response history analysis (Case IV).**

## Appendix E: M-PARS Statistical Parameters for the Bridge Matrix

In Tables E.1 through E.27, we tabulated the statistical parameters of  $G(EDP|IM)$  for the bridge matrix obtained from application of the M-PARS formulation. Three *EDPs* are considered: deck rotation ( $\theta_{rot}$ ), abutment unseating ( $\delta_{unseat}$ ), and column drift ratio ( $\theta_{col}$ ). The parameters tabulated here are  $\mathbf{a}_{0S_{11}}$  and  $\mathbf{a}_{1S_{11}}$  [see Equation (5.8)] with the dispersion of  $\beta_{S_{11}}$  (i.e.,  $\beta_{EDP|S_{11},IM}$ ); and similarly,  $\mathbf{a}_{0S_{12}}$  and  $\mathbf{a}_{1S_{12}}$  [see Equation (5.9)] with the dispersion of  $\beta_{S_{12}}$  (i.e.,  $\beta_{EDP|S_{12},IM}$ ). The last four columns of the tables display the medians ( $\eta_{BC}$  and  $\eta_{SKF}$ ) and dispersions ( $\beta_{BC}$  and  $\beta_{SKF}$ ) of the fragility curves of the BC and SKF states. A blank cell in the tables indicates that there was not an adequate amount of data to perform a meaningful regression for that specific case. For instance, the blank cell for “ $\eta_{BC}$ ” in Table E.2 for ALS0S indicates that there is no bridge collapse in any of the 240 response history analyses.

**Table E.1 Statistical parameters for Bridge A with pulse-like ground motion and a deck rotation EDP.**

Bridges	$a_{0S11}$	$a_{1S11}$	$\beta_{S11}$	$a_{0S12}$	$a_{1S12}$	$\beta_{S12}$	$\eta_{BC}$	$\beta_{BC}$	$\eta_{SKF}$	$\beta_{SKF}$
ALS0P	0.000	1.287	2.095	5.332	-0.347	2.760	164.108	0.255	104.812	0.134
ALS1P	0.110	-0.066	0.161	0.140	0.773	0.454	82.239	0.285	105.441	0.147
ALS2P	0.092	0.095	0.155	0.158	0.764	0.358	101.351	0.303	104.646	0.147
ALS3P	0.126	0.080	0.119	0.399	0.544	0.406	103.041	0.305	104.222	0.138
ALS4P	0.094	0.212	0.136	0.173	0.676	0.442	91.756	0.258	104.704	0.142
ALA0P	0.008	0.301	0.785	0.046	1.044	0.401	124.177	0.267	103.413	0.140
ALA1P	0.147	-0.109	0.178	0.033	1.129	0.475	98.144	0.291	103.911	0.147
ALA2P	0.080	0.127	0.091	0.112	0.863	0.361	83.869	0.319	104.016	0.139
ALA3P	0.144	0.056	0.137	0.072	0.919	0.455	118.937	0.248	104.724	0.136
ALA4P	0.108	0.174	0.108	0.133	0.740	0.448	83.660	0.258	104.388	0.148
AHS0P	0.000	0.508	1.014	4.748	-0.307	2.308	159.754	0.496	101.164	0.119
AHS1P	0.037	0.223	0.263	0.065	1.023	0.649	113.782	0.347	101.534	0.126
AHS2P	0.081	0.156	0.103	0.103	0.908	0.439	124.517	0.333	101.833	0.126
AHS3P	0.070	0.255	0.120	0.024	1.200	0.418	118.922	0.271	101.703	0.125
AHS4P	0.117	0.186	0.130	0.032	1.073	0.379	116.823	0.276	99.484	0.130
AHA0P	0.001	0.621	1.067	0.054	1.076	0.520	190.782	0.355	99.709	0.119
AHA1P	0.042	0.202	0.272	0.059	1.067	0.482	119.904	0.397	101.143	0.130
AHA2P	0.107	0.099	0.101	0.070	1.014	0.436	119.613	0.358	103.039	0.121
AHA3P	0.075	0.236	0.114	0.021	1.246	0.457	140.831	0.270	101.429	0.123
AHA4P	0.102	0.208	0.116	0.022	1.155	0.502	114.454	0.298	97.813	0.110

**Table E.2 Statistical parameters for Bridge A with soil-site ground motion and a deck rotation EDP.**

Bridges	$a_{0S11}$	$a_{1S11}$	$\beta_{S11}$	$a_{0S12}$	$a_{1S12}$	$\beta_{S12}$	$\eta_{BC}$	$\beta_{BC}$	$\eta_{SKF}$	$\beta_{SKF}$
ALS0S	0.000	1.967	1.819	0.268	0.259	2.670			81.203	0.245
ALS1S	0.010	0.509	0.235	0.051	1.045	0.287			75.629	0.256
ALS2S	0.016	0.526	0.181	0.031	1.146	0.253			73.694	0.245
ALS3S	0.022	0.522	0.152	0.013	1.320	0.129			72.131	0.239
ALS4S	0.031	0.496	0.206	0.010	1.314	0.103	132.900	0.000	69.266	0.206
ALA0S	0.001	0.720	0.482	0.093	0.904	0.368			71.771	0.267
ALA1S	0.011	0.504	0.229	0.050	1.076	0.509			74.071	0.247
ALA2S	0.018	0.512	0.164	0.014	1.305	0.299			74.332	0.249
ALA3S	0.022	0.516	0.159	0.010	1.378	0.180			70.692	0.225
ALA4S	0.033	0.474	0.169	0.015	1.215	0.187	132.900	0.000	67.236	0.202
AHS0S	0.000	1.615	1.512	0.676	0.160	1.809			65.746	0.232
AHS1S	0.008	0.593	0.223	0.194	0.762	0.544			64.233	0.226
AHS2S	0.015	0.591	0.187	0.055	1.060	0.365	90.971	0.246	62.034	0.225
AHS3S	0.020	0.569	0.181	0.093	0.893	0.292	123.330	0.115	61.145	0.204
AHS4S	0.035	0.475	0.187	0.039	1.046	0.138	128.680	0.080	57.311	0.187
AHA0S	0.001	0.783	0.773	0.224	0.749	0.456			63.891	0.224
AHA1S	0.010	0.548	0.233	0.150	0.842	0.411			63.758	0.226
AHA2S	0.017	0.549	0.171	0.050	1.078	0.250	132.900	0.000	61.424	0.217
AHA3S	0.019	0.583	0.164	0.091	0.904	0.285	123.330	0.115	59.529	0.208
AHA4S	0.031	0.505	0.204	0.031	1.115	0.115	126.735	0.095	58.833	0.195

**Table E.3 Statistical parameters for Bridge A with rock-site ground motion and a deck rotation EDP.**

Bridges	$a_{0S11}$	$a_{1S11}$	$\beta_{S11}$	$a_{0S12}$	$a_{1S12}$	$\beta_{S12}$	$\eta_{BC}$	$\beta_{BC}$	$\eta_{SKF}$	$\beta_{SKF}$
ALS0R	0.000	2.202	1.116	0.093	0.414	2.190			51.739	0.130
ALS1R	0.009	0.608	0.247	0.359	0.465	0.710			51.739	0.130
ALS2R	0.015	0.614	0.142	0.681	0.286	0.160			49.132	0.148
ALS3R	0.019	0.622	0.140	3.271	-0.127	0.110			50.975	0.136
ALS4R	0.025	0.617	0.152	1.026	0.135	0.053			54.516	0.126
ALA0R	0.001	0.984	0.436	0.129	0.798	0.477			48.644	0.140
ALA1R	0.010	0.626	0.233	0.502	0.481	0.360			49.350	0.140
ALA2R	0.013	0.664	0.161	0.827	0.321	0.096			50.021	0.144
ALA3R	0.020	0.598	0.140	0.445	0.423	0.107			51.583	0.139
ALA4R	0.025	0.615	0.135	0.100	0.734	0.120			52.736	0.125
AHS0R	0.000	2.650	1.686	1.213	-0.142	1.133			52.577	0.149
AHS1R	0.008	0.654	0.178	0.337	0.544	0.510			50.260	0.153
AHS2R	0.013	0.693	0.153	0.173	0.715	0.322			49.961	0.162
AHS3R	0.017	0.660	0.153	0.531	0.381	0.229			50.462	0.161
AHS4R	0.025	0.625	0.156	0.178	0.622	0.088	29.112	0.059	50.680	0.148
AHA0R	0.000	1.278	0.639	0.055	1.026	0.496			49.332	0.176
AHA1R	0.007	0.698	0.180	0.696	0.379	0.285			49.749	0.176
AHA2R	0.012	0.699	0.153	0.364	0.519	0.255			49.793	0.163
AHA3R	0.017	0.669	0.150	0.475	0.414	0.213			50.462	0.161
AHA4R	0.024	0.630	0.162	0.142	0.688	0.117			52.358	0.159

**Table E.4 Statistical parameters for Bridge B with pulse-like ground motion and a deck rotation EDP.**

Bridges	$a_{0S11}$	$a_{1S11}$	$\beta_{S11}$	$a_{0S12}$	$a_{1S12}$	$\beta_{S12}$	$\eta_{BC}$	$\beta_{BC}$	$\eta_{SKF}$	$\beta_{SKF}$
BLS0P	0.000	1.162	1.767	0.001	1.736	0.621	156.827	0.135	106.980	0.103
BLS1P	0.004	0.863	0.480	6.507	-0.030	0.344	96.411	0.273	109.151	0.147
BLS2P	0.007	0.825	0.355	1.278	0.279	0.216	101.970	0.261	107.126	0.151
BLS3P	0.004	1.030	0.345	0.577	0.430	0.234	135.248	0.248	97.001	0.093
BLS4P	0.006	0.962	0.235	0.216	0.570	0.191	120.086	0.251	100.630	0.125
BLA0P	0.000	1.122	2.102	3.085	0.126	0.177	113.389	0.342	107.663	0.139
BLA1P	0.003	0.885	0.463	1.438	0.287	0.295	139.622	0.352	108.188	0.156
BLA2P	0.007	0.829	0.313	1.115	0.326	0.254	148.035	0.182	106.440	0.147
BLA3P	0.005	0.977	0.313	0.327	0.523	0.167	132.150	0.227	102.490	0.139
BLA4P	0.005	1.021	0.265	0.107	0.722	0.187	108.538	0.257	101.378	0.127
BHS0P	0.000	0.780	1.405	0.029	1.078	0.339	119.969	0.242	111.210	0.132
BHS1P	0.013	0.615	0.333	0.504	0.584	0.240	121.587	0.266	105.778	0.136
BHS2P	0.015	0.709	0.324	0.695	0.477	0.213	119.085	0.228	108.804	0.140
BHS3P	0.017	0.724	0.239	0.909	0.331	0.160	124.738	0.245	101.244	0.106
BHS4P	0.005	1.025	0.231	1.489	0.202	0.185	110.460	0.244	97.799	0.096
BHA0P	0.000	0.947	1.567	0.315	0.636	0.227	129.596	0.194	109.438	0.129
BHA1P	0.011	0.677	0.386	1.154	0.392	0.201	130.741	0.239	106.740	0.146
BHA2P	0.016	0.702	0.352	1.808	0.259	0.182	97.193	0.249	106.810	0.114
BHA3P	0.024	0.654	0.206	3.872	0.042	0.162	115.675	0.261	100.985	0.101
BHA4P	0.012	0.832	0.221	0.675	0.361	0.164	101.359	0.234	96.354	0.082

**Table E.5 Statistical parameters for Bridge B with soil-site ground motion and a deck rotation EDP.**

Bridges	$a_{0S11}$	$a_{1S11}$	$\beta_{S11}$	$a_{0S12}$	$a_{1S12}$	$\beta_{S12}$	$\eta_{BC}$	$\beta_{BC}$	$\eta_{SKF}$	$\beta_{SKF}$
BLS0S	0.000	0.936	0.833							
BLS1S	0.001	1.302	0.482				86.590	0.278		
BLS2S	0.001	1.306	0.381				132.900	0.000		
BLS3S	0.001	1.334	0.344	0.001	1.711	0.257	97.515	0.351	119.825	0.113
BLS4S	0.004	1.113	0.282	0.005	1.394	0.197	97.141	0.411	99.387	0.113
BLA0S	0.000	1.099	1.317	1.020	0.347	0.147			130.418	0.056
BLA1S	0.002	1.081	0.350							
BLA2S	0.002	1.200	0.342				132.900	0.000		
BLA3S	0.001	1.366	0.375				82.956	0.513		
BLA4S	0.004	1.125	0.283	42.552	-0.545	0.195	99.865	0.319	123.658	0.130
BHS0S	0.000	1.095	0.982							
BHS1S	0.002	1.109	0.522	0.000	2.405	0.090			130.263	0.060
BHS2S	0.005	1.047	0.369	0.014	1.288	0.131	132.900	0.000	101.982	0.175
BHS3S	0.004	1.197	0.296	0.246	0.531	0.065	114.088	0.229	103.287	0.203
BHS4S	0.006	1.079	0.240	0.007	1.375	0.139	81.037	0.285	99.387	0.113
BHA0S	0.000	1.180	1.126							
BHA1S	0.004	0.963	0.421	0.000	2.360	0.114			119.574	0.115
BHA2S	0.006	0.997	0.345	0.003	1.594	0.054	40.628	0.614	92.823	0.166
BHA3S	0.004	1.164	0.280	0.540	0.352	0.033	108.773	0.246	95.724	0.188
BHA4S	0.005	1.108	0.243	0.683	0.350	0.204	87.268	0.287	111.538	0.144

**Table E.6 Statistical parameters for Bridge B with rock-site ground motion and a deck rotation EDP.**

Bridges	$a_{0S11}$	$a_{1S11}$	$\beta_{S11}$	$a_{0S12}$	$a_{1S12}$	$\beta_{S12}$	$\eta_{BC}$	$\beta_{BC}$	$\eta_{SKF}$	$\beta_{SKF}$
BLS0R	0.000	0.947	0.451							
BLS1R	0.000	1.744	0.676							
BLS2R	0.000	1.709	0.552							
BLS3R	0.001	1.623	0.378				41.006	0.048		
BLS4R	0.004	1.195	0.237							
BLA0R	0.000	1.380	0.759							
BLA1R	0.000	1.564	0.632							
BLA2R	0.001	1.600	0.528							
BLA3R	0.001	1.603	0.401							
BLA4R	0.003	1.210	0.248				38.940	0.349		
BHS0R	0.000	1.520	0.765							
BHS1R	0.000	1.701	0.500							
BHS2R	0.001	1.596	0.458	2164.048	-1.538	0.006	33.516	0.542	67.121	0.060
BHS3R	0.001	1.529	0.356	3.337	-0.004	0.002	42.609	0.340	67.121	0.060
BHS4R	0.004	1.197	0.226				41.628	0.271		
AHA0R	0.000	1.380	0.759							
BHA1R	0.001	1.415	0.407							
BHA2R	0.001	1.546	0.364	0.001	1.546	0.364	31.425	0.387	61.228	0.000
BHA3R	0.001	1.472	0.338							
BHA4R	0.004	1.195	0.228				33.682	0.342		

**Table E.7 Statistical parameters for Bridge C with pulse-like ground motion and a deck rotation EDP.**

Bridges	$a_{0S11}$	$a_{1S11}$	$\beta_{S11}$	$a_{0S12}$	$a_{1S12}$	$\beta_{S12}$	$\eta_{BC}$	$\beta_{BC}$	$\eta_{SKF}$	$\beta_{SKF}$
CLS0P	0.000	1.828	2.093	9.864	-0.390	0.923	117.011	0.229	103.341	0.132
CLS1P	0.001	1.427	0.527	0.724	0.356	0.274	105.043	0.208	99.709	0.148
CLS2P	0.003	1.200	0.363	0.961	0.300	0.260	107.871	0.203	99.834	0.128
CLS3P	0.005	1.117	0.245	0.062	0.905	0.194	108.809	0.199	94.435	0.127
CLS4P	0.001	1.439	0.184	0.085	0.845	0.264	112.442	0.188	89.573	0.142
CLA0P	0.000	1.766	1.612	10.689	-0.267	0.361	110.782	0.195	100.595	0.150
CLA1P	0.001	1.287	0.633	0.116	0.757	0.282	112.531	0.211	98.330	0.132
CLA2P	0.002	1.266	0.417	0.464	0.458	0.202	108.180	0.194	96.307	0.144
CLA3P	0.003	1.244	0.238	0.146	0.732	0.203	109.739	0.198	93.846	0.117
CLA4P	0.005	1.150	0.212	0.031	1.073	0.218	112.187	0.182	87.772	0.131
CHS0P	0.000	2.125	2.686	24.927	-0.527	0.864	116.273	0.228	97.740	0.160
CHS1P	0.002	1.281	0.543	0.046	1.061	0.363	114.660	0.222	94.018	0.165
CHS2P	0.003	1.249	0.349	0.074	0.937	0.268	113.725	0.190	88.485	0.154
CHS3P	0.006	1.124	0.239	0.143	0.758	0.174	109.483	0.186	84.341	0.160
CHS4P	0.007	1.076	0.125	0.119	0.781	0.257	107.911	0.186	82.030	0.147
CHA0P	0.000	1.769	2.628	5.927	-0.100	0.502	115.542	0.222	96.376	0.158
CHA1P	0.001	1.384	0.597	0.115	0.856	0.408	105.965	0.219	95.727	0.166
CHA2P	0.002	1.330	0.401	0.148	0.789	0.239	113.330	0.185	90.404	0.159
CHA3P	0.003	1.332	0.218	0.186	0.711	0.169	107.515	0.190	84.823	0.164
CHA4P	0.005	1.148	0.119	0.084	0.862	0.254	108.851	0.183	84.506	0.159

**Table E.8 Statistical parameters for Bridge C with soil-site ground motion and a deck rotation EDP.**

Bridges	$a_{0S11}$	$a_{1S11}$	$\beta_{S11}$	$a_{0S12}$	$a_{1S12}$	$\beta_{S12}$	$\eta_{BC}$	$\beta_{BC}$	$\eta_{SKF}$	$\beta_{SKF}$
CLS0S	0.000	1.421	1.314	99.156	-0.909	0.867	79.481	0.411	78.372	0.155
CLS1S	0.001	1.400	0.443	0.360	0.504	0.171	94.508	0.313	65.968	0.139
CLS2S	0.004	1.228	0.311	0.340	0.537	0.132	96.815	0.271	65.597	0.149
CLS3S	0.005	1.214	0.276	1.007	0.252	0.107	65.318	0.421	61.972	0.149
CLS4S	0.007	1.145	0.221	0.505	0.396	0.065	87.626	0.298	58.591	0.145
CLA0S	0.000	1.727	1.220	0.312	0.581	0.062	81.329	0.393	65.672	0.173
CLA1S	0.002	1.383	0.542	0.085	0.897	0.094	88.076	0.421	66.017	0.138
CLA2S	0.005	1.158	0.348	0.133	0.761	0.082	87.781	0.325	64.827	0.142
CLA3S	0.006	1.191	0.290	0.381	0.502	0.123	69.328	0.348	60.140	0.177
CLA4S	0.007	1.155	0.221	0.318	0.525	0.076	67.929	0.342	59.305	0.146
CHS0S	0.000	2.246	1.789	16.054	-0.408	0.607	78.097	0.395	64.734	0.203
CHS1S	0.002	1.442	0.389	0.258	0.696	0.152	72.843	0.373	60.631	0.209
CHS2S	0.006	1.173	0.271	0.155	0.790	0.134	65.013	0.358	55.711	0.172
CHS3S	0.009	1.132	0.169	0.227	0.704	0.163	69.495	0.342	54.212	0.168
CHS4S	0.011	1.069	0.133	0.301	0.627	0.155	63.665	0.366	53.480	0.149
CHA0S	0.000	2.387	1.474	1.133	0.306	0.246	67.282	0.420	59.598	0.198
CHA1S	0.003	1.279	0.363	0.122	0.867	0.164	56.968	0.372	59.052	0.202
CHA2S	0.006	1.189	0.251	0.154	0.787	0.128	74.860	0.304	55.083	0.183
CHA3S	0.008	1.163	0.174	0.171	0.777	0.152	66.355	0.324	55.597	0.173
CHA4S	0.011	1.073	0.129	0.095	0.922	0.137	79.252	0.302	53.033	0.150

**Table E.9 Statistical parameters for Bridge C with rock-site ground motion and a deck rotation EDP.**

Bridges	$a_{0S11}$	$a_{1S11}$	$\beta_{S11}$	$a_{0S12}$	$a_{1S12}$	$\beta_{S12}$	$\eta_{BC}$	$\beta_{BC}$	$\eta_{SKF}$	$\beta_{SKF}$
CLS0R	0.209	-0.599	1.769	5.095	-0.333	0.868	35.868	0.322	18.545	0.409
CLS1R	0.806	-0.536	0.863	4.301	-0.125	0.179	31.736	0.391	17.630	0.378
CLS2R	1.275	-0.501	0.615	3.057	0.013	0.152	29.100	0.433	20.554	0.412
CLS3R	1.217	-0.414	0.601	2.861	-0.003	0.111	27.718	0.418	18.599	0.324
CLS4R	1.077	-0.376	0.517	2.880	-0.044	0.074	35.688	0.356	17.414	0.288
CLA0R	1.533	-0.882	1.777	5.235	-0.128	0.087	35.029	0.360	18.153	0.368
CLA1R	0.772	-0.468	0.946	2.547	0.120	0.135	37.066	0.378	16.796	0.359
CLA2R	0.818	-0.352	0.642	1.420	0.280	0.087	35.942	0.392	15.851	0.331
CLA3R	1.316	-0.438	0.598	2.259	0.091	0.143	28.083	0.380	18.769	0.348
CLA4R	1.207	-0.412	0.527	1.987	0.106	0.090	30.405	0.343	18.275	0.327
CHS0R	0.124	-0.646	2.917	7.741	-0.317	0.587	32.800	0.355	20.000	0.361
CHS1R	0.479	-0.276	0.874	4.821	-0.020	0.217	31.560	0.365	20.408	0.368
CHS2R	0.454	-0.124	0.591	1.888	0.227	0.182	25.435	0.348	19.965	0.322
CHS3R	0.810	-0.228	0.458	2.111	0.195	0.198	26.355	0.393	19.955	0.335
CHS4R	0.931	-0.284	0.384	4.538	-0.071	0.181	25.645	0.376	20.364	0.342
CHA0R	0.418	-0.760	2.747	4.102	-0.010	0.257	32.801	0.367	20.568	0.348
CHA1R	0.390	-0.231	0.733	3.254	0.088	0.258	27.668	0.364	21.079	0.360
CHA2R	0.537	-0.166	0.580	1.937	0.211	0.184	29.427	0.371	20.145	0.332
CHA3R	0.952	-0.283	0.468	2.973	0.095	0.213	25.992	0.374	20.272	0.340
CHA4R	1.010	-0.304	0.382	3.712	0.001	0.197	24.419	0.388	21.217	0.334

**Table E.10 Statistical parameters for Bridge A with pulse-like ground motion and an abutment unseating EDP.**

Bridges	$a_{0S11}$	$a_{1S11}$	$\beta_{S11}$	$a_{0S12}$	$a_{1S12}$	$\beta_{S12}$	$\eta_{BC}$	$\beta_{BC}$	$\eta_{SKF}$	$\beta_{SKF}$
ALS0P	0.011	1.176	0.302	1.525	0.274	0.225	164.108	0.255	104.812	0.134
ALS1P	0.011	1.165	0.284	3.462	0.109	0.264	82.239	0.285	105.441	0.147
ALS2P	0.012	1.135	0.281	0.892	0.419	0.490	101.351	0.303	104.646	0.147
ALS3P	0.019	0.994	0.252	0.252	0.715	0.551	103.041	0.305	104.222	0.138
ALS4P	0.014	1.012	0.242	0.201	0.686	0.835	91.756	0.258	104.704	0.142
ALA0P	0.003	1.437	0.355	0.722	0.407	0.337	124.177	0.267	103.413	0.140
ALA1P	0.004	1.368	0.340	0.322	0.619	0.303	98.144	0.291	103.911	0.147
ALA2P	0.005	1.314	0.338	0.218	0.749	0.370	83.869	0.319	104.016	0.139
ALA3P	0.007	1.178	0.309	0.029	1.182	0.547	118.937	0.248	104.724	0.136
ALA4P	0.013	0.999	0.281	0.078	0.909	0.853	83.660	0.258	104.388	0.148
AHS0P	0.033	1.071	0.221	0.052	1.050	0.189	159.754	0.496	101.164	0.119
AHS1P	0.042	1.007	0.217	0.021	1.285	0.287	113.782	0.347	101.534	0.126
AHS2P	0.041	0.993	0.204	0.012	1.402	0.375	124.517	0.333	101.833	0.126
AHS3P	0.054	0.892	0.197	0.007	1.533	0.479	118.922	0.271	101.703	0.125
AHS4P	0.061	0.794	0.178	0.003	1.654	0.671	116.823	0.276	99.484	0.130
AHA0P	0.022	1.141	0.257	0.024	1.202	0.212	190.782	0.355	99.709	0.119
AHA1P	0.023	1.126	0.258	0.036	1.160	0.248	119.904	0.397	101.143	0.130
AHA2P	0.036	0.999	0.243	0.055	1.098	0.426	119.613	0.358	103.039	0.121
AHA3P	0.028	1.025	0.219	0.005	1.634	0.474	140.831	0.270	101.429	0.123
AHA4P	0.050	0.829	0.214	0.002	1.718	0.778	114.454	0.298	97.813	0.110

**Table E.11 Statistical parameters for Bridge A with soil-site ground motion and an abutment unseating EDP.**

Bridges	$a_{0S11}$	$a_{1S11}$	$\beta_{S11}$	$a_{0S12}$	$a_{1S12}$	$\beta_{S12}$	$\eta_{BC}$	$\beta_{BC}$	$\eta_{SKF}$	$\beta_{SKF}$
ALS0S	0.034	0.987	0.278	0.058	0.989	0.160			81.203	0.245
ALS1S	0.035	0.966	0.269	0.018	1.238	0.234			75.629	0.256
ALS2S	0.033	0.964	0.264	0.005	1.567	0.235			73.694	0.245
ALS3S	0.028	0.969	0.255	0.002	1.678	0.489			72.131	0.239
ALS4S	0.024	0.940	0.255	0.034	0.981	0.464	132.900	0.000	69.266	0.206
ALA0S	0.007	1.338	0.609	0.014	1.298	0.166			71.771	0.267
ALA1S	0.007	1.330	0.605	0.013	1.296	0.367			74.071	0.247
ALA2S	0.008	1.288	0.497	0.006	1.518	0.366			74.332	0.249
ALA3S	0.009	1.209	0.402	0.002	1.737	0.527			70.692	0.225
ALA4S	0.013	1.081	0.318	0.013	1.252	0.730	132.900	0.000	67.236	0.202
AHS0S	0.110	0.839	0.148	0.136	0.843	0.094			65.746	0.232
AHS1S	0.110	0.829	0.151	0.124	0.895	0.138			64.233	0.226
AHS2S	0.101	0.829	0.150	0.113	0.926	0.236	90.971	0.246	62.034	0.225
AHS3S	0.083	0.838	0.145	0.018	1.350	0.331	123.330	0.115	61.145	0.204
AHS4S	0.061	0.853	0.147	0.005	1.619	0.305	128.680	0.080	57.311	0.187
AHA0S	0.052	0.997	0.220	0.090	0.921	0.106			63.891	0.224
AHA1S	0.051	0.993	0.221	0.051	1.073	0.194			63.758	0.226
AHA2S	0.048	0.991	0.216	0.050	1.116	0.215	132.900	0.000	61.424	0.217
AHA3S	0.040	1.002	0.204	0.029	1.244	0.336	123.330	0.115	59.529	0.208
AHA4S	0.035	0.976	0.188	0.010	1.463	0.356	126.735	0.095	58.833	0.195

**Table E.12 Statistical parameters for Bridge A with rock-site ground motion and an abutment unseating EDP.**

Bridges	$a_{0S11}$	$a_{1S11}$	$\beta_{S11}$	$a_{0S12}$	$a_{1S12}$	$\beta_{S12}$	$\eta_{BC}$	$\beta_{BC}$	$\eta_{SKF}$	$\beta_{SKF}$
ALS0R	0.025	1.092	0.283	0.009	1.360	0.169			51.739	0.130
ALS1R	0.024	1.098	0.274	0.010	1.350	0.260			51.739	0.130
ALS2R	0.024	1.087	0.254	0.013	1.277	0.297			49.132	0.148
ALS3R	0.021	1.090	0.232	0.006	1.500	0.425			50.975	0.136
ALS4R	0.018	1.081	0.203	0.004	1.582	0.444			54.516	0.126
ALA0R	0.002	1.678	1.148	0.002	1.748	0.196			48.644	0.140
ALA1R	0.003	1.639	1.080	0.004	1.528	0.515			49.350	0.140
ALA2R	0.004	1.548	0.699	0.006	1.501	0.625			50.021	0.144
ALA3R	0.005	1.437	0.526	0.000	2.202	0.420			51.583	0.139
ALA4R	0.008	1.252	0.301	0.000	2.835	0.411			52.736	0.125
AHS0R	0.059	1.008	0.236	0.077	0.936	0.117			52.577	0.149
AHS1R	0.058	1.005	0.232	0.035	1.147	0.239			50.260	0.153
AHS2R	0.052	1.013	0.225	0.028	1.216	0.399			49.961	0.162
AHS3R	0.046	1.006	0.213	0.036	1.157	0.434			50.462	0.161
AHS4R	0.035	1.009	0.198	0.002	1.915	0.490	29.112	0.059	50.680	0.148
AHA0R	0.013	1.379	0.657	0.098	0.852	0.202			49.332	0.176
AHA1R	0.014	1.353	0.562	0.015	1.332	0.311			49.749	0.176
AHA2R	0.010	1.424	0.753	0.013	1.378	0.605			49.793	0.163
AHA3R	0.011	1.367	0.612	0.130	0.830	0.604			50.462	0.161
AHA4R	0.013	1.250	0.366	0.003	1.737	0.602			52.358	0.159

**Table E.13 Statistical parameters for Bridge B with pulse-like ground motion and abutment unseating EDP.**

Bridges	$a_{0S11}$	$a_{1S11}$	$\beta_{S11}$	$a_{0S12}$	$a_{1S12}$	$\beta_{S12}$	$\eta_{BC}$	$\beta_{BC}$	$\eta_{SKF}$	$\beta_{SKF}$
BLS0P	0.067	0.904	0.192	0.067	0.988	0.140	156.827	0.135	106.980	0.103
BLS1P	0.095	0.813	0.172	0.743	0.513	0.139	96.411	0.273	109.151	0.147
BLS2P	0.084	0.824	0.146	0.950	0.452	0.229	101.970	0.261	107.126	0.151
BLS3P	0.149	0.673	0.119	0.643	0.523	0.349	135.248	0.248	97.001	0.093
BLS4P	0.100	0.729	0.103	0.521	0.597	0.266	120.086	0.251	100.630	0.125
BLA0P	0.060	0.922	0.201	0.344	0.638	0.149	113.389	0.342	107.663	0.139
BLA1P	0.054	0.935	0.197	0.313	0.668	0.226	139.622	0.352	108.188	0.156
BLA2P	0.068	0.871	0.162	0.636	0.543	0.281	148.035	0.182	106.440	0.147
BLA3P	0.136	0.692	0.123	0.169	0.797	0.341	132.150	0.227	102.490	0.139
BLA4P	0.104	0.725	0.112	0.271	0.748	0.265	108.538	0.257	101.378	0.127
BHS0P	0.147	0.791	0.150	0.160	0.848	0.131	119.969	0.242	111.210	0.132
BHS1P	0.151	0.778	0.136	0.659	0.583	0.157	121.587	0.266	105.778	0.136
BHS2P	0.248	0.642	0.119	0.668	0.581	0.183	119.085	0.228	108.804	0.140
BHS3P	0.288	0.575	0.112	0.072	1.023	0.167	124.738	0.245	101.244	0.106
BHS4P	0.151	0.682	0.088	0.355	0.717	0.238	110.460	0.244	97.799	0.096
BHA0P	0.115	0.835	0.165	0.299	0.715	0.119	129.596	0.194	109.438	0.129
BHA1P	0.118	0.825	0.144	0.562	0.585	0.168	130.741	0.239	106.740	0.146
BHA2P	0.256	0.630	0.127	0.075	1.049	0.119	97.193	0.249	106.810	0.114
BHA3P	0.329	0.540	0.114	0.142	0.885	0.174	115.675	0.261	100.985	0.101
BHA4P	0.243	0.577	0.081	3.109	0.247	0.197	101.359	0.234	96.354	0.082

**Table E.14 Statistical parameters for Bridge B with soil-site ground motion and an abutment unseating EDP.**

Bridges	$a_{0S11}$	$a_{1S11}$	$\beta_{S11}$	$a_{0S12}$	$a_{1S12}$	$\beta_{S12}$	$\eta_{BC}$	$\beta_{BC}$	$\eta_{SKF}$	$\beta_{SKF}$
BLS0S	0.149	0.755	0.103							
BLS1S	0.149	0.753	0.099				86.590	0.278		
BLS2S	0.152	0.737	0.091				132.900	0.000		
BLS3S	0.122	0.771	0.098	0.000	2.969	0.220	97.515	0.351	119.825	0.113
BLS4S	0.100	0.786	0.094	0.000	3.204	0.027	97.141	0.411	99.387	0.113
BLA0S	0.084	0.882	0.138	0.000	2.161	0.028			130.418	0.056
BLA1S	0.090	0.865	0.128							
BLA2S	0.106	0.820	0.114				132.900	0.000		
BLA3S	0.098	0.823	0.109				82.956	0.513		
BLA4S	0.103	0.781	0.093	0.000	2.333	0.281	99.865	0.319	123.658	0.130
BHS0S	0.222	0.729	0.107							
BHS1S	0.240	0.704	0.098	0.347	0.748	0.169			130.263	0.060
BHS2S	0.245	0.691	0.089	0.023	1.280	0.174	132.900	0.000	101.982	0.175
BHS3S	0.229	0.681	0.087	0.011	1.420	0.040	114.088	0.229	103.287	0.203
BHS4S	0.216	0.650	0.081	0.009	1.495	0.055	81.037	0.285	99.387	0.113
BHA0S	0.167	0.789	0.108							
BHA1S	0.195	0.748	0.100	0.005	1.618	0.106			119.574	0.115
BHA2S	0.204	0.730	0.094	0.004	1.661	0.275	40.628	0.614	92.823	0.166
BHA3S	0.218	0.688	0.092	0.016	1.329	0.030	108.773	0.246	95.724	0.188
BHA4S	0.226	0.640	0.080	0.025	1.277	0.063	87.268	0.287	111.538	0.144

**Table E.15 Statistical parameters for Bridge B with rock-site ground motion and an abutment unseating EDP.**

Bridges	$a_{0S11}$	$a_{1S11}$	$\beta_{S11}$	$a_{0S12}$	$a_{1S12}$	$\beta_{S12}$	$\eta_{BC}$	$\beta_{BC}$	$\eta_{SKF}$	$\beta_{SKF}$
BLS0R	0.117	0.813	0.177							
BLS1R	0.116	0.816	0.174							
BLS2R	0.114	0.814	0.159							
BLS3R	0.078	0.898	0.133				41.006	0.048		
BLS4R	0.053	0.948	0.133							
BLA0R	0.031	1.147	0.574							
BLA1R	0.042	1.067	0.417							
BLA2R	0.057	0.985	0.266							
BLA3R	0.054	0.990	0.162							
BLA4R	0.053	0.950	0.132				38.940	0.349		
BHS0R	0.133	0.843	0.146							
BHS1R	0.122	0.868	0.140							
BHS2R	0.117	0.872	0.138	1639.592	-1.249	0.002	33.516	0.542	67.121	0.060
BHS3R	0.112	0.862	0.116	10.051	-0.018	0.013	42.609	0.340	67.121	0.060
BHS4R	0.075	0.912	0.122				41.628	0.271		
BHA0R	0.064	1.023	0.341							
BHA1R	0.051	1.086	0.408							
BHA2R	0.051	1.093	0.224	0.051	1.093	0.224	31.425	0.387	61.228	0.000
BHA3R	0.091	0.909	0.141							
BHA4R	0.085	0.880	0.112				33.682	0.342		

**Table E.16 Statistical parameters for Bridge C with pulse-like ground motion and an abutment unseating EDP.**

Bridges	$a_{0S11}$	$a_{1S11}$	$\beta_{S11}$	$a_{0S12}$	$a_{1S12}$	$\beta_{S12}$	$\eta_{BC}$	$\beta_{BC}$	$\eta_{SKF}$	$\beta_{SKF}$
CLS0P	0.075	0.970	0.231	0.739	0.518	0.252	117.011	0.229	103.341	0.132
CLS1P	0.143	0.808	0.191	0.042	1.127	0.246	105.043	0.208	99.709	0.148
CLS2P	0.121	0.833	0.170	0.413	0.642	0.360	107.871	0.203	99.834	0.128
CLS3P	0.174	0.727	0.172	0.109	0.955	0.396	108.809	0.199	94.435	0.127
CLS4P	0.058	0.967	0.118	0.046	1.201	0.472	112.442	0.188	89.573	0.142
CLA0P	0.086	0.929	0.225	0.070	0.995	0.277	110.782	0.195	100.595	0.150
CLA1P	0.071	0.976	0.204	0.093	0.949	0.309	112.531	0.211	98.330	0.132
CLA2P	0.116	0.839	0.191	0.515	0.591	0.346	108.180	0.194	96.307	0.144
CLA3P	0.143	0.773	0.144	0.094	1.001	0.452	109.739	0.198	93.846	0.117
CLA4P	0.159	0.716	0.119	0.029	1.308	0.426	112.187	0.182	87.772	0.131
CHS0P	0.084	1.025	0.202	1.376	0.434	0.294	116.273	0.228	97.740	0.160
CHS1P	0.028	1.298	0.179	0.312	0.759	0.267	114.660	0.222	94.018	0.165
CHS2P	0.024	1.319	0.128	0.450	0.704	0.274	113.725	0.190	88.485	0.154
CHS3P	0.213	0.742	0.125	0.426	0.709	0.261	109.483	0.186	84.341	0.160
CHS4P	0.203	0.721	0.094	0.090	1.083	0.385	107.911	0.186	82.030	0.147
CHA0P	0.113	0.941	0.217	0.554	0.630	0.286	115.542	0.222	96.376	0.158
CHA1P	0.029	1.269	0.151	0.575	0.618	0.294	105.965	0.219	95.727	0.166
CHA2P	0.026	1.287	0.152	0.331	0.771	0.232	113.330	0.185	90.404	0.159
CHA3P	0.157	0.809	0.121	0.474	0.694	0.301	107.515	0.190	84.823	0.164
CHA4P	0.209	0.718	0.091	0.176	0.935	0.374	108.851	0.183	84.506	0.159

**Table E.17 Statistical parameters for Bridge C with soil-site ground motion and an abutment unseating EDP.**

Bridges	$a_{0S11}$	$a_{1S11}$	$\beta_{S11}$	$a_{0S12}$	$a_{1S12}$	$\beta_{S12}$	$\eta_{BC}$	$\beta_{BC}$	$\eta_{SKF}$	$\beta_{SKF}$
CLS0S	0.144	0.872	0.164	0.020	1.370	0.094	79.481	0.411	78.372	0.155
CLS1S	0.159	0.843	0.136	0.076	1.053	0.214	94.508	0.313	65.968	0.139
CLS2S	0.176	0.806	0.121	0.109	0.981	0.357	96.815	0.271	65.597	0.149
CLS3S	0.159	0.817	0.120	4.848	0.054	0.397	65.318	0.421	61.972	0.149
CLS4S	0.149	0.805	0.111	0.423	0.658	0.459	87.626	0.298	58.591	0.145
CLA0S	0.108	0.940	0.182	0.045	1.162	0.131	81.329	0.393	65.672	0.173
CLA1S	0.120	0.909	0.159	0.089	1.027	0.238	88.076	0.421	66.017	0.138
CLA2S	0.144	0.855	0.132	0.420	0.649	0.327	87.781	0.325	64.827	0.142
CLA3S	0.157	0.822	0.127	3.504	0.169	0.476	69.328	0.348	60.140	0.177
CLA4S	0.153	0.802	0.110	0.292	0.780	0.544	67.929	0.342	59.305	0.146
CHS0S	0.229	0.856	0.199	0.202	0.914	0.189	78.097	0.395	64.734	0.203
CHS1S	0.265	0.809	0.209	0.167	0.972	0.186	72.843	0.373	60.631	0.209
CHS2S	0.322	0.733	0.180	0.415	0.765	0.199	65.013	0.358	55.711	0.172
CHS3S	0.325	0.710	0.137	0.678	0.673	0.257	69.495	0.342	54.212	0.168
CHS4S	0.255	0.731	0.102	0.741	0.641	0.409	63.665	0.366	53.480	0.149
CHA0S	0.212	0.860	0.204	0.173	0.944	0.193	67.282	0.420	59.598	0.198
CHA1S	0.236	0.826	0.212	0.073	1.158	0.214	56.968	0.372	59.052	0.202
CHA2S	0.297	0.746	0.187	0.437	0.758	0.175	74.860	0.304	55.083	0.183
CHA3S	0.298	0.734	0.154	0.274	0.887	0.304	66.355	0.324	55.597	0.173
CHA4S	0.243	0.754	0.106	0.391	0.818	0.369	79.252	0.302	53.033	0.150

**Table E.18 Statistical parameters for Bridge C with rock-site ground motion and an abutment unseating EDP.**

Bridges	$a_{0S11}$	$a_{1S11}$	$\beta_{S11}$	$a_{0S12}$	$a_{1S12}$	$\beta_{S12}$	$\eta_{BC}$	$\beta_{BC}$	$\eta_{SKF}$	$\beta_{SKF}$
CLS0R	5.976	-0.217	0.362	3.160	0.303	0.190	35.868	0.322	18.545	0.409
CLS1R	4.782	-0.162	0.311	4.005	0.150	0.269	31.736	0.391	17.630	0.378
CLS2R	4.628	-0.163	0.274	3.289	0.219	0.400	29.100	0.433	20.554	0.412
CLS3R	4.484	-0.172	0.281	3.824	0.154	0.390	27.718	0.418	18.599	0.324
CLS4R	4.843	-0.234	0.262	3.016	0.247	0.470	35.688	0.356	17.414	0.288
CLA0R	6.296	-0.260	0.395	4.033	0.127	0.255	35.029	0.360	18.153	0.368
CLA1R	4.198	-0.135	0.355	3.543	0.211	0.280	37.066	0.378	16.796	0.359
CLA2R	4.274	-0.150	0.304	2.451	0.329	0.311	35.942	0.392	15.851	0.331
CLA3R	4.769	-0.199	0.289	4.431	0.152	0.470	28.083	0.380	18.769	0.348
CLA4R	5.112	-0.249	0.264	2.094	0.412	0.525	30.405	0.343	18.275	0.327
CHS0R	5.930	-0.109	0.377	6.765	0.100	0.290	32.800	0.355	20.000	0.361
CHS1R	5.557	-0.108	0.365	7.808	0.054	0.312	31.560	0.365	20.408	0.368
CHS2R	4.366	-0.061	0.306	5.113	0.191	0.248	25.435	0.348	19.965	0.322
CHS3R	3.901	-0.042	0.256	6.101	0.166	0.292	26.355	0.393	19.955	0.335
CHS4R	3.620	-0.068	0.230	7.452	0.080	0.435	25.645	0.376	20.364	0.342
CHA0R	6.128	-0.150	0.385	6.814	0.064	0.301	32.801	0.367	20.568	0.348
CHA1R	4.318	-0.057	0.373	7.825	0.023	0.388	27.668	0.364	21.079	0.360
CHA2R	5.073	-0.116	0.316	5.189	0.191	0.228	29.427	0.371	20.145	0.332
CHA3R	4.113	-0.067	0.279	9.086	0.029	0.388	25.992	0.374	20.272	0.340
CHA4R	3.766	-0.073	0.243	5.412	0.203	0.402	24.419	0.388	21.217	0.334

**Table E.19 Statistical parameters for Bridge A with pulse-like ground motion and a column drift ratio EDP.**

Bridges	$a_{0S11}$	$a_{1S11}$	$\beta_{S11}$	$a_{0S12}$	$a_{1S12}$	$\beta_{S12}$	$\eta_{BC}$	$\beta_{BC}$	$\eta_{SKF}$	$\beta_{SKF}$
ALS0P	0.010	1.042	0.230	0.603	0.370	0.090	164.108	0.255	104.812	0.134
ALS1P	0.011	1.027	0.227	0.267	0.524	0.149	82.239	0.285	105.441	0.147
ALS2P	0.009	1.066	0.232	0.280	0.514	0.125	101.351	0.303	104.646	0.147
ALS3P	0.011	1.014	0.222	0.164	0.623	0.169	103.041	0.305	104.222	0.138
ALS4P	0.007	1.105	0.220	0.222	0.559	0.155	91.756	0.258	104.704	0.142
ALA0P	0.010	1.050	0.218	0.176	0.608	0.147	124.177	0.267	103.413	0.140
ALA1P	0.012	0.998	0.209	0.064	0.825	0.148	98.144	0.291	103.911	0.147
ALA2P	0.008	1.090	0.198	0.039	0.932	0.163	83.869	0.319	104.016	0.139
ALA3P	0.012	0.994	0.215	0.077	0.778	0.172	118.937	0.248	104.724	0.136
ALA4P	0.010	1.044	0.207	0.144	0.656	0.173	83.660	0.258	104.388	0.148
AHS0P	0.010	1.078	0.192	0.011	1.221	0.107	159.754	0.496	101.164	0.119
AHS1P	0.013	1.016	0.192	0.007	1.306	0.126	113.782	0.347	101.534	0.126
AHS2P	0.016	0.964	0.196	0.005	1.347	0.132	124.517	0.333	101.833	0.126
AHS3P	0.014	0.994	0.169	0.016	1.103	0.145	118.922	0.271	101.703	0.125
AHS4P	0.019	0.933	0.165	0.025	0.992	0.209	116.823	0.276	99.484	0.130
AHA0P	0.014	1.000	0.191	0.005	1.386	0.112	190.782	0.355	99.709	0.119
AHA1P	0.016	0.974	0.194	0.010	1.224	0.112	119.904	0.397	101.143	0.130
AHA2P	0.022	0.894	0.188	0.012	1.182	0.123	119.613	0.358	103.039	0.121
AHA3P	0.015	0.994	0.172	0.019	1.069	0.151	140.831	0.270	101.429	0.123
AHA4P	0.023	0.899	0.168	0.021	1.027	0.218	114.454	0.298	97.813	0.110

**Table E.20 Statistical parameters for Bridge A with soil-site ground motion and a column drift ratio EDP.**

Bridges	$a_{0S11}$	$a_{1S11}$	$\beta_{S11}$	$a_{0S12}$	$a_{1S12}$	$\beta_{S12}$	$\eta_{BC}$	$\beta_{BC}$	$\eta_{SKF}$	$\beta_{SKF}$
ALS0S	0.018	0.963	0.219	0.017	1.134	0.079			81.203	0.245
ALS1S	0.018	0.960	0.219	0.017	1.129	0.091			75.629	0.256
ALS2S	0.016	0.983	0.225	0.015	1.123	0.133			73.694	0.245
ALS3S	0.015	1.010	0.226	0.015	1.149	0.086			72.131	0.239
ALS4S	0.014	1.034	0.235	0.019	1.083	0.095	132.900	0.000	69.266	0.206
ALA0S	0.031	0.830	0.170	0.013	1.182	0.067			71.771	0.267
ALA1S	0.029	0.843	0.174	0.010	1.242	0.105			74.071	0.247
ALA2S	0.028	0.857	0.175	0.013	1.168	0.100			74.332	0.249
ALA3S	0.026	0.870	0.180	0.016	1.130	0.109			70.692	0.225
ALA4S	0.025	0.889	0.191	0.020	1.068	0.095	132.900	0.000	67.236	0.202
AHS0S	0.024	0.922	0.130	0.024	1.043	0.061			65.746	0.232
AHS1S	0.025	0.905	0.128	0.019	1.089	0.049			64.233	0.226
AHS2S	0.024	0.912	0.126	0.024	1.031	0.042	90.971	0.246	62.034	0.225
AHS3S	0.025	0.913	0.127	0.027	0.992	0.056	123.330	0.115	61.145	0.204
AHS4S	0.023	0.939	0.133	0.023	1.036	0.044	128.680	0.080	57.311	0.187
AHA0S	0.035	0.823	0.116	0.019	1.085	0.060			63.891	0.224
AHA1S	0.037	0.813	0.112	0.017	1.102	0.047			63.758	0.226
AHA2S	0.036	0.824	0.110	0.016	1.129	0.048	132.900	0.000	61.424	0.217
AHA3S	0.036	0.832	0.106	0.018	1.091	0.058	123.330	0.115	59.529	0.208
AHA4S	0.034	0.856	0.111	0.021	1.064	0.038	126.735	0.095	58.833	0.195

**Table E.21 Statistical parameters for Bridge A with rock-site ground motion and a column drift ratio EDP.**

Bridges	$a_{0S11}$	$a_{1S11}$	$\beta_{S11}$	$a_{0S12}$	$a_{1S12}$	$\beta_{S12}$	$\eta_{BC}$	$\beta_{BC}$	$\eta_{SKF}$	$\beta_{SKF}$
ALS0R	0.016	1.036	0.180	0.148	0.557	0.040			51.739	0.130
ALS1R	0.015	1.052	0.181	0.140	0.562	0.038			51.739	0.130
ALS2R	0.014	1.077	0.185	0.203	0.458	0.037			49.132	0.148
ALS3R	0.012	1.118	0.188	0.217	0.441	0.025			50.975	0.136
ALS4R	0.011	1.149	0.195	0.396	0.302	0.020			54.516	0.126
ALA0R	0.027	0.904	0.133	0.105	0.625	0.051			48.644	0.140
ALA1R	0.026	0.918	0.132	0.146	0.545	0.047			49.350	0.140
ALA2R	0.024	0.942	0.134	0.139	0.553	0.037			50.021	0.144
ALA3R	0.022	0.965	0.138	0.177	0.490	0.022			51.583	0.139
ALA4R	0.020	0.996	0.146	0.124	0.584	0.022			52.736	0.125
AHS0R	0.016	1.041	0.177	0.392	0.312	0.107			52.577	0.149
AHS1R	0.017	1.021	0.178	0.124	0.594	0.087			50.260	0.153
AHS2R	0.016	1.035	0.192	0.076	0.706	0.077			49.961	0.162
AHS3R	0.016	1.049	0.208	0.068	0.718	0.080			50.462	0.161
AHS4R	0.014	1.089	0.227	0.116	0.572	0.045	29.112	0.059	50.680	0.148
AHA0R	0.031	0.869	0.120	0.090	0.677	0.111			49.332	0.176
AHA1R	0.031	0.866	0.122	0.069	0.742	0.086			49.749	0.176
AHA2R	0.031	0.877	0.130	0.105	0.622	0.078			49.793	0.163
AHA3R	0.029	0.898	0.147	0.068	0.715	0.081			50.462	0.161
AHA4R	0.026	0.936	0.166	0.089	0.642	0.060			52.358	0.159

**Table E.22 Statistical parameters for Bridge B with a pulse-like ground motion and a column drift ratio EDP.**

Bridges	$a_{0S11}$	$a_{1S11}$	$\beta_{S11}$	$a_{0S12}$	$a_{1S12}$	$\beta_{S12}$	$\eta_{BC}$	$\beta_{BC}$	$\eta_{SKF}$	$\beta_{SKF}$
BLS0P	0.030	0.906	0.188	0.121	0.791	0.060	156.827	0.135	106.980	0.103
BLS1P	0.040	0.827	0.166	0.433	0.482	0.083	96.411	0.273	109.151	0.147
BLS2P	0.038	0.847	0.154	0.325	0.540	0.080	101.970	0.261	107.126	0.151
BLS3P	0.051	0.797	0.131	0.606	0.416	0.097	135.248	0.248	97.001	0.093
BLS4P	0.038	0.899	0.113	0.247	0.618	0.128	120.086	0.251	100.630	0.125
BLA0P	0.035	0.866	0.180	0.236	0.607	0.092	113.389	0.342	107.663	0.139
BLA1P	0.032	0.885	0.170	0.342	0.520	0.092	139.622	0.352	108.188	0.156
BLA2P	0.037	0.853	0.156	0.300	0.560	0.101	148.035	0.182	106.440	0.147
BLA3P	0.047	0.817	0.132	0.349	0.534	0.078	132.150	0.227	102.490	0.139
BLA4P	0.040	0.895	0.126	0.271	0.599	0.131	108.538	0.257	101.378	0.127
BHS0P	0.038	0.816	0.149	0.360	0.509	0.072	119.969	0.242	111.210	0.132
BHS1P	0.036	0.824	0.142	0.203	0.625	0.137	121.587	0.266	105.778	0.136
BHS2P	0.056	0.729	0.132	0.151	0.684	0.121	119.085	0.228	108.804	0.140
BHS3P	0.058	0.731	0.102	0.288	0.529	0.126	124.738	0.245	101.244	0.106
BHS4P	0.045	0.823	0.084	0.025	1.068	0.169	110.460	0.244	97.799	0.096
BHA0P	0.039	0.810	0.150	0.312	0.536	0.067	129.596	0.194	109.438	0.129
BHA1P	0.038	0.817	0.138	0.350	0.495	0.151	130.741	0.239	106.740	0.146
BHA2P	0.053	0.749	0.126	1.904	0.153	0.124	97.193	0.249	106.810	0.114
BHA3P	0.067	0.700	0.101	0.824	0.320	0.136	115.675	0.261	100.985	0.101
BHA4P	0.041	0.856	0.077	0.012	1.248	0.196	101.359	0.234	96.354	0.082

**Table E.23 Statistical parameters for Bridge B with soil-site ground motion and a column drift ratio EDP.**

Bridges	$a_{0S11}$	$a_{1S11}$	$\beta_{S11}$	$a_{0S12}$	$a_{1S12}$	$\beta_{S12}$	$\eta_{BC}$	$\beta_{BC}$	$\eta_{SKF}$	$\beta_{SKF}$
BLS0S	0.049	0.824	0.087							
BLS1S	0.050	0.825	0.088				86.590	0.278		
BLS2S	0.056	0.804	0.078				132.900	0.000		
BLS3S	0.061	0.803	0.080	0.123	0.783	0.017	97.515	0.351	119.825	0.113
BLS4S	0.068	0.814	0.084	0.088	0.882	0.034	97.141	0.411	99.387	0.113
BLA0S	0.071	0.734	0.078	0.000	2.103	0.019			130.418	0.056
BLA1S	0.066	0.755	0.079							
BLA2S	0.066	0.765	0.073				132.900	0.000		
BLA3S	0.058	0.818	0.083				82.956	0.513		
BLA4S	0.069	0.812	0.089	0.023	1.156	0.000	99.865	0.319	123.658	0.130
BHS0S	0.048	0.799	0.088							
BHS1S	0.051	0.786	0.086	0.002	1.630	0.028			130.263	0.060
BHS2S	0.060	0.755	0.080	0.015	1.146	0.028	132.900	0.000	101.982	0.175
BHS3S	0.072	0.727	0.085	0.012	1.201	0.041	114.088	0.229	103.287	0.203
BHS4S	0.103	0.666	0.089	0.809	0.386	0.032	81.037	0.285	99.387	0.113
BHA0S	0.057	0.764	0.085							
BHA1S	0.067	0.722	0.079	0.005	1.418	0.031			119.574	0.115
BHA2S	0.068	0.722	0.077	0.008	1.290	0.060	40.628	0.614	92.823	0.166
BHA3S	0.076	0.711	0.081	0.015	1.159	0.048	108.773	0.246	95.724	0.188
BHA4S	0.100	0.676	0.091	0.143	0.767	0.021	87.268	0.287	111.538	0.144

**Table E.24** Statistical parameters for Bridge B with rock-site ground motion and a column drift ratio EDP.

Bridges	$a_{0S11}$	$a_{1S11}$	$\beta_{S11}$	$a_{0S12}$	$a_{1S12}$	$\beta_{S12}$	$\eta_{BC}$	$\beta_{BC}$	$\eta_{SKF}$	$\beta_{SKF}$
BLS0R	0.042	0.873	0.135							
BLS1R	0.045	0.855	0.135							
BLS2R	0.051	0.822	0.124							
BLS3R	0.046	0.870	0.112				41.006	0.048		
BLS4R	0.042	0.915	0.131							
BLA0R	0.069	0.742	0.088							
BLA1R	0.071	0.734	0.094							
BLA2R	0.071	0.738	0.099							
BLA3R	0.052	0.841	0.104							
BLA4R	0.043	0.904	0.130				38.940	0.349		
BHS0R	0.034	0.871	0.112							
BHS1R	0.035	0.871	0.111							
BHS2R	0.035	0.883	0.116	3.465	-0.185	0.010	33.516	0.542	67.121	0.060
BHS3R	0.038	0.879	0.107	35.118	-0.745	0.005	42.609	0.340	67.121	0.060
BHS4R	0.041	0.871	0.132				41.628	0.271		
BHA0R	0.060	0.721	0.091							
BHA1R	0.058	0.736	0.087							
BHA2R	0.046	0.812	0.079	0.046	0.812	0.079	31.425	0.387	61.228	0.000
BHA3R	0.041	0.857	0.103							
BHA4R	0.043	0.852	0.131				33.682	0.342		

**Table E.25 Statistical parameters for Bridge C with pulse-like ground motion and a column drift ratio EDP.**

Bridges	$a_{0S11}$	$a_{1S11}$	$\beta_{S11}$	$a_{0S12}$	$a_{1S12}$	$\beta_{S12}$	$\eta_{BC}$	$\beta_{BC}$	$\eta_{SKF}$	$\beta_{SKF}$
CLS0P	0.008	1.309	0.113	0.578	0.473	0.095	117.011	0.229	103.341	0.132
CLS1P	0.011	1.239	0.106	0.078	0.871	0.080	105.043	0.208	99.709	0.148
CLS2P	0.011	1.231	0.107	0.141	0.744	0.065	107.871	0.203	99.834	0.128
CLS3P	0.021	1.088	0.114	0.061	0.925	0.076	108.809	0.199	94.435	0.127
CLS4P	0.008	1.313	0.123	0.018	1.186	0.111	112.442	0.188	89.573	0.142
CLA0P	0.010	1.263	0.117	0.103	0.825	0.081	110.782	0.195	100.595	0.150
CLA1P	0.010	1.267	0.113	0.078	0.880	0.097	112.531	0.211	98.330	0.132
CLA2P	0.012	1.228	0.122	0.085	0.847	0.079	108.180	0.194	96.307	0.144
CLA3P	0.016	1.147	0.109	0.067	0.917	0.074	109.739	0.198	93.846	0.117
CLA4P	0.016	1.121	0.235	0.047	0.953	0.134	112.187	0.182	87.772	0.131
CHS0P	0.003	1.525	0.115	0.096	0.809	0.116	116.273	0.228	97.740	0.160
CHS1P	0.005	1.405	0.113	0.053	0.943	0.103	114.660	0.222	94.018	0.165
CHS2P	0.005	1.421	0.137	0.089	0.811	0.117	113.725	0.190	88.485	0.154
CHS3P	0.010	1.260	0.120	0.165	0.665	0.097	109.483	0.186	84.341	0.160
CHS4P	0.009	1.262	0.096	0.024	1.084	0.152	107.911	0.186	82.030	0.147
CHA0P	0.005	1.398	0.115	0.092	0.822	0.110	115.542	0.222	96.376	0.158
CHA1P	0.005	1.387	0.110	0.105	0.799	0.092	105.965	0.219	95.727	0.166
CHA2P	0.005	1.416	0.123	0.129	0.736	0.106	113.330	0.185	90.404	0.159
CHA3P	0.009	1.280	0.119	0.206	0.619	0.098	107.515	0.190	84.823	0.164
CHA4P	0.011	1.191	0.237	0.003	1.566	0.428	108.851	0.183	84.506	0.159

**Table E.26 Statistical parameters for Bridge C with soil-site ground motion and a column drift ratio EDP.**

Bridges	$a_{0S11}$	$a_{1S11}$	$\beta_{S11}$	$a_{0S12}$	$a_{1S12}$	$\beta_{S12}$	$\eta_{BC}$	$\beta_{BC}$	$\eta_{SKF}$	$\beta_{SKF}$
CLS0S	0.058	0.902	0.074	0.017	1.260	0.085	79.481	0.411	78.372	0.155
CLS1S	0.067	0.857	0.072	0.017	1.265	0.066	94.508	0.313	65.968	0.139
CLS2S	0.075	0.826	0.069	0.019	1.262	0.056	96.815	0.271	65.597	0.149
CLS3S	0.072	0.838	0.076	0.042	1.050	0.057	65.318	0.421	61.972	0.149
CLS4S	0.072	0.822	0.239	0.022	1.197	0.068	87.626	0.298	58.591	0.145
CLA0S	0.067	0.860	0.073	0.023	1.206	0.043	81.329	0.393	65.672	0.173
CLA1S	0.068	0.856	0.072	0.009	1.423	0.048	88.076	0.421	66.017	0.138
CLA2S	0.080	0.808	0.070	0.022	1.212	0.042	87.781	0.325	64.827	0.142
CLA3S	0.079	0.816	0.078	0.051	1.015	0.066	69.328	0.348	60.140	0.177
CLA4S	0.059	0.867	0.231	0.111	0.724	0.978	67.929	0.342	59.305	0.146
CHS0S	0.060	0.868	0.127	0.029	1.123	0.080	78.097	0.395	64.734	0.203
CHS1S	0.070	0.818	0.125	0.038	1.063	0.132	72.843	0.373	60.631	0.209
CHS2S	0.095	0.719	0.125	0.054	0.971	0.125	65.013	0.358	55.711	0.172
CHS3S	0.102	0.705	0.126	0.063	0.944	0.140	69.495	0.342	54.212	0.168
CHS4S	0.065	0.832	0.136	0.052	0.923	0.955	63.665	0.366	53.480	0.149
CHA0S	0.072	0.816	0.112	0.062	0.956	0.095	67.282	0.420	59.598	0.198
CHA1S	0.086	0.761	0.120	0.029	1.125	0.133	56.968	0.372	59.052	0.202
CHA2S	0.102	0.704	0.127	0.055	0.970	0.129	74.860	0.304	55.083	0.183
CHA3S	0.107	0.696	0.124	0.042	1.038	0.147	66.355	0.324	55.597	0.173
CHA4S	0.072	0.794	0.272	0.022	1.166	0.138	79.252	0.302	53.033	0.150

**Table E.27 Statistical parameters for Bridge C with a rock-site ground motion and a column drift ratio EDP.**

Bridges	$a_{0S11}$	$a_{1S11}$	$\beta_{S11}$	$a_{0S12}$	$a_{1S12}$	$\beta_{S12}$	$\eta_{BC}$	$\beta_{BC}$	$\eta_{SKF}$	$\beta_{SKF}$
CLS0R	2.450	-0.189	0.289	1.273	0.395	0.120	35.868	0.322	18.545	0.409
CLS1R	2.277	-0.183	0.251	2.379	0.123	0.153	31.736	0.391	17.630	0.378
CLS2R	2.450	-0.208	0.226	2.538	0.112	0.160	29.100	0.433	20.554	0.412
CLS3R	2.427	-0.205	0.242	1.989	0.159	0.122	27.718	0.418	18.599	0.324
CLS4R	1.947	-0.159	0.406	3.454	-0.066	0.157	35.688	0.356	17.414	0.288
CLA0R	2.437	-0.198	0.256	2.827	0.086	0.180	35.029	0.360	18.153	0.368
CLA1R	2.096	-0.154	0.243	2.240	0.167	0.153	37.066	0.378	16.796	0.359
CLA2R	2.175	-0.172	0.222	1.979	0.189	0.118	35.942	0.392	15.851	0.331
CLA3R	2.553	-0.223	0.235	1.791	0.196	0.146	28.083	0.380	18.769	0.348
CLA4R	2.149	-0.205	0.420	1.603	0.097	1.008	30.405	0.343	18.275	0.327
CHS0R	1.593	-0.105	0.310	2.421	0.083	0.236	32.800	0.355	20.000	0.361
CHS1R	1.565	-0.116	0.284	2.542	0.060	0.282	31.560	0.365	20.408	0.368
CHS2R	1.358	-0.091	0.244	1.183	0.275	0.198	25.435	0.348	19.965	0.322
CHS3R	1.156	-0.028	0.244	2.110	0.091	0.225	26.355	0.393	19.955	0.335
CHS4R	1.462	-0.107	0.300	0.807	0.304	0.982	25.645	0.376	20.364	0.342
CHA0R	1.798	-0.151	0.274	2.801	0.037	0.207	32.801	0.367	20.568	0.348
CHA1R	1.343	-0.077	0.255	2.027	0.114	0.292	27.668	0.364	21.079	0.360
CHA2R	1.502	-0.114	0.242	1.474	0.204	0.223	29.427	0.371	20.145	0.332
CHA3R	1.257	-0.055	0.237	2.575	0.027	0.262	25.992	0.374	20.272	0.340
CHA4R	1.375	-0.097	0.422	1.745	0.091	0.231	24.419	0.388	21.217	0.334



## PEER REPORTS

PEER reports are available as a free PDF download from [http://peer.berkeley.edu/publications/peer\\_reports\\_complete.html](http://peer.berkeley.edu/publications/peer_reports_complete.html). Printed hard copies of PEER reports can be ordered directly from our printer by following the instructions at [http://peer.berkeley.edu/publications/peer\\_reports.html](http://peer.berkeley.edu/publications/peer_reports.html). For other related questions about the PEER Report Series, contact the Pacific Earthquake Engineering Research Center, 325 Davis Hall mail code 1792, Berkeley, CA 94720. Tel.: (510) 642-3437; Fax: (510) 665-1655; Email: [peer\\_editor@berkeley.edu](mailto:peer_editor@berkeley.edu)

- PEER 2014/01** *Performance-Based Seismic Assessment of Skewed Bridges*. Peyman Kaviani, Farzin Zareian, and Ertugrul Taciroglu. January 2014.
- PEER 2013/25** *Earthquake Engineering for Resilient Communities: 2013 PEER Internship Program Research Report Collection*. Heidi Tremayne (Editor), Stephen A. Mahin (Editor), Jorge Archbold Monterossa, Matt Brosman, Shelly Dean, Katherine deLaveaga, Curtis Fong, Donovan Holder, Rakeeb Khan, Elizabeth Jachens, David Lam, Daniela Martinez Lopez, Mara Minner, Geffen Oren, Julia Pavicic, Melissa Quinonez, Lorena Rodriguez, Sean Salazar, Kelli Slaven, Vivian Steyert, Jenny Taing, and Salvador Tena. December 2013.
- PEER 2013/24** *NGA-West2 Ground Motion Prediction Equations for Vertical Ground Motions*. September 2013.
- PEER 2013/23** *Coordinated Planning and Preparedness for Fire Following Major Earthquakes*. Charles Scawthorn. November 2013.
- PEER 2013/22** *GEM-PEER Task 3 Project: Selection of a Global Set of Ground Motion Prediction Equations*. Jonathan P. Stewart, John Douglas, Mohammad B. Javanbarg, Carola Di Alessandro, Yousef Bozorgnia, Norman A. Abrahamson, David M. Boore, Kenneth W. Campbell, Elise Delavaud, Mustafa Erdik and Peter J. Stafford. December 2013.
- PEER 2013/21** *Seismic Design and Performance of Bridges with Columns on Rocking Foundations*. Grigorios Antonellis and Marios Panagiotou. September 2013.
- PEER 2013/20** *Experimental and Analytical Studies on the Seismic Behavior of Conventional and Hybrid Braced Frames*. Jiun-Wei Lai and Stephen A. Mahin. September 2013.
- PEER 2013/19** *Toward Resilient Communities: A Performance-Based Engineering Framework for Design and Evaluation of the Built Environment*. Michael William Mieler, Bozidar Stojadinovic, Robert J. Budnitz, Stephen A. Mahin and Mary C. Comerio. September 2013.
- PEER 2013/18** *Identification of Site Parameters that Improve Predictions of Site Amplification*. Ellen M. Rathje and Sara Navidi. July 2013.
- PEER 2013/17** *Response Spectrum Analysis of Concrete Gravity Dams Including Dam-Water-Foundation Interaction*. Arnkjell Lokke and Anil K. Chopra. July 2013.
- PEER 2013/16** *Effect of hoop reinforcement spacing on the cyclic response of large reinforced concrete special moment frame beams*. Marios Panagiotou, Tea Visnjic, Grigorios Antonellis, Panagiotis Galanis, and Jack P. Moehle. June 2013.
- PEER 2013/15** *A Probabilistic Framework to Include the Effects of Near-Fault Directivity in Seismic Hazard Assessment*. Shrey Kumar Shahi, Jack W. Baker. October 2013.
- PEER 2013/14** *Hanging-Wall Scaling using Finite-Fault Simulations*. Jennifer L. Donahue and Norman A. Abrahamson. September 2013.
- PEER 2013/13** *Semi-Empirical Nonlinear Site Amplification and its Application in NEHRP Site Factors*. Jonathan P. Stewart and Emel Seyhan. November 2013.
- PEER 2013/12** *Nonlinear Horizontal Site Response for the NGA-West2 Project*. Ronnie Kamai, Norman A. Abramson, Walter J. Silva. May 2013.
- PEER 2013/11** *Epistemic Uncertainty for NGA-West2 Models*. Linda Al Atik and Robert R. Youngs. May 2013.
- PEER 2013/10** *NGA-West 2 Models for Ground-Motion Directionality*. Shrey K. Shahi and Jack W. Baker. May 2013.
- PEER 2013/09** *Final Report of the NGA-West2 Directivity Working Group*. Paul Spudich, Jeffrey R. Bayless, Jack W. Baker, Brian S.J. Chiou, Badie Rowshandel, Shrey Shahi, and Paul Somerville. May 2013.
- PEER 2013/08** *NGA-West2 Model for Estimating Average Horizontal Values of Pseudo-Absolute Spectral Accelerations Generated by Crustal Earthquakes*. I. M. Idriss. May 2013.

- PEER 2013/07** *Update of the Chiou and Youngs NGA Ground Motion Model for Average Horizontal Component of Peak Ground Motion and Response Spectra.* Brian Chiou and Robert Youngs. May 2013.
- PEER 2013/06** *NGA-West2 Campbell-Bozorgnia Ground Motion Model for the Horizontal Components of PGA, PGV, and 5%-Damped Elastic Pseudo-Acceleration Response Spectra for Periods Ranging from 0.01 to 10 sec.* Kenneth W. Campbell and Yousef Bozorgnia. May 2013.
- PEER 2013/05** *NGA-West 2 Equations for Predicting Response Spectral Accelerations for Shallow Crustal Earthquakes.* David M. Boore, Jonathan P. Stewart, Emel Seyhan, Gail M. Atkinson. May 2013.
- PEER 2013/04** *Update of the AS08 Ground-Motion Prediction Equations Based on the NGA-West2 Data Set.* Norman Abrahamson, Walter Silva, and Ronnie Kamai. May 2013.
- PEER 2013/03** *PEER NGA-West2 Database.* Timothy D. Ancheta, Robert B. Darragh, Jonathan P. Stewart, Emel Seyhan, Walter J. Silva, Brian S.J. Chiou, Katie E. Wooddell, Robert W. Graves, Albert R. Kottke, David M. Boore, Tadahiro Kishida, and Jennifer L. Donahue. May 2013.
- PEER 2013/02** *Hybrid Simulation of the Seismic Response of Squat Reinforced Concrete Shear Walls.* Catherine A. Whyte and Bozidar Stojadinovic. May 2013.
- PEER 2013/01** *Housing Recovery in Chile: A Qualitative Mid-program Review.* Mary C. Comerio. February 2013.
- PEER 2012/08** *Guidelines for Estimation of Shear Wave Velocity.* Bernard R. Wair, Jason T. DeJong, and Thomas Shantz. December 2012.
- PEER 2012/07** *Earthquake Engineering for Resilient Communities: 2012 PEER Internship Program Research Report Collection.* Heidi Tremayne (Editor), Stephen A. Mahin (Editor), Collin Anderson, Dustin Cook, Michael Erceg, Carlos Esparza, Jose Jimenez, Dorian Krausz, Andrew Lo, Stephanie Lopez, Nicole McCurdy, Paul Shipman, Alexander Strum, Eduardo Vega. December 2012.
- PEER 2012/06** *Fragilities for Precarious Rocks at Yucca Mountain.* Matthew D. Purvance, Rasool Anooshehpour, and James N. Brune. December 2012.
- PEER 2012/05** *Development of Simplified Analysis Procedure for Piles in Laterally Spreading Layered Soils.* Christopher R. McGann, Pedro Arduino, and Peter Mackenzie-Helwein. December 2012.
- PEER 2012/04** *Unbonded Pre-Tensioned Columns for Bridges in Seismic Regions.* Phillip M. Davis, Todd M. Janes, Marc O. Eberhard, and John F. Stanton. December 2012.
- PEER 2012/03** *Experimental and Analytical Studies on Reinforced Concrete Buildings with Seismically Vulnerable Beam-Column Joints.* Sangjoon Park and Khalid M. Mosalam. October 2012.
- PEER 2012/02** *Seismic Performance of Reinforced Concrete Bridges Allowed to Uplift during Multi-Directional Excitation.* Andres Oscar Espinoza and Stephen A. Mahin. July 2012.
- PEER 2012/01** *Spectral Damping Scaling Factors for Shallow Crustal Earthquakes in Active Tectonic Regions.* Sanaz Rezaeian, Yousef Bozorgnia, I. M. Idriss, Kenneth Campbell, Norman Abrahamson, and Walter Silva. July 2012.
- PEER 2011/10** *Earthquake Engineering for Resilient Communities: 2011 PEER Internship Program Research Report Collection.* Eds. Heidi Faison and Stephen A. Mahin. December 2011.
- PEER 2011/09** *Calibration of Semi-Stochastic Procedure for Simulating High-Frequency Ground Motions.* Jonathan P. Stewart, Emel Seyhan, and Robert W. Graves. December 2011.
- PEER 2011/08** *Water Supply in regard to Fire Following Earthquake.* Charles Scawthorn. November 2011.
- PEER 2011/07** *Seismic Risk Management in Urban Areas. Proceedings of a U.S.-Iran-Turkey Seismic Workshop.* September 2011.
- PEER 2011/06** *The Use of Base Isolation Systems to Achieve Complex Seismic Performance Objectives.* Troy A. Morgan and Stephen A. Mahin. July 2011.
- PEER 2011/05** *Case Studies of the Seismic Performance of Tall Buildings Designed by Alternative Means.* Task 12 Report for the Tall Buildings Initiative. Jack Moehle, Yousef Bozorgnia, Nirmal Jayaram, Pierson Jones, Mohsen Rahnama, Nilesh Shome, Zeynep Tuna, John Wallace, Tony Yang, and Farzin Zareian. July 2011.
- PEER 2011/04** *Recommended Design Practice for Pile Foundations in Laterally Spreading Ground.* Scott A. Ashford, Ross W. Boulanger, and Scott J. Brandenburg. June 2011.
- PEER 2011/03** *New Ground Motion Selection Procedures and Selected Motions for the PEER Transportation Research Program.* Jack W. Baker, Ting Lin, Shrey K. Shahi, and Nirmal Jayaram. March 2011.
- PEER 2011/02** *A Bayesian Network Methodology for Infrastructure Seismic Risk Assessment and Decision Support.* Michelle T. Bensi, Armen Der Kiureghian, and Daniel Straub. March 2011.

- PEER 2011/01** *Demand Fragility Surfaces for Bridges in Liquefied and Laterally Spreading Ground.* Scott J. Brandenberg, Jian Zhang, Pirooz Kashighandi, Yili Huo, and Minxing Zhao. March 2011.
- PEER 2010/05** *Guidelines for Performance-Based Seismic Design of Tall Buildings.* Developed by the Tall Buildings Initiative. November 2010.
- PEER 2010/04** *Application Guide for the Design of Flexible and Rigid Bus Connections between Substation Equipment Subjected to Earthquakes.* Jean-Bernard Dastous and Armen Der Kiureghian. September 2010.
- PEER 2010/03** *Shear Wave Velocity as a Statistical Function of Standard Penetration Test Resistance and Vertical Effective Stress at Caltrans Bridge Sites.* Scott J. Brandenberg, Naresh Bellana, and Thomas Shantz. June 2010.
- PEER 2010/02** *Stochastic Modeling and Simulation of Ground Motions for Performance-Based Earthquake Engineering.* Sanaz Rezaeian and Armen Der Kiureghian. June 2010.
- PEER 2010/01** *Structural Response and Cost Characterization of Bridge Construction Using Seismic Performance Enhancement Strategies.* Ady Aviram, Božidar Stojadinović, Gustavo J. Parra-Montesinos, and Kevin R. Mackie. March 2010.
- PEER 2009/03** *The Integration of Experimental and Simulation Data in the Study of Reinforced Concrete Bridge Systems Including Soil-Foundation-Structure Interaction.* Matthew Dryden and Gregory L. Fenves. November 2009.
- PEER 2009/02** *Improving Earthquake Mitigation through Innovations and Applications in Seismic Science, Engineering, Communication, and Response. Proceedings of a U.S.-Iran Seismic Workshop.* October 2009.
- PEER 2009/01** *Evaluation of Ground Motion Selection and Modification Methods: Predicting Median Interstory Drift Response of Buildings.* Curt B. Haselton, Ed. June 2009.
- PEER 2008/10** *Technical Manual for Strata.* Albert R. Kottke and Ellen M. Rathje. February 2009.
- PEER 2008/09** *NGA Model for Average Horizontal Component of Peak Ground Motion and Response Spectra.* Brian S.-J. Chiou and Robert R. Youngs. November 2008.
- PEER 2008/08** *Toward Earthquake-Resistant Design of Concentrically Braced Steel Structures.* Patxi Uriz and Stephen A. Mahin. November 2008.
- PEER 2008/07** *Using OpenSees for Performance-Based Evaluation of Bridges on Liquefiable Soils.* Stephen L. Kramer, Pedro Arduino, and HyungSuk Shin. November 2008.
- PEER 2008/06** *Shaking Table Tests and Numerical Investigation of Self-Centering Reinforced Concrete Bridge Columns.* Hyung IL Jeong, Junichi Sakai, and Stephen A. Mahin. September 2008.
- PEER 2008/05** *Performance-Based Earthquake Engineering Design Evaluation Procedure for Bridge Foundations Undergoing Liquefaction-Induced Lateral Ground Displacement.* Christian A. Ledezma and Jonathan D. Bray. August 2008.
- PEER 2008/04** *Benchmarking of Nonlinear Geotechnical Ground Response Analysis Procedures.* Jonathan P. Stewart, Annie On-Lei Kwok, Youssef M. A. Hashash, Neven Matasovic, Robert Pyke, Zhiliang Wang, and Zhaohui Yang. August 2008.
- PEER 2008/03** *Guidelines for Nonlinear Analysis of Bridge Structures in California.* Ady Aviram, Kevin R. Mackie, and Božidar Stojadinović. August 2008.
- PEER 2008/02** *Treatment of Uncertainties in Seismic-Risk Analysis of Transportation Systems.* Evangelos Stergiou and Anne S. Kiremidjian. July 2008.
- PEER 2008/01** *Seismic Performance Objectives for Tall Buildings.* William T. Holmes, Charles Kircher, William Petak, and Nabih Youssef. August 2008.
- PEER 2007/12** *An Assessment to Benchmark the Seismic Performance of a Code-Conforming Reinforced Concrete Moment-Frame Building.* Curt Haselton, Christine A. Goulet, Judith Mitrani-Reiser, James L. Beck, Gregory G. Deierlein, Keith A. Porter, Jonathan P. Stewart, and Ertugrul Taciroglu. August 2008.
- PEER 2007/11** *Bar Buckling in Reinforced Concrete Bridge Columns.* Wayne A. Brown, Dawn E. Lehman, and John F. Stanton. February 2008.
- PEER 2007/10** *Computational Modeling of Progressive Collapse in Reinforced Concrete Frame Structures.* Mohamed M. Talaat and Khalid M. Mosalam. May 2008.
- PEER 2007/09** *Integrated Probabilistic Performance-Based Evaluation of Benchmark Reinforced Concrete Bridges.* Kevin R. Mackie, John-Michael Wong, and Božidar Stojadinović. January 2008.
- PEER 2007/08** *Assessing Seismic Collapse Safety of Modern Reinforced Concrete Moment-Frame Buildings.* Curt B. Haselton and Gregory G. Deierlein. February 2008.
- PEER 2007/07** *Performance Modeling Strategies for Modern Reinforced Concrete Bridge Columns.* Michael P. Berry and Marc O. Eberhard. April 2008.

- PEER 2007/06** *Development of Improved Procedures for Seismic Design of Buried and Partially Buried Structures.* Linda Al Atik and Nicholas Sitar. June 2007.
- PEER 2007/05** *Uncertainty and Correlation in Seismic Risk Assessment of Transportation Systems.* Renee G. Lee and Anne S. Kiremidjian. July 2007.
- PEER 2007/04** *Numerical Models for Analysis and Performance-Based Design of Shallow Foundations Subjected to Seismic Loading.* Sivapalan Gajan, Tara C. Hutchinson, Bruce L. Kutter, Prishati Raychowdhury, José A. Ugalde, and Jonathan P. Stewart. May 2008.
- PEER 2007/03** *Beam-Column Element Model Calibrated for Predicting Flexural Response Leading to Global Collapse of RC Frame Buildings.* Curt B. Haselton, Abbie B. Liel, Sarah Taylor Lange, and Gregory G. Deierlein. May 2008.
- PEER 2007/02** *Campbell-Bozorgnia NGA Ground Motion Relations for the Geometric Mean Horizontal Component of Peak and Spectral Ground Motion Parameters.* Kenneth W. Campbell and Yousef Bozorgnia. May 2007.
- PEER 2007/01** *Boore-Atkinson NGA Ground Motion Relations for the Geometric Mean Horizontal Component of Peak and Spectral Ground Motion Parameters.* David M. Boore and Gail M. Atkinson. May 2007.
- PEER 2006/12** *Societal Implications of Performance-Based Earthquake Engineering.* Peter J. May. May 2007.
- PEER 2006/11** *Probabilistic Seismic Demand Analysis Using Advanced Ground Motion Intensity Measures, Attenuation Relationships, and Near-Fault Effects.* Polsak Tothong and C. Allin Cornell. March 2007.
- PEER 2006/10** *Application of the PEER PBEE Methodology to the I-880 Viaduct.* Sashi Kunnath. February 2007.
- PEER 2006/09** *Quantifying Economic Losses from Travel Forgone Following a Large Metropolitan Earthquake.* James Moore, Sungbin Cho, Yue Yue Fan, and Stuart Werner. November 2006.
- PEER 2006/08** *Vector-Valued Ground Motion Intensity Measures for Probabilistic Seismic Demand Analysis.* Jack W. Baker and C. Allin Cornell. October 2006.
- PEER 2006/07** *Analytical Modeling of Reinforced Concrete Walls for Predicting Flexural and Coupled-Shear-Flexural Responses.* Kutay Orakcal, Leonardo M. Massone, and John W. Wallace. October 2006.
- PEER 2006/06** *Nonlinear Analysis of a Soil-Drilled Pier System under Static and Dynamic Axial Loading.* Gang Wang and Nicholas Sitar. November 2006.
- PEER 2006/05** *Advanced Seismic Assessment Guidelines.* Paolo Bazzurro, C. Allin Cornell, Charles Menun, Maziar Motahari, and Nicolas Luco. September 2006.
- PEER 2006/04** *Probabilistic Seismic Evaluation of Reinforced Concrete Structural Components and Systems.* Tae Hyung Lee and Khalid M. Mosalam. August 2006.
- PEER 2006/03** *Performance of Lifelines Subjected to Lateral Spreading.* Scott A. Ashford and Teerawut Juirnarongrit. July 2006.
- PEER 2006/02** *Pacific Earthquake Engineering Research Center Highway Demonstration Project.* Anne Kiremidjian, James Moore, Yue Yue Fan, Nesrin Basoz, Ozgur Yazali, and Meredith Williams. April 2006.
- PEER 2006/01** *Bracing Berkeley. A Guide to Seismic Safety on the UC Berkeley Campus.* Mary C. Comerio, Stephen Tوبرiner, and Ariane Fehrenkamp. January 2006.
- PEER 2005/16** *Seismic Response and Reliability of Electrical Substation Equipment and Systems.* Junho Song, Armen Der Kiureghian, and Jerome L. Sackman. April 2006.
- PEER 2005/15** *CPT-Based Probabilistic Assessment of Seismic Soil Liquefaction Initiation.* R. E. S. Moss, R. B. Seed, R. E. Kayen, J. P. Stewart, and A. Der Kiureghian. April 2006.
- PEER 2005/14** *Workshop on Modeling of Nonlinear Cyclic Load-Deformation Behavior of Shallow Foundations.* Bruce L. Kutter, Geoffrey Martin, Tara Hutchinson, Chad Harden, Sivapalan Gajan, and Justin Phalen. March 2006.
- PEER 2005/13** *Stochastic Characterization and Decision Bases under Time-Dependent Aftershock Risk in Performance-Based Earthquake Engineering.* Gee Liek Yeo and C. Allin Cornell. July 2005.
- PEER 2005/12** *PEER Testbed Study on a Laboratory Building: Exercising Seismic Performance Assessment.* Mary C. Comerio, editor. November 2005.
- PEER 2005/11** *Van Nuys Hotel Building Testbed Report: Exercising Seismic Performance Assessment.* Helmut Krawinkler, editor. October 2005.
- PEER 2005/10** *First NEES/E-Defense Workshop on Collapse Simulation of Reinforced Concrete Building Structures.* September 2005.
- PEER 2005/09** *Test Applications of Advanced Seismic Assessment Guidelines.* Joe Maffei, Karl Telleen, Danya Mohr, William Holmes, and Yuki Nakayama. August 2006.

- PEER 2005/08** *Damage Accumulation in Lightly Confined Reinforced Concrete Bridge Columns.* R. Tyler Ranf, Jared M. Nelson, Zach Price, Marc O. Eberhard, and John F. Stanton. April 2006.
- PEER 2005/07** *Experimental and Analytical Studies on the Seismic Response of Freestanding and Anchored Laboratory Equipment.* Dimitrios Konstantinidis and Nicos Makris. January 2005.
- PEER 2005/06** *Global Collapse of Frame Structures under Seismic Excitations.* Luis F. Ibarra and Helmut Krawinkler. September 2005.
- PEER 2005/05** *Performance Characterization of Bench- and Shelf-Mounted Equipment.* Samit Ray Chaudhuri and Tara C. Hutchinson. May 2006.
- PEER 2005/04** *Numerical Modeling of the Nonlinear Cyclic Response of Shallow Foundations.* Chad Harden, Tara Hutchinson, Geoffrey R. Martin, and Bruce L. Kutter. August 2005.
- PEER 2005/03** *A Taxonomy of Building Components for Performance-Based Earthquake Engineering.* Keith A. Porter. September 2005.
- PEER 2005/02** *Fragility Basis for California Highway Overpass Bridge Seismic Decision Making.* Kevin R. Mackie and Božidar Stojadinović. June 2005.
- PEER 2005/01** *Empirical Characterization of Site Conditions on Strong Ground Motion.* Jonathan P. Stewart, Yoojoong Choi, and Robert W. Graves. June 2005.
- PEER 2004/09** *Electrical Substation Equipment Interaction: Experimental Rigid Conductor Studies.* Christopher Stearns and André Filiatrault. February 2005.
- PEER 2004/08** *Seismic Qualification and Fragility Testing of Line Break 550-kV Disconnect Switches.* Shakhzod M. Takhirov, Gregory L. Fenves, and Eric Fujisaki. January 2005.
- PEER 2004/07** *Ground Motions for Earthquake Simulator Qualification of Electrical Substation Equipment.* Shakhzod M. Takhirov, Gregory L. Fenves, Eric Fujisaki, and Don Clyde. January 2005.
- PEER 2004/06** *Performance-Based Regulation and Regulatory Regimes.* Peter J. May and Chris Koski. September 2004.
- PEER 2004/05** *Performance-Based Seismic Design Concepts and Implementation: Proceedings of an International Workshop.* Peter Fajfar and Helmut Krawinkler, editors. September 2004.
- PEER 2004/04** *Seismic Performance of an Instrumented Tilt-up Wall Building.* James C. Anderson and Vitelmo V. Bertero. July 2004.
- PEER 2004/03** *Evaluation and Application of Concrete Tilt-up Assessment Methodologies.* Timothy Graf and James O. Malley. October 2004.
- PEER 2004/02** *Analytical Investigations of New Methods for Reducing Residual Displacements of Reinforced Concrete Bridge Columns.* Junichi Sakai and Stephen A. Mahin. August 2004.
- PEER 2004/01** *Seismic Performance of Masonry Buildings and Design Implications.* Kerri Anne Taeko Tokoro, James C. Anderson, and Vitelmo V. Bertero. February 2004.
- PEER 2003/18** *Performance Models for Flexural Damage in Reinforced Concrete Columns.* Michael Berry and Marc Eberhard. August 2003.
- PEER 2003/17** *Predicting Earthquake Damage in Older Reinforced Concrete Beam-Column Joints.* Catherine Pagni and Laura Lowes. October 2004.
- PEER 2003/16** *Seismic Demands for Performance-Based Design of Bridges.* Kevin Mackie and Božidar Stojadinović. August 2003.
- PEER 2003/15** *Seismic Demands for Nondeteriorating Frame Structures and Their Dependence on Ground Motions.* Ricardo Antonio Medina and Helmut Krawinkler. May 2004.
- PEER 2003/14** *Finite Element Reliability and Sensitivity Methods for Performance-Based Earthquake Engineering.* Terje Haukaas and Armen Der Kiureghian. April 2004.
- PEER 2003/13** *Effects of Connection Hysteretic Degradation on the Seismic Behavior of Steel Moment-Resisting Frames.* Janise E. Rodgers and Stephen A. Mahin. March 2004.
- PEER 2003/12** *Implementation Manual for the Seismic Protection of Laboratory Contents: Format and Case Studies.* William T. Holmes and Mary C. Comerio. October 2003.
- PEER 2003/11** *Fifth U.S.-Japan Workshop on Performance-Based Earthquake Engineering Methodology for Reinforced Concrete Building Structures.* February 2004.
- PEER 2003/10** *A Beam-Column Joint Model for Simulating the Earthquake Response of Reinforced Concrete Frames.* Laura N. Lowes, Nilanjan Mitra, and Arash Altoontash. February 2004.

- PEER 2003/09** *Sequencing Repairs after an Earthquake: An Economic Approach.* Marco Casari and Simon J. Wilkie. April 2004.
- PEER 2003/08** *A Technical Framework for Probability-Based Demand and Capacity Factor Design (DCFD) Seismic Formats.* Fatemeh Jalayer and C. Allin Cornell. November 2003.
- PEER 2003/07** *Uncertainty Specification and Propagation for Loss Estimation Using FOSM Methods.* Jack W. Baker and C. Allin Cornell. September 2003.
- PEER 2003/06** *Performance of Circular Reinforced Concrete Bridge Columns under Bidirectional Earthquake Loading.* Mahmoud M. Hachem, Stephen A. Mahin, and Jack P. Moehle. February 2003.
- PEER 2003/05** *Response Assessment for Building-Specific Loss Estimation.* Eduardo Miranda and Shahram Taghavi. September 2003.
- PEER 2003/04** *Experimental Assessment of Columns with Short Lap Splices Subjected to Cyclic Loads.* Murat Melek, John W. Wallace, and Joel Conte. April 2003.
- PEER 2003/03** *Probabilistic Response Assessment for Building-Specific Loss Estimation.* Eduardo Miranda and Hesameddin Aslani. September 2003.
- PEER 2003/02** *Software Framework for Collaborative Development of Nonlinear Dynamic Analysis Program.* Jun Peng and Kincho H. Law. September 2003.
- PEER 2003/01** *Shake Table Tests and Analytical Studies on the Gravity Load Collapse of Reinforced Concrete Frames.* Kenneth John Elwood and Jack P. Moehle. November 2003.
- PEER 2002/24** *Performance of Beam to Column Bridge Joints Subjected to a Large Velocity Pulse.* Natalie Gibson, André Filiatrault, and Scott A. Ashford. April 2002.
- PEER 2002/23** *Effects of Large Velocity Pulses on Reinforced Concrete Bridge Columns.* Greg L. Orozco and Scott A. Ashford. April 2002.
- PEER 2002/22** *Characterization of Large Velocity Pulses for Laboratory Testing.* Kenneth E. Cox and Scott A. Ashford. April 2002.
- PEER 2002/21** *Fourth U.S.-Japan Workshop on Performance-Based Earthquake Engineering Methodology for Reinforced Concrete Building Structures.* December 2002.
- PEER 2002/20** *Barriers to Adoption and Implementation of PBEE Innovations.* Peter J. May. August 2002.
- PEER 2002/19** *Economic-Engineered Integrated Models for Earthquakes: Socioeconomic Impacts.* Peter Gordon, James E. Moore II, and Harry W. Richardson. July 2002.
- PEER 2002/18** *Assessment of Reinforced Concrete Building Exterior Joints with Substandard Details.* Chris P. Pantelides, Jon Hansen, Justin Nadauld, and Lawrence D. Reaveley. May 2002.
- PEER 2002/17** *Structural Characterization and Seismic Response Analysis of a Highway Overcrossing Equipped with Elastomeric Bearings and Fluid Dampers: A Case Study.* Nicos Makris and Jian Zhang. November 2002.
- PEER 2002/16** *Estimation of Uncertainty in Geotechnical Properties for Performance-Based Earthquake Engineering.* Allen L. Jones, Steven L. Kramer, and Pedro Arduino. December 2002.
- PEER 2002/15** *Seismic Behavior of Bridge Columns Subjected to Various Loading Patterns.* Asadollah Esmaeily-Gh. and Yan Xiao. December 2002.
- PEER 2002/14** *Inelastic Seismic Response of Extended Pile Shaft Supported Bridge Structures.* T.C. Hutchinson, R.W. Boulanger, Y.H. Chai, and I.M. Idriss. December 2002.
- PEER 2002/13** *Probabilistic Models and Fragility Estimates for Bridge Components and Systems.* Paolo Gardoni, Armen Der Kiureghian, and Khalid M. Mosalam. June 2002.
- PEER 2002/12** *Effects of Fault Dip and Slip Rake on Near-Source Ground Motions: Why Chi-Chi Was a Relatively Mild M7.6 Earthquake.* Brad T. Aagaard, John F. Hall, and Thomas H. Heaton. December 2002.
- PEER 2002/11** *Analytical and Experimental Study of Fiber-Reinforced Strip Isolators.* James M. Kelly and Shakhzod M. Takhirov. September 2002.
- PEER 2002/10** *Centrifuge Modeling of Settlement and Lateral Spreading with Comparisons to Numerical Analyses.* Sivapalan Gajan and Bruce L. Kutter. January 2003.
- PEER 2002/09** *Documentation and Analysis of Field Case Histories of Seismic Compression during the 1994 Northridge, California, Earthquake.* Jonathan P. Stewart, Patrick M. Smith, Daniel H. Whang, and Jonathan D. Bray. October 2002.
- PEER 2002/08** *Component Testing, Stability Analysis and Characterization of Buckling-Restrained Unbonded Braces™.* Cameron Black, Nicos Makris, and Ian Aiken. September 2002.

- PEER 2002/07** *Seismic Performance of Pile-Wharf Connections*. Charles W. Roeder, Robert Graff, Jennifer Soderstrom, and Jun Han Yoo. December 2001.
- PEER 2002/06** *The Use of Benefit-Cost Analysis for Evaluation of Performance-Based Earthquake Engineering Decisions*. Richard O. Zerbe and Anthony Falit-Baiamonte. September 2001.
- PEER 2002/05** *Guidelines, Specifications, and Seismic Performance Characterization of Nonstructural Building Components and Equipment*. André Filiatrault, Constantin Christopoulos, and Christopher Stearns. September 2001.
- PEER 2002/04** *Consortium of Organizations for Strong-Motion Observation Systems and the Pacific Earthquake Engineering Research Center Lifelines Program: Invited Workshop on Archiving and Web Dissemination of Geotechnical Data, 4–5 October 2001*. September 2002.
- PEER 2002/03** *Investigation of Sensitivity of Building Loss Estimates to Major Uncertain Variables for the Van Nuys Testbed*. Keith A. Porter, James L. Beck, and Rustem V. Shaikhutdinov. August 2002.
- PEER 2002/02** *The Third U.S.-Japan Workshop on Performance-Based Earthquake Engineering Methodology for Reinforced Concrete Building Structures*. July 2002.
- PEER 2002/01** *Nonstructural Loss Estimation: The UC Berkeley Case Study*. Mary C. Comerio and John C. Stallmeyer. December 2001.
- PEER 2001/16** *Statistics of SDF-System Estimate of Roof Displacement for Pushover Analysis of Buildings*. Anil K. Chopra, Rakesh K. Goel, and Chatpan Chintanapakdee. December 2001.
- PEER 2001/15** *Damage to Bridges during the 2001 Nisqually Earthquake*. R. Tyler Ranf, Marc O. Eberhard, and Michael P. Berry. November 2001.
- PEER 2001/14** *Rocking Response of Equipment Anchored to a Base Foundation*. Nicos Makris and Cameron J. Black. September 2001.
- PEER 2001/13** *Modeling Soil Liquefaction Hazards for Performance-Based Earthquake Engineering*. Steven L. Kramer and Ahmed-W. Elgamal. February 2001.
- PEER 2001/12** *Development of Geotechnical Capabilities in OpenSees*. Boris Jeremić. September 2001.
- PEER 2001/11** *Analytical and Experimental Study of Fiber-Reinforced Elastomeric Isolators*. James M. Kelly and Shakhzod M. Takhirov. September 2001.
- PEER 2001/10** *Amplification Factors for Spectral Acceleration in Active Regions*. Jonathan P. Stewart, Andrew H. Liu, Yoojoong Choi, and Mehmet B. Baturay. December 2001.
- PEER 2001/09** *Ground Motion Evaluation Procedures for Performance-Based Design*. Jonathan P. Stewart, Shyh-Jeng Chiou, Jonathan D. Bray, Robert W. Graves, Paul G. Somerville, and Norman A. Abrahamson. September 2001.
- PEER 2001/08** *Experimental and Computational Evaluation of Reinforced Concrete Bridge Beam-Column Connections for Seismic Performance*. Clay J. Naito, Jack P. Moehle, and Khalid M. Mosalam. November 2001.
- PEER 2001/07** *The Rocking Spectrum and the Shortcomings of Design Guidelines*. Nicos Makris and Dimitrios Konstantinidis. August 2001.
- PEER 2001/06** *Development of an Electrical Substation Equipment Performance Database for Evaluation of Equipment Fragilities*. Thalia Agnanos. April 1999.
- PEER 2001/05** *Stiffness Analysis of Fiber-Reinforced Elastomeric Isolators*. Hsiang-Chuan Tsai and James M. Kelly. May 2001.
- PEER 2001/04** *Organizational and Societal Considerations for Performance-Based Earthquake Engineering*. Peter J. May. April 2001.
- PEER 2001/03** *A Modal Pushover Analysis Procedure to Estimate Seismic Demands for Buildings: Theory and Preliminary Evaluation*. Anil K. Chopra and Rakesh K. Goel. January 2001.
- PEER 2001/02** *Seismic Response Analysis of Highway Overcrossings Including Soil-Structure Interaction*. Jian Zhang and Nicos Makris. March 2001.
- PEER 2001/01** *Experimental Study of Large Seismic Steel Beam-to-Column Connections*. Egor P. Popov and Shakhzod M. Takhirov. November 2000.
- PEER 2000/10** *The Second U.S.-Japan Workshop on Performance-Based Earthquake Engineering Methodology for Reinforced Concrete Building Structures*. March 2000.
- PEER 2000/09** *Structural Engineering Reconnaissance of the August 17, 1999 Earthquake: Kocaeli (Izmit), Turkey*. Halil Sezen, Kenneth J. Elwood, Andrew S. Whittaker, Khalid Mosalam, John J. Wallace, and John F. Stanton. December 2000.

- PEER 2000/08** *Behavior of Reinforced Concrete Bridge Columns Having Varying Aspect Ratios and Varying Lengths of Confinement.* Anthony J. Calderone, Dawn E. Lehman, and Jack P. Moehle. January 2001.
- PEER 2000/07** *Cover-Plate and Flange-Plate Reinforced Steel Moment-Resisting Connections.* Taejin Kim, Andrew S. Whittaker, Amir S. Gilani, Vitelmo V. Bertero, and Shakhzod M. Takhirov. September 2000.
- PEER 2000/06** *Seismic Evaluation and Analysis of 230-kV Disconnect Switches.* Amir S. J. Gilani, Andrew S. Whittaker, Gregory L. Fenves, Chun-Hao Chen, Henry Ho, and Eric Fujisaki. July 2000.
- PEER 2000/05** *Performance-Based Evaluation of Exterior Reinforced Concrete Building Joints for Seismic Excitation.* Chandra Clyde, Chris P. Pantelides, and Lawrence D. Reaveley. July 2000.
- PEER 2000/04** *An Evaluation of Seismic Energy Demand: An Attenuation Approach.* Chung-Che Chou and Chia-Ming Uang. July 1999.
- PEER 2000/03** *Framing Earthquake Retrofitting Decisions: The Case of Hillside Homes in Los Angeles.* Detlof von Winterfeldt, Nels Roselund, and Alicia Kitsuse. March 2000.
- PEER 2000/02** *U.S.-Japan Workshop on the Effects of Near-Field Earthquake Shaking.* Andrew Whittaker, ed. July 2000.
- PEER 2000/01** *Further Studies on Seismic Interaction in Interconnected Electrical Substation Equipment.* Armen Der Kiureghian, Kee-Jeung Hong, and Jerome L. Sackman. November 1999.
- PEER 1999/14** *Seismic Evaluation and Retrofit of 230-kV Porcelain Transformer Bushings.* Amir S. Gilani, Andrew S. Whittaker, Gregory L. Fenves, and Eric Fujisaki. December 1999.
- PEER 1999/13** *Building Vulnerability Studies: Modeling and Evaluation of Tilt-up and Steel Reinforced Concrete Buildings.* John W. Wallace, Jonathan P. Stewart, and Andrew S. Whittaker, editors. December 1999.
- PEER 1999/12** *Rehabilitation of Nonductile RC Frame Building Using Encasement Plates and Energy-Dissipating Devices.* Mehrdad Sasani, Vitelmo V. Bertero, James C. Anderson. December 1999.
- PEER 1999/11** *Performance Evaluation Database for Concrete Bridge Components and Systems under Simulated Seismic Loads.* Yael D. Hose and Frieder Seible. November 1999.
- PEER 1999/10** *U.S.-Japan Workshop on Performance-Based Earthquake Engineering Methodology for Reinforced Concrete Building Structures.* December 1999.
- PEER 1999/09** *Performance Improvement of Long Period Building Structures Subjected to Severe Pulse-Type Ground Motions.* James C. Anderson, Vitelmo V. Bertero, and Raul Bertero. October 1999.
- PEER 1999/08** *Envelopes for Seismic Response Vectors.* Charles Menun and Armen Der Kiureghian. July 1999.
- PEER 1999/07** *Documentation of Strengths and Weaknesses of Current Computer Analysis Methods for Seismic Performance of Reinforced Concrete Members.* William F. Cofer. November 1999.
- PEER 1999/06** *Rocking Response and Overturning of Anchored Equipment under Seismic Excitations.* Nicos Makris and Jian Zhang. November 1999.
- PEER 1999/05** *Seismic Evaluation of 550 kV Porcelain Transformer Bushings.* Amir S. Gilani, Andrew S. Whittaker, Gregory L. Fenves, and Eric Fujisaki. October 1999.
- PEER 1999/04** *Adoption and Enforcement of Earthquake Risk-Reduction Measures.* Peter J. May, Raymond J. Burby, T. Jens Feeley, and Robert Wood.
- PEER 1999/03** *Task 3 Characterization of Site Response General Site Categories.* Adrian Rodriguez-Marek, Jonathan D. Bray, and Norman Abrahamson. February 1999.
- PEER 1999/02** *Capacity-Demand-Diagram Methods for Estimating Seismic Deformation of Inelastic Structures: SDF Systems.* Anil K. Chopra and Rakesh Goel. April 1999.
- PEER 1999/01** *Interaction in Interconnected Electrical Substation Equipment Subjected to Earthquake Ground Motions.* Armen Der Kiureghian, Jerome L. Sackman, and Kee-Jeung Hong. February 1999.
- PEER 1998/08** *Behavior and Failure Analysis of a Multiple-Frame Highway Bridge in the 1994 Northridge Earthquake.* Gregory L. Fenves and Michael Ellery. December 1998.
- PEER 1998/07** *Empirical Evaluation of Inertial Soil-Structure Interaction Effects.* Jonathan P. Stewart, Raymond B. Seed, and Gregory L. Fenves. November 1998.
- PEER 1998/06** *Effect of Damping Mechanisms on the Response of Seismic Isolated Structures.* Nicos Makris and Shih-Po Chang. November 1998.
- PEER 1998/05** *Rocking Response and Overturning of Equipment under Horizontal Pulse-Type Motions.* Nicos Makris and Yiannis Roussos. October 1998.

- PEER 1998/04** *Pacific Earthquake Engineering Research Invitational Workshop Proceedings, May 14–15, 1998: Defining the Links between Planning, Policy Analysis, Economics and Earthquake Engineering.* Mary Comerio and Peter Gordon. September 1998.
- PEER 1998/03** *Repair/Upgrade Procedures for Welded Beam to Column Connections.* James C. Anderson and Xiaojing Duan. May 1998.
- PEER 1998/02** *Seismic Evaluation of 196 kV Porcelain Transformer Bushings.* Amir S. Gilani, Juan W. Chavez, Gregory L. Fennes, and Andrew S. Whittaker. May 1998.
- PEER 1998/01** *Seismic Performance of Well-Confined Concrete Bridge Columns.* Dawn E. Lehman and Jack P. Moehle. December 2000.

## ONLINE PEER REPORTS

The following PEER reports are available by Internet only at [http://peer.berkeley.edu/publications/peer\\_reports\\_complete.html](http://peer.berkeley.edu/publications/peer_reports_complete.html).

- PEER 2012/103** *Performance-Based Seismic Demand Assessment of Concentrically Braced Steel Frame Buildings*. Chui-Hsin Chen and Stephen A. Mahin. December 2012.
- PEER 2012/102** *Procedure to Restart an Interrupted Hybrid Simulation: Addendum to PEER Report 2010/103*. Vesna Terzic and Božidar Stojadinovic. October 2012.
- PEER 2012/101** *Mechanics of Fiber Reinforced Bearings*. James M. Kelly and Andrea Calabrese. February 2012.
- PEER 2011/107** *Nonlinear Site Response and Seismic Compression at Vertical Array Strongly Shaken by 2007 Niigata-ken Chuetsu-oki Earthquake*. Eric Yee, Jonathan P. Stewart, and Kohji Tokimatsu. December 2011.
- PEER 2011/106** *Self Compacting Hybrid Fiber Reinforced Concrete Composites for Bridge Columns*. Pardeep Kumar, Gabriel Jen, William Trono, Marios Panagiotou, and Claudia Ostertag. September 2011.
- PEER 2011/105** *Stochastic Dynamic Analysis of Bridges Subjected to Spatially Varying Ground Motions*. Katerina Konakli and Armen Der Kiureghian. August 2011.
- PEER 2011/104** *Design and Instrumentation of the 2010 E-Defense Four-Story Reinforced Concrete and Post-Tensioned Concrete Buildings*. Takuya Nagae, Kenichi Tahara, Taizo Matsumori, Hitoshi Shiohara, Toshimi Kabeyasawa, Susumu Kono, Minehiro Nishiyama (Japanese Research Team) and John Wallace, Wassim Ghannoum, Jack Moehle, Richard Sause, Wesley Keller, Zeynep Tuna (U.S. Research Team). June 2011.
- PEER 2011/103** *In-Situ Monitoring of the Force Output of Fluid Dampers: Experimental Investigation*. Dimitrios Konstantinidis, James M. Kelly, and Nicos Makris. April 2011.
- PEER 2011/102** *Ground-motion prediction equations 1964 - 2010*. John Douglas. April 2011.
- PEER 2011/101** *Report of the Eighth Planning Meeting of NEES/E-Defense Collaborative Research on Earthquake Engineering*. Convened by the Hyogo Earthquake Engineering Research Center (NIED), NEES Consortium, Inc. February 2011.
- PEER 2010/111** *Modeling and Acceptance Criteria for Seismic Design and Analysis of Tall Buildings*. Task 7 Report for the Tall Buildings Initiative - Published jointly by the Applied Technology Council. October 2010.
- PEER 2010/110** *Seismic Performance Assessment and Probabilistic Repair Cost Analysis of Precast Concrete Cladding Systems for Multistory Buildings*. Jeffrey P. Hunt and Božidar Stojadinovic. November 2010.
- PEER 2010/109** *Report of the Seventh Joint Planning Meeting of NEES/E-Defense Collaboration on Earthquake Engineering. Held at the E-Defense, Miki, and Shin-Kobe, Japan, September 18–19, 2009*. August 2010.
- PEER 2010/108** *Probabilistic Tsunami Hazard in California*. Hong Kie Thio, Paul Somerville, and Jascha Polet, preparers. October 2010.
- PEER 2010/107** *Performance and Reliability of Exposed Column Base Plate Connections for Steel Moment-Resisting Frames*. Ady Aviram, Božidar Stojadinovic, and Armen Der Kiureghian. August 2010.
- PEER 2010/106** *Verification of Probabilistic Seismic Hazard Analysis Computer Programs*. Patricia Thomas, Ivan Wong, and Norman Abrahamson. May 2010.
- PEER 2010/105** *Structural Engineering Reconnaissance of the April 6, 2009, Abruzzo, Italy, Earthquake, and Lessons Learned*. M. Selim Günay and Khalid M. Mosalam. April 2010.
- PEER 2010/104** *Simulating the Inelastic Seismic Behavior of Steel Braced Frames, Including the Effects of Low-Cycle Fatigue*. Yuli Huang and Stephen A. Mahin. April 2010.
- PEER 2010/103** *Post-Earthquake Traffic Capacity of Modern Bridges in California*. Vesna Terzic and Božidar Stojadinović. March 2010.
- PEER 2010/102** *Analysis of Cumulative Absolute Velocity (CAV) and JMA Instrumental Seismic Intensity ( $I_{JMA}$ ) Using the PEER-NGA Strong Motion Database*. Kenneth W. Campbell and Yousef Bozorgnia. February 2010.
- PEER 2010/101** *Rocking Response of Bridges on Shallow Foundations*. Jose A. Ugalde, Bruce L. Kutter, and Boris Jeremic. April 2010.
- PEER 2009/109** *Simulation and Performance-Based Earthquake Engineering Assessment of Self-Centering Post-Tensioned Concrete Bridge Systems*. Won K. Lee and Sarah L. Billington. December 2009.
- PEER 2009/108** *PEER Lifelines Geotechnical Virtual Data Center*. J. Carl Stepp, Daniel J. Ponti, Loren L. Turner, Jennifer N. Swift, Sean Devlin, Yang Zhu, Jean Benoit, and John Bobbitt. September 2009.
- PEER 2009/107** *Experimental and Computational Evaluation of Current and Innovative In-Span Hinge Details in Reinforced Concrete Box-Girder Bridges: Part 2: Post-Test Analysis and Design Recommendations*. Matias A. Hube and Khalid M. Mosalam. December 2009.

- PEER 2009/106** *Shear Strength Models of Exterior Beam-Column Joints without Transverse Reinforcement.* Sangjoon Park and Khalid M. Mosalam. November 2009.
- PEER 2009/105** *Reduced Uncertainty of Ground Motion Prediction Equations through Bayesian Variance Analysis.* Robb Eric S. Moss. November 2009.
- PEER 2009/104** *Advanced Implementation of Hybrid Simulation.* Andreas H. Schellenberg, Stephen A. Mahin, Gregory L. Fenves. November 2009.
- PEER 2009/103** *Performance Evaluation of Innovative Steel Braced Frames.* T. Y. Yang, Jack P. Moehle, and Božidar Stojadinovic. August 2009.
- PEER 2009/102** *Reinvestigation of Liquefaction and Nonliquefaction Case Histories from the 1976 Tangshan Earthquake.* Robb Eric Moss, Robert E. Kayen, Liyuan Tong, Songyu Liu, Guojun Cai, and Jiaer Wu. August 2009.
- PEER 2009/101** *Report of the First Joint Planning Meeting for the Second Phase of NEES/E-Defense Collaborative Research on Earthquake Engineering.* Stephen A. Mahin et al. July 2009.
- PEER 2008/104** *Experimental and Analytical Study of the Seismic Performance of Retaining Structures.* Linda Al Atik and Nicholas Sitar. January 2009.
- PEER 2008/103** *Experimental and Computational Evaluation of Current and Innovative In-Span Hinge Details in Reinforced Concrete Box-Girder Bridges. Part 1: Experimental Findings and Pre-Test Analysis.* Matias A. Hube and Khalid M. Mosalam. January 2009.
- PEER 2008/102** *Modeling of Unreinforced Masonry Infill Walls Considering In-Plane and Out-of-Plane Interaction.* Stephen Kadysiewski and Khalid M. Mosalam. January 2009.
- PEER 2008/101** *Seismic Performance Objectives for Tall Buildings.* William T. Holmes, Charles Kircher, William Petak, and Nabih Youssef. August 2008.
- PEER 2007/101** *Generalized Hybrid Simulation Framework for Structural Systems Subjected to Seismic Loading.* Tarek Elkhoraibi and Khalid M. Mosalam. July 2007.
- PEER 2007/100** *Seismic Evaluation of Reinforced Concrete Buildings Including Effects of Masonry Infill Walls.* Alidad Hashemi and Khalid M. Mosalam. July 2007.

The Pacific Earthquake Engineering Research Center (PEER) is a multi-institutional research and education center with headquarters at the University of California, Berkeley. Investigators from over 20 universities, several consulting companies, and researchers at various state and federal government agencies contribute to research programs focused on performance-based earthquake engineering.

These research programs aim to identify and reduce the risks from major earthquakes to life safety and to the economy by including research in a wide variety of disciplines including structural and geotechnical engineering, geology/seismology, lifelines, transportation, architecture, economics, risk management, and public policy.

PEER is supported by federal, state, local, and regional agencies, together with industry partners.



PEER Core Institutions:  
University of California, Berkeley (Lead Institution)  
California Institute of Technology  
Oregon State University  
Stanford University  
University of California, Davis  
University of California, Irvine  
University of California, Los Angeles  
University of California, San Diego  
University of Southern California  
University of Washington

PEER reports can be ordered at [http://peer.berkeley.edu/publications/peer\\_reports.html](http://peer.berkeley.edu/publications/peer_reports.html) or by contacting

Pacific Earthquake Engineering Research Center  
University of California, Berkeley  
325 Davis Hall, mail code 1792  
Berkeley, CA 94720-1792  
Tel: 510-642-3437  
Fax: 510-642-1655  
Email: [peer\\_editor@berkeley.edu](mailto:peer_editor@berkeley.edu)

ISSN 1547-0587X